Field Excursion to the Southern Pyrenean and Ebro Foreland Basins, Spain

26th April to 4th May, 2003

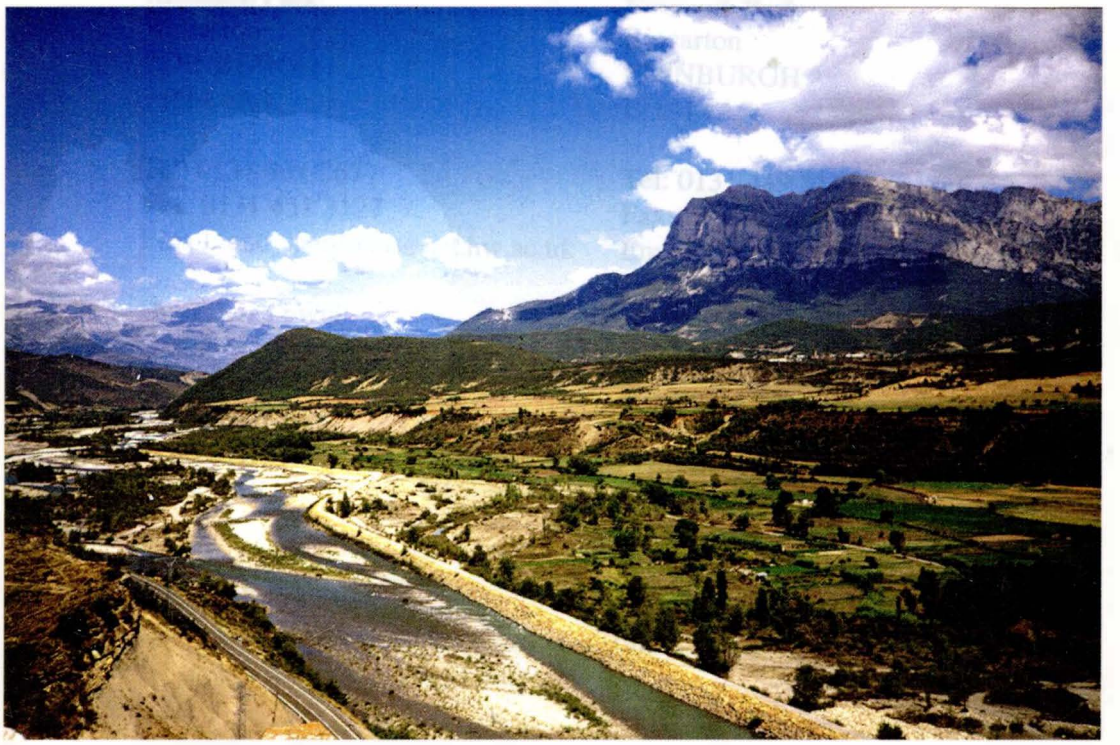

Leaders
Andy Gardiner, Patrick Corbett and Helen Lewis

Brochure compiled by
Andy Gardiner
with contributions from
Patrick Corbett, Julian Clark and Rob Ferguson

CONTENTS

Chapters Page

1 INTRODUCTION 1.1

1.1 GENERAL GEOLOGICAL INFORMATION 1.1

1.2 AIMS OF THE EXCURSION 1.1

1.3 FORMAT OF THE GUIDEBOOK 1.1

1.4 ACKNOWLEDGEMENTS 1.2

2 GEOLOGICAL HISTORY OF THE SOUTHERN PYRENEES 2.1

2.1 INTRODUCTION TO THE PYRENEES 2.1

2.2 DEVELOPMENT OF THE PYRENEES 2.1

2.2.1 Stephanian - Late Aptian Rifting 2.1
2.2.2 Late Aptian - Late Cretaceous Strike-slip Deformation 2.2
2.2.3 Late Cretaceous - Miocene Compression 2.2

2.3 STRUCTURAL INTERPRETATIONS OF THE PYRENEES 2.2

2.3.1 Thin-skinned Model 2.2
2.3.2 Thick-skinned Model 2.2
2.3.3 Inhomogeneous Strain Model 2.3
2.3.4 The Evidence of the ECORS Profile 2.3

2.4 STRATIGRAPHICAL AND STRUCTURAL DEVELOPMENT OF THE SOUTH PYRENEAN BASIN 2.3

2.4.1 Pre-compression Stratigraphy (Post-Hercynian) 2.4
2.4.2 Syn- and Post-Compression Stratigraphy 2.4
2.4.3 Key Structures of the Spanish Pyrenees 2.5

2.5 THE UPPER CRETACEOUS VALLCARGA BASIN - EXTENSION AND INVERSION 2.6

2.6 THE EOCENE SOUTH PYRENEAN FORELAND BASINS 2.7

2.6.1 Introduction 2.7
2.6.2 The Ager Sub-basin 2.8
2.6.3 The Tremp-Graus Sub-basin 2.8
2.6.4 The Ainsa Sub-basin 2.10
2.6.5 The Jaca Sub-basin 2.11

2.7 THE UPPER EOCENE - OLIGOCENE JACA BASIN-FILL 2.11

2.8 THE EBRO BASIN 2.12

2b REFERENCES 2b.1

3 FIELD LOCALITIES - THE VALLCARGA BASIN

4 FIELD LOCALITIES - THE TREMP-GRAUS SUB-BASIN

5 FIELD LOCALITIES - THE AINSA SUB-BASIN

6 FIELD LOCALITIES - THE JACA SUB-BASIN

7 FIELD LOCALITIES - THE EXTERNAL SIERRAS AND EBRO BASIN

8 GENERAL DIAGRAMS

9 NOTES

10 GEOLOGICAL MAP

11 LOCALITY MAP

Itinerary

Day 1 (Saturday 26th April)

Fly to Barcelona
Drive to Tremp (approx. 2-3 hours).

Due to the unavoidable late flight times, we will not have time on the Saturday evening to do our usual brief introduction to the geology of the Pyrenees. Instead, we will drive straight to Tremp for a late dinner.

Night at Tremp

Day 2 (Sunday 27th April)

Introduction to the tectonic setting and sedimentary fill of the southern Pyrenean foreland basins.

Shallow marine sediments in the Vallcarga Basin. The Vallcarga Basin is a small, extensional basin which was active before the main Pyrenean deformation, and so pre-dates the southern Pyrenean foreland Basins. The upper part of its fill includes the laterally extensive Arén sandstone (or Arén Formation).

- Latest Paleocene Aren sandstone around Isona. The well-exposed shallow marine/shoreline deposits of the Aren sandstone will be examined to the east of the town of Isona. Later in the day, after examination of the fluvial sediments around Montañana, we may also visit the Aren sandstone at the type locality, to allow comparison of the formation in the different localities.

Fluvial and shallow marine sediments in the Tremp-Graus Basin

- Introduction to the tectonic setting and sedimentary fill of the Tremp-Graus Basin.

- Examination of excellently-exposed fluvial sediments in the Montañana area. These include classic examples of ribbon-like meandering channel sandstones, often with excellently-preserved lateral accretion surfaces, as well as multi-storey/multi-lateral fluvial sheet sandstones. The overbank sediments commonly contain calcareous soil horizons (calcretes) and these will be examined.

- Oligocene fluvial conglomerates N of Benabarre

- The Sis palaeo-valley - a long-lasting sediment supply conduit into the Tremp-Graus and Ebro basins

Night at Serradúy

Day 3 (Monday 28th April)

Shallow marine Roda Sandstone

- Shallow-marine/estuarine sandbar sandstones of the Roda Sandstone near Roda.

Ainsa Basin turbidite sediments.

- Foradada Fault. Strike-slip fault at the northern margin of the Ainsa Basin
- Overview of the Ainsa Basin from Griébal. From the viewpoint at Griébal, it is possible to see the gross stratigraphy of the deep-water sediments which form the lower part of the fill of the Ainsa Basin. Complex channnel sandbodies occur within a dominantly fine-grained succession, of inferred submarine slope origin
- Ainsa I and II overview. View, across the reservoir, of the Ainsa I channel sandbody, exposed in a quarry S of Ainsa. The Ainsa II sandbody forms the first cliff at the top of the shale-domianted slope above the quarry.
- Morillo channel complex. Detailed examination of a complex channel sandbody. Examination of the sedimentary succession and comparison with a Gamma Log measured in the field.

Night at Ainsa

Day 4 (Tuesday 29th April)

Modelling of stacked turbidite channels

- Examination of the Ainsa II channel complex. Identification and correlation of individual sandbodies within the complex. Discussion of seismic resolution of similar successions in the subsurface.
- Discussion of modelling issues. Identification of modelling elements. Discussion of parameters likely to control reservoir behaviour.
- Generation of 2D models of the Ainsa II channel complex. Flow simulation (using Eclipse). Variation of the models to examine sensitivities.

Night at Ainsa

Day 5 (Wednesday 30th April)

Summary of the Ainsa Basin

- Guaso overview. View of northern part of the Ainsa Basin, showing context of the deep-water sediments and the overlying deltaic, shallow marine and fluvial sediments which complete the fill of the basin.
- 'Sobrarbe delta' shallow marine sediments south of Guaso.
- Escanilla Fm. fluvial sediments at Olsón,

Introduction to the Jaca Basin

Day 7 (Friday 2nd May)

The Huesca fluvial distributary system

Continued examination of the Huesca fluvial distributary system

Examination of the higher net-to-gross intervals

- Pertusa. Higher net-to-gross succession in a more proximal part of the fluvial distributary system. Estimation of the ratio of channel to non-channel facies. Identification of modelling elements and logging of short section to establish likely reservoir parameters.

- Angüés. Additional high net-to-gross section to add to database for modelling studies.

Drive to Caspe

Modelling

- Late afternoon/early evening in hotel – discussion of fluvial modelling issues. Measurement of outcrop panels and digital photographs to identify sandbody dimensions.

Night at Caspe

Day 8 (Saturday, 3rd May)

Finish modelling exercise

- Build a range of 2D fluvial models, to examine the impact of different net-to-gross ratios, sandbody dimensions, floodplain characteristics and petrophysics. Flow simulation through the models

Exhumed fluvial channels and channel belts in the southern Ebro Basin.

- Exhumed fluvial channels and channel belts in the Caspe area. Erosion of the intervening floodplain fines has left many fluvial channels exposed as sandstone ridges. The channels typically have low aspect ratios and commonly stack to form narrow multi-storey sandbodies. The planform shape of these sandbodies can be clearly demonstrated, and the contact between sandbodies can be demonstrated at several localities. This area is the subject of a current GPR (Ground Penetrating Radar) study by the Genetic Units Project at Heriot-Watt.

Summary meeting/de-briefing

Night at Caspe

Day 9 (Sunday 4th May)

Due to the early flight time, we will leave Caspe before breakfast, to arrive in Barcelona (approximately 3-4 hours from Caspe) in time for check-in.
Return to UK

Hotel addresses

Date	Hotel	Phone (00 34 9)	Fax
Saturday, 26th April	Hotel Segle XX Plaça de la Creu, 8 DP 25620 Tremp	73 650 000	73 652 612
Sunday, 27th April	Hotel Casa Peix Serradúy	74 544 430	74 544 460
Mon. 28th and Tues. 29th April	Hotel Dos Rios Avda. Central DP 22330 Ainsa	74 500 961 74 500 043	74 510 025
Wednesday, 30th April	Hotel Ramiro 1 C. del Carmen 23 DP 22700 Jaca	74 361 367	74 361 361
Thursday 1st May	Hostal Joachín Costa C. Joachín Costa DP 22003 Huesca	74 241 774	74 241 315
Friday 2nd May Saturday 3rd May	Hotel Magallón Plaza Obispo Cubeles DP 50700 Caspe Email: hotelmag@infonegocio.com www.iawol.com/hotelmagallon	76 630 222	76 630 003

1 Introduction

1.1 GENERAL GEOLOGICAL INFORMATION

The Southern Pyrenean basins formed during the Tertiary, as foreland basins to the developing Pyrenean mountain chain. The main Southern Pyrenean Basin, which consists of four sub-basins, the Ager, Temp-Graus, Ainsa and Jaca sub-basins, was active during the Eocene. Its sedimentary fill is dominated by a westerly directed axial depositional system, which deposited mainly clastic sediments in a wide range of deposition environments. The eastern part of the basin is dominated by fluvial sediments, which pass westwards into shoreline and shelf deposits and finally into marine turbidites. Due to renewed thrust activity, deposition was restricted during the late Eocene and Oligocene to the westernmost Jaca External Sub-basin. Later thrusts propagated further southwards, forming the External Sierras where they cut up-section. This led to the development of a second foreland basin, the Ebro Basin, to the south of the External Sierras. Deposition in the Ebro Basin, during the Oligo-Miocene, was dominated by alluvial fan, fluvial and lacustrine systems.

1.2 AIMS OF THE EXCURSION

The aims of the excursion are to examine the sedimentary fills of the Southern Pyrenean Basin and the northern part of the Ebro Basin and their relationship to contemporaneous tectonic activity. In recent years, attempts have been made to describe the succession in terms of sequence stratigraphic models, and the applicability of these models to foreland basins will be discussed.

Although we will consider exploration-scale issues during the excursion, we will concentrate on the reservoir scale and will discuss the likely reservoir behaviour of the sandbodies seen at outcrop. The excellent exposures allow the 2-dimensional and 3-dimensional geometry of the sand bodies, and their interconnectedness, to be examined in detail and we will discuss a range of reservoir issues, including reservoir description, model building, flow simulation and well testing, at outcrop. To enable us to do this, we will draw on a wide range of studies in geoscience and engineering which have been carried out at Heriot-Watt University.

1.3 FORMAT OF THE GUIDEBOOK

The Southern Pyrenean area has been the subject of much detailed work during the last twenty five years. The area has been well described in the literature and several field guides to the area exist. Section 2 of this guidebook contains a brief summary of the geological history of the Southern Pyrenean and Ebro basins and is followed by an extensive bibliography. Following this summary, the bulk of the information on individual localities (Sections 3 to 7) takes the form of diagrams, including maps, sedimentary logs, cross-sections and depositional models. These diagrams will form the basis of discussions in the field.

1.4 ACKNOWLEDGEMENTS

The geological summary in Section 2 is based on an earlier summary of the Southern Pyrenean basins by Trevor Elliott of Liverpool University, which has been updated and extended to cover the Ebro Basin. Many of the diagrams used in the guidebook are based on publications listed in the bibliography, for which we thank the authors. We also thank Julian Clark for providing much new material on the Ainsa Basin.
This excursion received financial support from Shell Expro and the Aberdeen Formation Evaluation Society, for which we offer our sincere thanks.

2 Geological History of the Southern Pyrenees

2.1 INTRODUCTION TO THE PYRENEES

The Pyrenees are part of the Alpine Mountain Belt of Southern Europe, extending from the Asturias in Northern Spain eastwards to Provence in Southern France. The mountain belt developed from the late Cretaceous to Pliocene times. A north-south cross section through the Pyrenees reveals several distinctive structural zones (Figures 2.1 and 2.2).

i) The Aquitaine Basin in Southern France which is, in part, a foreland basin to the Pyrenees.

ii) A zone of north-vergent thrusts and folds.

iii) The North Pyrenean Fault Zone - a steep fault zone with locally developed zones of high strain in Mesozoic metasediments and lherzolite pods.

iv) The Axial Zone, composed of ?Precambrian to Carboniferous metasediments, gneiss domes and granitoides, which constitute a Hercynian massif.

v) A zone of south-vergent thrusts and folds on the Spanish side of the Pyrenees.

vi) A southern system of foreland basins to the mountain belt - the South Pyrenean Basin (Ager, Tremp-Graus, Ainsa and Jaca Sub-basins) and the Ebro Basin.

The excursion is concerned exclusively with the evolution of foreland basins on the southern, Spanish side of the Pyrenees and their links with deformation in the south-vergent thrust belt and the axial zone

2.2 DEVELOPMENT OF THE PYRENEES

Three principal stages can be recognised in the development of the Pyrenean Mountain Belt:

2.2.1 Stephanian to Late Aptian Rifting

Stephanian to late Aptian rifting between Iberia and France began in post-Hercynian times, during the late Stephanian and Permian, and created intra-continental extensional or transtensional basins (Speksnijder, 1985). Continued rifting and subsidence in the Triassic and Liassic eventually resulted in the formation of a marine basin which persisted throughout the Lower and Middle Jurassic (Puigdefábregas and Souquet, 1986). The principal rifting phase began during the Kimmeridgian and continued into the late Aptian, heralding the opening of the Bay of Biscay (Pinet et al., 1987). A rifted margin was produced at the Biscay margin of the French plate and numerous other basins were enhanced at this time (e.g. the Parentis Basin). There is no evidence for the existence of oceanic crust between the Iberian and European plates in the Pyrenean region.

2.2.2 Late Aptian to Late Cretaceous Strike-slip Deformation

Late Aptian to late Cretaceous strike-slip deformation. Northward extension of the Atlantic spreading centre and the initiation of sea-floor spreading in the Bay of Biscay in late Aptian/early Albian (J-anomaly, 110 Ma) caused a major change in plate motions, with Iberia beginning to move south-east in a sinistral sense with respect to the French plate (Boillot, 1984). This change in plate motions was almost entirely accommodated in the Central Pyrenees; normal faults were reactivated as strike-slip faults and flower structures were produced locally, particularly on the northern (French) side. Transtension associated with the opening of Bay of Biscay formed extensional basins (e.g. the Vallcarga Basin, see Section 2.5) which were active until the beginning of alpine compression.

2.2.3 Late Cretaceous to Miocene Compression

Compression resulted from a further change in plate motion, which was caused by the northward extension of the North Atlantic spreading centre and the cessation of sea floor spreading in the Bay of Biscay. The timing of this change is dated at 75 Ma by the age of the last sea-floor magnetic stripe in the Bay of Biscay. According to Puigdefábregas and Souquet (1986) the earliest Alpine shortening may have been due to transpressional strike-slip but, by the Paleocene, a convergent margin had developed and the European plate was being subducted beneath Iberia. Thrusting per se was confined to the immediate vicinity of the mountain belt, but associated deformation extended northwards, causing inversion of earlier basins on the French side and initiating diapirism (Pinet et al., 1987). The compressional direction was NNE-SSW and estimates of shortening have a mean value of around 100 km.

2.3 STRUCTURAL INTERPRETATIONS OF THE PYRENEES

Numerous models have been proposed to explain the structural style and development of the Pyrenees during the alpine orogeny. To date, none of these models have achieved a consensus; the main areas of contention are i) the attitude of the thrust at depth; ii) the significance of the North Pyrenean fault; and iii) the origin and significance of a 15 km southward downstep in the Moho beneath the North Pyrenean fault, which was identified in early seismic work. Three models can be identified at present.

2.3.1 Thin-skinned Model

This model is favoured by Williams and Fischer (1984) who interpret a system of high-level thrusts, which link downwards into a low-angle sole thrust which dips north at 6 degrees (Figure 2.3). Most of the shortening is directed southwards and the northward shortening on the French side is attributed to a backthrust fan which branches from the sole thrust, with its extension inferred to lie beneath the Aquitaine Basin. The evidence for the Moho step directly beneath the present outcrop of the North Pyrenean fault is ignored in this model.

2.3.2 Thick-skinned Model

Deramond et al. (1984) interpret a thin-skinned thrust system at high levels, which steepens at depth, cuts the crust-mantle boundary and passes into a décollement between the crust and mantle north of the North Pyrenean fault. The restored lower crust is more attenuated in this interpretation, which is in keeping with the earlier extensional and transtensional history of the area. Once again, however, the Moho step is ignored in this model.

2.3.3 Inhomogeneous Strain Model

This model, involving high-level brittle displacements and deeper level ductile, shear zone deformation, is favoured by Seguret and Danieres (1986) and follows earlier work by French researchers. They consider the Moho step to be directly related to the North Pyrenean Fault and believe that it is a long-lived feature inherited from the late Cretaceous, when the fault was active. The North Pyrenean Fault is used as a pin-line in their reconstructions and as a result the restored section shows thinned lower crust beneath the Aquitaine Basin and normal thickness crust south of the fault. This is compatible with the prevalence of thick Jurassic - Cretaceous basin fill successions in the Aquitaine Basin.

2.3.4 The Evidence of the ECORS Profile

Publication of the ECORS deep seismic reflection profile across the Pyrenees provided crucial evidence relating to the deep structure of the mountain belt (ECORS, 1988). The line is 225 km long and extends from the Ebro Basin to the Aquitaine Basin slightly east of the centre of the Pyrenees. With the exception of the axial zone, the entire crustal profile shows clear reflectors (Figure 2.4). The deeper part of the profile is well layered and the base of this zone is interpreted as the Moho. On the Spanish side, the Moho is at 10-12 seconds twtt and dips northwards towards the axial zone, where it is at 20 seconds. On the French side, beneath the Aquitaine Basin, the Moho is located between 7-10 seconds and dips gently southwards into the axial zone. The crust is thicker on the Spanish side and the observed dipping of the Moho into the axial zone is considered to reflect overthrusting towards the forelands. Thrust stacking in the axial zone is considered to be responsible for the thickening of the Spanish crust. The North Pyrenean Fault separates the regions of deep, northward-dipping and shallow, southward-dipping reflectors and is therefore interpreted as the boundary between the Spanish and French plates. Deformation of the fault is interpreted, with the lower crust on the French side indenting into the thicker crust on the Spanish side. At shallower levels on the Spanish side, it is clear that the basement is not involved in deformation at the thrust front and the deformation is therefore thin-skinned, but when traced northwards towards the axial zone the décollement level steepness slightly and connects with the lower crustal reflectors. Crustal-scale thrusts are therefore interpreted, favouring a variant of the thick-skinned, inhomogenous strain model of Seguret and Dagnieres (1986).

2.4 STRATIGRAPHICAL AND STRUCTURAL DEVELOPMENT OF THE SOUTH PYRENEAN BASIN

The earliest evidence for alpine compression in the Pyrenees is during the Maastrichtian in the east of the area. The onset of compression was diachronous, becoming younger westwards. In a regional sense, the Paleocene, which comprises a continental red-bed succession (the Tremp Formation; Figure 2.5) transgressively overlain by a marine limestone (the Alveolina Limestone Formation), corresponds to a structural hiatus between extension during the Cretaceous and compression during the Tertiary. These formations are of relatively constant thickness and facies throughout the area, suggesting a lack of differential subsidence at this time and hence relative tectonic quiescence.

2.4.1 Pre-compression Stratigraphy (Post-Hercynian)

Coal-bearing Carboniferous successions, Permian and Triassic continental red-bed successions and volcanics/volcaniclastics accumulated in extensional basins which immediately post-dated the Hercynian orogeny (Nagtegaal, 1969; Speksnijder, 1985). The Triassic Bunter facies is overlain by a suite of limestones, marls, gypsum, halite and gabbroic ('ophite') intrusions which are Muschelkalk and Keuper in age. This stratigraphical level is

critical, since the gypsum and halite lithologies constitute one of the key décollement levels of the alpine compression. The Jurassic is composed of marine limestones, which are mainly exposed in the east of the Pyrenees. This early part of the pre-compression stratigraphy cannot, at this stage, be restored to its original configuration due to a lack of high quality information on thickness and facies variations of the formations, and on the early history of faults which may have influenced deposition. In contrast, the Cretaceous is characterised by well documented thickness and facies variations, which permit the reconstruction of basin development during this period (Puigdefábregas and Souquet, 1986).

During Aptian - early Albian, transtension formed a series of NW-SE trending lozenge-shaped extensional basins which formed a connection between the Tethys and the Atlantic. In the middle Albian, these basins were re-set by activity along the North Pyrenean Fault Zone, which gave rise to a series of E-W trending transtensional, 'flysch noire' basins on the French side. These basins widened during the Cenomanian eustatic sea level rise, resulting in widespread carbonate deposition. A renewal of extensional faulting in the late Santonian resulted in a widespread unconformity, basin development and carbonate platform collapse into the evolving basin (e.g. the Vallcarga Basin, see Section 2.5). Compressional tectonics commenced in the Maastrichtian in the eastern Pyrenees, causing inversion of former extensional faults in, for example, the San Corneli anticline.

2.4.2 Syn- and Post-Compression Stratigraphy

The Tertiary fill of basins associated with compressional deformation comprises a wide range of predominantly clastic rocks. These vary in age, thickness and facies in concert with the structural development of the foreland. Three key basins are involved in the Tertiary foreland basin-fill; the South Pyrenean basin, the Jaca Basin and the Ebro Basin (Figure 2.6). The South Pyrenean basin has a predominantly Eocene fill, which accumulated in a series of structurally defined sub-basins - the Ager, Tremp-Graus and Ainsa Basins and an early phase of the Jaca Basin; the later phase of the Jaca Basin is Upper Eocene/Oligocene in age and resulted from a displacement of thrust belt activity to the south. As younger basins were initiated, older basins were terminated, uplifted and began to provide sediments to the active basin. The stratigraphy of the South Pyrenean Basin is complex, but a seismic sequence/systems tract view of the stratigraphy was been proposed in the 1980s by Mutti *et al.* (1985a). The succession is bounded by the Paleocene Alveolina Limestone, which marks transgression over the underlying continental Tremp Formation (and represents the initiation of the south Pyrenean Basin), and the Bartonian - Priabonian shallow marine facies (related to the Biarritzian transgression), which separates the Eocene and Upper Eocene - Oligocene clastic wedges filling the basins. The Eocene clastic wedge fill of the Temp-Graus, Ainsa and Jaca Sub-basins is divided into seven depositional sequences, which are considered to be bounded by surfaces which are either angular unconformities, major erosional contacts (subaerial and submarine) or abrupt facies contacts.

The sequences are named i) Figols; ii) Montañana; iii) Castisent; iv) Charo; v) Santa Liestra; vi) Banaston; vii) Ainsa. In general, the lower sequences are exposed in the eastern part of the area and the higher sequences in the western part (Figure 2.6). This scheme has been constructed by the use of aerial photographs and fieldwork aimed at tracing critical sequence boundaries.

The basin fill is dominated by an axially-directed suite of depositional systems comprising fluvial systems in the east, shoreline and shelf systems in the central area, a basin slope and an extensive turbidite basin in the west. Sandstone-rich turbidite intervals are considered to correlate with erosional sequence boundaries in the fluvial and shoreline-shelf systems tracts to the east and the entire basin-fill is therefore interpreted to have accumulated in a similar

manner to passive margin sequences. Sandstone-rich turbidite deposition is considered to be related to lowstand periods, when the shallower-water parts of the basin were being eroded, whereas more fine-sediment-dominated turbidite intervals correspond to highstand periods, when the fluvial and shoreline-shelf systems were prograding and aggrading. Lowstand canyons are regarded as by-pass zones when the sandstone-rich lobe facies were being deposited in the deeper part of the basin; the canyons are considered to have acquired their fill later, presumably during the early stages of the subsequent onlap.

Major fanglomerate bodies are locally directed southwards from the axial zone and thrust belt into the westerly directed systems (the San Esteban and Campanue fanglomerates). Syn-tectonic structures such as the Boltaña anticline, which developed during basin deposition and separated the Ainsa and Jaca I sub-basins, are an essential feature of the stratigraphical evolution of the basin (see Section 2.6.4).

The Upper Eocene to Oligocene Jaca Basin formed in response to the onset of thrust-related deformation, which culminated in the 'Gavarnie' phase of thrusting. The effect of the early thrusting was to terminate the earlier system of basins and shift the active depocentre to the south and west. The basin succession commences with a distinctive glauconitic sandstone (the Sabiñánigo Sandstone), which is felt to record the Biarritzian transgression (Upper Eocene). This unit is overlain by a westerly-prograding clastic wedge which records filling of the basin. The wedge comprises the marine Pamplona Marls, deltaic shorelines of the Belsue-Atares Formations and a thick alluvial succession termed the Campodarbe Group (Figure 2.8). Deposition of the Campodarbe Group was influenced by a southerly-migrating thrust front which was responsible for deforming the Eocene fill of the Jaca Sub-basin.

Development of the External Sierras in the Oligo - Miocene terminated the Jaca Basin and displaced the basin depocentre southwards to the Ebro Basin. At this time, the Ebro Basin was an entirely continental, terminal basin with no outlet. Small thrust-front alluvial fans accumulated during thrust belt activity on the south side of the External Sierras and larger alluvial fans were located where lateral ramps intersected the margin of the Ebro Basin (see Section 2.9). In the central part of the basin, fine-grained, lacustrine sedimentation prevailed, with occasional discrete fluvial channel sandstone bodies.

2.4.3 Key Structures of the Spanish Pyrenees

Tertiary basins in the Spanish Pyrenees are controlled by the geometry and evolution of thrusts and thrust-related structures. In keeping with other mountain belts with long and varied research histories, the terminology of structures is complex. The following is a brief guide to the key structures relevant to this excursion (Figures 2.6 and 2.9):

i) The Cotiella-Monsech thrust sheet - this thrust sheet is limited to the eastern end of the Central Pyrenees; the frontal structure of the sheet is generally taken as the line of the Monsech thrust, but it seems more likely that this was a splay of the thrust and the actual thrust front was located farther south in what is now the External Sierras; the easterly limit of the structure is the oblique-slip Segre Fault; the western limit can be seen near Peña Montañesa but is then buried by Tertiary sediments. This thrust sheet was emplaced during the early Eocene and was a major influence on the Tremp-Graus and Ainsa Sub-basins.

ii) The Mediano diapir is a salt diapir which formed beyond the limit of the Cotiella-Monsech thrust sheet, in response to loading by the thrust sheet. The structure has a two-fold history: a positive ballooning phase in the Upper Eocene and a dissolution collapse phase during the uppermost Eocene and Oligo - Miocene (Reynolds, 1987).

iii) The Boltaña anticline is a major north-south trending structure which formed as a growth structure during deposition in the Ainsa and Jaca Sub-basins in the Upper Eocene. It is interpreted as a fold to a lateral ramp and is considered to be part of a westerly propagating system of lateral ramp folds which developed at this time (see Section 2.8).

iv) The Gavarnie thrust sheet - this term is often applied to thrust sheets responsible for producing the External Sierras, which represent the southerly limit of Pyrenean thrusting. This phase occurring during the Oligo - Miocene and is considered to have affected the entire central part of the Pyrenees, transporting the Cotiella-Monsech thrust sheet in its hangingwall and also influencing the area further westwards. There are, however, problems in linking these thrusts throughout the area, particularly to the Gavarnie thrust of the axial zone and between the western and eastern sectors of the External Sierras. Throughout this guide, the term Gavarnie thrust sheet is placed in parentheses and is used to refer collectively to a group of thrusts which were active during the Oligo - Miocene, but were not necessarily a single, linked system. Other workers sub-divide the 'Gavarnie' unit into a Gavarnie-Boltaña unit and a Guarga unit which contains the Jaca Basin.

2.5 THE UPPER CRETACEOUS VALLCARGA BASIN - EXTENSION AND INVERSION

The Vallcarga Basin is an Upper Cretaceous basin located on the hangingwall side of northward-dipping extensional faults which were later inverted in the early phases of alpine compression. The footwall side of these faults was characterised by shallow carbonate platforms and frequent disconformities, but the hangingwall side was the site of a deep, rapidly subsiding clastic basin for much of the Upper Cretaceous. The fill of the Vallcarga Basin is dominated by marls, turbidites, slumps and large-scale olisthostrome complexes. As differential subsidence decreased and inversion commenced, the basin was filled by a westerly prograding sand-dominated coastal system (the Aren Sandstone). The initial deep-water, turbidite, phase of the basin-fill has not been investigated in detail. The turbidites are thinly bedded, siliciclastic beds with westerly-directed palaeocurrents, which are axial to the half-graben basin. Folded slump intervals of carbonates derived from the footwalls of the faults are commonly interbedded with the turbidites. In the Esera section, the basin-fill includes the Campo Breccia, which comprises up to 385m of breccia composed largely of Upper Cretaceous limestone clasts, with subordinate Triassic clasts. The largest clast sizes occur at the base of the unit, with sizes of 15m being common and a maximum size of 1km being recorded (van Hoorn, 1970). The Campo Breccia is interpreted as the product of fault-induced collapse of a footwall carbonate platform. Periods of fault activity resulted in olisthostrome complexes being shed into the hangingwall. The exposure of older formations in the footwall could account for the local presence of 'exotic' Triassic clasts in the breccia.

The upper part of the basin-fill succession is dominated by the Aren Sandstone which, in turn, is overlain by the continental, red-bed Tremp Formation. The Aren Sandstone comprises two large-scale, wave-dominated upward-coarsening sequences, each of which represents a prograding coastal system (Ghibaudo et al., 1974). Both sequences indicate westerly progradation along the axis of the half-graben; the lower sequence pinches out just west of Aren, but the upper sequence extends to the Esera Valley and, therefore, prograded more than 95km.

Complex facies relationships in the east of the area, around Orcau, indicate a range of tidal inlet, lagoonal and fluvial settings associated with the coastal barrier (Nagtegaal, 1972; Nagtegaal et al., 1983). The range of environments in the Aren Sandstone, coupled with the large progradation distance of the upper sequence, suggests that it is best considered as a wave-dominated delta system. A distinctive feature of the Aren Sandstone coastal progradation system is the occurrence of turbidite sandbodies. The turbidites occur as discrete, localised and often channelised bodies. Ghibaudo et al. (1974) attributed these turbidites to tectonic instability of the coastal system, whereas Nagtegaal et al. (1983) attributed them to abrupt deepening of the basin as the coastal system prograded away from growth anticlines (see below).

The Arén Sandstone displays clear evidence that it was deposited during a period of active deformation (Ghibaudo et al., 1974; Nagtegaal et al., 1983; Simo and Puigdefábregas, 1985). Structures such as the San Corneli, Boixols and Isona anticlines display numerous features which suggest that they were growth anticlines during Upper Cretaceous deposition. Campanian and Maastrichtian intervals thin and onlap the San Corneli anticline and localised syn-tectonic unconformities occur in the vicinity of the structure. Facies variations in the Aren Sandstone occur near the anticlines and it is also possible that the complex configuration of the basin margin produced by the structures may have influenced the physical processes of sedimentation (e.g. amplification of tidal currents in narrow gulfs between anticlines). These anticlines are interpreted as inversion structures formed by compression of the earlier half-graben basins (Simo and Puigdefábregas, 1985; Reynolds, 1987). Mutti and Sgavetti (1987) have recently re-interpreted the stratigraphy of the Aren Sandstone interval in terms of seismic stratigraphic sequences. They identify two unconformity-bounded, first-order sequences termed the Orcau and Aren Sequences which they attribute to third-order cycles of global sea-level fluctuation. Deposition within the Aren sequence is sub-divided into a series of second-order sequences which are considered to relate to tectonic events in the depositional area.

2.6 THE EOCENE SOUTH PYRENEAN FORELAND BASINS

2.6.1 Introduction

The South Pyrenean Basin is a narrow, elongate basin developed on the southern, Spanish, side of the Pyrenees. The elongation of the basin is parallel to the strike of the mountain belt and the fill of the basin is predominantly axial, directed westwards along the length of the basin. Deposition in the basin was intimately associated with thrust-belt deformation at a variety of scales. At the largest scale, the South Pyrenean Basin can be divided into a series of structurally defined sub-basins. These will form the basis of the field excursion and are introduced below (Figures 2.6 and 2.9):

1. The Ager Sub-basin is a localised basin developed in the footwall of the Cotiella-Monsech thrust sheet south of the Tremp-Graus Sub-basin.

2. The Tremp-Graus Sub-basin is situated in the east of the area and is a thrust-sheet-top basin developed on the Cotiella-Monsech thrust sheet.

3. The Ainsa Sub-basin is situated west of the Tremp-Graus Sub-basin beyond the lateral margin of the Cotiella-Monsech thrust sheet and is further defined by growth structures which were active during deposition (the Boltaña anticline and Mediano diapir).

4. The Jaca Sub-basin extends west of the Boltaña anticline and is associated with the Gavarnie thrust sheet; this basin has a two-phase sedimentation history involving an Eocene phase which is linked to deposition in the Tremp-Graus and Ainsa Sub-basins, and a later Upper Eocene to Oligocene phase which is largely restricted to the Jaca Basin area. The Ebro Basin is a younger, Oligo-Miocene Basin which is developed south of the External Sierras (see Section 2.9).

2.6.2 The Ager Sub-basin

The Tertiary fill of the Ager Basin ranges from the Upper Paleocene to Lower Eocene. The present configuration of the basin is an asymmetrical syncline which is a footwall structure to the Monsech Thrust (Figure 5.1). Several features of the basin-fill succession highlighted by Mutti et al. (1985b) suggest that the northern margin of the basin was active during Tertiary deposition. The succession commences with the transgressive Alveolina Limestone, which disconformably overlies the Tremp Formation. The limestone contains clasts of Cretaceous limestone, thought to be derived from the Monsech and both the Alveolina Limestone and overlying Figols sequence thin and onlap towards the Monsech structure to the north. The thinning and onlap of the Figols sequence is due to a syn-tectonic unconformity at the base of the sequence on the northern side of the syncline. Mutti et al. (1985b) consider that the Monsech Thrust was active at this time but Reynolds (1987) considers that contemporaneous thrusting was minimal and that instead a northward-dipping extensional fault was being inverted (see Ribagorzana cross-section). This deformation was associated with initiation of the basin and the basin was terminated by the later deformation phase which produced the Cotiella-Monsech thrust and footwall syncline (see below). This latter phase began during deposition of the Figols and Montañana sequences and produced an emergent thrust tip to the south, which confined the Ager Basin. Upper Eocene/Oligocene conglomerates unconformably overlie the basin-fill succession and the Monsech Thrust.

The most thoroughly investigated unit of the Ager basin-fill is the Baronia Formation, which comprises bioclastic and siliciclastic facies deposited by tidal currents in a restricted, gulf-like basin (Mutti et al., 1985b). Tidal flats, estuarine channels and shoals have been recognised, but the most important elements are upwards-coarsening sequences which are interpreted as elongate, flow parallel 'tidal bars'. Sandbodies associated with the bars are up to 10m thick, 2-3km long, at least 0.5km wide. They have lenticular cross sections with flat bases and convex-up top surfaces and are considered to have frontal offlapping dip surfaces. Internally, they are dominated by sets of cross bedding, many of which have a distinctive sigmoidal shape. Facies organisation is complex and includes opposed cross bed cosets in a single bar. In part, these tidal bars resemble tidal sand ridges, but their development in a very narrow confined basin means that they are not identical. The composite thickness of these sandbodies is up to 200m and they extend along the length of the basin for at least 10km. The sediment was derived from the south rather than from the Monsech Thrust to the north. This may suggest that the thrust front at this time was located beyond the Monsech structure and that the Ager Sub-basin was a thrust-sheet-top basin to the southerly thrust.

2.6.3 The Tremp-Graus Sub-basin

The Tremp-Graus Sub-basin is a thrust-sheet-top basin developed on the Cotiella-Monsech thrust sheet. The thrust movements which terminated the Ager Sub-basin during the Figols-Montañana sequences were responsible for establishing the Tremp-Graus Sub-basin. The early history of the two basins is, therefore, similar. The Tremp-Graus Sub-basin commences with the Alveolina Limestone, which disconformably overlies the continental Tremp Formation and passes gradationally upwards into marine marls of the Figols Sequence. The unconformity observed between the Alveolina Limestone and Figols Sequence in the Ager

Sub-basin is absent. In the eastern part of the basin (Ribagorzana Section) the passage from the Figols sequence into the Montañana sequence records a transition into continental, fluviatile facies. These facies dominate the basin-fill in this area, attaining a thickness of 1.5km. Variations in coarse member and palaeosol characteristics permit distinct formations to be recognised within this thickness (Nijman and Nio, 1975; Puigdefábregas and van Vliet, 1978; Atkinson, 1983; 1986). One particularly notable formation is the Castisent Sandstone, which is a major fluvial system which can be traced extensively across the basin. It is composite, multi-storey/multi-lateral sandstone body, 40m thick in the east of the basin where it has been interpreted as a coarse-grained meander-belt system (Nijman and Puigdefábregas, 1983). The system flowed towards the northwest, but has a clear axial zone provenance. It is therefore, considered to have been southward directed and then diverted to the northwest by a thrust-related intrabasinal high. In the systems tract scheme of Mutti et al. (1985a, Figure 2.7) the Castisent Sandstone constitutes a sequence.

Traced westwards along the axis of the basin, the fluvial facies pass gradationally into coastal plain and, eventually, shoreline and shelf facies (Figure 6.1). The coastal plain facies comprise fluvial and tidal channel sandstones set in brackish to marine grey marls (Nijman and Nio, 1975). Lateral accretion surfaces are common in the channel sandstones (?tidal limit meander belts), but the coastal plain facies have not been studied in detail. The shoreline sequences are extremely varied and include both tide and storm-dominated shorelines. At Perrarua in the Esera valley, vertically stacked upward-coarsening sequences reflect repeated shoreline progradation and transgression. The sequence are commonly storm-dominated (hummocky cross stratification and graded nummulite beds), but occasionally include erosive-based tidal sandstone units representing tidal inlets at the top of the sequence. There are three notable departures from the arrangement of depositional facies and systems outlined above:

i) The Roda Sandstone is a depositional system locally developed in the marine marls of the Figols Sequence (Nio, 1976; Nio and Siegenthaler, 1978). It is noteworthy for the development of large-scale sets of cross bedding up to 20m thick. Smaller scale sets of cross bedding intimately linked with the large scale sets display abundant evidence of tidal current processes and for this reason the sandstone bodies which constitute the Roda Sandstone were originally interpreted as the product of major flow transverse, tidal sandwave bedforms. More recently, the large scale sets have been interpreted as Gilbert-type foresets associated with a fan delta. The reason for locally developing a significant sand body within an otherwise marl-dominated setting is that a syncline at the basin margin acted as a preferred route of clastic supply into the basin.

ii) The San Esteban Conglomerate is an alluvial fan body directed south-south-westward into the westerly prograding Figols-Montañana Sequence. The provenance of the conglomerate is from the axial zone.

iii) The Campanue Conglomerate is a fan delta body which is also directed southwards into the basin, where it interfingers with shoreline sequences of the Santa Liestra Sequence (Nijman and Nio, 1975; Crumeyrolle, 1987). The conglomerate is 600m thick and is underlain by an unconformity which dies out into the basin. The fan delta is thought to record development of the triangle zone at the northern margin of the basin (see Esera section), with the predominantly Cretaceous and Paleocene limestone clast petrography being derived from the backthrusting cover to the triangle zone (Reynolds, 1987).

2.6.4 The Ainsa Sub-basin

The Ainsa Sub-basin is generally defined by the lateral ramp of the Cotiella-Monsech thrust sheet, the Boltaña anticline and the Mediano diapir (Nijman and Nio, 1975, Figure 2.6). For some time it was felt that the lateral ramp was a distinct feature which controlled the shelf-slope break of the South Pyrenean Basin, but recent work has cast doubt on the significance of this structure. Firstly, structural cross-section constraints argue that the thrust sheet was emplaced during the Figols/Montañana sequence, eroded back and subsequently buried (Reynolds, 1987). Key exposures at La Atiart show the upper surface of the thrust sheet being buried by early Eocene (Cuisian, pre-Castisent Sequence) marls. The exposed levels of the Ainsa Sub-basin (Charo-Ainsa Sequences) were therefore, deposited at a time when the structure had been largely buried. Secondly, the sequence stratigraphy of Mutti et al. (1985a) argues for greater environmental continuity across this area, albeit with many of the lowstand canyons occurring in this area. Originally, it was felt that the Boltaña anticline existed throughout the fill of the Ainsa Sub-basin (Nijman and Nio, 1975) but, more recently, Mutti et al. (1985) argued that it did not form until late in the basin-fill succession (Banaston Sequence), implying that, for much of the time, the Ainsa and Jaca Sub-basins were linked. The Mediano diapir was characterised by a positive, ballooning phase during the Eocene as evidenced by localised carbonate bodies, syn-tectonic unconformities and slumps directed away from the diapir.

The deep water fill of the Ainsa Sub-basin is 3km thick and is dominated by deep basin marls in which a range of turbidite sandstone bodies are interbedded. This formation is termed the Hecho Group and extends westwards into the Jaca Sub-basin. The turbidite bodies include lenticular, channelised units up to 50m thick and generally a few kms wide, thinly bedded channel margin facies and interchannel bundles of turbidites separated by mudstone intervals. Originally, these facies were interpreted in a submarine fan model (Mutti, 1977), but later work by Mutti et al. (1985a) argued that the turbidite succession comprises a series of facies units which result from sea-level fluctuations rather than fan progradation. More recently, Pickering and Corregidor (2002) place the Ainsa channel complexes in a toe of slope setting.

In this work (Mutti et al., 1985a) the Hecho Group is sub-divided into four main sandstone-dominated turbidite intervals separated vertically by thick wedges of finer-grained facies. In the Ainsa Sub-basin, the sandstone intervals are characterised by wide canyons or channels which occur at the base of each of the exposed sequences. The finer grained intervals are composed of mudstones with numerous slump scar disconformities, thin (cm-scale) turbidites and small-scale turbidite channels. These intervals are interpreted as channel-levee complexes deposited by small volume, mud-rich flows.

The sandstone-dominated intervals are interpreted as lowstand deposits formed by resedimentation of fluvio-deltaic sediments, whereas the fine-grained intervals were deposited during highstand conditions by resedimentation of the mud-rich distal parts of the delta-shelf system.

Downcurrent, the sandstone-dominated intervals are considered to correlate with a non-channelised, tabular turbidite lobe facies in the Jaca Sub-basin (see below). The inferred time relationships between the components of the turbidite system are complex. Commencing during a lowstand period, sand was initially deposited in the lobe systems; the channels and canyons acquired their fill later (?during the early stages of the highstand). The evidence for the regional correlations between the Ainsa and Jaca Sub-basins and the time relationships is not clear.

2.6.5 The Jaca Sub-basin

As noted earlier (Section 2.6.1), the Jaca Basin has a two phase history: an Eocene phase which is linked to the Tremp-Graus and Ainsa Sub-basins, and an Upper Eocene - Oligocene phase which is discussed in the following section (Section 2.8).

The Eocene phase involves a narrow, elongate turbidite basin which extends westwards from the Boltaña anticline (Figures 2.10 and 2.11). The present, shortened width of the basin is 20km and the turbidites which dominate the basin fill were directed westwards, axially down the basin. A shallow water carbonate platform existed on the southern side of the basin and projected northwards to connect with the Boltaña anticline. It is possible that there was also a carbonate platform on the northern side of the basin (see below).

The turbidite fill of the basin attains a maximum thickness of 3km and is dominated by distinctive, thin-bedded turbidites. Upward-thickening sequences are interpreted as lobe deposits and are considered to be common (Mutti, 1977; Mutti et al., 1985a). However, in many exposures no trends are discernible and the turbidites are perhaps best considered as basin plain deposits.

Set into these thin-bedded turbidites are occasional exceptionally thick turbidites referred to as mega-beds (Rupke 1976a, b; Johns et al., 1981; Labaume et al., 1983; Seguret et al., 1984). A complete mega-bed has three components: i) a basal olisthostrome or slump unit which can be up to 200m thick (sometimes absent), at least locally); ii) a sand-grade turbidite 5m-20m thick; and iii) a marl unit up to 5m-15m thick.

The mega-beds range in thickness from several metres to more than 200m. Large examples can be traced laterally and form useful marker horizons which appear to be basin-wide. Labaume et al. (1983) map nine examples and Johns et al. (1981) trace one example (the Roncal unit or 'Chinese Wall') 60km along the strike of the basin and 12km across the basin. A further distinctive feature of the mega-beds is that both the clasts of the olisthostrome/slump unit and the turbidite sediment are composed of platform carbonate material. The basal units result from large-scale mass gravity transport and the turbidites and marls represent re-sedimented platform sediments. The marls probably result from rapid deposition by high concentration, fine-grained turbidity currents. The mega-beds are thought to be derived either from the southern extant platform or from a northern platform which has subsequently been obliterated by thrusting. Initiation of the mega-beds is though to involve thrust-induced seismicity or oversteepening of the carbonate platform by the propagation of blind thrusts (Rupke, 1976a; Labaume et al., 1983). One mega-bed (MT3 of Labaume et al., 1983) includes km-scale clasts of Paleocene and early Eocene limestones. In this case the mega-bed might have resulted from a thrust sheet breaking the surface of the basin and evolving into a mass flow.

2.7 THE UPPER EOCENE - OLIGOCENE JACA BASIN-FILL

The stratigraphy of this phase of the Jaca Basin comprises a thick succession of deep basin and slope marls termed the Pamplona marls, prograding fluvio-deltaic sequences termed the Belsue and Atares Formations, and a thick alluvial succession termed the Campodarbe Formation (Figure 2.7). The succession is exposed in a major east-west trending syncline - the Guarga syncline.

Growth structures related to thrust propagation during the accumulation of this basin-fill succession are evident in the Pamplona and Belsue-Atares Formations as north-south

trending folds which are interpreted as tip folds to blind oblique ramps (Puigdefábregas, 1975; Puigdefábregas et al., 1975). An easterly progression of these structures can be demonstrated by the relationships to the basin fill. Delta progradation in the Belsue-Atares Formation was influenced by the growth synclines, with vertically stacked delta front sequences being concentrated in the synclines and thinner, inter-deltaic sequences over the anticlines. Dipping depositional surfaces which imitate delta foresets were produced locally by tilting of the surface during growth fold formation.

The Campodarbe Formation is composed of up to 3km of alluvial facies which include conglomeratic and sandstone-dominated fluvial channels, overbank intervals with well developed calcrete palaeosols, and large fanglomerate bodies (e.g. the Santa Orosia conglomerate; Figure 2.7). Sandstone-dominated fluvial channel conglomerates of the fanglomerate bodies were directed southwards (Puigdefábregas, 1975).

2.8 THE EBRO BASIN

The Ebro Basin was the main depocentre during the Oligo-Miocene. The basin was an internal basin which acquired its fill during and after the formation of the External Sierras. The basin lies beyond the southern limit of Pyrenean thrusting and is, therefore, the final foreland basin to the Pyrenees. In the east of the area, south of the Tremp-Graus Basin, the thrusts associated with the External Sierras involved both Triassic and Upper Eocene salt horizons, with the latter forming the main décollement horizon (see the Ribagorzana and Esera cross-sections). Structures in the External Sierras in this area include steep, tight folds which owe their form to salt mobility during thrusting.

In addition, immediately in front of the thrust front in this area is a major east-west trending fold known as the Barbastro anticline, which is a salt-cored fold formed by the migration of salt from beneath the advancing thrust sheet. In the west of the area, south of the Jaca Basin, the External Sierras formed on a Triassic salt décollement, but salt diapirism was limited. In both sectors of the External Sierras, northerly-directed backthrusting is identified. Further insights into the formation of the External Sierras can be gained from conglomerates deposited at the southern, thrust front margin with the Ebro Basin, which show clear evidence of having been deposited during thrust deformation (Nichols, 1987a). The conglomerates are thick, localised bodies which accumulated in alluvial fans at the thrust front. Evidence for deformation during deposition of these alluvial fans includes folding of early fanglomerate deposits and syn-tectonic unconformities truncating these folds, pronounced stratal wedging into the basin and growth folds (Nichols, 1987a). These fans are composed entirely of clasts derived from the External Sierras and they die out within a few kilometres of the basin margin. The dominant processes in these fans are sheet-floods; stream channels are subordinate and debris flows are rare to absent. Whilst the conglomerate fans are spectacular and informative, they are relatively minor contributors to the fill of the Ebro Basin. Two main fan systems have been identified at the margin of the Ebro Basin; the Huesca and Luna Fans (Hirst and Nicols, 1986; Nichols, 1987b). These are large, fluvial distributary fan systems which extends over 2000-3000 sq km across the basin and up to 70km into the basin. They are composed of material derived from the axial zone and the emergent Tremp-Graus and Jaca Basins. Conglomeratic facies are restricted to the apical regions of the fans, which in this case of the Huesca fan was largely located in the Tremp-Graus Basin (see 7.2.2).

The medial and distal parts of the fans comprise sandstone-dominated channels with a radial pattern. Sandstone body size and frequency decreases down-fan and there are also systematic changes in sandstone body geometry. Sheet and subordinate ribbon bodies occur in the medial region, but ribbon bodies (Huesca System) or weakly channelised sheets (Luna

System) predominate in the distal region. A critical point concerning the fans is that their location is controlled by the structural geometry of the thrust front. The Huesca fan emerges from the lateral ramp zone which separates the eastern and western sectors of the Sierras, whereas the apex of the Luna fan occurs at the westerly tip fold of the Sierras. In both cases, these areas are topographic lows along the thrust front.

Subsidence in the Ebro Basin was asymmetric, being greatest in the immediate vicinity of the thrust front and decreasing basinwards. Facies in the central part of the basin are dominated by lacustrine marls, limestones and gypsum. Fluvial channel sandstones in fine-sediment-dominated parts of the Ebro Basin are often spectacularly exposed as ribbon bodies, with either a straight or meandering pattern, which represent exhumed palaeochannels (Puigdefábregas, 1973; Friend et al., 1979; Friend et al., 1981; Friend et al., 1986).

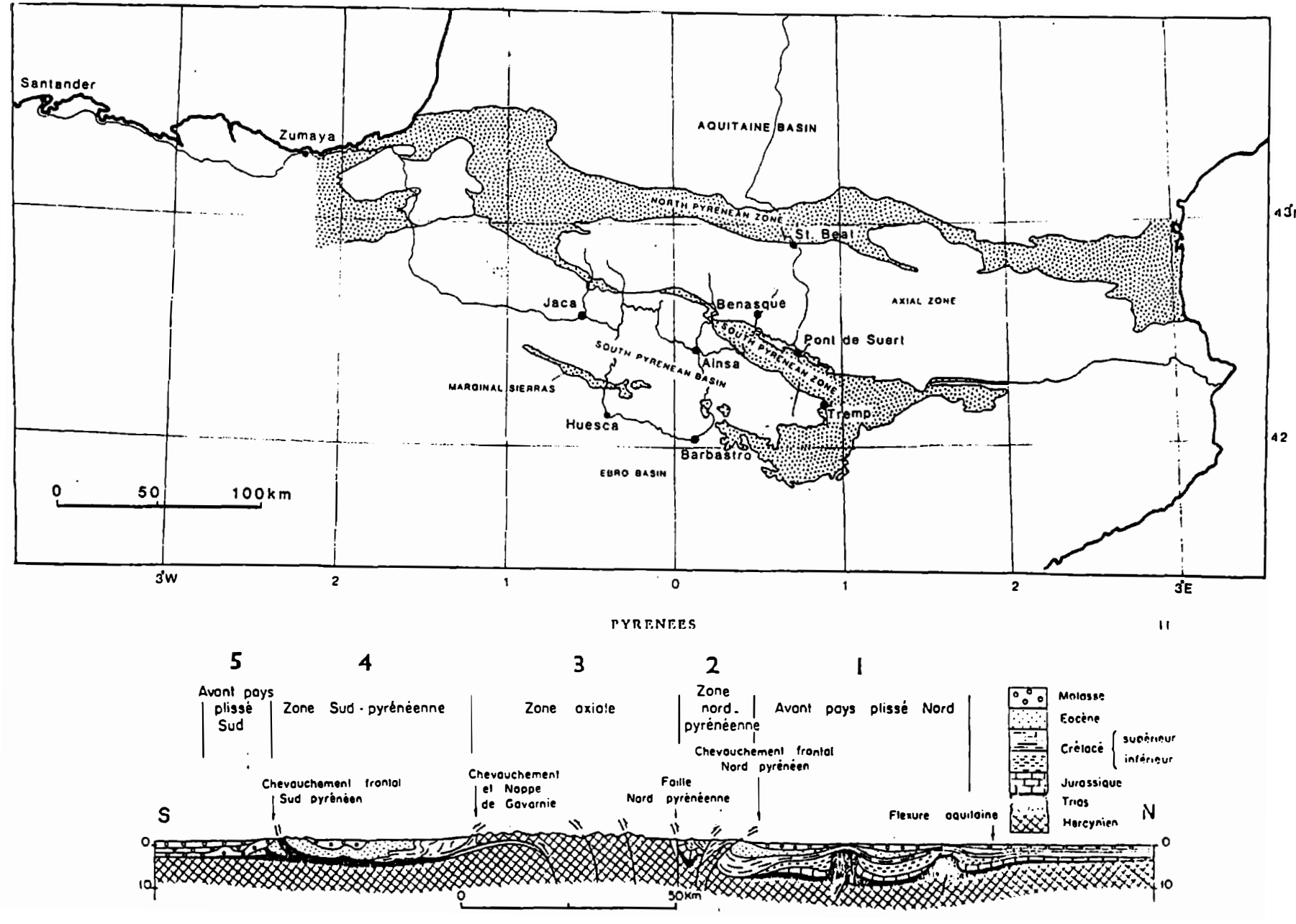

Figure 2.1 a. Main tectonic elements of the Pyrenees and the associated foreland basins
b. N-S cross-section through the Pyrenees

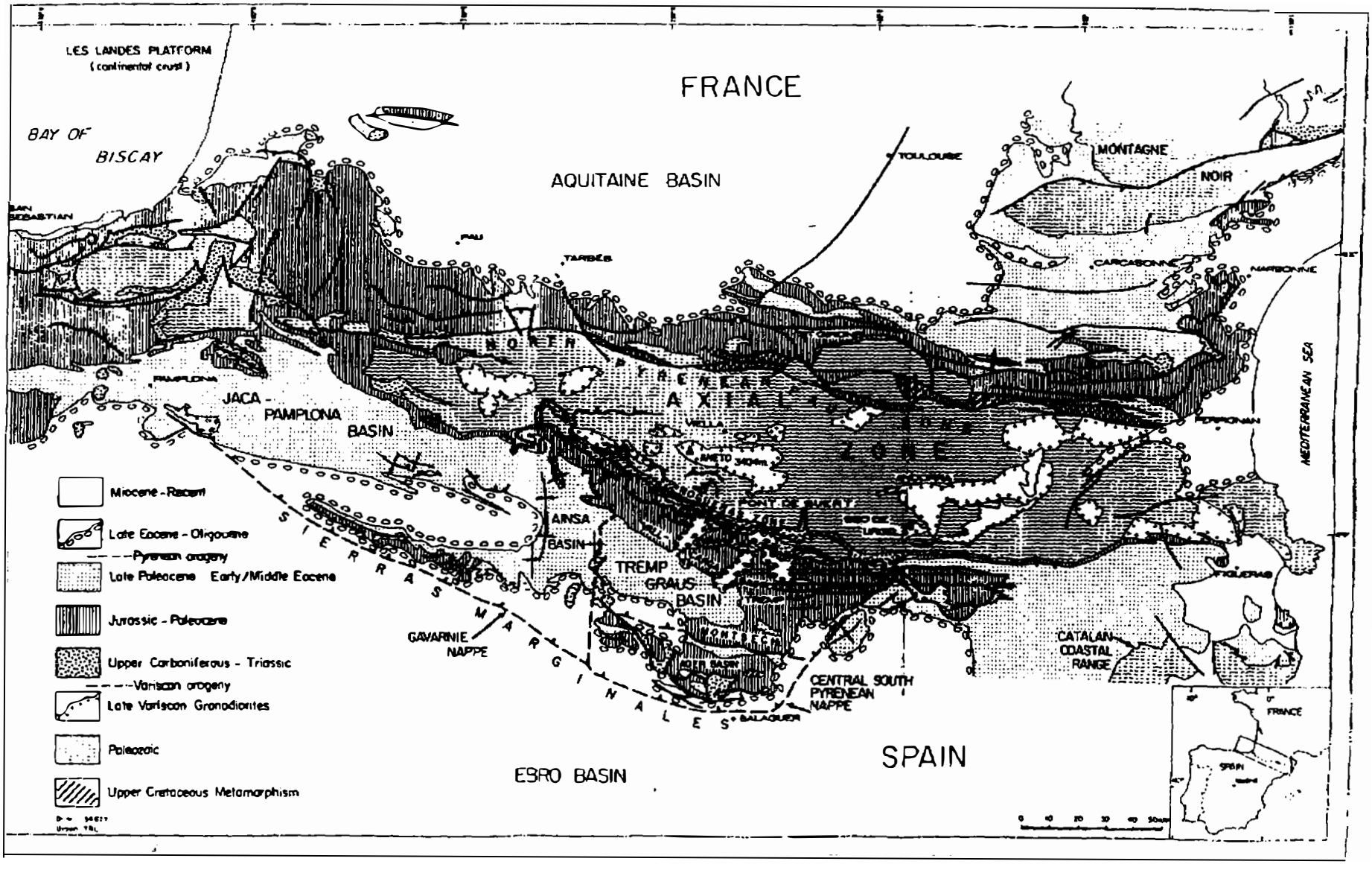

Figure 2.2 Structural sketch map of the Pyrenees (simplified after Choukroune and Seguret)

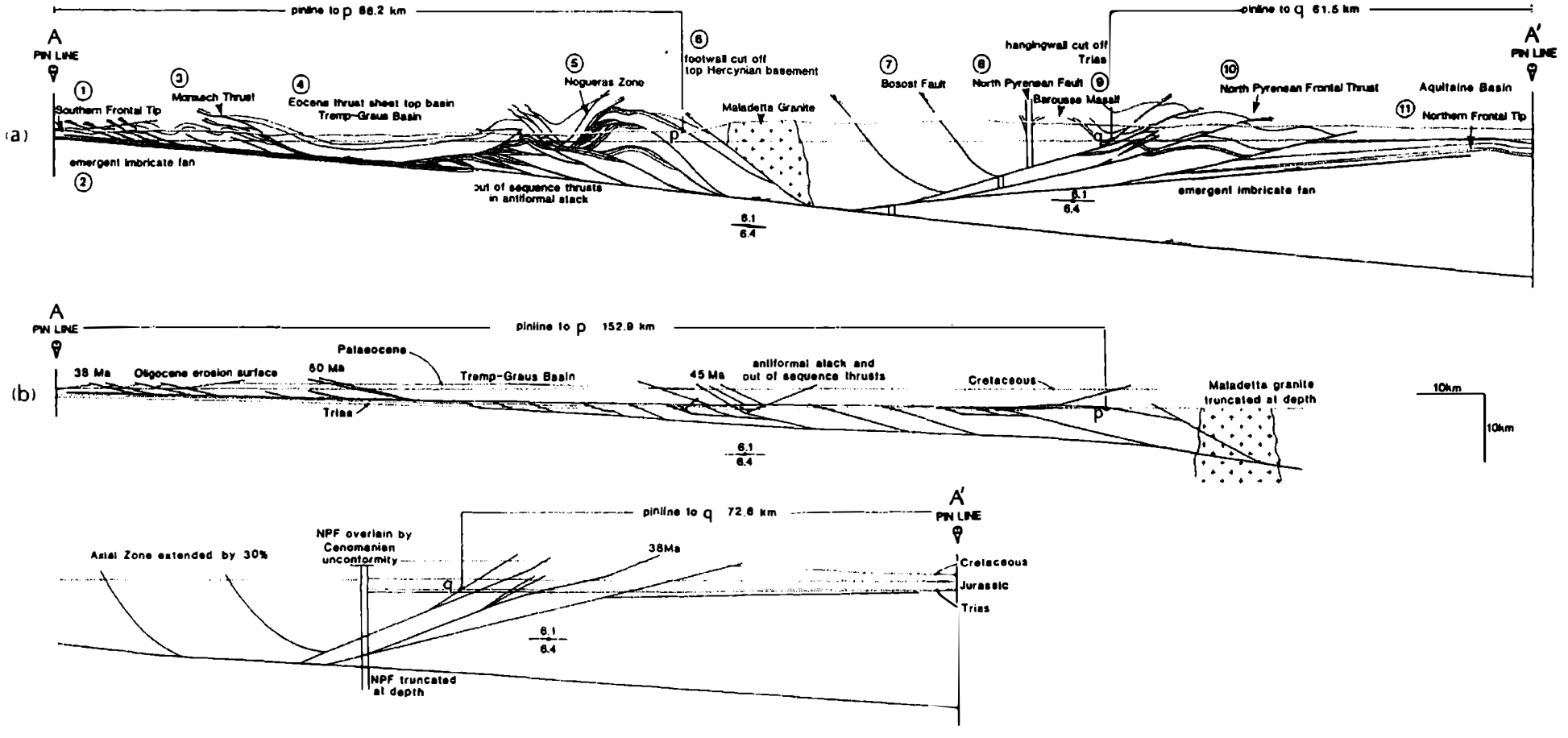

Figure 2.3 (a) Balanced and (b) restored cross section through the central Pyrenees. From Williams and Fischer, 1984.

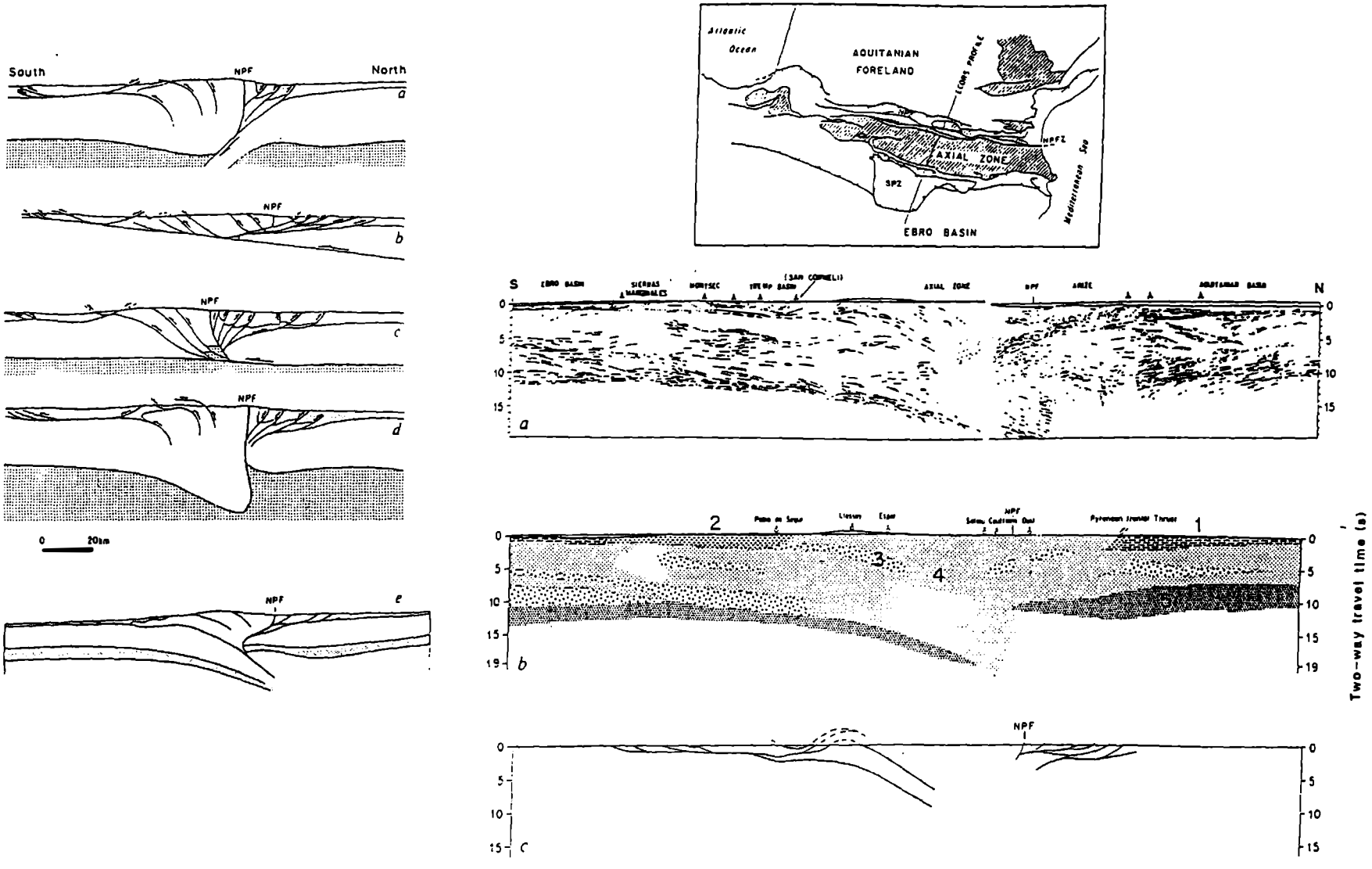

Figure 2.4 Seismic data and interpretations from the ECORS profile (see top right for line of section). At right, a. shows a line drawing of the profile, whilst b. shows the seismic facies, and c. shows the geometry of external thrusts identified from seismic and geological data. The profiles on the left show a range of interpretations of the structure of the Pyrenees (NPF = North Pyrenean Fault). Section e is consistent with the ECORS data. From ECORS Pyrenees Team, 1988.

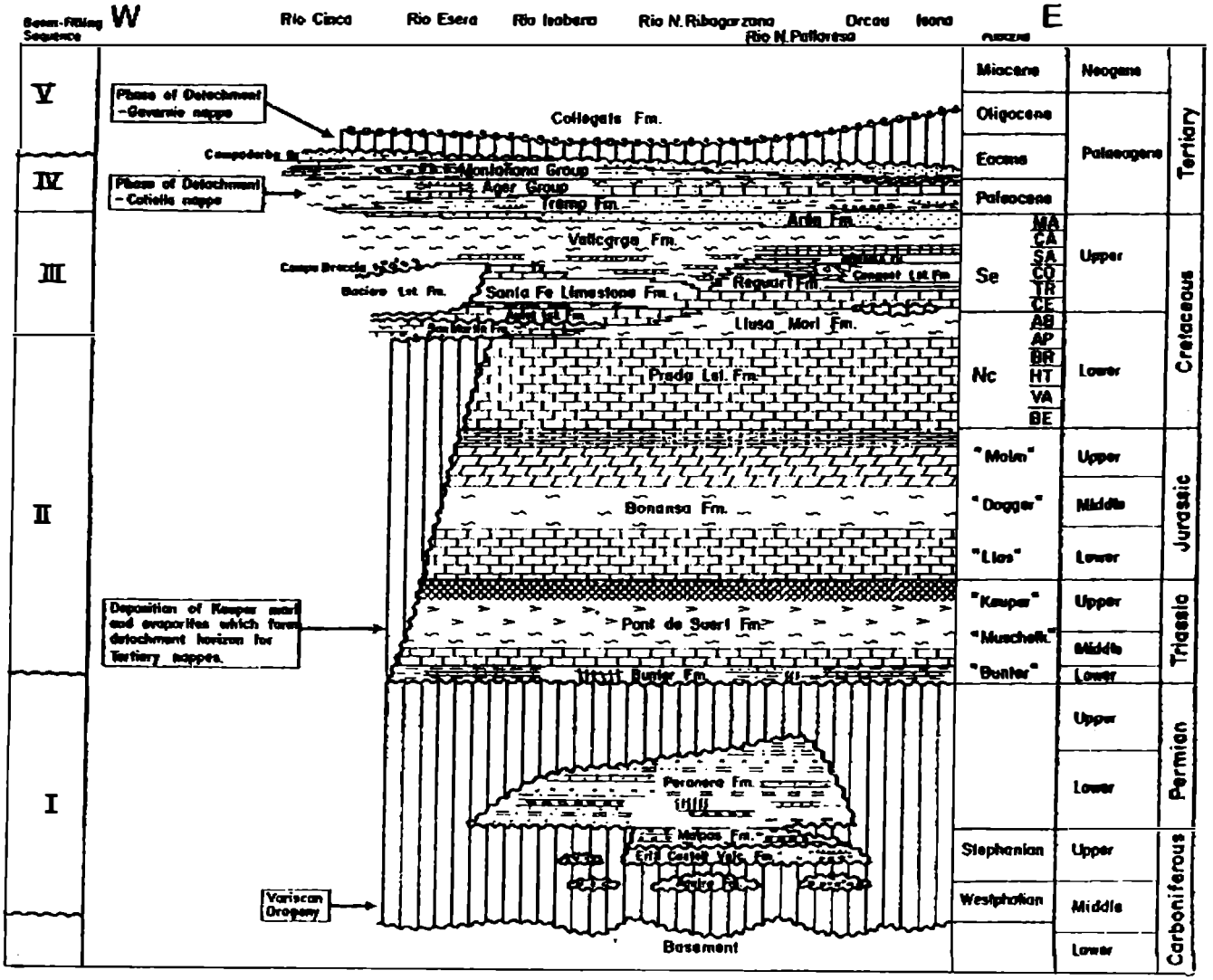

Figure 2.5 Stratigraphy, formations and facies for the post-Variscan of the south-central Pyrenees

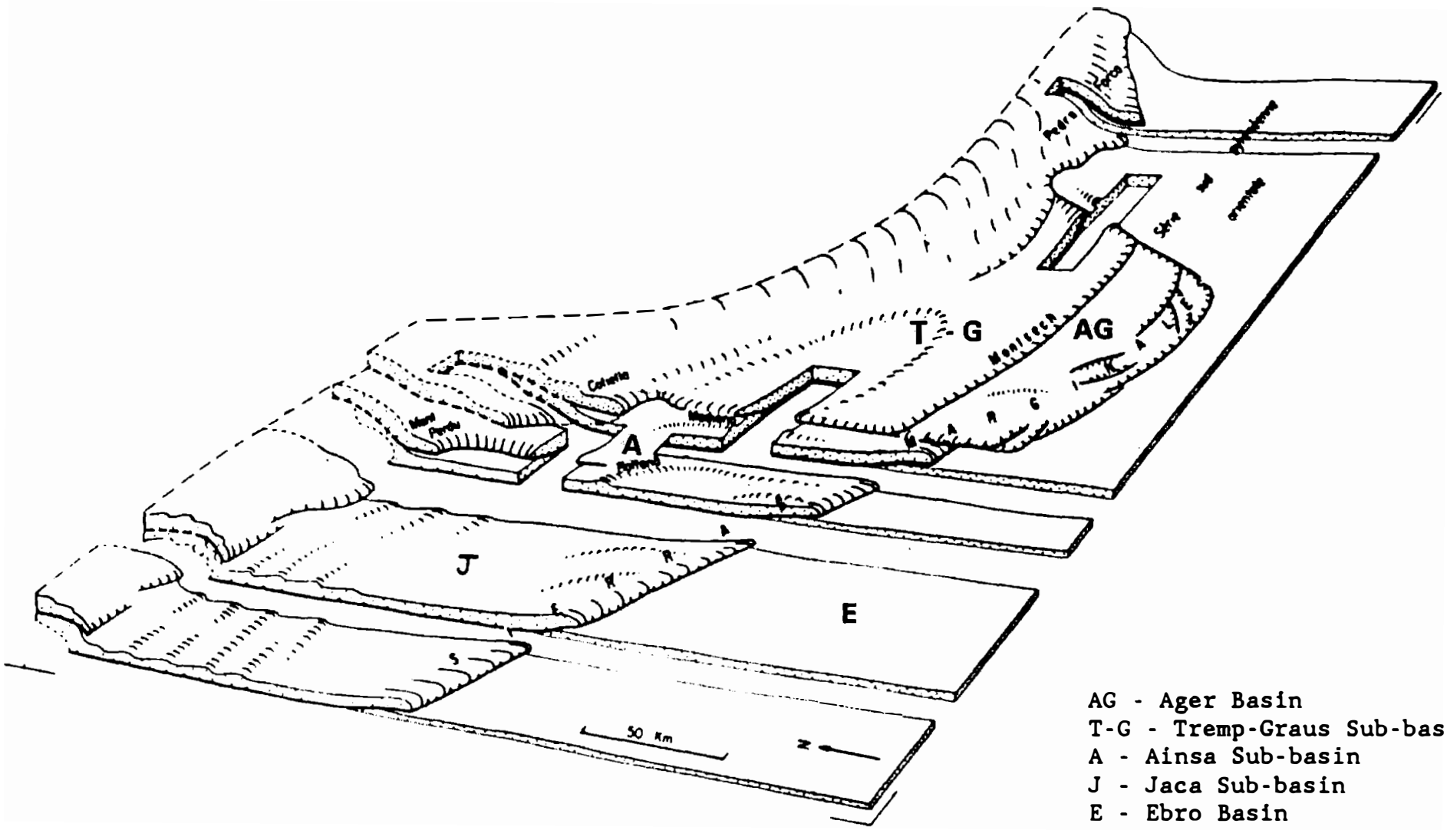

Figure 2.6 Block diagram of the south side of the Pyrenees at top Cretaceous, looking towards the NE. Note the 'piggy-back' nature of the Tremp-Graus Basin

LOWER AND MIDDLE EOCENE DEPOSITIONAL SEQUENCES AND SYSTEMS IN THE EASTERN AND CENTRAL SECTORS OF THE TREMP-PAMPLONA BASIN, SOUTH-CENTRAL PYRENEES

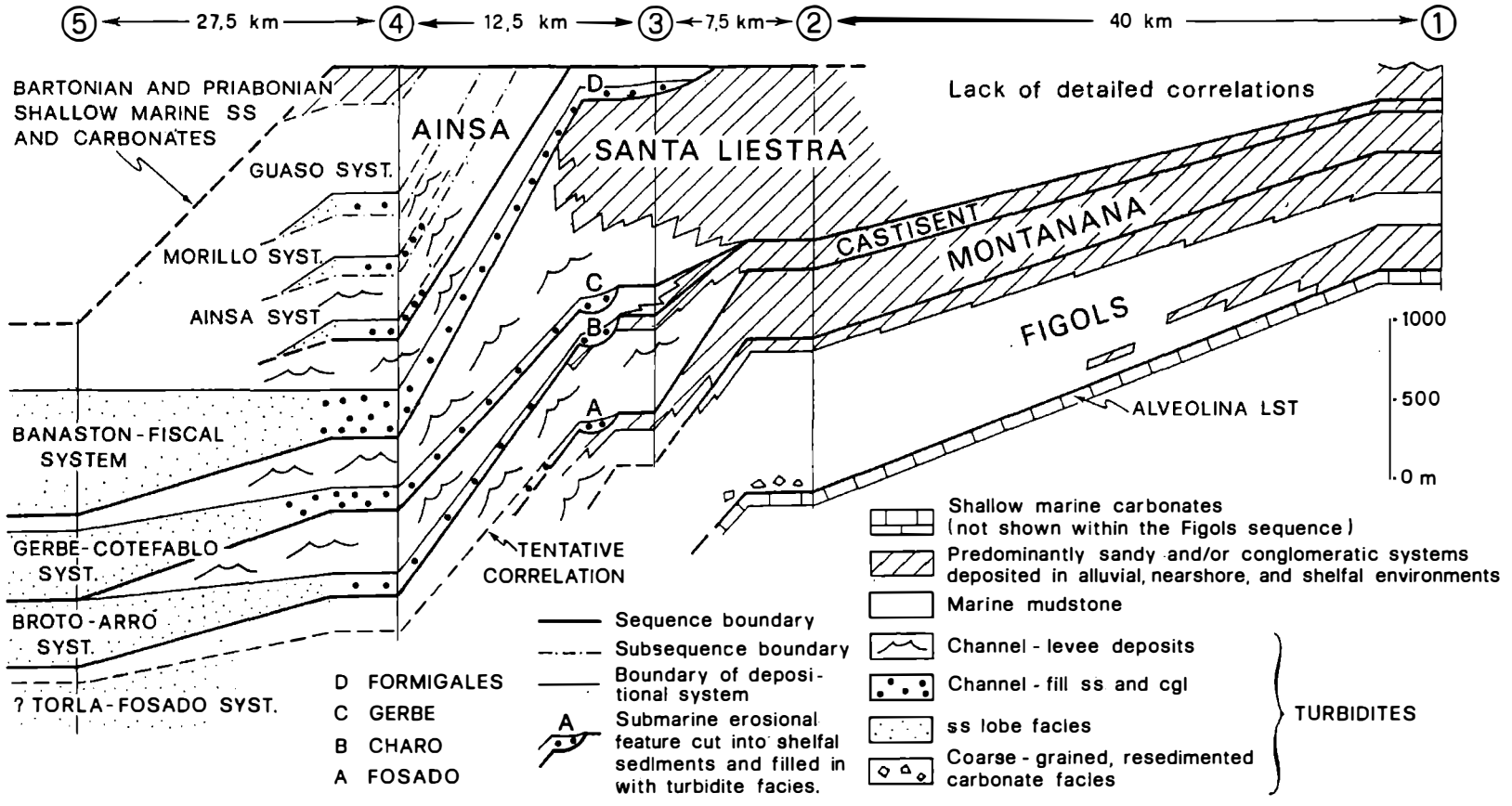

Figure 2.7 Stratigraphic cross-section between the eastern and western sectors of the Southern Pyrenean Basin, showing a proposed correlation between the fluvial and shallow marine sediments in the east and the deep water sediments in the west. After Mutti *et al.*, 1985

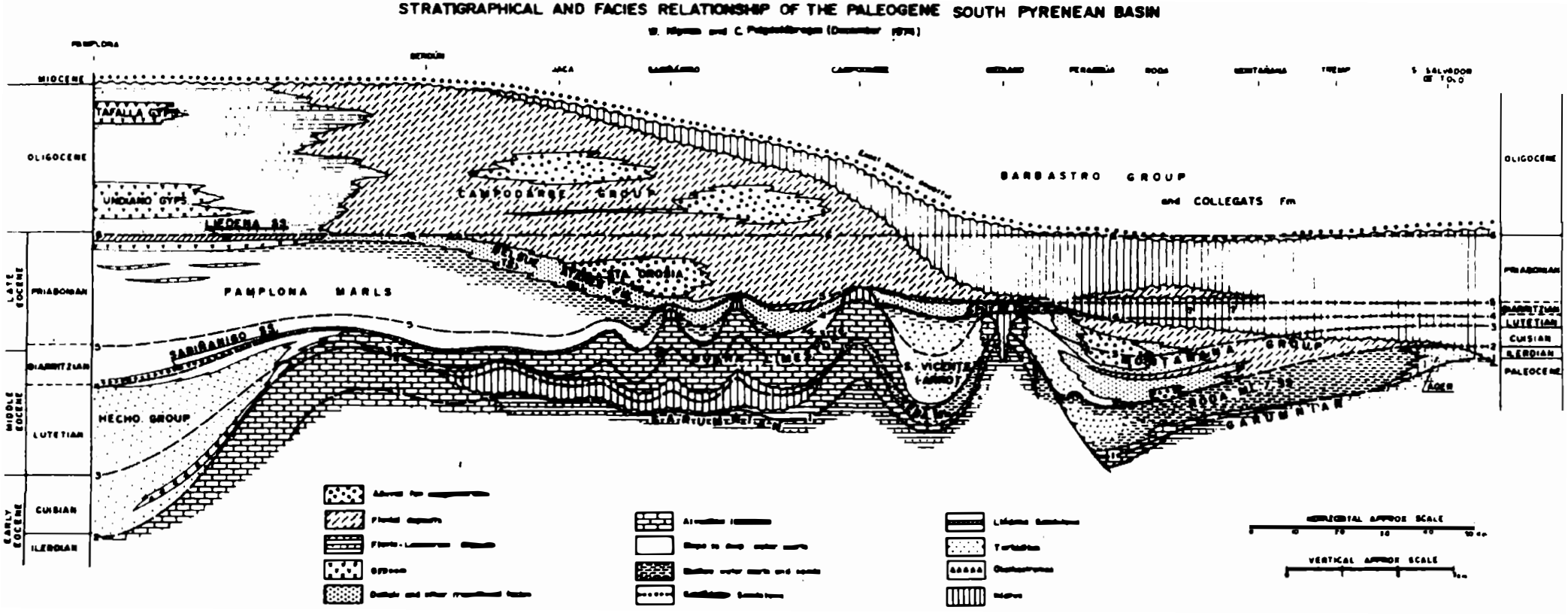

Figure 2.8 Stratigraphic and facies relationships in the Palaeogene of the South Pyrenean Basin (from Nijman and Puigdefabregas).

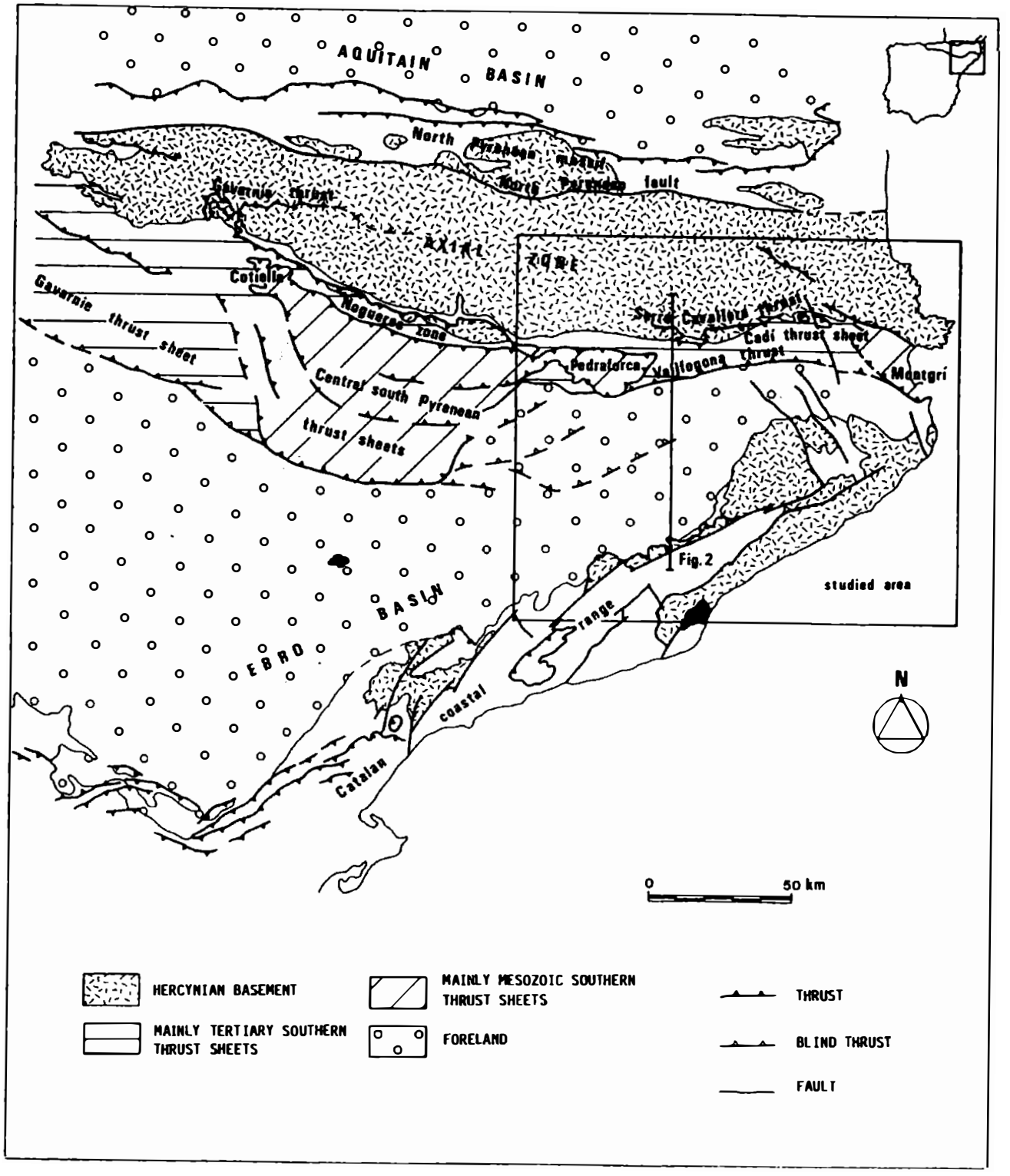

Figure 2.9 Simplified geological map showing the distribution of thrust sheets in the north and south Pyrenean thrust zones and in the Catalan Coastal Range. From Puigdefabregas *et al.*, 1986.

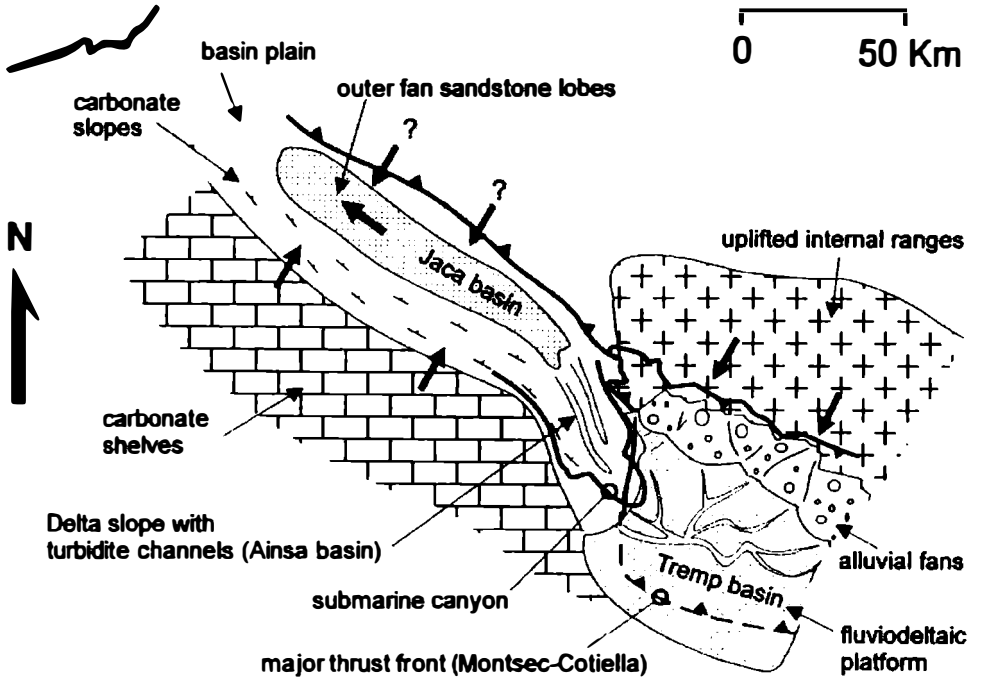

Figure 2.10 Palaeogeography of the south Pyrenean foreland basin during Early Lutetian. Turbiditic systems of the Ainsa basin had feeder fluvial systems in the Tremp Basin. Clast composition is dominated by limestone clasts derived from Palaeocene and Mesozoic rocks, but also includes granites, volcanic rocks and others, which correlate with the exposed rocks in the hinterland, as is also indicated by the composition of the alluvial-fan conglomerates fringing the northern Ebro basin. From Marzo *et al.*, 1998.

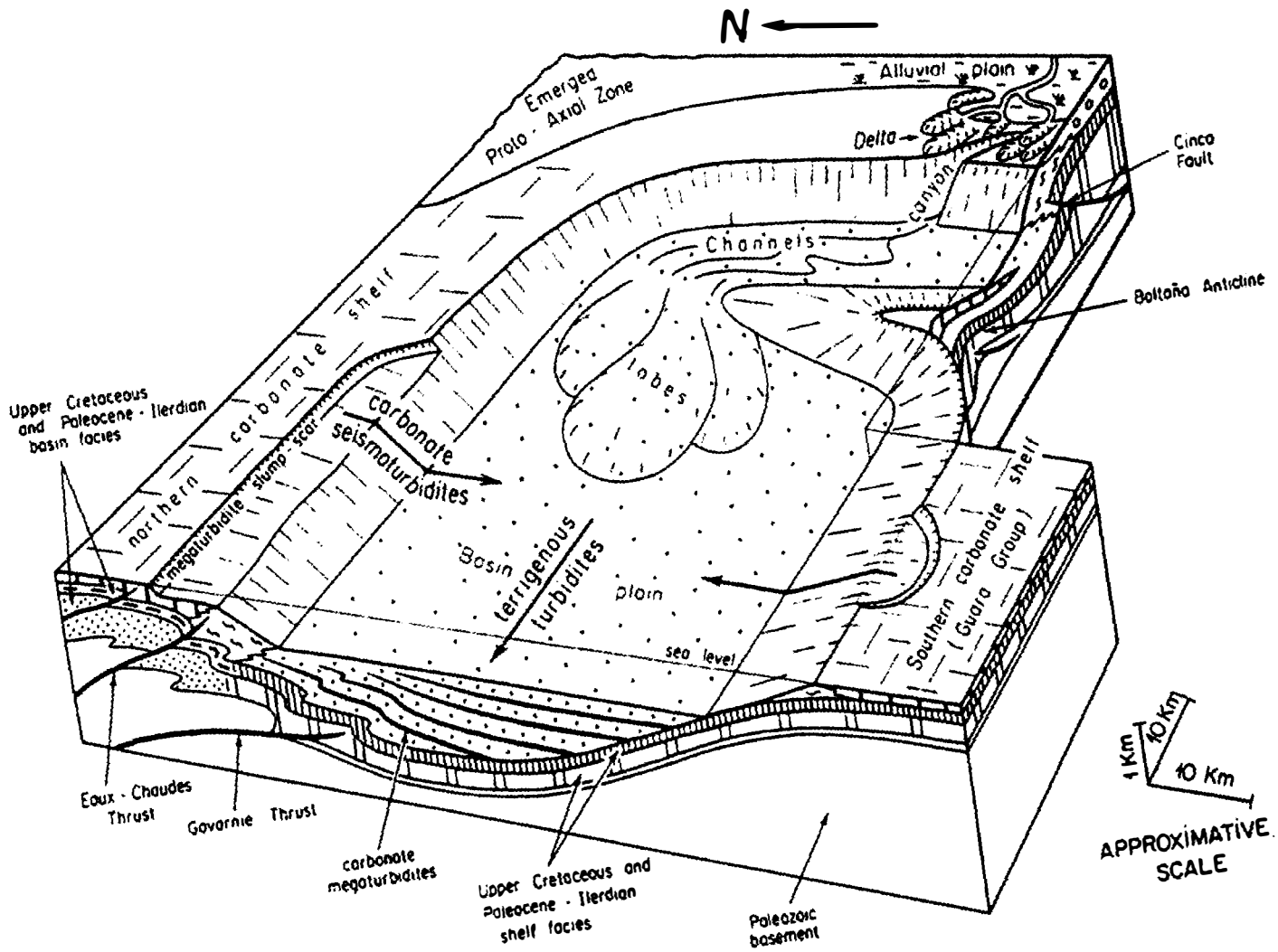

Figure 2.11 General geometry and sedimentary environments of the early and middle Eocene Southern Pyrenean Basin

2b References

PYRENEES REFERENCES

ALLEN, P.A., AND MANGE-RAJETZKY, M., 1982. Sediment dispersal and palaeohydraulics of Oligocene Rivers in the Eastern Ebro Basin. Sedimentology, v. 29, p. 705-716.

ALLEN, P.A., CABRERA, Ll., COLOMBO, F. AND MATTER, A., 1983. Variations in fluvial style on the Eocene - Oligocene alluvial fan of the Scala Dei Group, SE Ebro Basin, Spain. J. Geol. Soc. London, v. 140, p. 133-146.

ALLEN, P.A., HOMEWOOD, P., AND WILLIAMS, G.D., 1986. Foreland basins: an introduction. In: Allen, P.A. and Homewood, P. (eds.). Foreland Basins. Int. Assoc. Sedimentol. Spec. Publ. 8, p. 3-12.

ANADÓN, P, CABRERA, LL., COLLDEFORNS, B., COLOMBO, F., CUEVAS, J. L. AND MARZO, M., 1989. Alluvial fan evolution in the S.E. Ebro Basin: response to tectonics and lacustrine base level changes. Guidebook Series of the 4th International Conference on Fluvial Sedimentology. Publicacions del Servei Geològic de Catalunya. pp. 91.

ANADÓN, P., CABRERA, Ll., COLOMBO, F., MARZO, M. AND RIBA, O., 1986. Syntectonic intraformational unconformities in alluvial fan deposits, eastern Ebro Basin margins (NE Spain). In: Allen, P.A. and Homewood, P. (eds.), Foreland Basins. Int. Assoc. Sedimentol. Spec. Publ. 8, p. 259-272.

ANADÓN, P., CABRERA, Ll., GUIMERÀ, J. AND SANTANACH, P., 1985a. Paleogene strike-slip deformation, basin formation and sedimentation along the southeastern margin of the Ebro Basin. In: Biddle K.T. and Christie-Blick, N. (eds.). Strike-slip deformation, basin formation and sedimentation. Soc. Econ. Palaeontol. Mineral. Spec. Publ. 37, p. 303-318.

ANADÓN, P., MARZO, M., AND PUIGDEFÀBREGAS, C., 1985b. The Eocene fan-delta of Montserrat (Southeastern Ebro Basin, Spain). In: Milá, M.D. and Rosell, J. (eds.). Excursion Guidebook, Int. Assoc. Sedimentol. 6th Eur. Reg. Meeting, Lleida, Spain. Excursion No. 3, p109-146.

ATKINSON, C.D., 1983. Comparative sequences of ancient fluvial deposits in the Tertiary South Pyrenean basin, northern Spain. Unpubl. PhD thesis, Univ. Coll. Swansea.

ATKINSON, C.D., 1986. Tectonic control on alluvial sedimentation as revealed by an ancient catena in the Capella Formation (Eocene) of northern Spain. In: Wright, V.P., (ed.) Palaeosols: their recognition and interpretation, p. 139-179.

BANDA, E. AND WICKHAM, S.M., 1986. The geological evolution of the Pyrenees - an introduction. Tectonophysics, v. 129, p. 1-7.

BANKS, C.J. AND WARBURTON, J., 1986. Passive-roof duplex geometry in the frontal structures of the Kirthar and Sulaiman Mountain Belts, Pakistan. J. Struct. Geol., v. 8, p. 229-237.

BENTHAM, P. A., BURBANK, D. W. AND PUIGDEFABREGAS, C., 1992. Temporal and spatial controls on the alluvial architecture of an axial drainage system: late Eocene Escanilla Formation, south Pyrenean foreland basin, Spain. Basin Research, v. 4, p. 335-352.

BILOTTE, M., 1991. Depositional sequences and block limits in the late Cretaceous and early Paleocene of the sub-Pyrenean foreland basin (Petites Pyrénées – Dômes Annexes, France). Bull. Centres Rech. Explor.-Prod. Elf-Aquitaine, v. 15, p. 411-437.

BIRNBAUM, S.J. AND COLEMAN, M., 1979. Source of sulphur in the Ebro Basin (Northern Spain). Tertiary non-marine evaporite deposits as evidenced by sulphur isotopes. Chemical. Geology, v. 26, p. 163-168.

BOILLOT, G., 1984. Some remarks on the continental margins of in the Aquitaine Basin and the French Pyrenees. Geol. Mag., v. 121, p. 407-412.

BOYER, S.E. AND ELLIOT, D., 1982. Thrust systems. Am. Assoc. Pet. Geol. Bull., v. 66, p. 1196-1230.

BURNS, B. A., HELLER. P. L. MARZO, M. AND PAOLA, C., 1997. Fluvial response in a sequence stratigraphic framework: example from the Montserrat fan delta, Spain. J. Sediment. Res., v. 67, p. 311-321.

CABRERA, Ll., COLOMBO, F. AND ROBLES, S., 1985. Sedimentation and tectonics interrelationships in the Paleogene marginal alluvial systems of the S.E. Ebro Basin. Transition from alluvial to shallow lacustrine environments. In: M. Milá and J. Rosell (eds.). Excursion guide book of the 6th European Regional IAS Meeting, Lleida, Spain. Excursion No.. 10, p. 393-492.

CABRERA, Ll., AND SÁEZ, A., 1987. Coal deposition in carbonate-rich shallow lacustrine systems: the Calaf and Mequinenza sequences (Oligocene, eastern Ebro Basin, NE Spain). J. Geol. Soc. London, v. 144, p. 451-461.

CHOUKROUNE, P. AND SEGURET, M., 1973. Carte structurale des Pyrénées. Université des Sciences et Techniques du Languedoc, Montpellier.

CHOUKROUNE, P. AND ECORS TEAM, 1989. The ECORS Pyrenean deep seismic profile reflection data and the overall structure of an orogenic belt. Tectonics, v. 8, p. 23-29.

CLARK, J.D. 1995. Detailed section across the Ainsa II Channel complex, south central Pyrenees, Spain. In: PICKERING, K.T., HISCOTT, R.N., KENYON, N.H., RICCI LUCCHI, F. & SMITH, R.D.A. (eds), Atlas of Deep Water Environments: architectural style in turbidite systems, 139-144. London: Chapman & Hall.

CLARK, J.D., KENYON, N.H. & PICKERING, K.T. 1992. Quantitative analysis of the geometry of submarine channels: Implications for the classification of submarine fans. Geology, **20**, 633-636.

CLARK, J.D. & PICKERING, K.T. 1996. Architectural elements of submarine channels, growth patterns, and application to hydrocarbon exploration. American Association of Petroleum Geologists Bulletin, **80**, 194-221.

COOK, T.W., BOUMA, A.H., CHAPIN, M.A. & ZHU, H. 1994. Facies architecture and reservoir characterisation of a submarine channel complex, Jackfork Formation, Arkansas. In:

WEIMER, P., BOUMA, A.H. & PERKINS, B.F. (eds) Submarine Fans and Turbidite Systems. Gulf Coast Section Society of Economic Palaeontologists and Mineralogists 15th Annual Research Conference, p. 69-81.

COSSEY, S.P.J. 1994. Reservoir modelling of deepwater clastic sequences: mesoscale architectural elements, aspect ratio and producability. In: Weimer, P., Bouma, A.H. & Perkins, B.F. (eds) Submarine Fans and Turbidite Systems. Gulf Coast Section Society of Economic Palaeontologists and Mineralogists 15th Annual Research Conference, p. 69-81.

CRIMES, T. P., 1973. From limestones to distal turbidites: a facies and trace fossil analysis in the Zumaya flysch (Paleocene–Eocene), North Spain. Sedimentology, v. 20, p. 105-131.

CROOK, K.A.W., 1974. Lithogenesis and geotectonics: the significance of compositional variations in flysch arenites (greywackes). In: DOTT, R.H., AND SHAVER, R.H. (eds.). Modern and ancient geosynclinal sedimentation. Soc. Econ. Paleontol. Mineral. Spec. Publ. 19, p. 304-310.

CRUMEYROLLE, P., 1987a. Stratigraphie physoque et sedimentologie des systemes de depot de la sequence de Santa Liestra (Eocene and sud-Pyreneen), Pyrenees Aragonaises, Espagne. Thes. Univ. de Bordeaux, p. 111.

CRUMEYROLLE, P. 1987b. Stratigraphice physique et sedimentologie des systems de depot de plate-forme de la Sequence de Santa Liestra (Bassin Eocene Sud-Pyreneen, province se Huesca, Espagne): C.R. Acad. Sc., Paris, **303**, serie II, n.7, p. 581-584.

CRUMEYROLLE, P., SOUDET, M.J. LÓPEZ-BLANCO, M., AND RODA TEAM, 1990. Partitioning of a deltaic reservoir controlled by base level changes. A case study: the Roda complex (NE Spain). 13th Int. Sedimentol. Congress, Nottingham, England. Abs., p. 114-115.

CUEVAS, M., DONSELAAR, M.E. AND NIO, S.D., 1985. Eocene clastic tidal deposit in the Tremp-Graus Basin (provs. of Lerida and Huesca). In: Milá, M.D. and Rosell, J. (eds.). Excursion Guidebook. Int. Assoc. Sediment. 6th European Region Meeting, Lleida, Spain. Excursion No.6, p. 215-266.

DERAMOND, J., FISCHER, M., HOSSACK, J., LABAUME, P., SEGURET, M., SOULA, J.C., VIALLARD, P. AND WILLIAMS, G.D., 1984. Field Guide of Conference Trip to the Pyrenees. Chevauchement et deformation conference, Toulouse. p. 1-28.

DONSELAAR, M.E. AND NIO, S.D., 1982. An Eocene tidal inlet washover type barrier island complex in the south Pyrenean marginal basin, Spain. Geologie en Mijnbouw, v. 61, p. 343-353.

DREYER, T., FÄLT, L.-M., HOY, T. KNARUD, R., STEEL, R. AND CUEVAS, J.-L., 1993 Sedimentary architecture of field analogues for reservoir information (SAFARI): a case study of the fluvial Escanilla Formation, Spanish Pyrenees. In: Flint, S. S. and Bryant, I. D. (eds.) The geological modelling of hydrocarbon reservoirs and outcrop analogues. Spec. Publs int. Ass. Sediment. (1993) 15, p. 57-80

DREYER, T., CORREGIDOR, J., ARBUES, P. AND PUIGDEFABREGAS, C., 1999. Architecture of the tectonically influenced Sobrarbe deltaic complex in the Ainsa Basin, northern Spain. Sedimentary Geology v. 127, p. 127-169

ECORS PYRENEES TEAM, 1988. The ECORS deep reflection seismic survey across the Pyrenees. Nature, v. 331, p. 508-511.

VAN EDEN, J.G., 1970. A reconnaissance of deltaic environment in the Middle Eocene of the South-Central Pyrenees, Spain. Geologie en Mijnbouw, v. 49, p. 145-157.

ESTRADA ALIBERAS, M.R. 1982. Lobulos deposicionales de la parte superior del Grupo de Hecho entre el anticlinal de Boltaña y el Rio Aragon (Huesca): Ph.D. thesis, Universidad Autonoma de Barcelona.

FARRELL, S.G. & EATON, S. 1987. Slump strain in the Tertiary of Cyprus and the Spanish Pyrenees. Definition of palaeoslopes and models of soft-sediment deformation. In JONES, M.E. & PRESTON, R.M.F. (eds), Deformation of sediments and sedimentary rocks. Geological Society, London, Special Publication **29**, 181-196. Oxford: Blackwell Scientific Publications.

FARREL, S.G., WILLIAMS, G.D. AND ATKINSON, C.D., 1987. Constraints on the age of movement of the Montsech and Cotiella Thrusts. South-Central Pyrenees, Spain. J. Geol. Soc. London, v. 144, p. 907-914.

FONTANA, D., ZUFFA, G.G. & GARZANTI, E. 1989. The interaction of eustacy and tectonism from provenance studies of the Eocene Hecho Group Turbidite Complex (South-Central Pyrenees). Basin Research **2**, 223-237.

FRIEND, P.F., MARZO, M.M., NIJMAN, W. AND PUIGDEFABREGAS, C., 1981. Fluvial sedimentology in the Tertiary South Pyrenean and Ebro Basins, Spain. In: Elliott, T. (ed.), Field Guide to Modern and Ancient Fluvial Systems in Britain and Spain. Proc. Second Intern. Conference on Fluvial Sedimentology : Modern and Ancient Fluvial Systems: Sedimentology and Processes. Univ. of Keele. P4.1-4.50

FRIEND, P.F., HIRST, J.P.P. AND NICHOLS, G.J. (1986). Sandstone-body structure and river process in the Ebro Basin of Aragon, Spain. Cuadernos de Geologica Iberica, v. 10, p. 9-30.

FRIEND, P.F., HIRST, J.P.P., HOGAN, P.J., JOLLEY, E.J., MCELROY, R., NICHOLS, G.J. AND RODRÍGUES VIDAL, J. (1989). Pyrenean Tectonic Control of Oligo-Miocene River Systems, Huesca, Aragon, Spain. Guidebook Series of the 4th International Conference on Fluvial Sedimentology. Publicacions del Servei Geològic de Catalunya. pp142

FRIEND, P.F., SLATER, M., AND WILLIAMS, R.C., 1979. Vertical and lateral building of river sandstone bodies, Ebro Basin, Spain. J. Geol. Soc. London, v. 136, p. 39-46.

GARRIDO MEGIAS, A., 1973, Estudio geologico y relacion entre tectonica y sedimentacion del Secundario y Terciario de la vertiente meridional pirenaica en su zona central (provincias de Huesca y Lerida): Ph.D. Thesis, University of Granada.

GARRIDO, H. M., MORER, E. L. P., CARDONA, M. A., AGUADO, A. L., URCIA, B. O., PEÑA, M. B. B. AND JUAN, A. P., 2000. Actividad tectónica registrada en los depósitos terciarios del frente meridional del Pirineo Central. Rev. Soc. Geol España, v. 13, p. 279-300.

GHIBAUDO, G., MUTTI, E. AND ROSELL, J., 1974. Le spiagge fossile delle Arenarie di Arén (Cretacico Superiore) nella Valle Noguera Ribagorzana (Pirinei Centro - Meridional, Provinci di Lerida e Huesca). Mem. Soc. Geol. Ital., v. 13, p. 497-537.

HEWARD, A.P., 1978. Alluvian-fan sequence and megasequences models, with examples from Westphalian D-Stephanian B Coalfields, Northern Spain. In: Miall, A.D., (ed.), Fluvial Sedimentology. Mem. Can. Soc. Petrol. Geol. 5, p. 669-702.

HIRST, J.P.P., 1991. Variations in alluvial architecture across the Oligo-Miocene Huesca fluvial system, Ebro Basin, Spain. In: Miall, A.D. and Tyler, N. (eds.), The three-dimensional facies architecture of terrigenous clastic sediments and its implications for hydrocarbon discovery and recovery. SEPM, Concepts in Sedimentology and Palaeontology, v. 3, p. 6-12.

HIRST, J.P.P. AND NICHOLS, G.J., 1986. Thrust tectonic controls on Miocene alluvial distribution patterns, southern Pyrenees. In: Allen, P.A. and Homewood, P. (eds.), Foreland Basins. Int. Assoc. Sedim. Spec. Publ. 8, p. 247-258.

JOHNS, D.R., MUTTI, E., ROSELL, J. AND SEGURET, M., 1981. Origin of a thick, redeposited carbonate bed in Eocene turbidites of the Hecho Group, South-central Pyrenees, Spain. Geology, v. 9, p. 161-164.

JOLLEY, E.J., 1987. Thrust tectonics and alluvial architecture of the Jaca Basin, Southern Pyrenees, Spain. University of Wales Unpublished Ph.D Thesis.

JONES, P.B., 1982. Oil and gas beneath east-dipping underthurst faults in the Alberta foothills. In: Powers, R.B. (ed.). Geological studies of the Cordilleran Thrust Belt. Rocky Mountain Association of Petroleum Geologists, v. 1, p. 61-74.

JONES, S. J., FROSTICK, L. E. AND ASTIN, T. R., 2001. Braided stream and flood plain architecture: the Rio Vero Formation, Spanish Pyrenees. Sedimentary Geology, v. 139, p. 229-260.

JUPP, P.E., SPURR, B.D., NICHOLS, G.J. AND HIRST, J.P.P, 1987. Statistical estimation of the apex of a sediment distribution system from palaeocurrent data. Mathematical geology, v. 19, p. 319-333.

KLEVERLAAN, K. AND COSSEY, S.P.J. 1993. Permeability barriers within sand-rich submarine fans: putcrop studies of the Tabernas Basin, SE Spain. *In*: ESCARD, R. & DOLIGEZ, B. (eds) *Subsurface Reservoir Characterisation from Outcrop Observations.* Éditions Technip, Paris, 161-164.

LABAUME, P., MUTTI, E., SEGURET, M. AND ROSELL, J., 1983. Megaturbidites carbonatées du basin turbiditique de l'Eocene inferieur et moyen sud-pyreneen. Bull. Soc. Geol. France, v. 25, p. 927-941.

LABAUME, P., SEGURET, M. AND SEYVE, C., 1985. Evolution of a turbidite foreland basin and analogy with an accretionary prism: example from the Eocene south Pyrenean Basin. Tectonics, v. 4, p. 661-685.

LEWIS, K.B. 1971. Slumping on a continental slope inclined at 1^{o}-4^{o}. Sedimentology **16**, 97-110.

MILLINGTON, J. & CLARK, J.D. 1995. Submarine canyon and associated base-of-slope sheet system: the Eocene Charo-Arro system, south-central Pyrenees, Spain. In: Pickering, K.T., Hiscott, R.N., Kenyon, N.H., Ricci Lucchi, F. & Smith, R.D.A. (eds), Atlas of Deep Water Environments: architectural style in turbidite systems, 150-156. London: Chapman & Hall.

MARZO, M. AND ANADON, P., 1988. Anatomy of a conglomeratic fan-delta complex: The Eocene Montserrat Conglomerate, Ebro Basin, northeastern Spain. In: Nemec, W. and Steel, R.J. (ed.) Sedimentology and tectonic settings. Blackie and Son. p. 318-340.

MCCAIG, A.M. AND WICKHAM, S.H., 1984. The tectonic evolution of the Pyrenees: a workshop. J. Geol. Soc. London, v. 141, p. 379-381.

MCCAIG, A.M., 1986. Thick and thin-skimmed tectonics in the Pyrenees. Tectonophysics, v. 129, p. 319-342.

MUÑOZ, J.A., MARTÍNEZ, A. AND VERGÈS, J., 1986. Thrust sequences in the Spanish Eastern Pyrenees. J. Struct. Geol., v. 8, p. 399-405.

MUTTI, E., 1977. Distinctive thin-bedded turbidite facies and related depositional environments in the Eocene Hecho Group (South Central Pyrenees, Spain). Sedimentology, v. 24, p. 107-131.

MUTTI, E. 1979. Turbidites et cones sous-marins profonds. In Homewood, P. (Ed.), Sedimentation Detrique (Fluviatile, Littorale et Marine): Institut de Geologie, University de Fribourg.

MUTTI, E. 1985. Turbidite systems and their relations to depositional systems. In Zuffa, G.G. (Ed.), Provenance of Arenites: NATO-ASI Series, Reidel Publishing Co., Dordrecht, The Netherlands, 65-93.

MUTTI, E. AND JOHNS, D.R., 1978. The role of sedimentary by-passing in the genesis of fan fringe and basin plain turbidites in the Hecho Group system (South-Central Pyrenees). Mem. Soc. Geol. It., v. 18, p. 15-22.

MUTTI, E. AND NORMARK, W.R. 1987. Comparing examples of modern and ancient turbidite systems: Problems and concepts. In LEGGET, J.K. & ZUFFA, G.G. (eds)., Deep Water Clastic Deposits: Models and Case Histories: Graham & Trotman, London, 1-38.

MUTTI, E. AND NORMARK, W.R. 1991. An integrated approach to the study of turbidite systems. In LINK, M.H. & WIEMER, P. (eds),: Seismic Facies and sedimentary Processes of Submarine Fans and Turbidite Systems, Springer-Verlag, New York.

MUTTI, E. AND SONNINO, M. 1981. Compensation cycles: A diagnostic feature of sandstone lobes: Abstracts II European Regional Meeting, International Association of Sedimentologists, Bologna, 120-123.

MUTTI, E. AND RICCI LUCCHI, F., 1972. Le torbiditi dell'Appennino Stentrionale: introduzione all'analisi di facies. Mem. Soc. Geol., It., v. 11, p. 161-199.

MUTTI, E., DAVOLI, G., MORA, S. AND PAPANI, L., 1994. Internal stacking patterns of ancient turbidite systems from collision basins. GCCSEPM Foundation 15th Annual Conference. Submarine Fans and Turbidite Systems, December 4-7, 1994, p. 257-268.

MUTTI, E., LUTERBACHER, H.P., FERRER, J. AND ROSSELL, J., 1972. Schema stratigrafico e lineamenti di facies del Paleogene marino della zona centrale sud-pirenaica tra Tremp (Catalogna) e Pamplona (Navarra). Mem. Soc. Geol. It., v. 11, p. 391-416.

MUTTI, E., FONNESU, F., RAMPONE, G. AND SONNINO, M., 1981. Channel-fill and associated overbank deposits in the Eocene Hecho Group, Ainsa-Boltaña region (South-Central Pyrenees). Abstr. 2nd Eur. Reg. Meet., I.A.S. Bologna, p. 113-116.

MUTTI, E., RICCHI LUCCHI, F., SEGURET, M. AND ZANZUCCHI, G., 1984a. Seismoturbidites: a new group of resedimented deposits. Marine Geology v. 55, p. 103-166.

MUTTI, E., ROSELL, J. AND ALLEN, G.P., 1984b. The tide-dominated Baronia delta complex in the upper Paleocene and lower Eocene Figols Sequence, Ager syncline, South-Central Pyrenees, Spain. Abstr. 5th Eur. Reg. Meet., I.A.S., Marseille, p. 314-315.

MUTTI, E., ROSELL, J., ALLEN, G.P., FONNESU, F. AND SGAVETTI, M., 1985. The Eocene Baroia tide dominated delta-shelf system in the Ager Basin. In: Milá, M.D. and Rosell, J. (eds.). Excursion Guidebook. Int. Assoc. Sediment. 6th European Regional Meeting, Lleida, Spain. Excursion No. 13, p. 579-600.

MUTTI, E., REMACHA E., SGAVETTI, M., ROSELL, J., VALLONI, R. AND ZAMORANO, M., 1985a. Stratigraphy and facies characteristics of the Eocene Hecho Group turbidite systems, south-central Pyrenees. In: Milá, M.D. and Rossel, J. (eds.). Excursion Guidebook. Int. Assoc. Sediment. 6th European Regional Meeting, Lleida, Spain, p. 521-576.

MUTTI, E. AND SGAVETTI, M., 1987. Sequence stratigraphy of the Maastrichtian Aren strata in the Orcau-Aren region, south-central Pyrenees, Spain: distinction between eustatically and tectonically controlled deposited sequences. Amm. dell. Univ. de. Ferrara, v. 1, p. 1-17.

MUTTI, E., SEGURET, M. & SGAVETTI, M. 1989. Sedimentation and deformation in the Tertiary Sequences of the Southern Pyrenees. American Association of Petroleum Geologists Mediterranean Basins Conference Guidebook Field Trip No. 7, Nice, Special Publication of the Institute of Geology, University of Parma.

NAGTEGAAL, P. J. C., 1969a. Microtextures in Recent and fossil caliche. Luidse Geologische Mededelingen, v. 42, p. 131-142.

NAGTEGAAL, P.J.C., 1969b. Sedimentology, palaeoclimatology and diagenesis of post-Hercynian continental deposits in the South-Central Pyrenees, Spain. Leids. Geol. Med., v. 42, p. 143-238.

NAGTEGAAL, P.J.C., 1972. Depositional history and clay minerals of the Upper Cretaceous basin in the South-Central Pyrenees, Spain. Leids. Geol. Med., v. 47, p. 251-275.

NAGTEGAAL, P.J.C., VAN VLIET, A., BROUWER, J., 1983. Syntectonic coastal offlap and concurrent turbidite deposition in the Upper Cretaceous Aren Sandstone in the South-Central Pyrenees, Spain. Sedim. Geol., v. 34, p. 185-218.

NICHOLS, G.J., 1987a. Syntectonic alluvian fan sedimentation, southern Pyrenees. Geol. Mag., v. 124, p. 121-133.

NICHOLS, G.J., 1987b. The structure and stratigraphy of the Western External Sierras of the Pyrenees, northern Spain. Geol. J., v. 22, p. 245-259.

NICHOLS, G.J., 1987c. Structural controls on fluvial distributary systems - the Luna System, Northern Spain. In: Ethridge, F.G., Flores, R.M. and Harvey, M.D. (eds.), Recent developments in fluvial sedimentology. SEPM, Spec. Publ. 39, p. 269-277.

NICKEL, E., 1982. Alluvial-fan carbonate facies with evaporites, Eocene Guarga Formation, Southern Pyrenees, Spain. Sedimentology, v. 29, p. 761-796.

NIJMAN, W. AND NIO, S.D., 1975. The Eocene Montañana Delta. In: The sedimentary evolution of the Paleogene South Pyrenean Basin, I.A.S. International Congress, Nice, part B.

NIJMAN, W. AND PUIGDEFABREGAS, C., 1978. Coarse-grained point bar structure in a mollase-type fluvial system, Eocene Castisent Formation, South Pyrenean basin. In: Miall, A.D. (ed.). Fluvial Sedimentology. Can. Soc. Pet. Geol. Mem. 5, p. 487-510.

NIJMAN, W., 1981. Fluvial sedimentology and basin architecture of the Eocene Montañana Group, South Pyrenean Tremp-Graus Basin. In: Elliott, T. (ed.). Field Guides to Modern and Ancient Fluvial Systems in Britain and Spain. Proceedings International Fluvial Conference. Keele, p. 3-27.

NIO, S.D., 1976. Marine transgression as a factor in the formaton of sandwave complexes. Geol. Mijn. v. 55, p. 18-40.

NIO, S.D. AND DONSELAAR, R., 1978. An Eocene transgressive barrier complex near Graus. Comp. Sed. Div., U trecht, v. 18, p. 45-58.

NIO, S.D. AND SIEGENTHALER, C., 1978. A Lower Eocene estuarine-shelf complex in the Isabena Valley. Comp. Sed. Div., Utrecht, v. 18, p. 1- 44.

ORI, G.G. AND FRIEND, P.F., 1984. Sedimentary basins formed and carried piggyback on active thrust sheets. Geology, v. 12, p. 475-478.

PARISH, M., 1984. A structural interpretation of a section of the Gavarnie nappe and its implication for Pyrenean geology. J. Struct. Geol., v. 6, p. 247-255.

PAYROS, A., PUJALTE, V., BACETA, J. I., BERNAOLA, G., ORUE-ETXEBARRIA, X., APELLANIZ, E., CABALLERO, F. AND FERRANDEZ, C., 2000. Lithostratigraphy and sequence stratigraphy of the Upper Thanetian to Middle Illerdian strata of the Campo section (southern Pyrenees, Spain): revision and new data. Rev. Soc. Geol España, v. 13, p. 213-225.

PICKERING, K. T. AND CORREGIDOR, J., 2000. 3D reservoir-scale study of Eocene confines submarine fans, south-central Spanish Pyrenees. GCCSEPM Foundation 20th Annual Conference. Deep-Water Reservoirs of the World, December 3-6, 2000, p. 776-781.

PICKERING, K. T. AND CORREGIDOR, J., 2002. Rates of lateral migration and growth of linear confined basin-floor fans, and importance of mass transport complexes (MTCs), Mid Eocene, south Spanish Pyrenees. Preprint.

PICKERING, K.T., HISCOTT, R.N. & HEIN, F.J. 1989. Deep marine environments: clastic sedimentation and tectonics. 416 pp. London: Chapman & Hall.

PICKERING, K.T., HISCOTT, R.N., KENYON, N.H., RICCI LUCCHI, F. & SMITH, R.D.A. (eds), Atlas of Deep Water Environments: architectural style in turbidite systems. London: Chapman & Hall.

PICKERING, K.T., CLARK, J.D., SMITH, R.D.A., HISCOTT, R.N., RICCI LUCCHI, F. & KENYON, N.H. 1995. Architectural element analysis of turbidite systems, and selected topical problems for sand-prone deep-water systems In: PICKERING, K.T., HISCOTT, R.N., KENYON, N.H., RICCI LUCCHI, F. & SMITH, R.D.A. (eds), Atlas of Deep Water Environments: architectural style in turbidite systems, 1-10. London: Chapman & Hall.

PINET, B., 1987. Crustal thinning on the Aquitaine shelf, Bay of Biscay, from deep seismic data. Nature, v. 235, p. 513-516.

PLATT, N. H., 1990. Basin evolution and fault reactivation in the western Cameros Basin, Northern Spain. J. Geol. Soc. London, v. 147, p. 165-175.

PUIGDEFABREGAS, C., 1973. Miocene point bar deposits in the Ebro Basin, northern Spain. Sedimentology, v. 20, p. 133-144.

PUIGDEFABREGAS, C., 1975. La sedimentatión molásica en la cuenca de Jaca. Pirineos, v. 104, p. 1-188, with map.

PUIGDEFABREGAS, C., RUPKE, N.A. AND SOLE SEDO, J., 1975. The sedimentary evolution of the Jaca Basin. In: Rosell, J. and Puigdefabregas, C., (eds.). The sedimentary evolution of the Paleogene South Pyrenean Basin. International Association of Sedimentologists. 9th International Congress. Nice. p.

PUIGDEFABREGAS, C. AND VAN VLIET, A., 1978. Meandering stream deposits from the Tertiary of the Southern Pyrenees. In: Miall, A.D. (ed.). Fluvial Sedimentology. Canadian Society of Petroleum Geologists Memoir 5, p. 469-487.

PUIGDEFABREGAS, C. AND SOUQUET, P., 1985. Tecto-sedimentary cycles and depositional sequences of the Mesozoic and Tertiary from the Pyrenees. Tectonophysics, v. 129, p. 173-203.

PUIGDEFABREGAS, C., MUÑOZ, J.A. AND MARZO, M., 1986. Thrust belt development in the Eastern Pyrenees and related depositional sequences in the southern foreland basin. In: Allen, P.A. and Homewood, P. (eds.), Foreland Basins. Int. Assoc. Sedimentol. Spec. Publ. 8, p. 229-246.

REMACHA, E. 1983. "Sand tongues" de la Unidad de Broto (Grupo Hecho) entre el anticlinal de Boltaña y Rio Osia (prov. de Huesca): Ph.D. thesis, Universidad Autonoma de Barcelona.

REYNOLDS, S.A., GALLOWAY, W.E. AND GLASFORD, J.L., 1989. Genetic stratigraphic sequences in non-marine basins. Abstracts of the 28th Int. Geological Congress, Washington, v. 2, p. 691-692.

REYNOLDS, A.D., 1987. Tectonically controlled fluvial sedimentation in the South-Central Pyrenees. Unpubl. PhD thesis, Univ. of Liverpool.

RIBA, O., 1976. Syntectonic unconformities of the Alto Cardener, Spanish Pyrenees: A genetic interpretation. Sediment. Geol. v. 15, p. 213-233.

ROBLES, S., 1982. Estudio comparativo del sistemo aluvial del borde suroccidental de Los Catal. 160 mides en la transversal de Prat de Compte (Tarragona) y los abanicos aluviales de Pobla de Segur (Prepirineo de Lérida). Acta Geologica Hispanica, v. 17, p. 255-269.

ROSELL, J. AND PUIGDEFABREGAS, C., 1975. The sedimentary evolution of the Paleogene South Pyrenean Basin. International Association of Sedimentologists. 9th International Congress, Nice, p.

RUPKE, N.A., 1976a. Large-scale slumping in a flysch basin, southwestern Pyrenees. J. Geol. Soc. London, v. 132, p. 121-130.

RUPKE, N.A., 1976b. Sedimentology of very thick calcarenite-marlstone beds in a flysch succession, south-western Pyrenees. Sedimentology, v. 23, p. 43-65.

SÁEZ, A. AND RIBA, O., 1986. Depósitos aluviales y lacustres paleógenos del margen pirenaico catalán de la Cuenca del Ebro. Guia de las Excursiones al XI Cong. Esp. de Sediment. (Barcelona). v. 6, p. 29.

SCHUPPERS, J.D. 1995. Characterization of Deep-Marine Clastic Sediments from Foreland Basins. Ph.D. Thesis, Delft University.

SEGURET, M., 1972a. Etude tectonique des nappes et series décollés de la partie central du versant sud des Pyrenees; cactere synsedimentaire, reh de la compression et de la gravité. Thes. Foc. Sei. Montpellier.

SEGURET, M. 1972b. Etude tectonique des nappes et series decollees de la patie centrale du versant sud des Pyrenees: Caractere Synsedimentarire, Role de la Compression et de la Gravite: Ser. Geol. Str., **2**, U.S.T.L., Montpellier, France.

SEGURET, M., LABAUME, P. AND MADARIAGA, R., 1984. Eocene seismicity in the Pyrenees from megaturbidites of the South Pyrenean Basin (North Spain). Marine Geology, Special Issue: Seismicity and Sedimentation Synposium. C.I.E.S.M., Cannes. 8 déc. 1982, v. 55, p. 117-131.

SEGURET, M. AND DAGNIERES, M., 1986. Crustal scale balanced cross sections of the Pyrenees: discussion. Tectonophysics, v. 129, p. 308-318.

SEIFERT, D., NEWBERY, J.D.H., RAMSEY, C. & LEWIS, J.J.M. 1997. Evaluation of field development plans using 3-D reservoir modelling. 4th International Reservoir Characterization Technical Conference, Houston, Texas, 2-4 March, 1997.

SIMÓ, A. AND PUIGDEFABREGAS, C., 1985. Transition from shelf to basin on an active slope, Upper Cretaceous, Tremp Aren, southern Pyrenees. In: Milá, M.D. and Rosell, J. (eds.). Excursion Guidebook, Int. Assoc. Sediment. 6th European Regional Meeting, Lleida, Spain. Excursion No. 2, p. 63-103.

SPEKSNIJDER, A., 1985. Anatomy of a strike-slip controlled sedimentary basin, Permian of the southern Pyrenees, Spain. Sediment. Geol., v. 44, p. 179-224.

STOCCHI, S. 1987. Il Sistema Torbiditico Guaso nella Sequenza Deposizionale de Ainsa (Eocene Medio della Zona Centrale Sud-Pirenaica, Provincia di Huesca, Spagna): Thesis, University of Parma, 406 p.

TEIXELL, A. AND MUÑOZ, J. A., 2000. Evolución tectono-sedimentaria del pirineo meridional durante el terciario: una síntesis basada en la transversal del Río Noguera Ribagorçana. Rev. Soc. Geol España, v. 13, p. 251-264.

TURNER, J., 1990. Structural and stratigraphic evolution of the West Jaca thrust-top basin, Spanish Pyrenees. J. Geol. Soc. London, v. 147, p. 177-184.

VALLONI, R., 1985. Reading provenance from modern marine sands. In: Zuffa, G.G. (ed.). Provenance of arenites, NATO-ASI Series, Reidal P.C., New York, in press.

VANN, I. R., GRAHAM, R. H. AND HAYWARD, A. B., 1986. The structure of mountain fronts. J. Struct. Geol., v. 8, p. 215-227.

VERGÉS, J. AND MUÑOZ, J.A., 1989. Thrust sequences in the Southern Central Pyrenees. Bull. Soc. Geol. France. (in press).

VINCENT, S.J. AND ELLIOTT, T., 1996. Long-lived palaeovalleys sited on structural lineaments in the Tertiary of the Spanish Pyrenees. In: Friend, P.F. and Dabrio, C.J. (eds.). Tertiary Basins of Spain, Cambridge University Press, p.161-165.

VINCENT, S.J. AND ELLIOTT, T., 1997. Long-lived transfer-zone paleovalleys in mountain belts: an example from the Tertiary of the Spanish Pyrenees. J. Sedim. Res. v. 67, p. 303-310.

WEBER, K.J. 1986. How Heterogeneity affects oil recovery. *In*: LAKE, L.W. & CARROLL, H.B. (eds) *Reservoir Characterization.* Proceedings of the Reservoir Characterization Technical Conference, Dallas April 29-May 1, Academic Press, p. 487-544.

WILLIAMS, G.D., 1985. Thrust tectonics in the South Central Pyrenees. J. Struct. Geol. v. 7, p. 11-17.

WILLIAMS, G.D. AND FISCHER, M.W., 1984. A balanced section across the Pyrenean orogenic belt. Tectonics. v. 3, p. 773-780.

Section 3

Field localities in the Vallcarga Basin

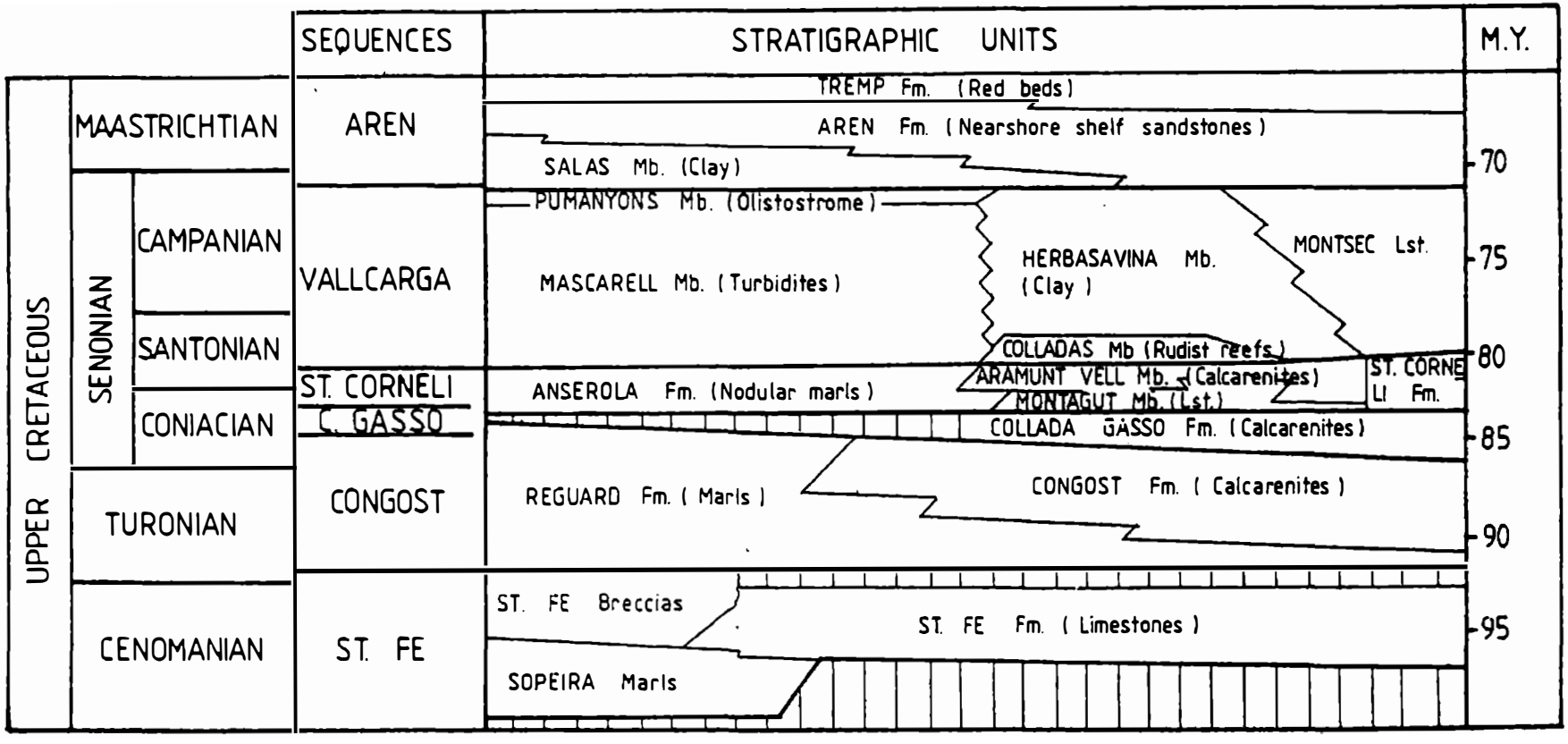

Figure 3.1 Upper Cretaceous stratigraphy in the Vallcarga Basin (from Simó and Puigdefabregas, 1985)

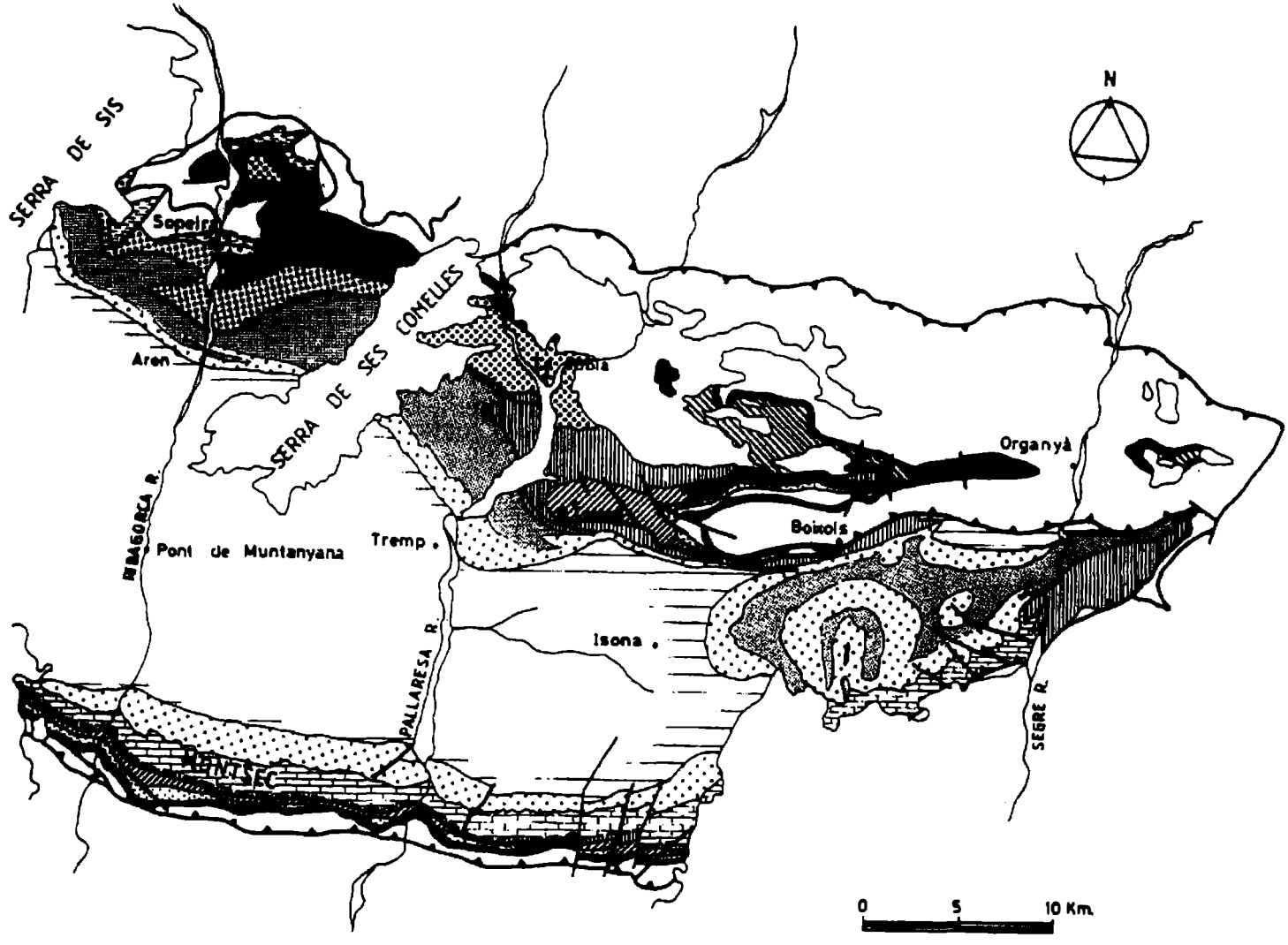

Figure 3.2 Distribution of the Arén Sandstone (Maastrichtian), shown in bold stipple (from Simó and Puigdefabregas, 1985).

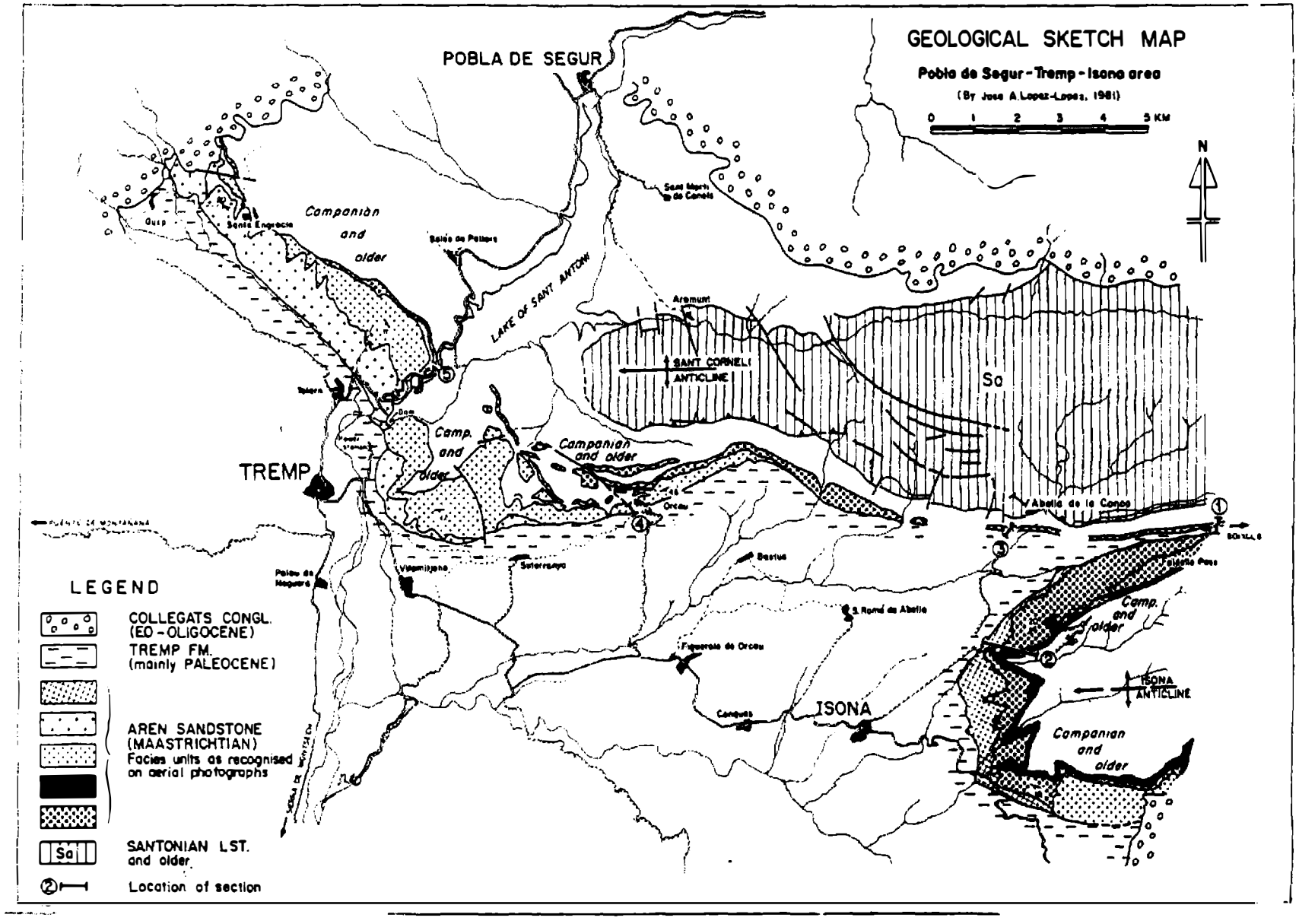

Figure 3.3 Geological sketch map of the Pobla de Segur - Tremp - Isona area (from Nagtegaal *et al.*, 1983)

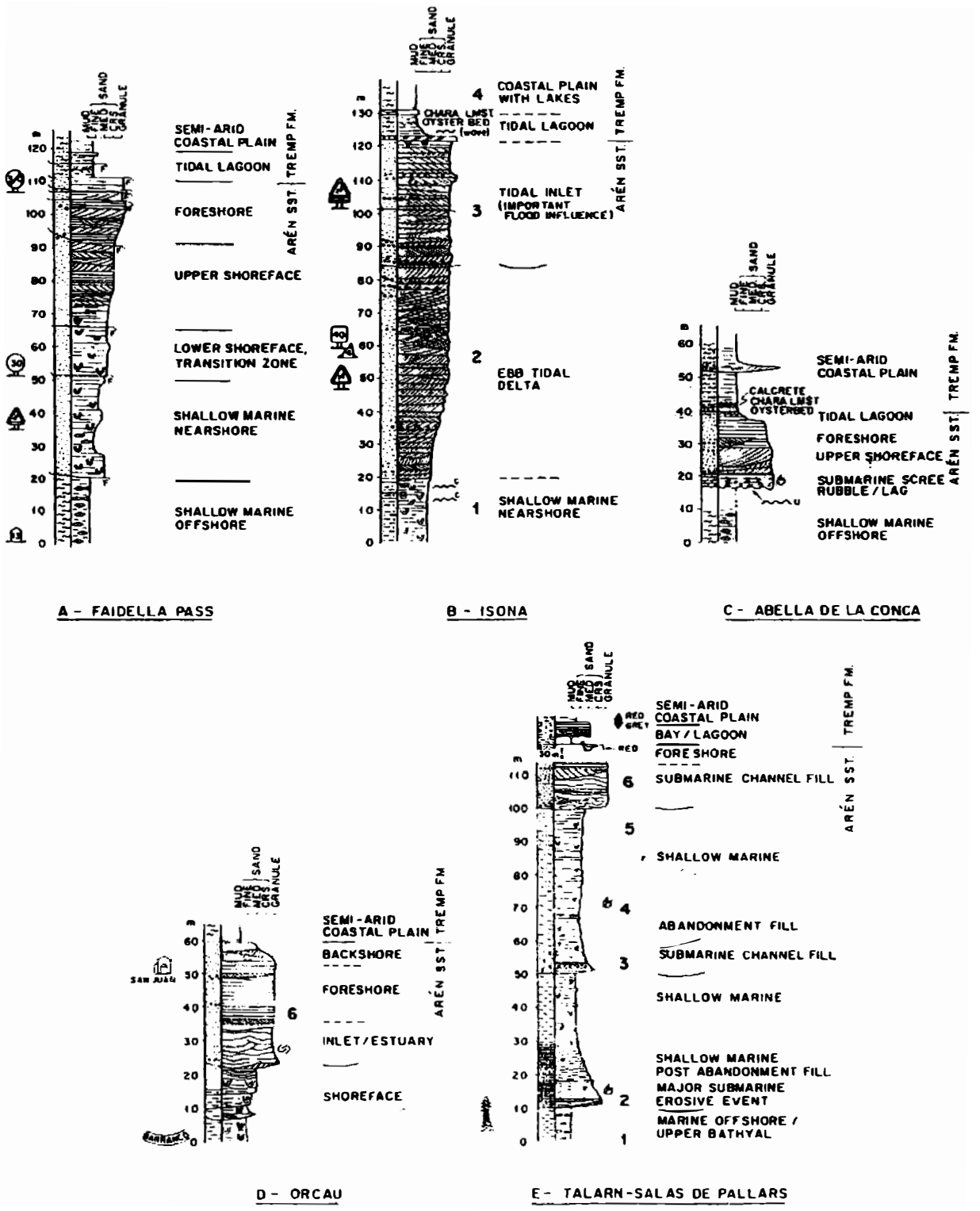

Figure 3.4 Sections through the Arén Sandstone, east of Tremp. A. Faidella Pass section (section 1 on Figure 3.3) .B. Isona section (section 2 on Figure 3.3). C. Abella de la Conca section (section 3 on Figure 3.3. D. Orcau section (Section 4 on Figure 3.3). E. Talarn-Salás de Pallars section (Section 5 on Figure 3.3) (from Nagtegaal *et al.*, 1983).

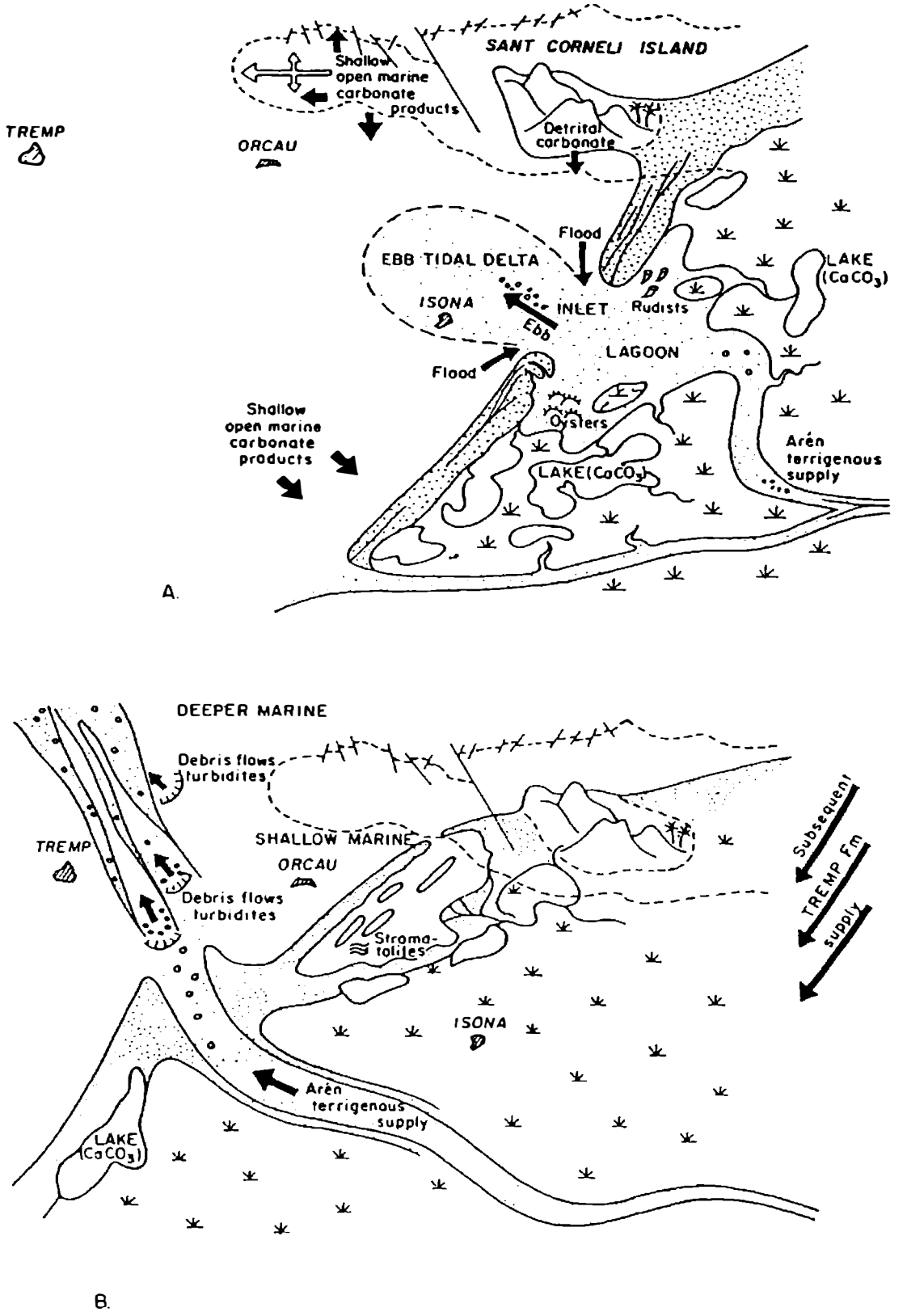

Figure 3.5 Models of the Arén depositional environment. A. at 'Isona time' and B. at 'Orcau-Tremp time' (from Nagtegaal *et al.*, 1983).

Section 4

Field localities in the Tremp-Graus sub-basin

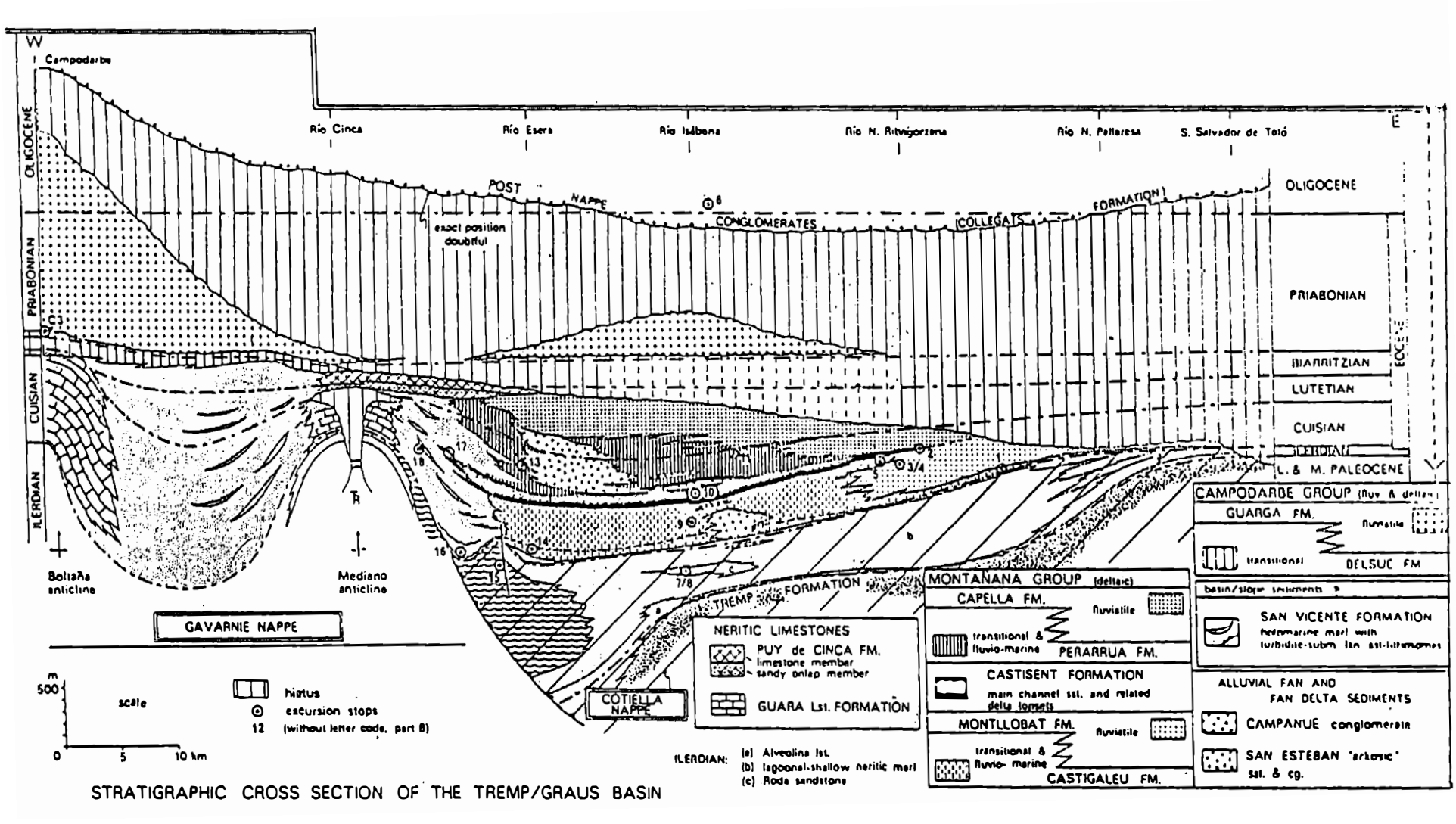

STRATIGRAPHIC CROSS SECTION OF THE TREMP/GRAUS BASIN

Figure 4.1 Stratigraphic cross-section of theTremp-Graus Basin. From Nio and Siegenthaler, 1978.

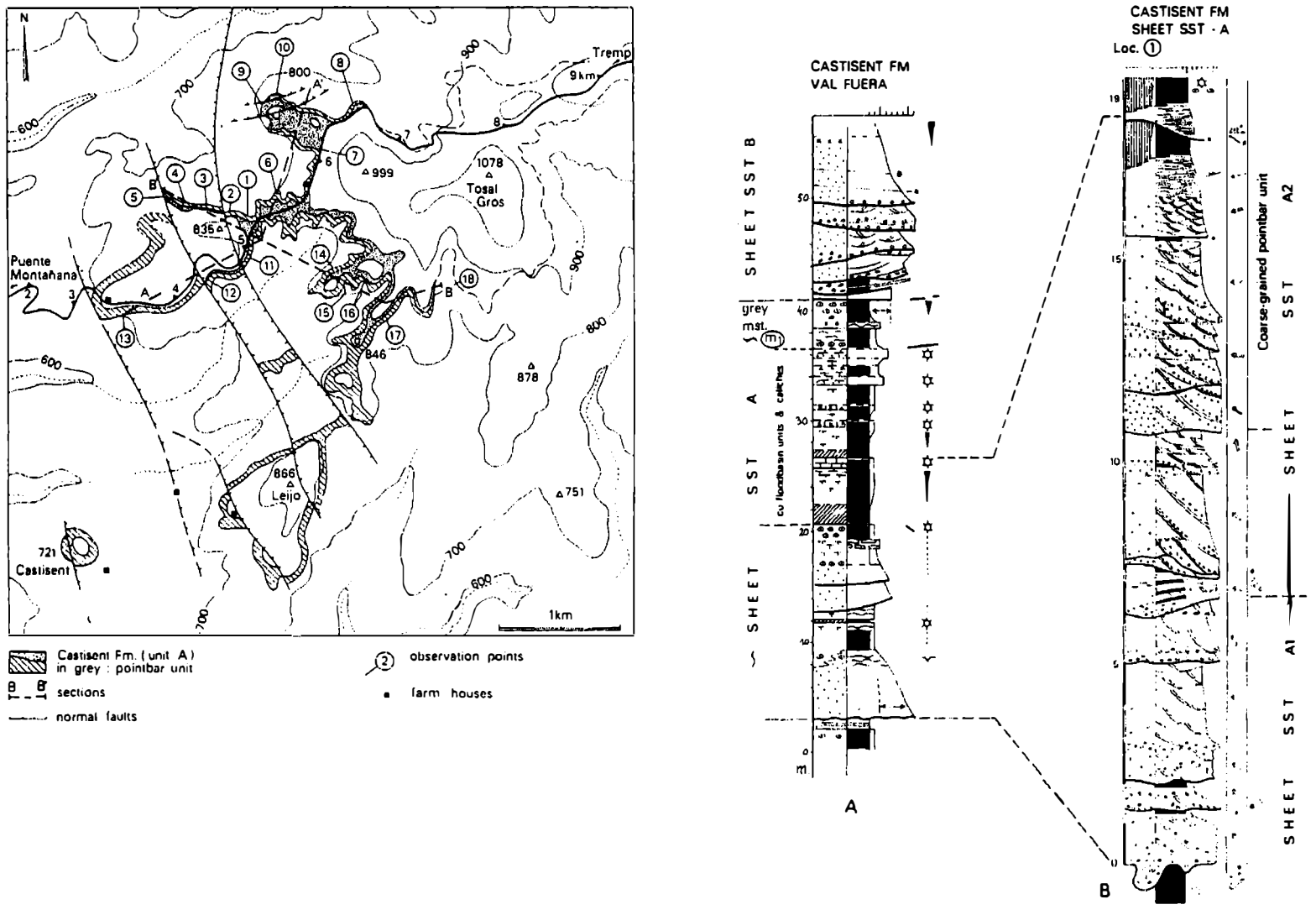

Figure 4.2 Map showing the extensive outcrop of sheet sandstone A of the Castisent Formation in the type area and sedimentary log of the formation near the western margin of the sheet sandstone. The expanded log shows the multi-storey nature of sandstone A. From Friend *et al.* 1981.

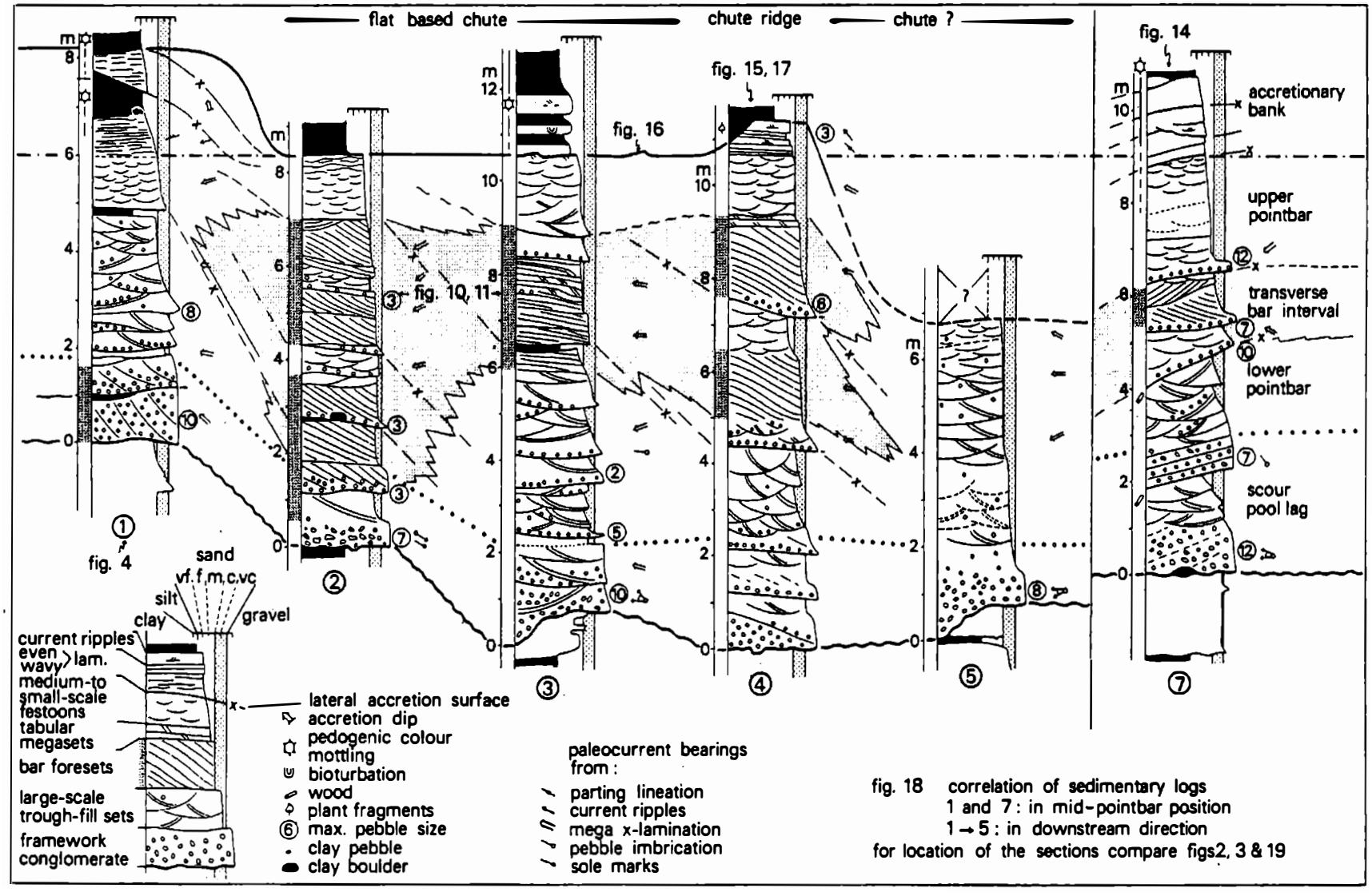

Figure 4.3 Correlation of sedimentary logs through an inferred point bar deposit in the Castisent Sandsone in the type area east of Montanana. From Nijman and Puigdefabregas, 1978.

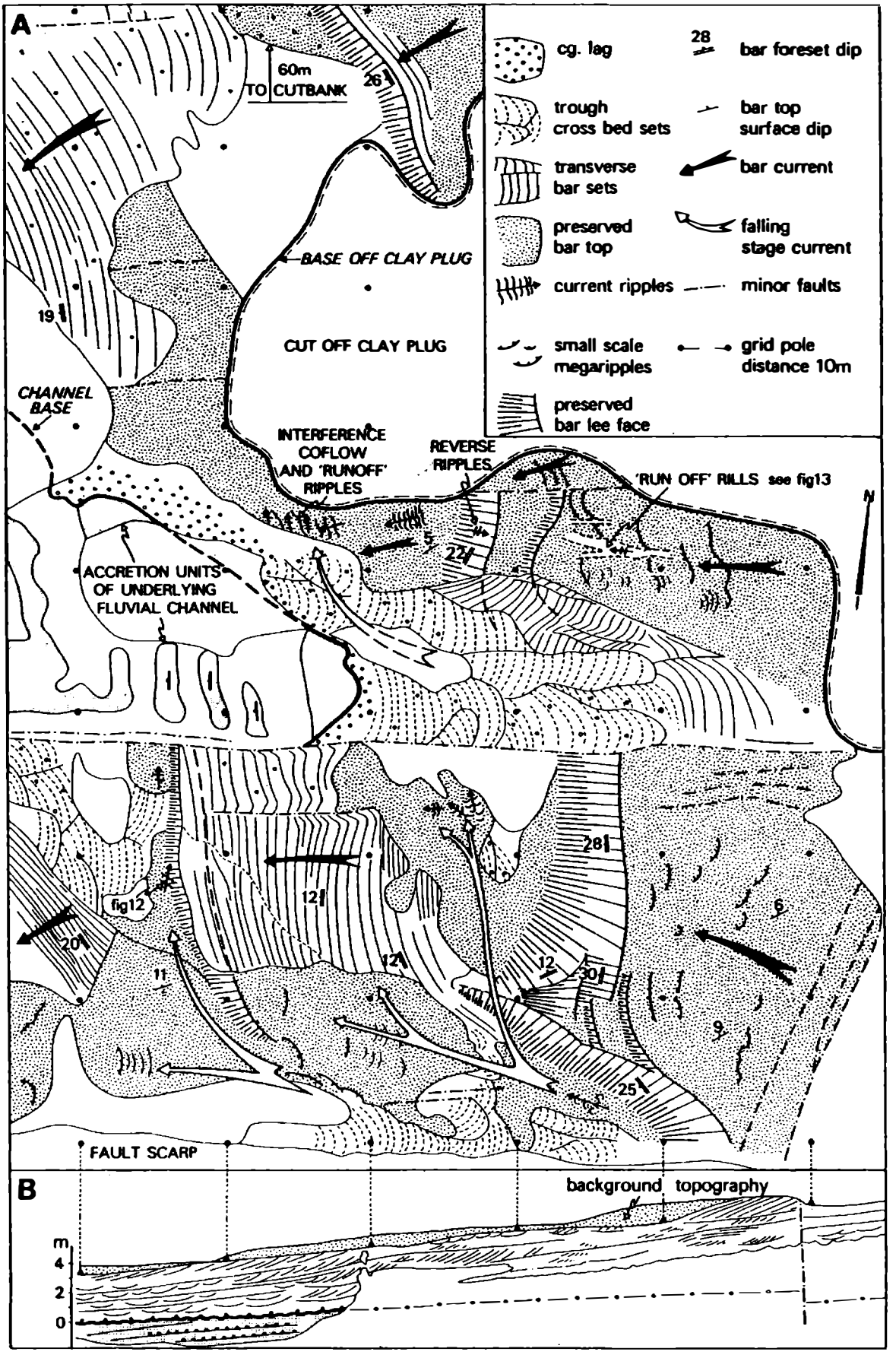

Figure 4.4 Plan view and cross-section of the inferred point bar deposit seen in Figures 4.2 and 4.3. From Nijman and Puigdefabregas, 1978.

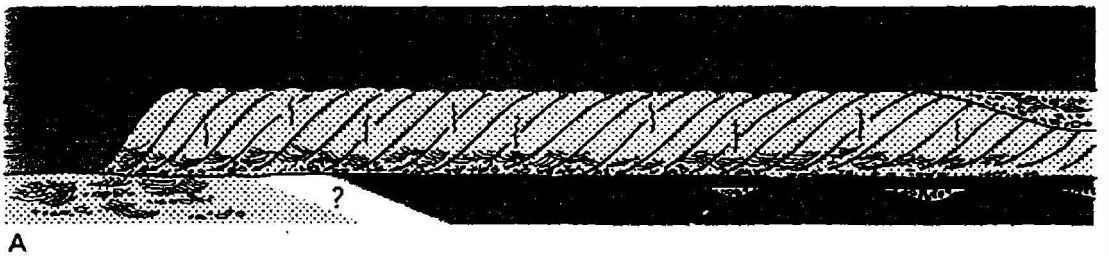

A

Scheme of upper channel cross-section as exposed in the northern valley wall of the Bco. de Montañana. Vertical scale exaggerated, horizontal distance approx. 250 m. Note clay plug and cutbank failure structure.

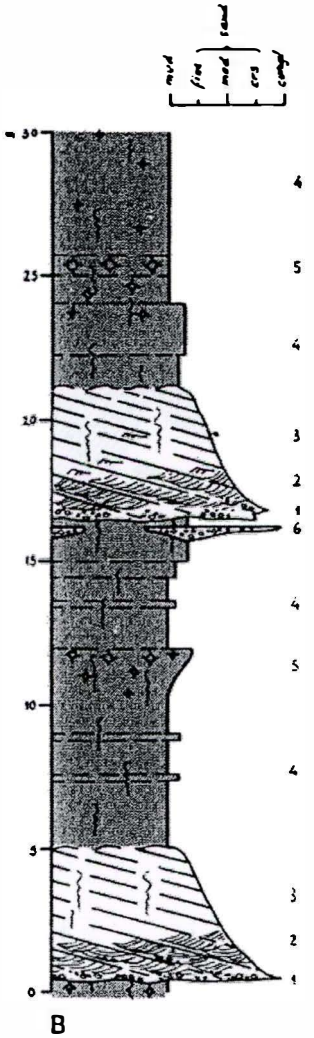

B

Generalised vertical section of the exposure north of the bridge.
1) scoured surface (locally overlain by lag deposits);
2) dm-scale trough cross-bedded sandstone;
3) inclined bedded homogenised muddy sandstone;
4) mottled mudstone;
5) calcrete horizons;
6) small channellised conglomerate bodies.
(Fig. 4.12 from Puigdefabregas and van Vliet, 1978).

Figure 4.5 Sedimentary log of the two laterally-accreted fluvial channels seen in the Baranco de Montanana and a cross-section of the upper channel. From Friend *et al.*, 1981 (after Puigdefabregas and van Vliet, 1978).

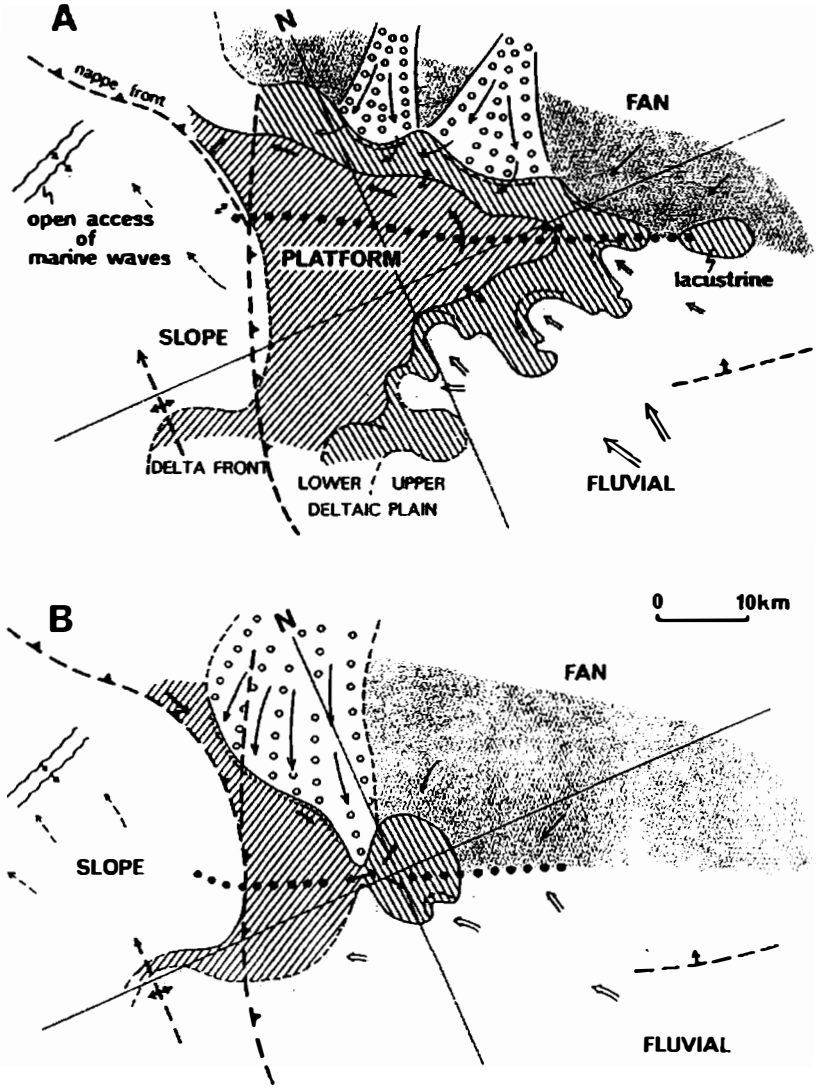

Fig. 4.6 **Basic configurations of the Montañana Group. A, during early stage; B, during more advanced stage of progradation.**

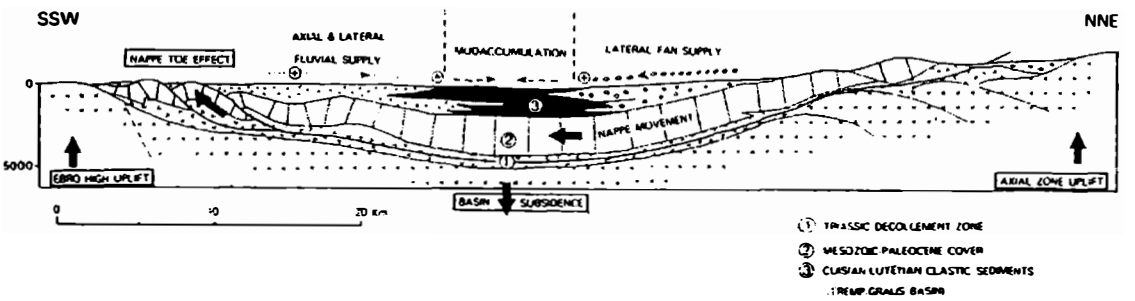

Figure 4.6 Basin configurations of the Montanana Group A. during early stage and B. during a more advanced stage of progradation. The Lower cross section shows a model for the tectonic control on sedimentation. From Friend *et al.*, 1978 (cross-section after Seguret, 1972).

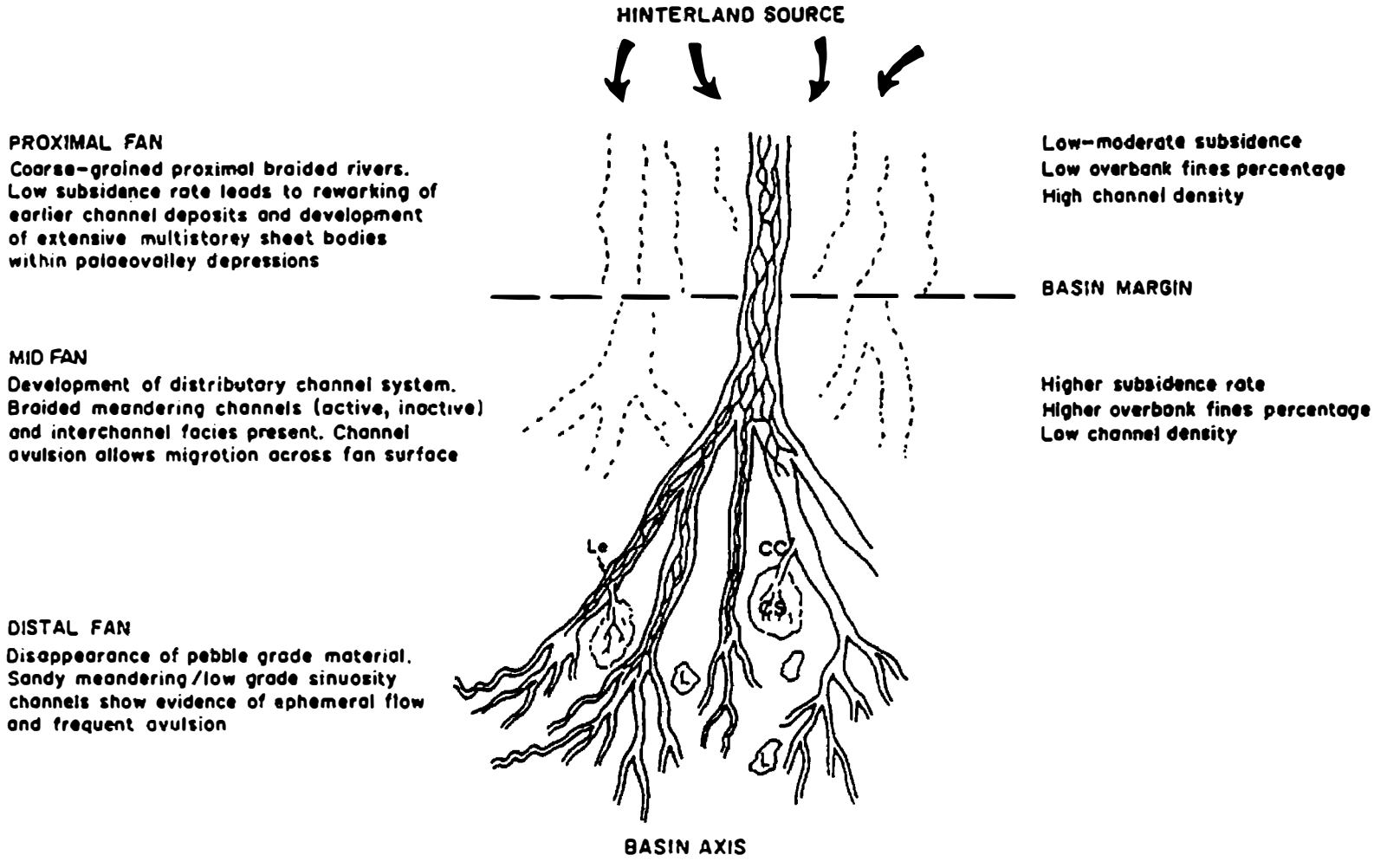

Figure 4.7 Idealised depositional model for the Montanana and Campodarbe humid alluvial fans. Le = levee, CC = crevasse channel, CS = crevasse splay and L = lacustrine. From Atkinson, 1986.

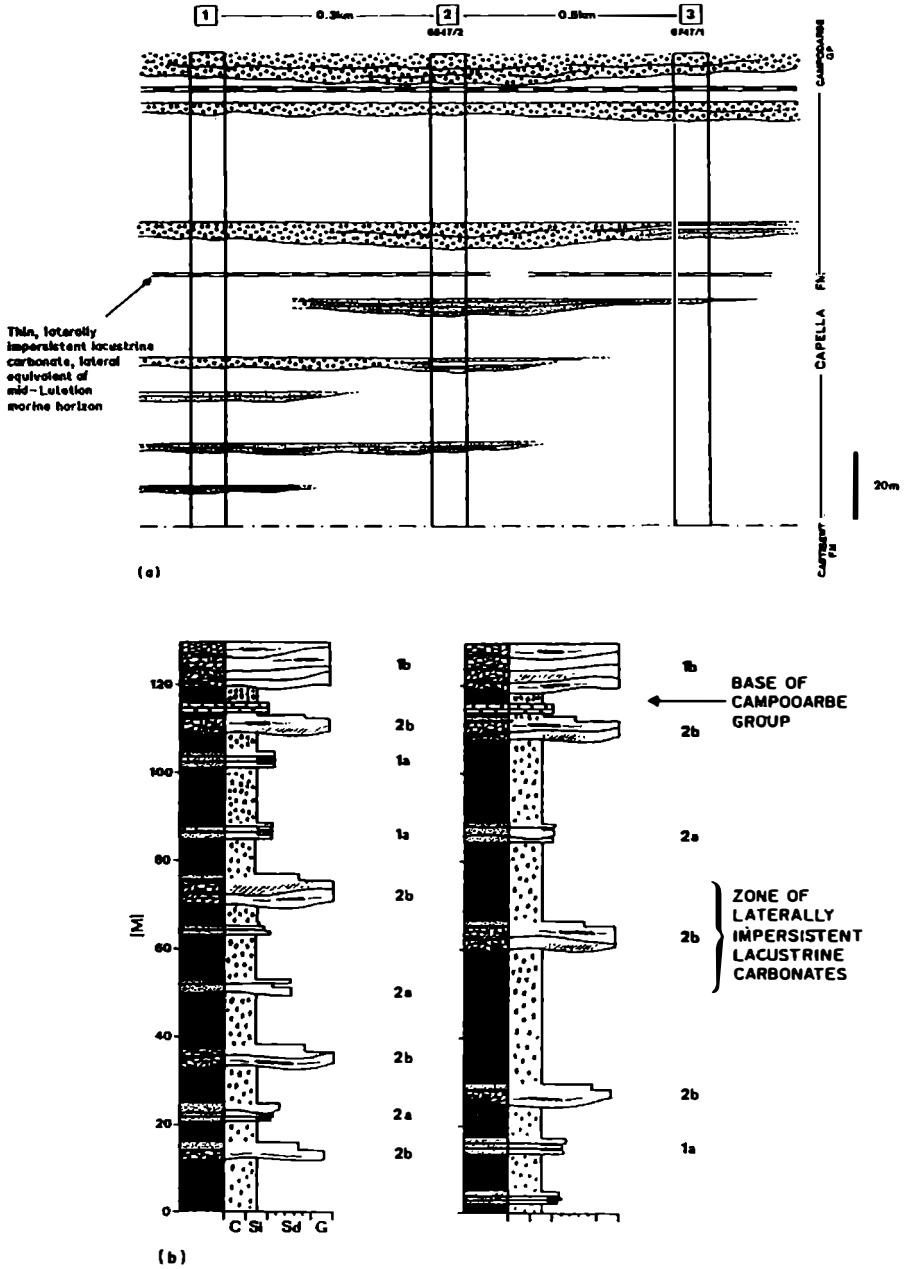

	Length of time for accumulation of sequence[1] (millions of years)	Thickness of sequence (metres)	Average floodplain aggradation rate (metres/year)	Average number of composite paleosol intervals	Average time between soil forming episodes (years)
Locality C1 Laguarres-Capella	1	300	0.3	72	14000
Locality C2 Valturo valley	1	c.120	0.12	26	40000
Locality C3 Torsal Gros[2]	3	c.150	0.046	no data	no data

[1]Based on time correlation of Mutti *et al.* (1972)
[2]Torsal Gros estimates are based on the whole Capella Formation.

c.

Figure 4.8 Diagrams showing the nature of the Capella Formation in the eastern Tremp-Graus Basin. a. simplified alluvial stratigraphy; b. vertical sedimentary profiles showing the development of soils between the channels and the presence of laterally impersistent limestones; c. table showing the rates of floodplain accretion and soil occurrence. From Atkinson, 1986.

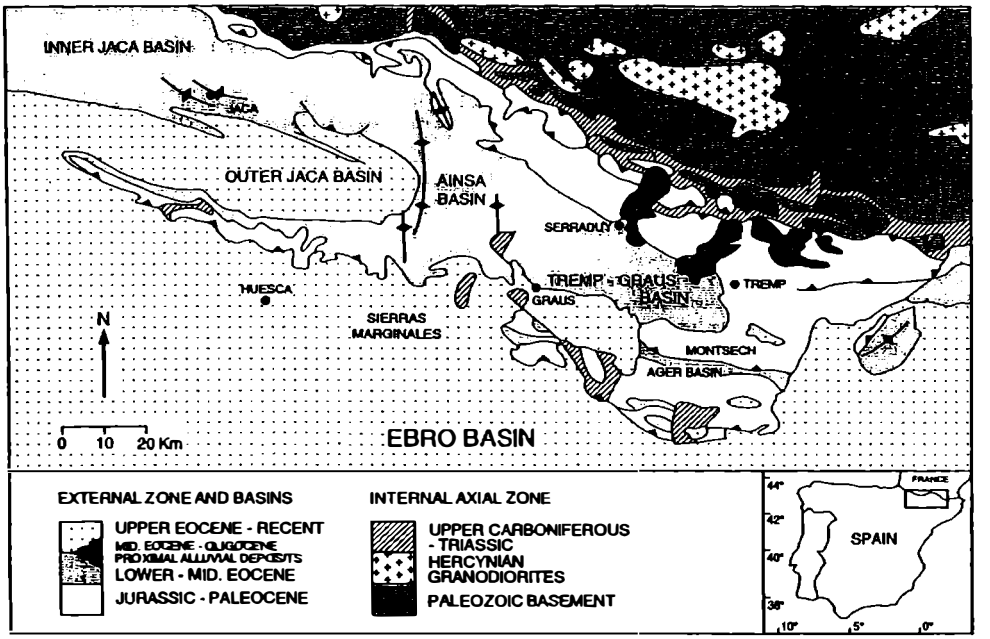

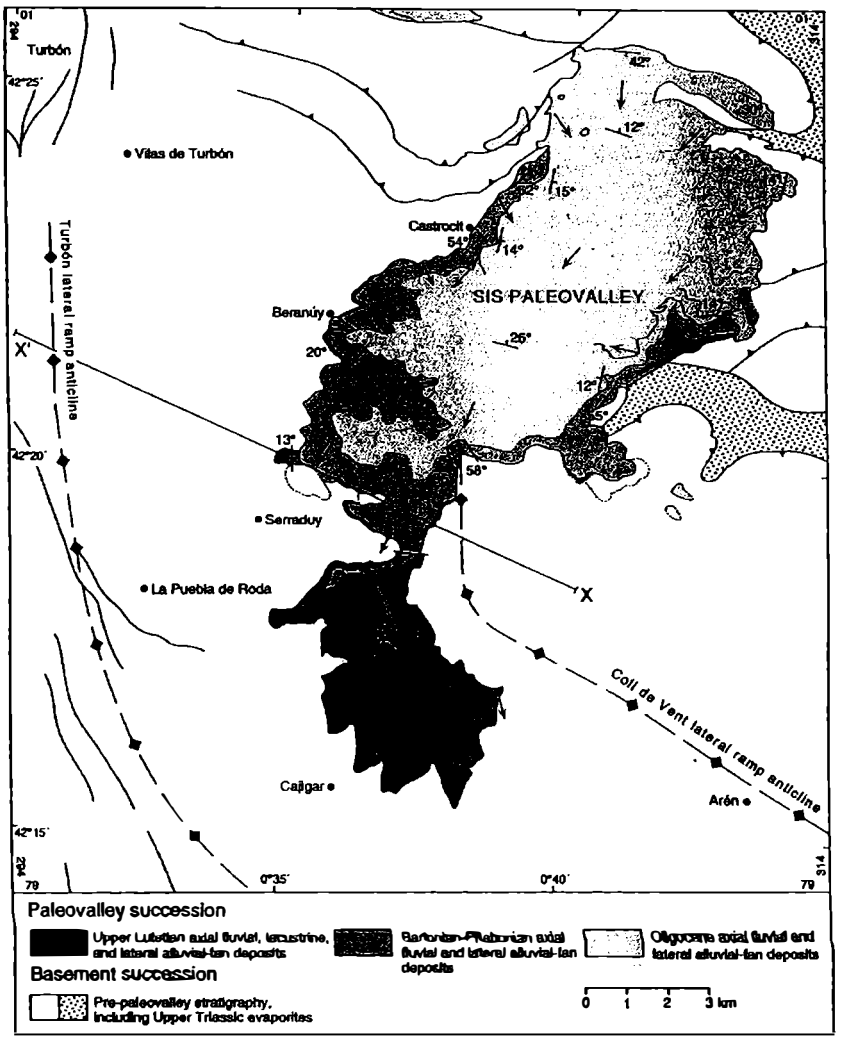

Figure 4.9 Geological map showing the location of the Sis (SC) and Gurp (GC) Conglomerate bodies and a more detailed facies map of the Sis palaeovalley. From Vincent and Elliott, 1997.

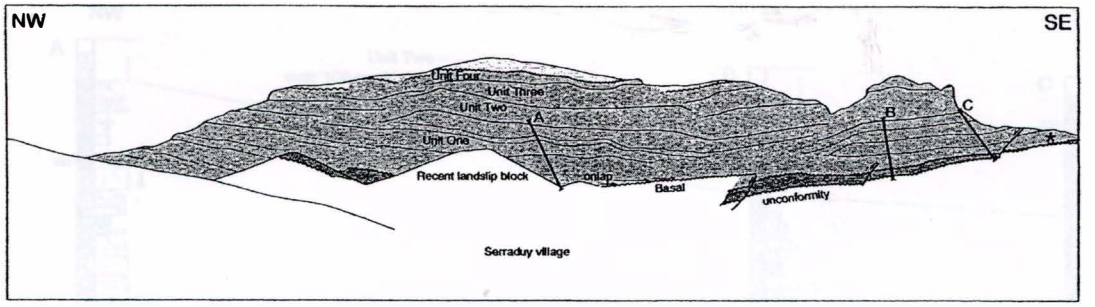

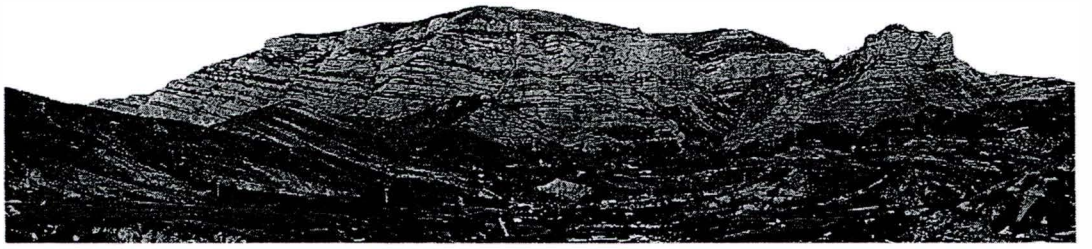

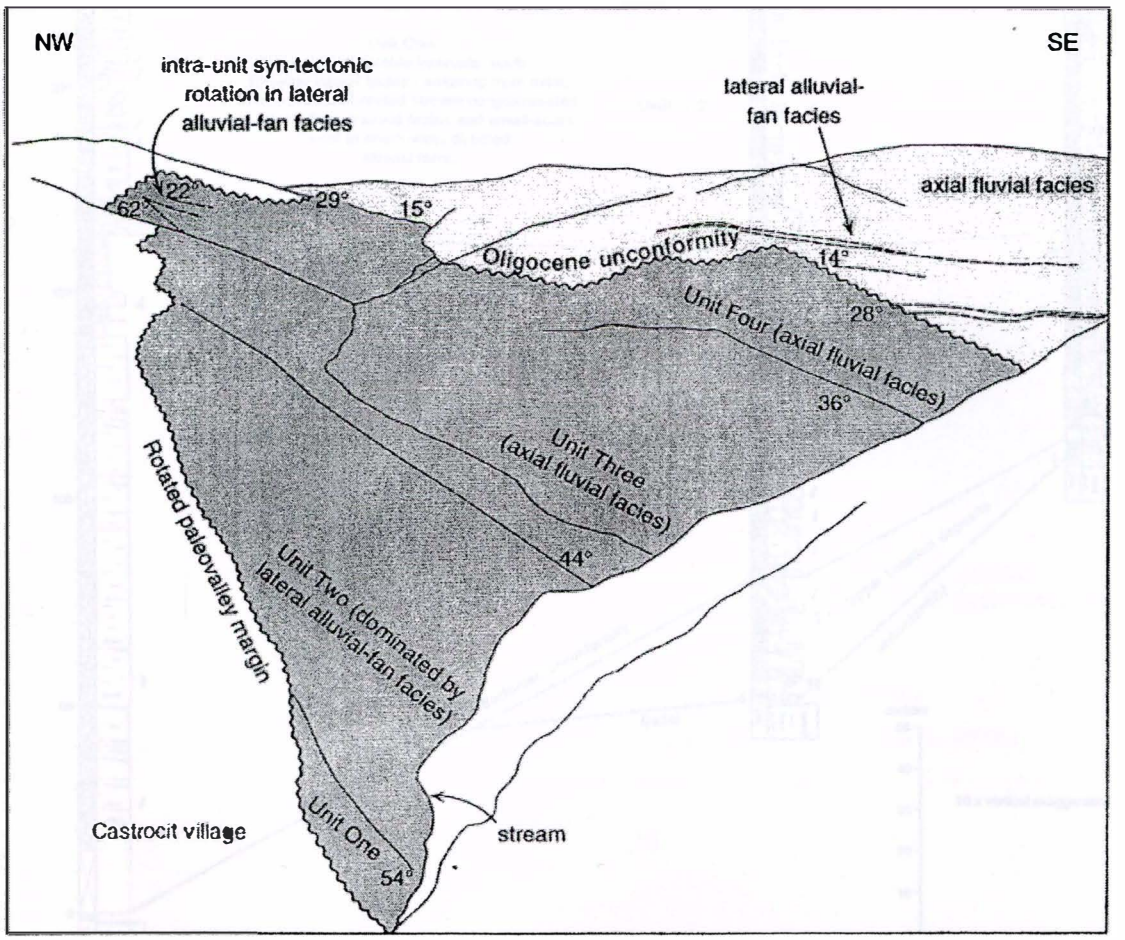

Figure 4.10 View and sketch interpretation of the southern (palaeocurrent-transverse) face of the Sis conglomerate. The conglomerate is 4km wide and 800m thick in this view. Lower diagram shows more detail of the western margin. From Vincent and Elliott, 1997.

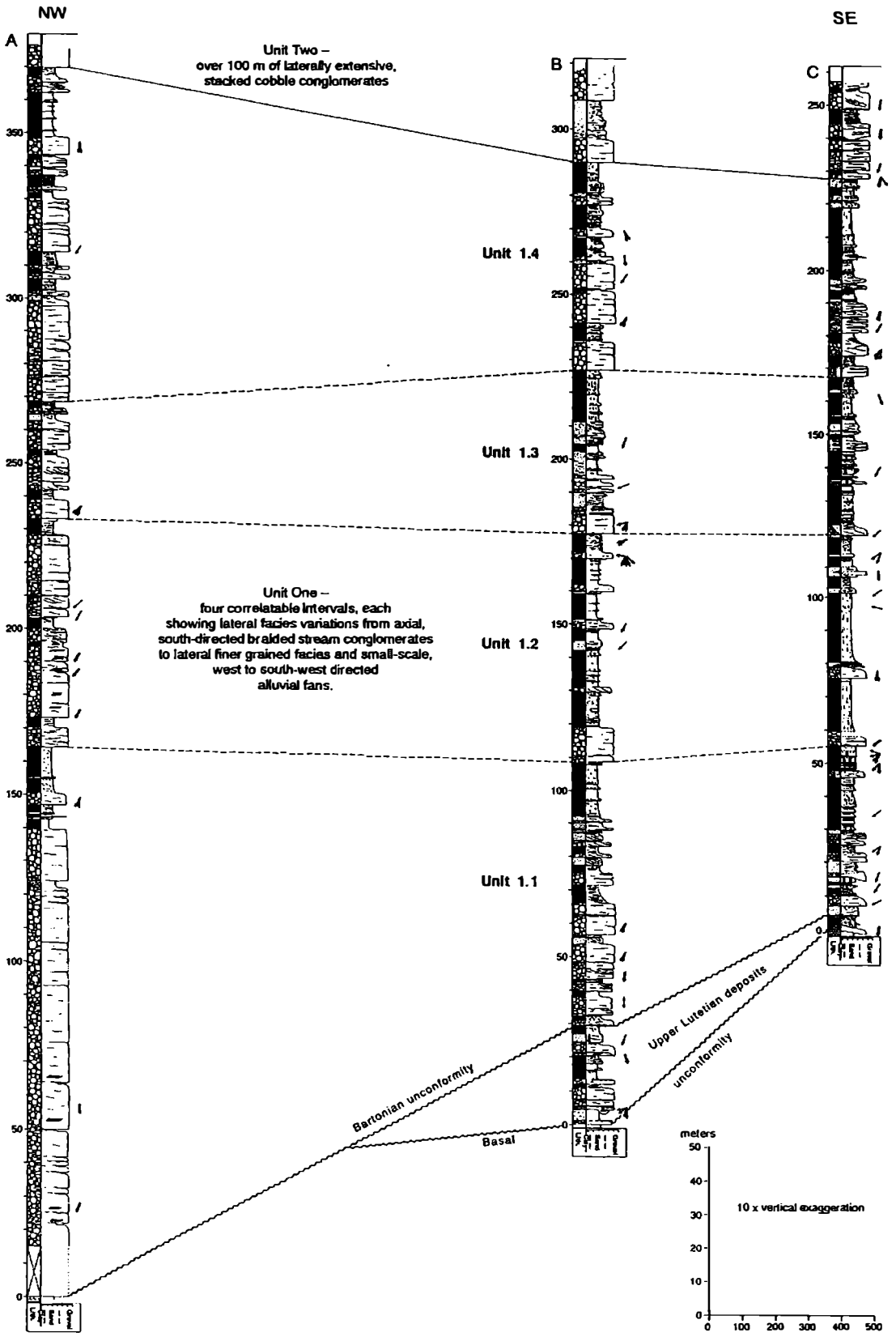

Figure 4.11 Graphic logs through the lower part of the southern face of the Sis conglomerate, showing the axial to lateral variation in facies and the large-scale onlap towards the eastern margin of the body. From Vincent and Elliott, 1997.

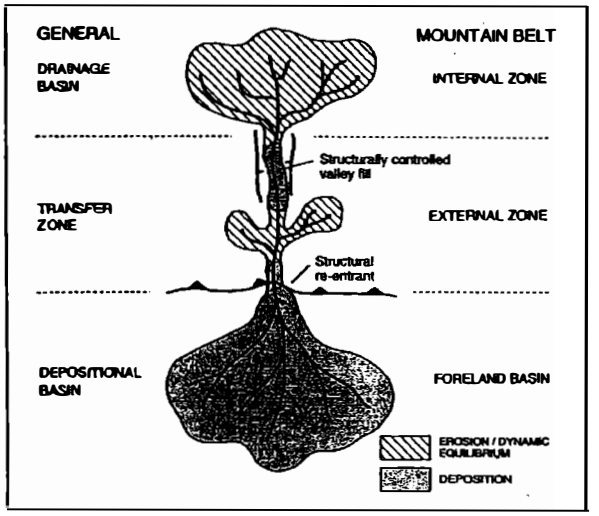

(a)

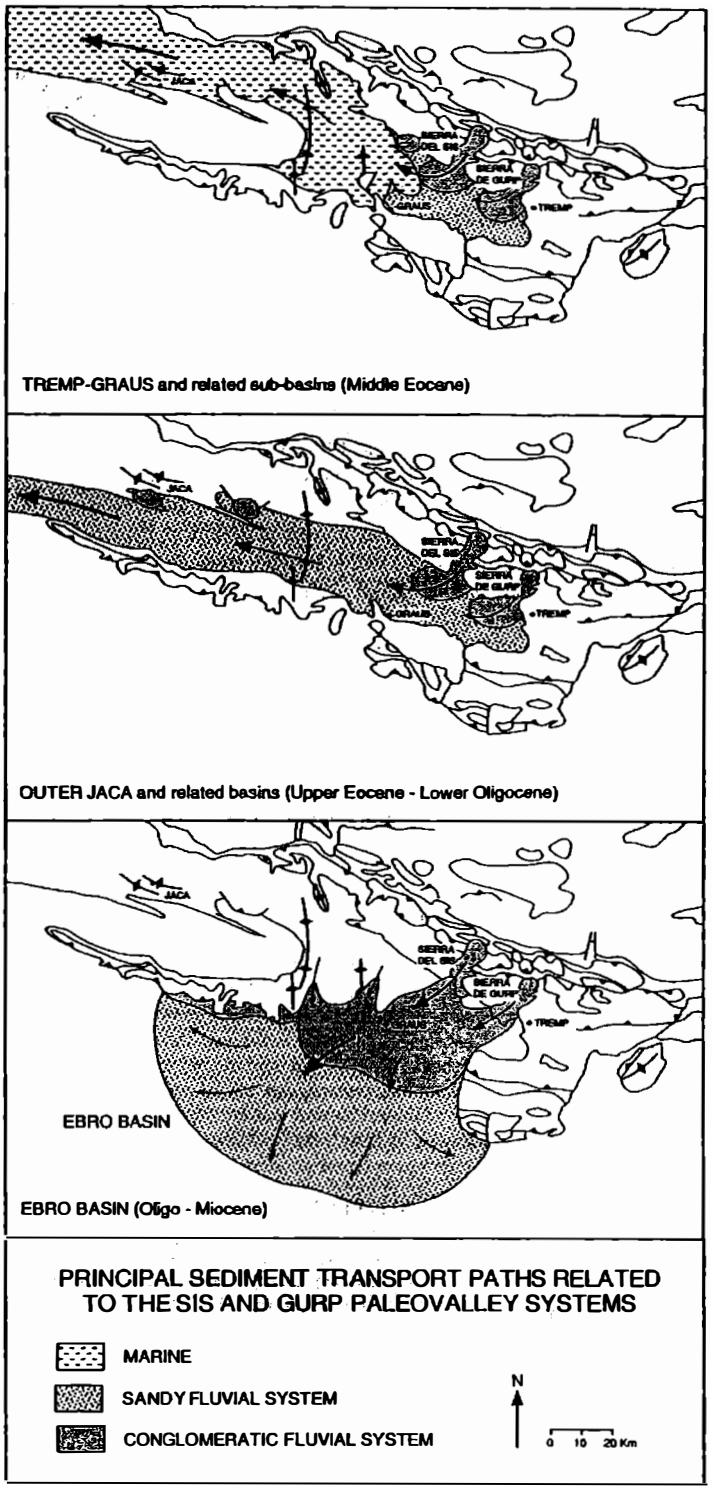

(b)

Figure 4.12 a. Simplified depositional model for fluvial systems and their relationship to mountain belts; b. diagrams showing the role of the Sis and Gurp palaeovalleys as fluvial transfer zones during the depositional history of the Southern Pyrenean and Ebro basins. From Vincent and Elliott, 1997.

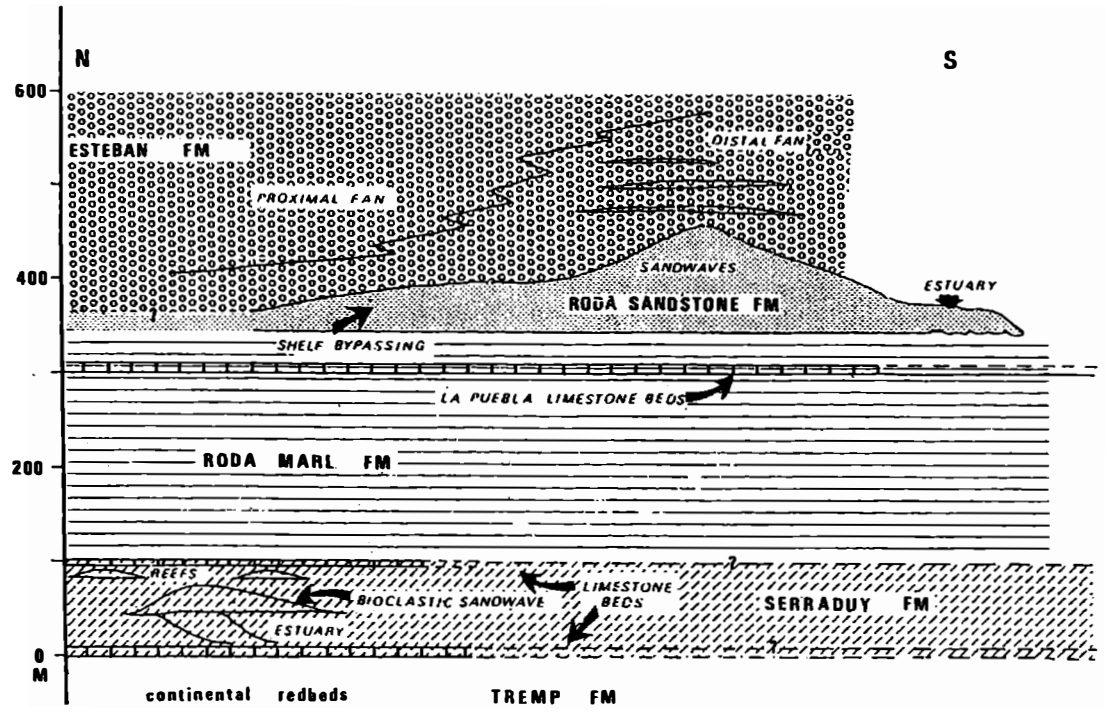

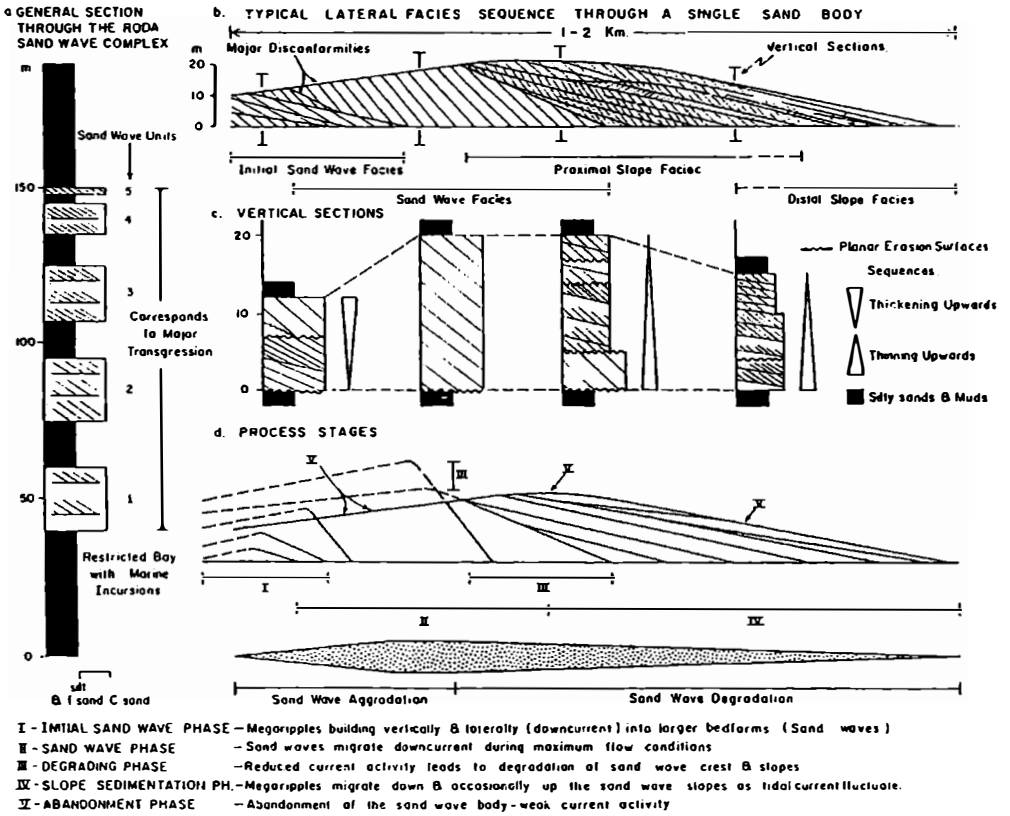

Figure 4.13 Lithostratigraphic cross-section through the Ager Group of the Isabena Valley and an idealised cross-section through a typical sandwave in the Roda Sandstone. From Nio and Siegenthaler, 1978.

Section 5

Field localities in the Ainsa sub-basin

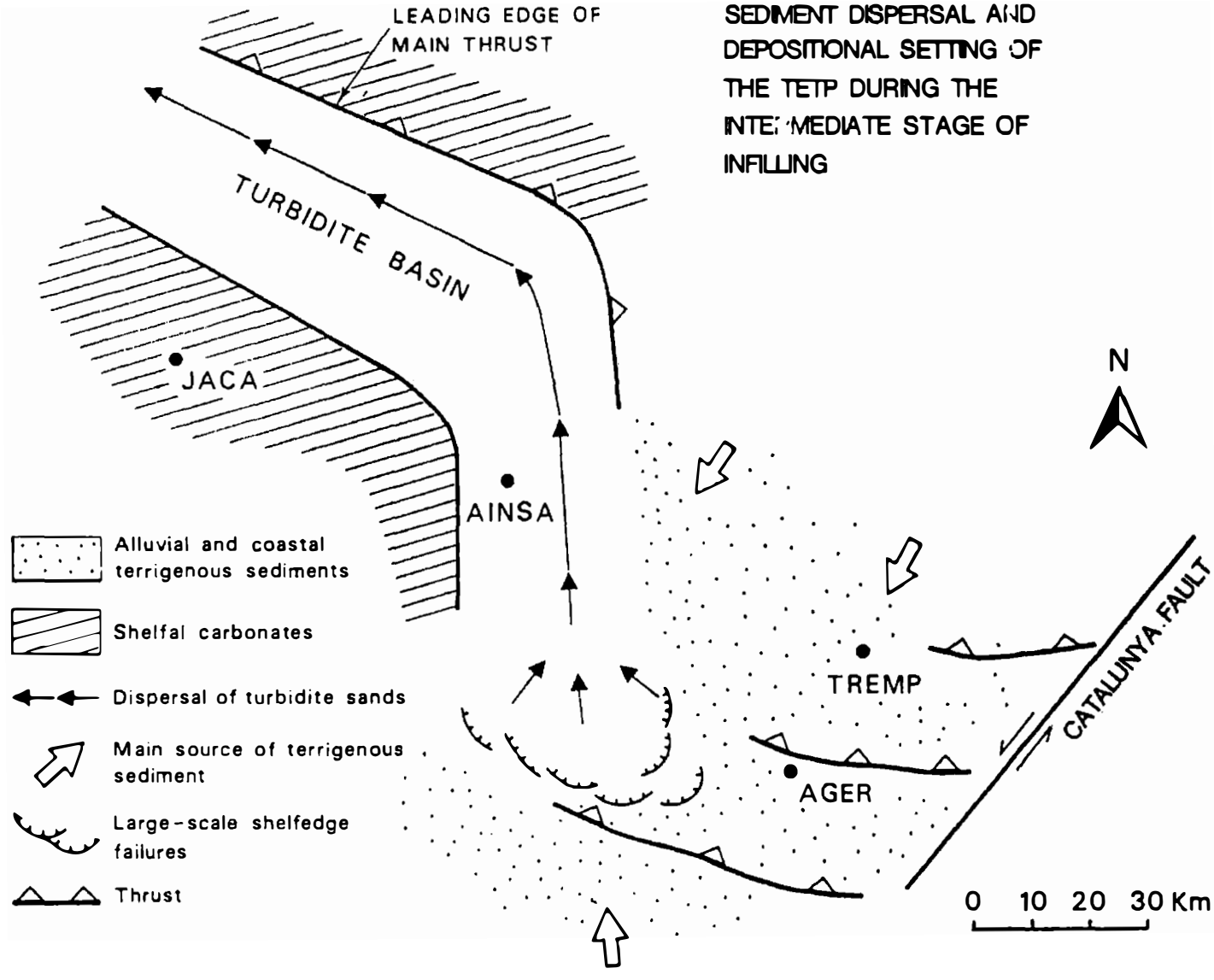

Figure 5.1 Palaeogeograpphic sketch map of the Southern Pyrenean Basin during the intermediate and main stage of basin development. Palaeocurrents and facies distributions suggest that the source of the Hecho Group turbidites was located close to the frontal thrust zone. From Mutti et al., 1985a.

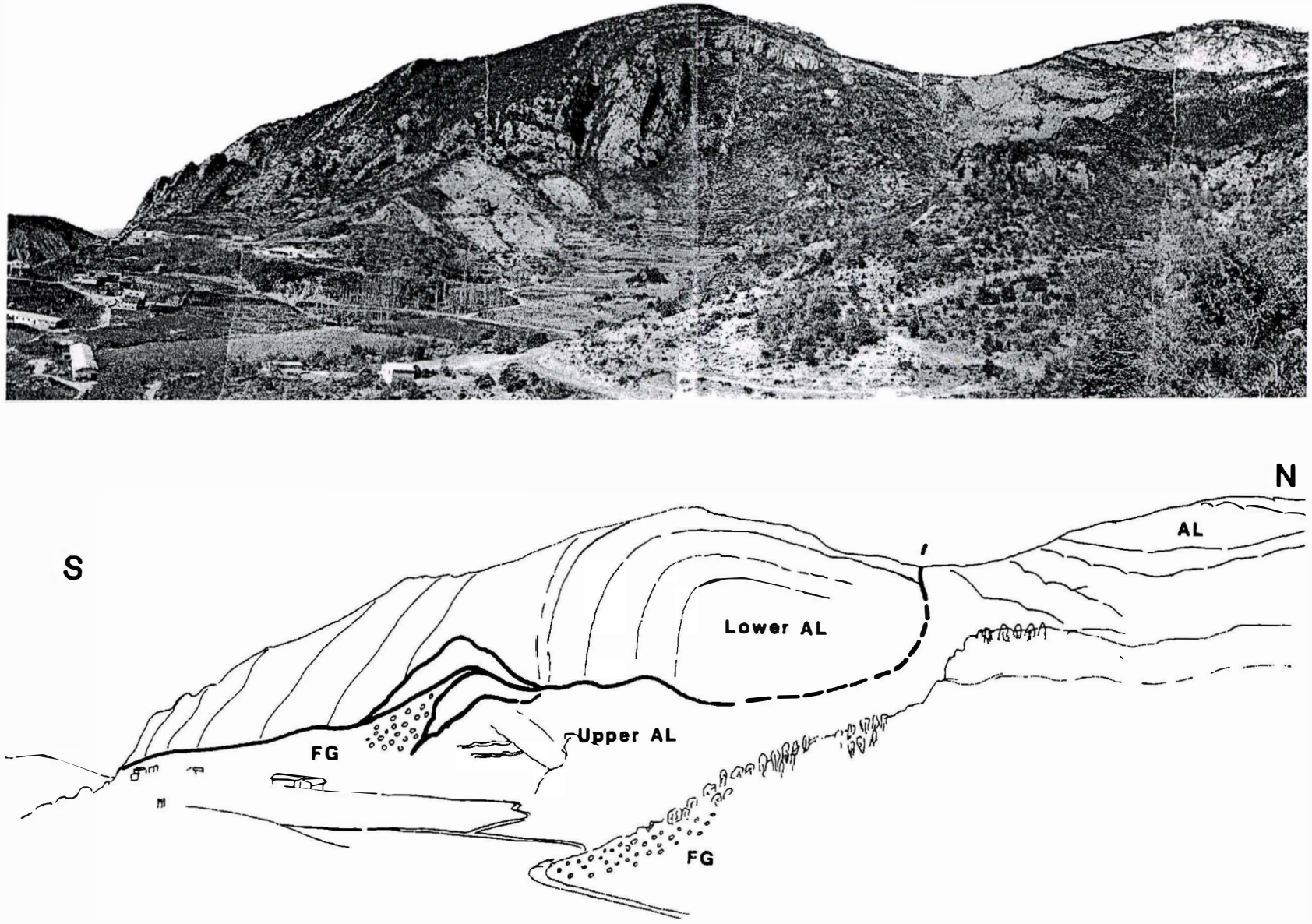

Figure 5.2 The Pena Montanesa frontal ramp anticline of the Cotiella Nappe and associated dextral tear fault (the Foradada Fault). From Mutti *et al.* (1989).

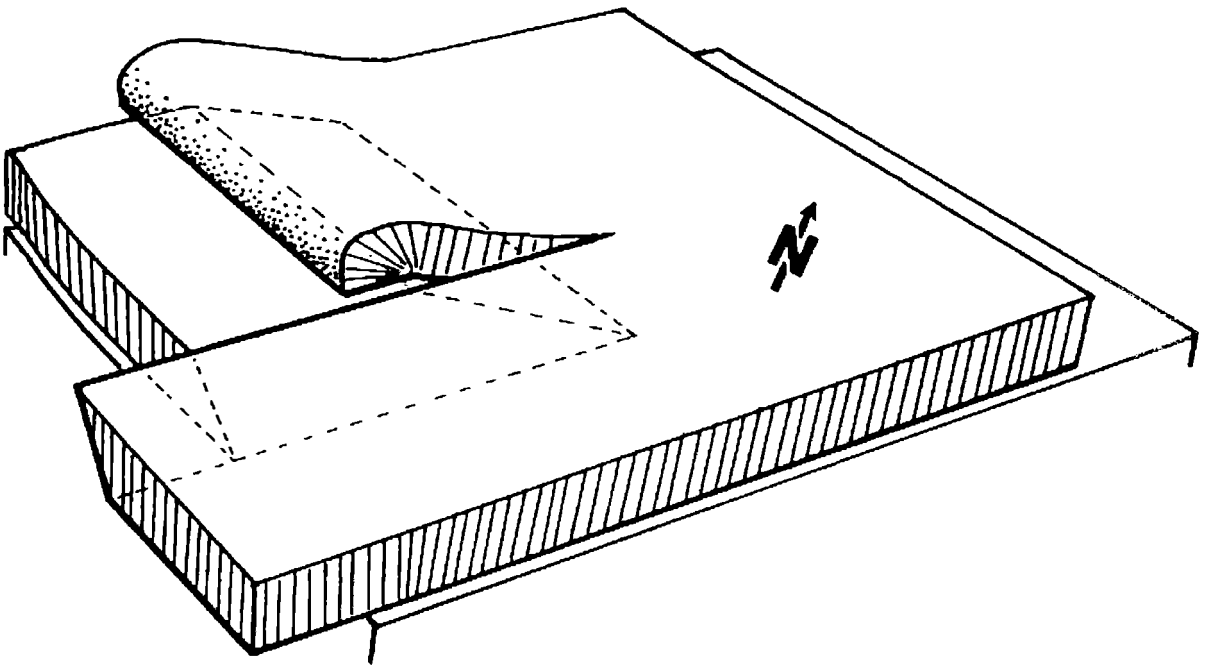

Figure 5.3 The Pena Montanesa frontal ramp anticline of the Cotiella Nappe and associated dextral tear fault. The thrust initiated in Figols time, post Alveolina Limestone Group. (From Mutti *et al.* 1989).

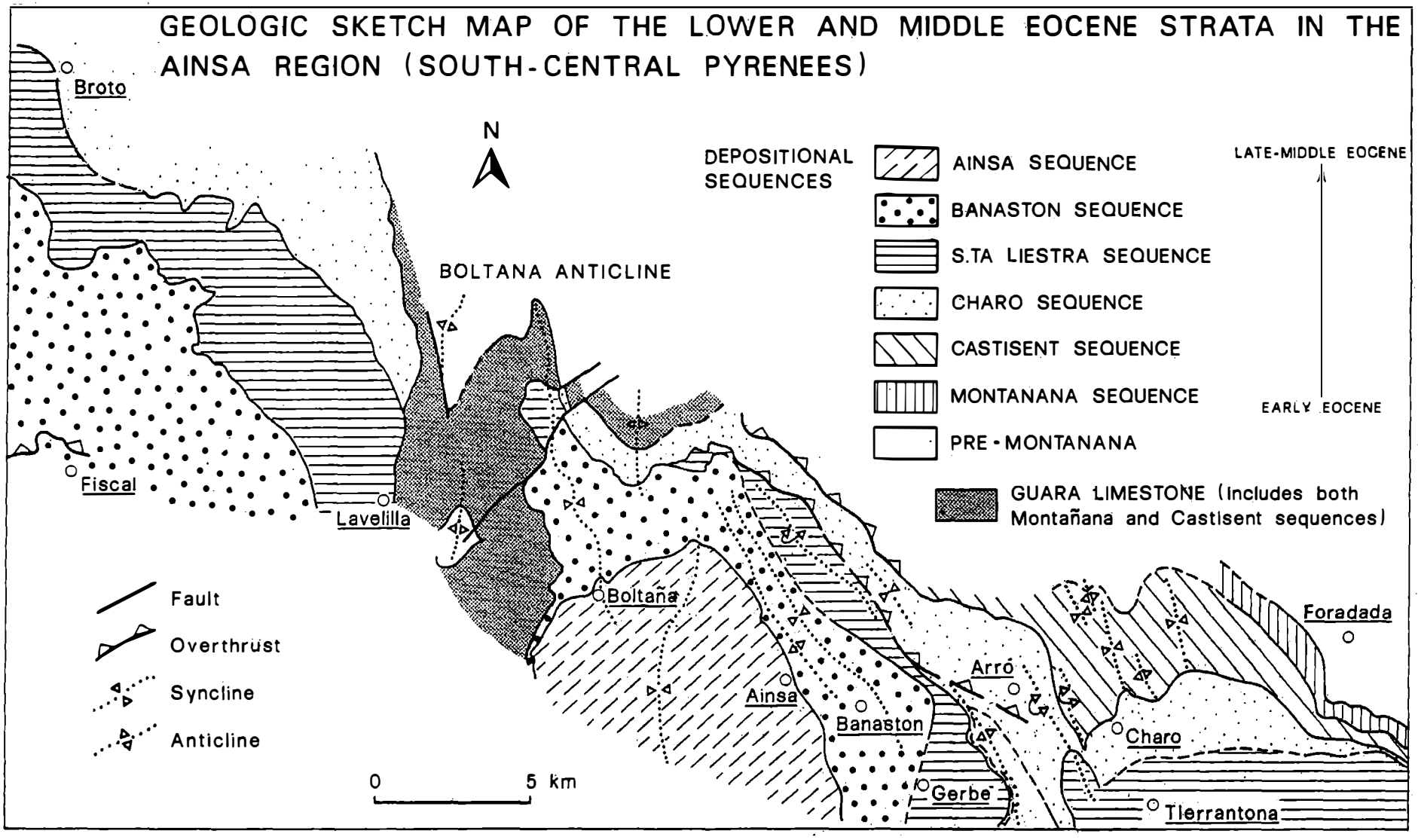

Figure 5.4 Geological sketch map of the depositional sequences in the transitional areas between the eastern and central areas (i.e. around the Ainsa sub-basin). From Mutti *et al.*, 1985a, after Mutti *et al.*, 1985b.

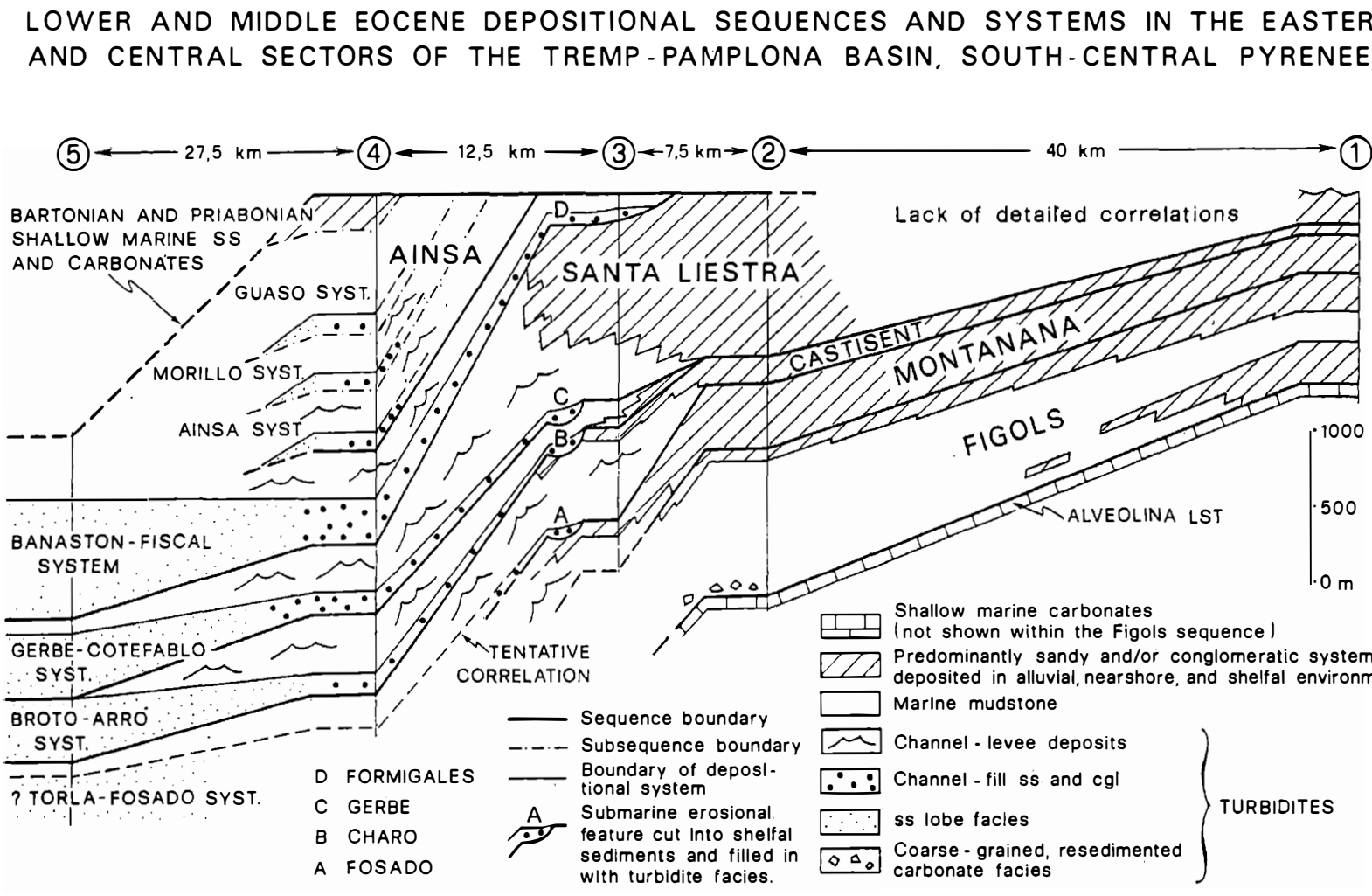

Figure 5.5 Stratigraphic cross-section between the eastern and western sectors of the Southern Pyrenean Basin, showing a proposed correlation between the fluvial and shallow marine sediments in the east and the deep water sediments in the west. After Mutti *et al.*, 1985a

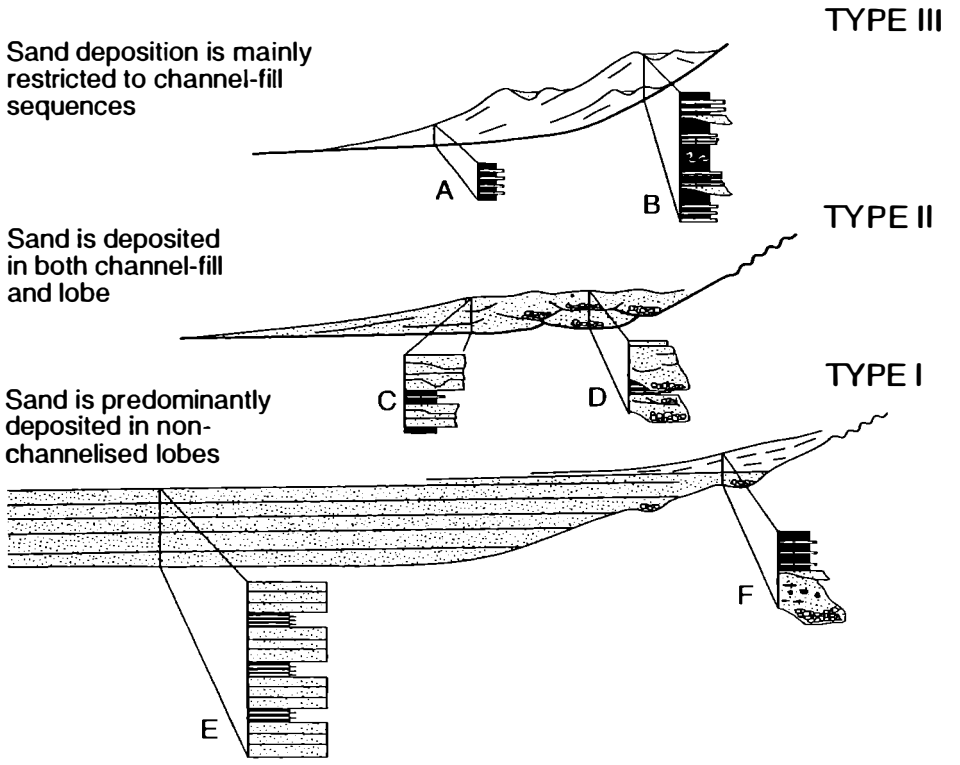

Schematic representation of the three main types of turbidite deposits as characterised by relative amount of and position within the deposit of the sandy component (Mutti & Normark 1987).

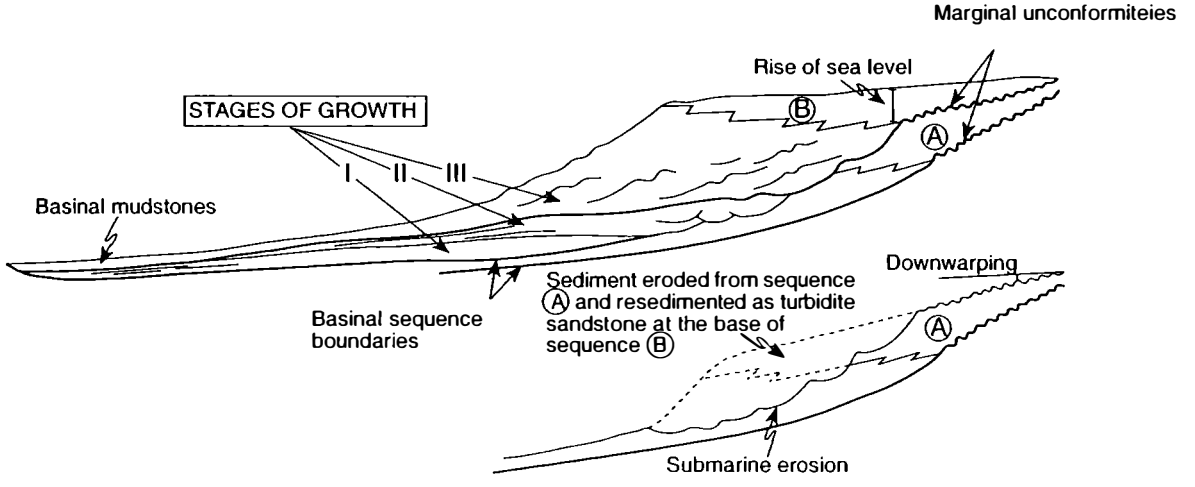

Figure 5.6 Conceptual diagram relating relative sea level changes and different stages of growth of turbidite systems with depositional sequnces developed in elongate basins (Mutti *et al.* 1985).

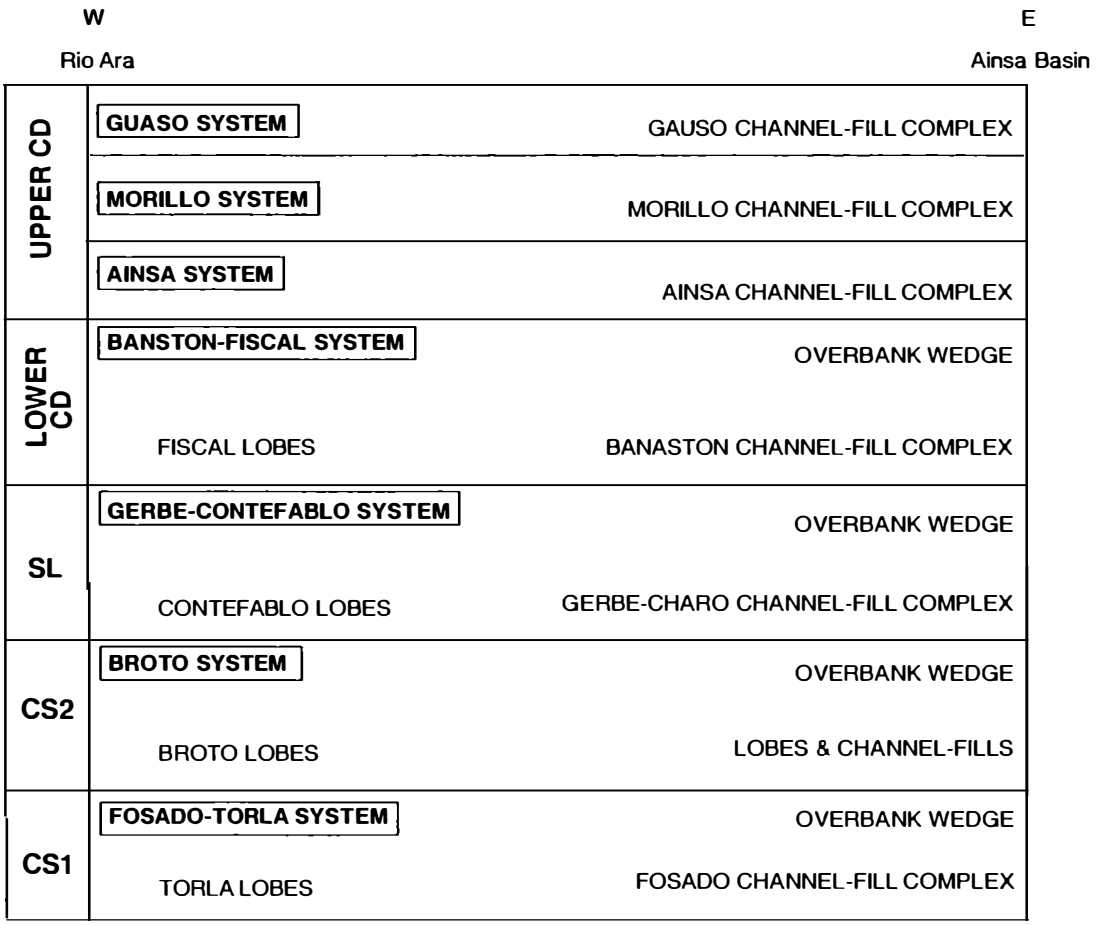

Figure 5.7 Distribution of turbidite systems in the stratigraphy of the Temp-Pamplona Basin, in the Río Ara and Ainsa areas (after Mutti *et al.* 1989).

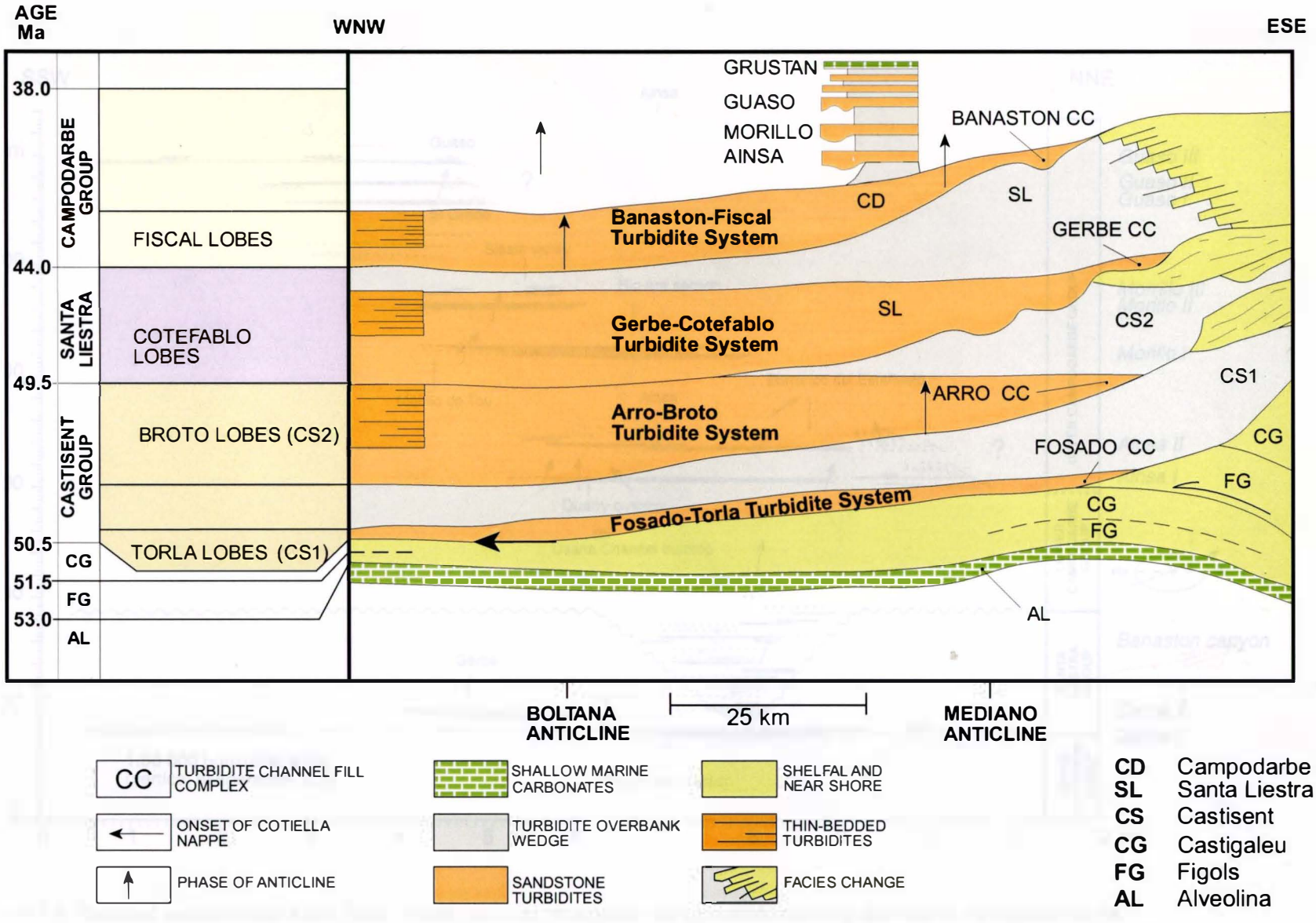

Figure 5.8 Depositional systems of the Eocene Hecho Group (after Mutti *et al.* 1989).

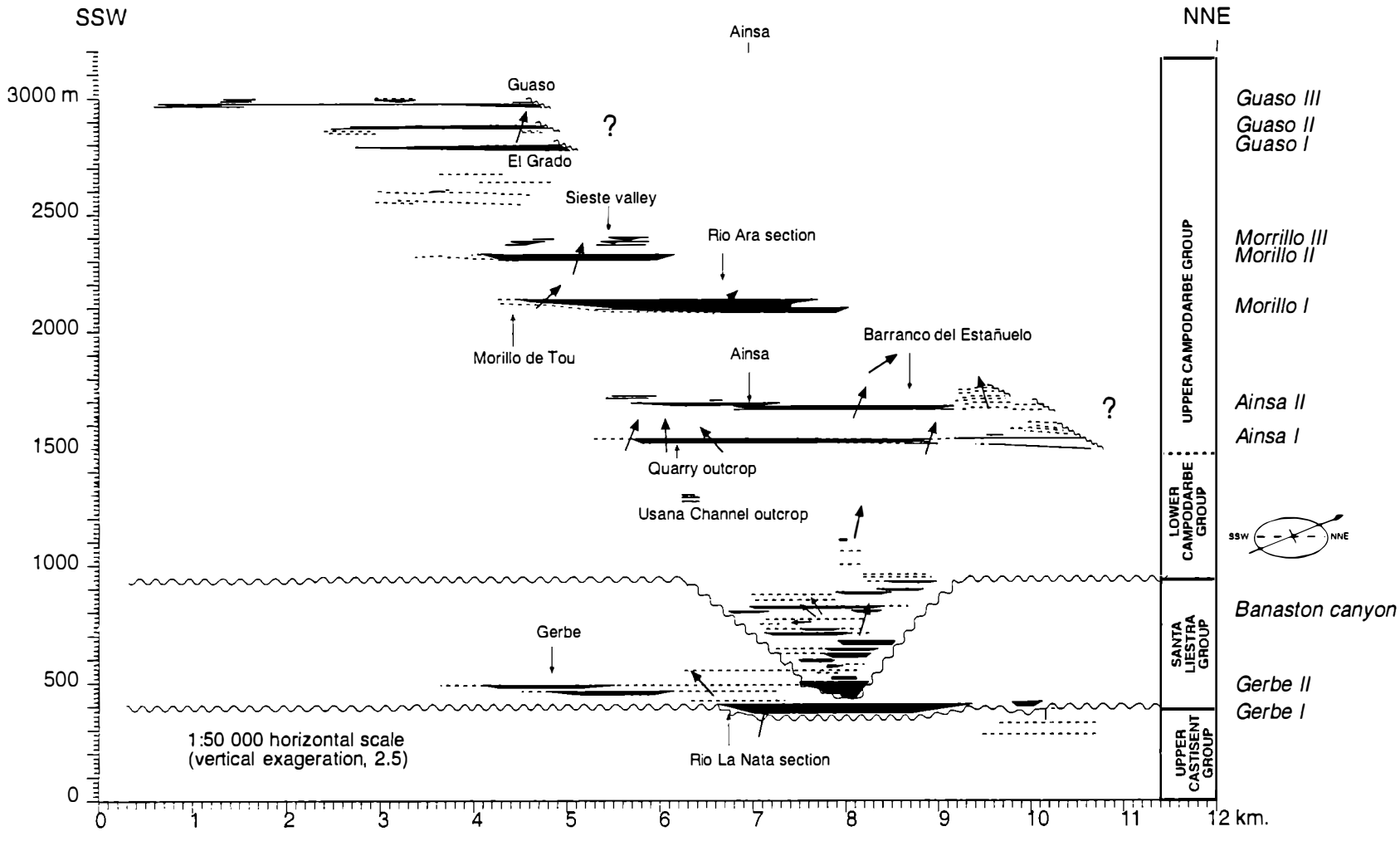

Figure 5.9 Restored section of the Ainsa Basin (based on aerial photograph interpretation) showing the vertical distribution of the channel-levee complexes. Palaeocurrent arrows are orientated with respect to the orientation of the section (SSW-NNE), *i.e.*, vertical arrows indicate palaeocurrent direction towards WNW (Clark 1994). Regional unconformities are those mapped by Mutti *et al.* (1989).

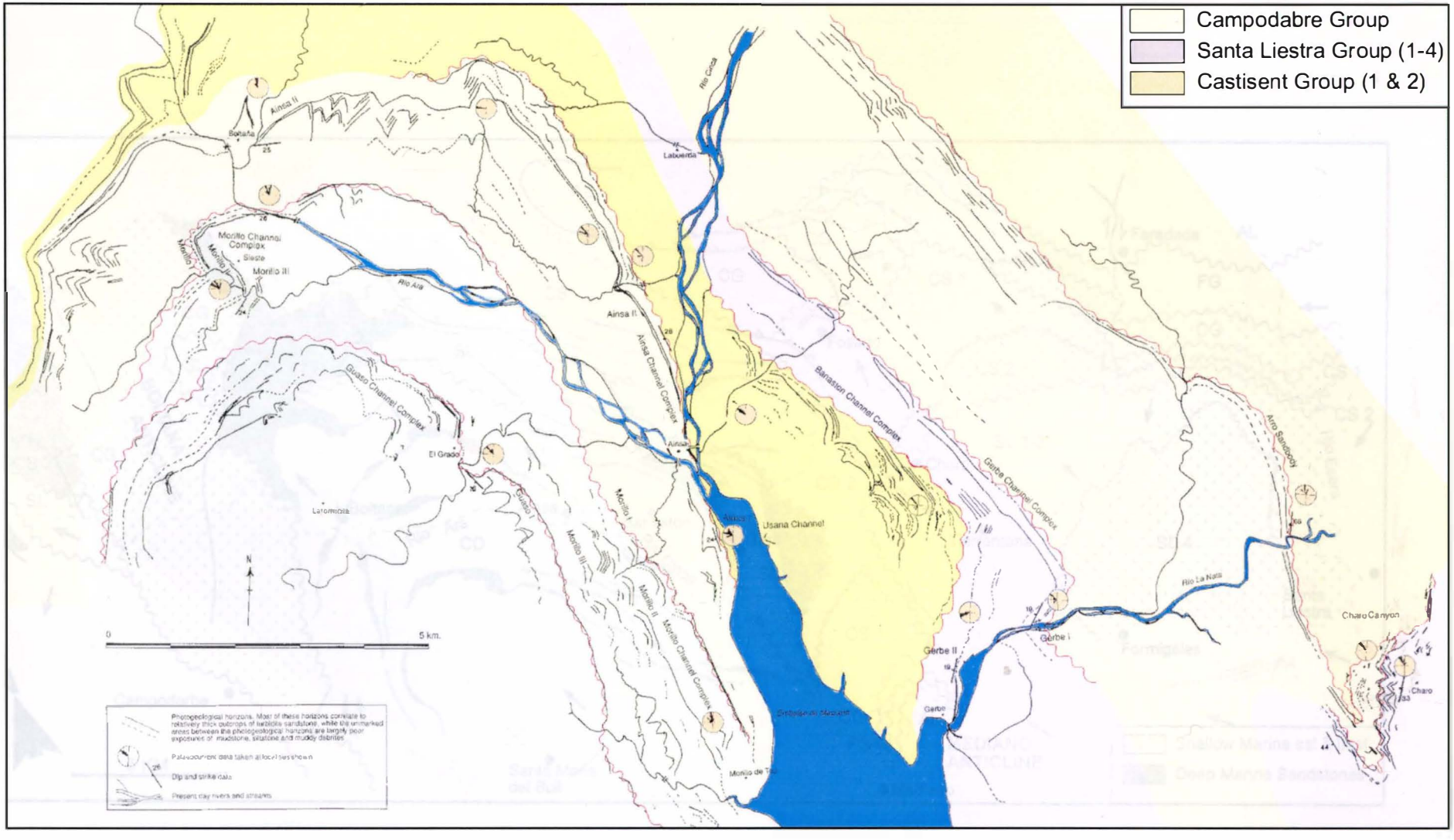

Figure 5.10 Detailed map (from aerial photograph interpretation) of sandstone bodies in the Santa Maria del Bruil Syncline (Clark 1994).

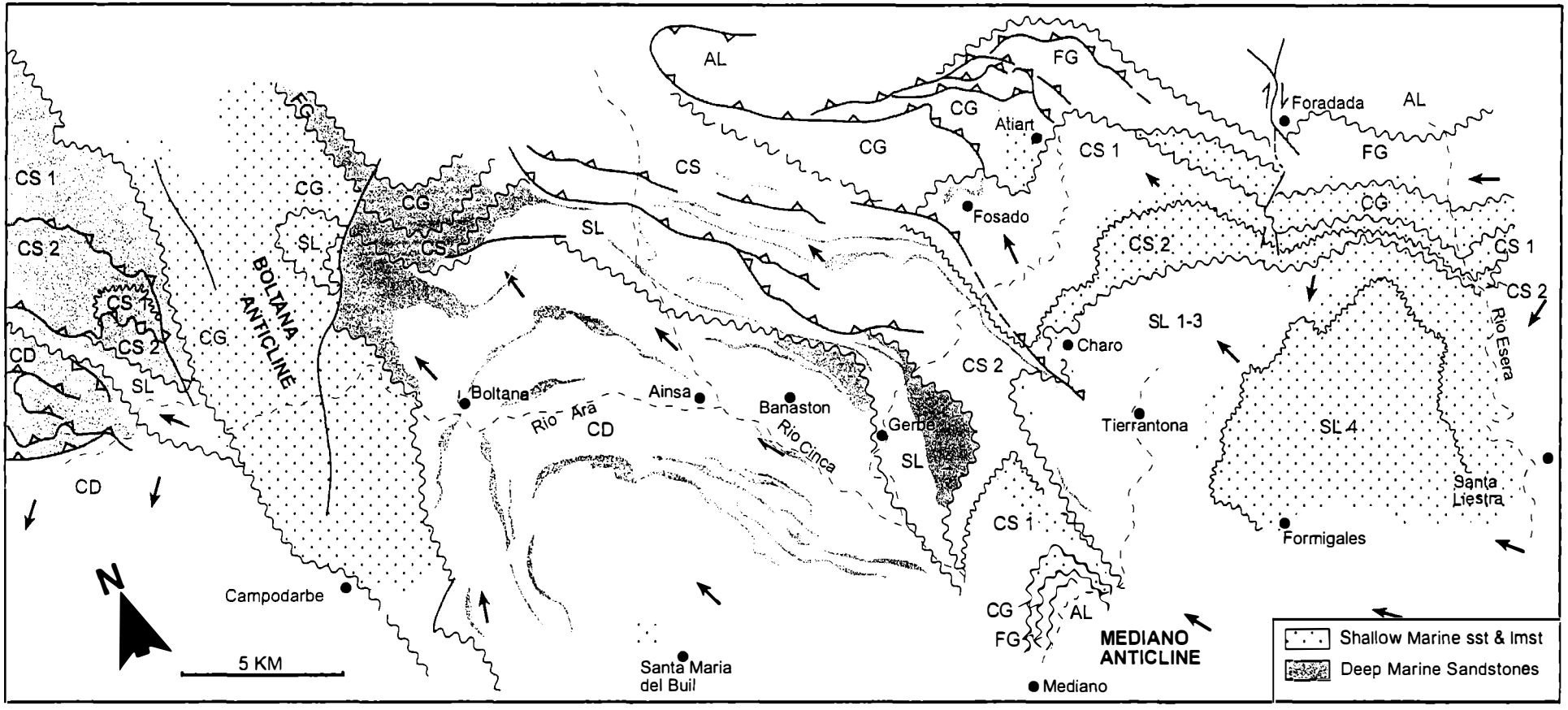

Figure 5.11 Palaeoenvironments of the Central Sector of the Tremp-Pamplona Basin (after Mutti *et al.* 1989).

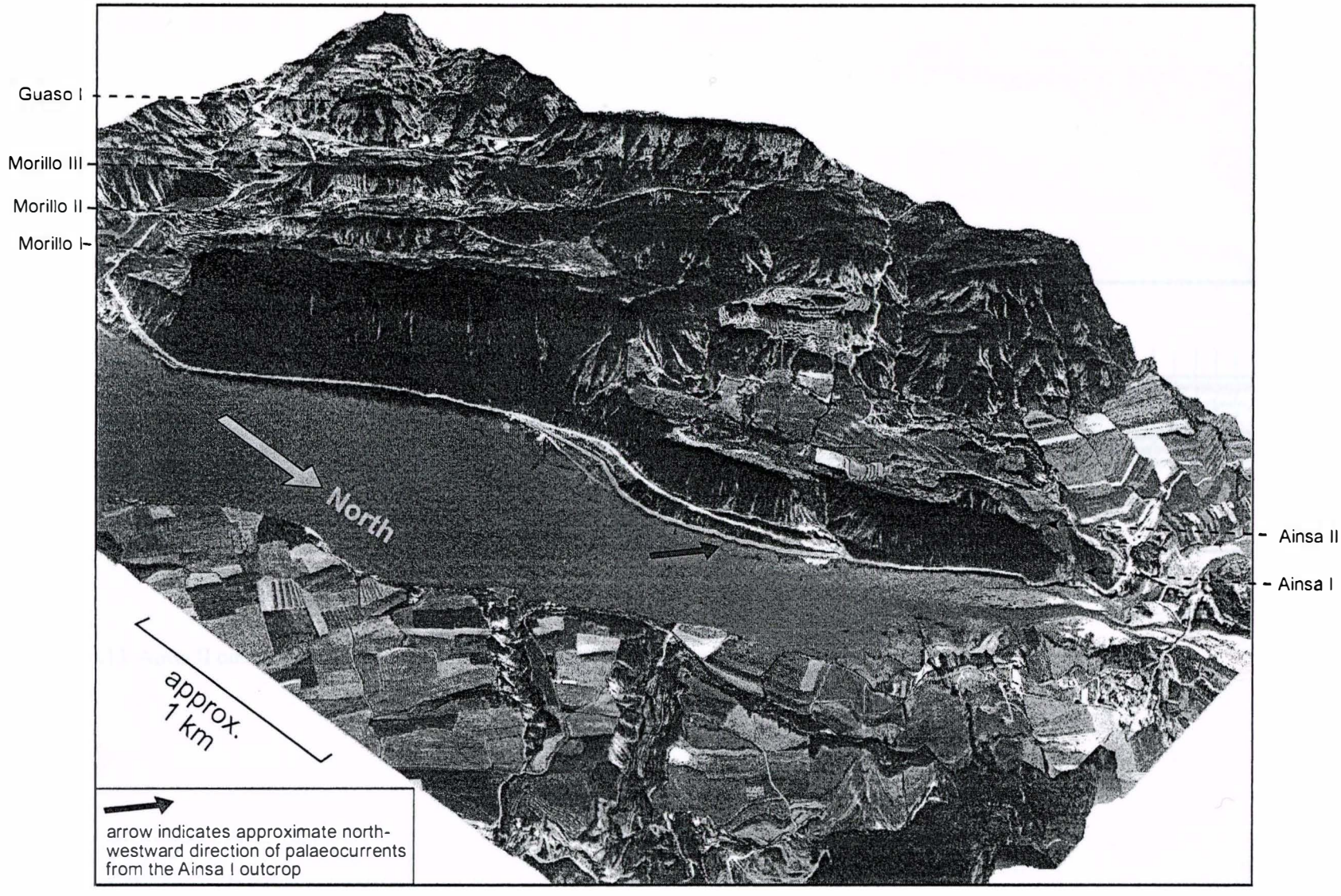

Figure 5.12 3D perspective view of the Upper Campodarbe deposits, south of Ainsa. The image was created using digital photogrammetric techniques from a pair of stereo aerial photographs. The digital photogrammetric software produces an orthorectified image which can be draped over the digital elevation model (DEM). This image can then be viewed from any angle, in this case, approximately along the dip of the beds. Furthermore, the resulting dataset can be used to make accurate measurements in 3D. Image courtesy of Jamie Pringle (Heriot-Watt University).

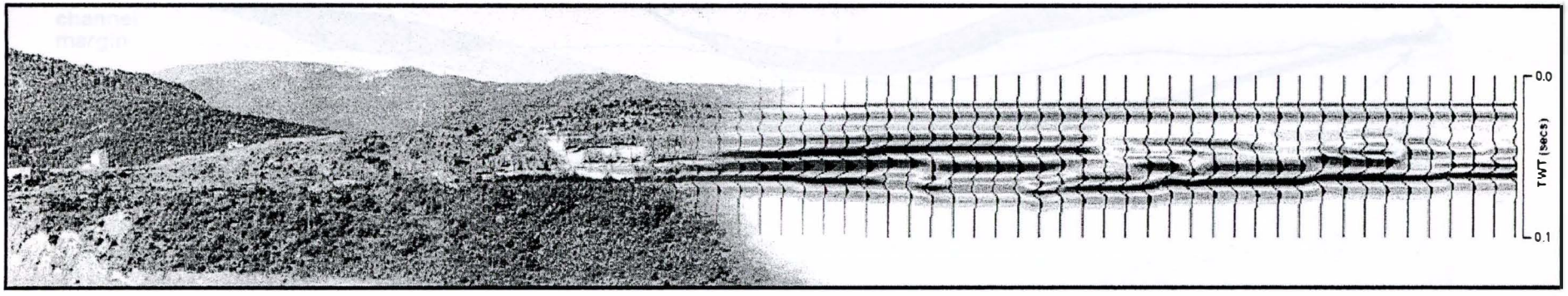

Figure 5.13 Ainsa II outcrop superimposed with high resolution synthetic seismic image (dominant Ricker wavelength = 78 Hz)

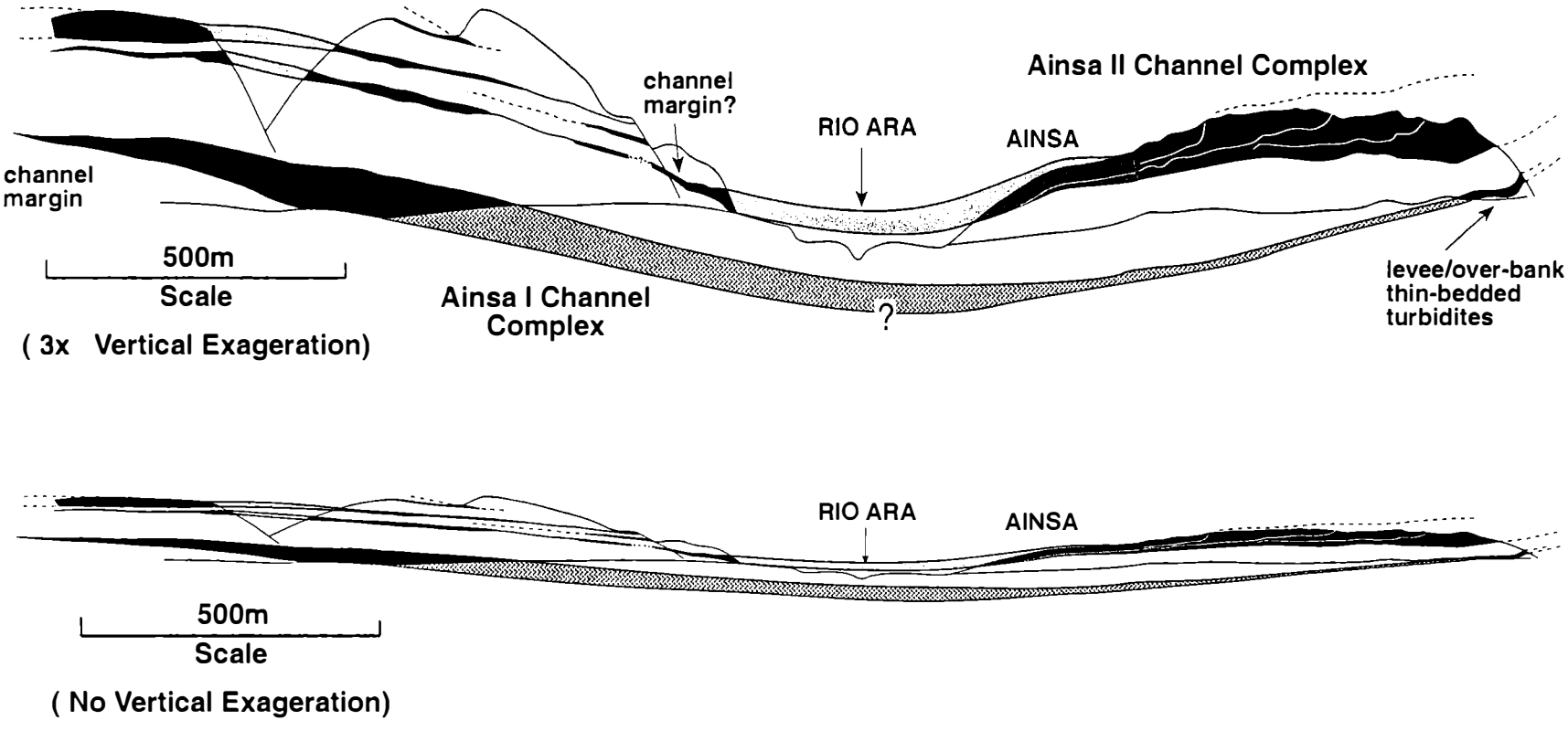

Figure 5.14 Interpretation showing the relationship between the Ainsa I Channel Complex north and south of Ainsa, and the overlying Ainsa II Channel Complex (Clark 1994).

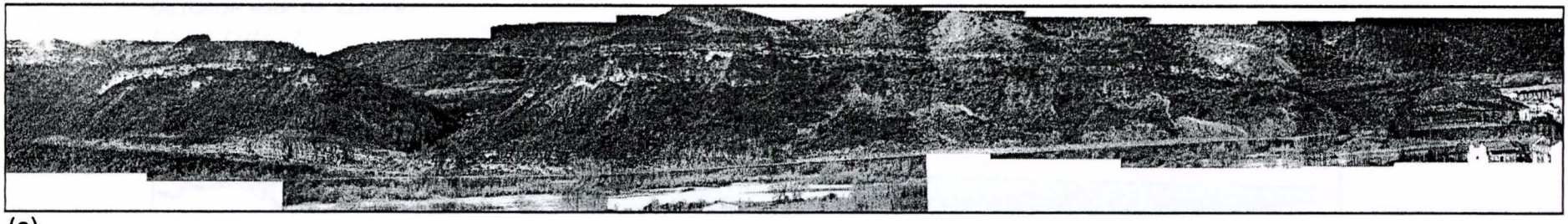

(a)

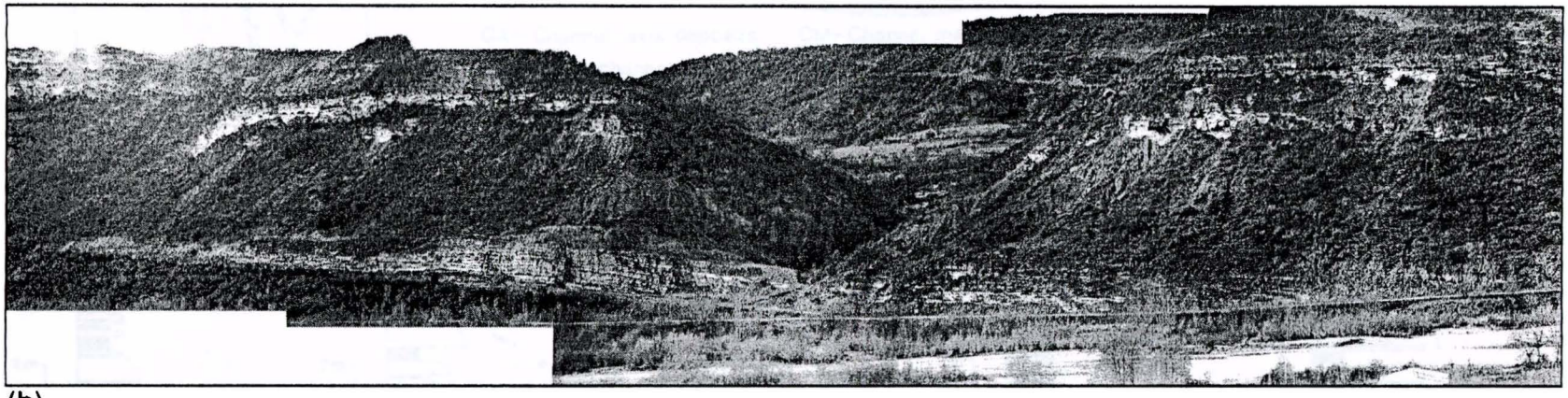

(b)

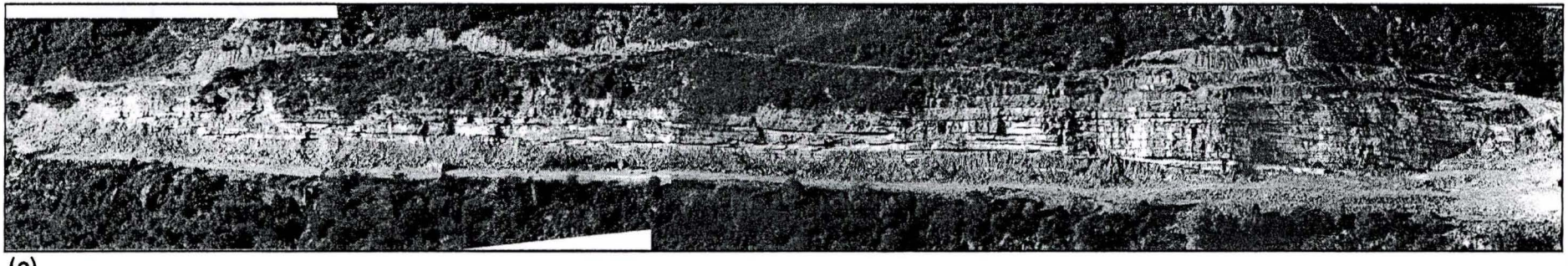

(c)

Figure 5.15 Photographs of the Ainsa I and Ainsa II channel complexes, south of Ainsa. (a) Field of view approximately 1.5 km, showing the relationship between the Ainsa I Channel (quarry exposure) and Ainsa II stacked channel complex (sandbodies at top of the main slope). (b) Detail of above, showing pinch-out of sands in the Ainsa I Channel. (c) Aerial photomontage of the Ainsa I Channel (quarry exposure) showing detailed bed architecture.

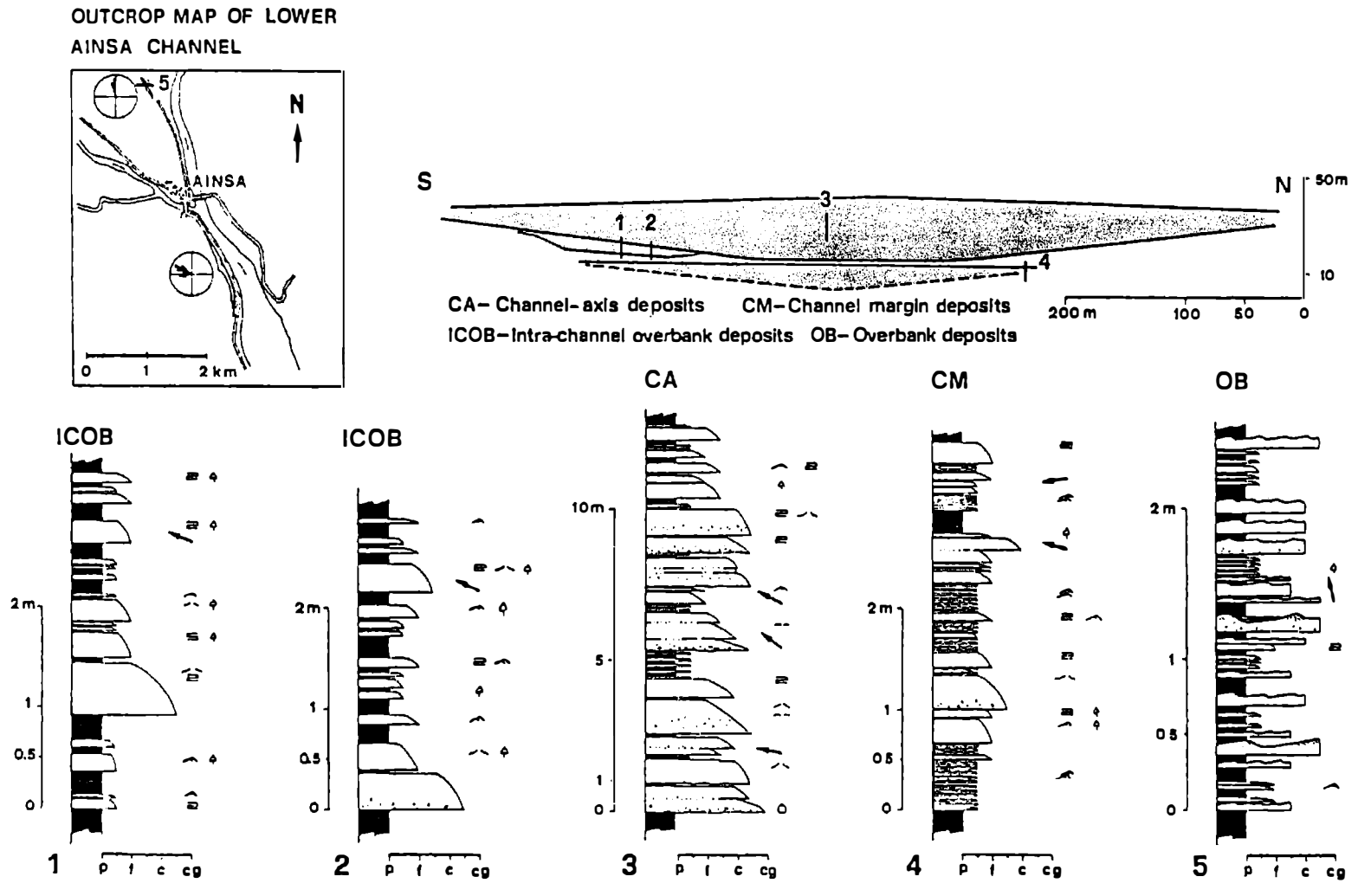

Figure 5.16 Diagramatic cross section of the Ainsa I Channel and facies samples from channel-fill and overbank deposits. (Mutti *et al.* 1985).

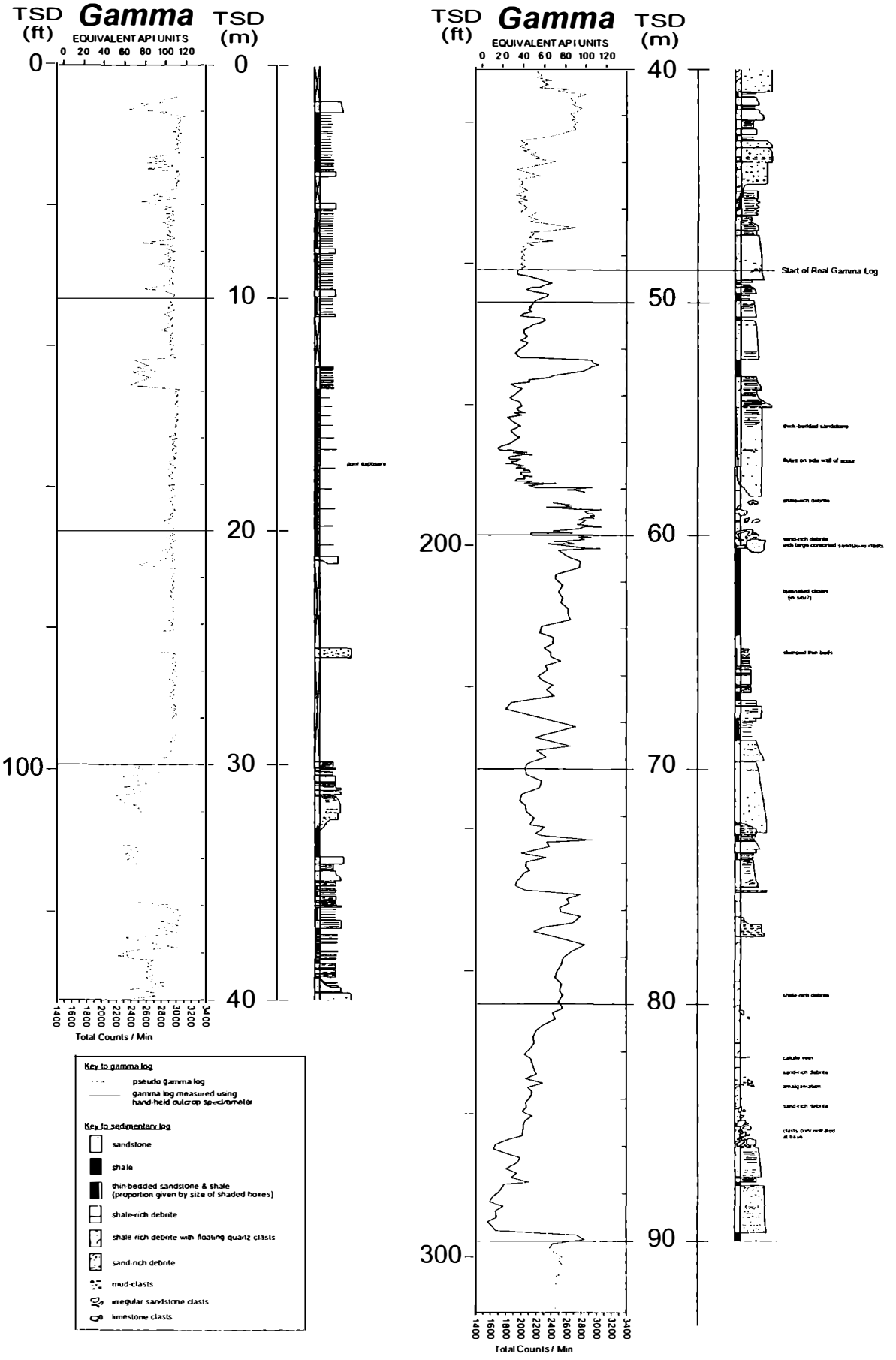

Figure 5.17 Sedimentary log with combined pseudo and measured gamma logs from the basal part of the Morillo Channel Complex, Rio Ara section. The measured gamma log was taken with an outcrop gamma spectrometer along the path.

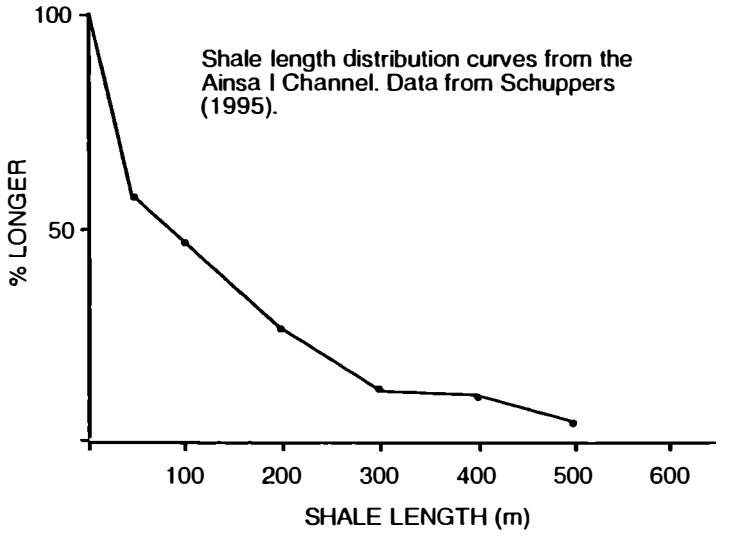

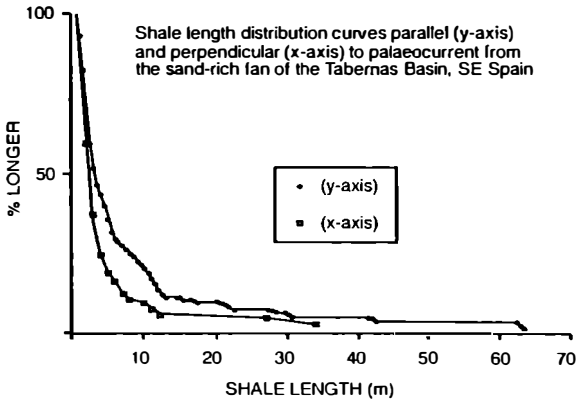

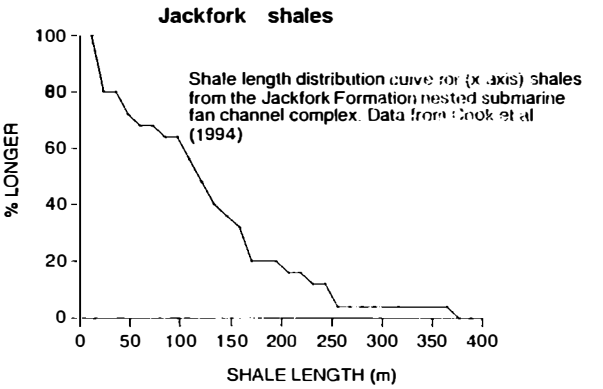

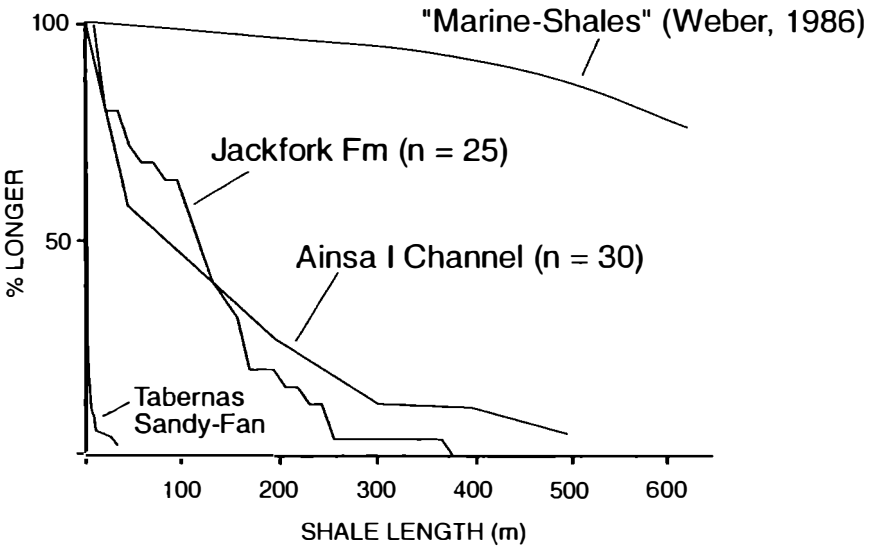

Figure 5.18 Comparative plot of shale length distribution curves from the Ainsa I Channel Complex (Schuppers 1995), Tabernas Basin (Kleverlaan & Cossey 1993), the Jackfork Formation Big Rock Quarry Channel Complex (Cook et al. 1994), and the "marine-shales" curve of Weber (1986).

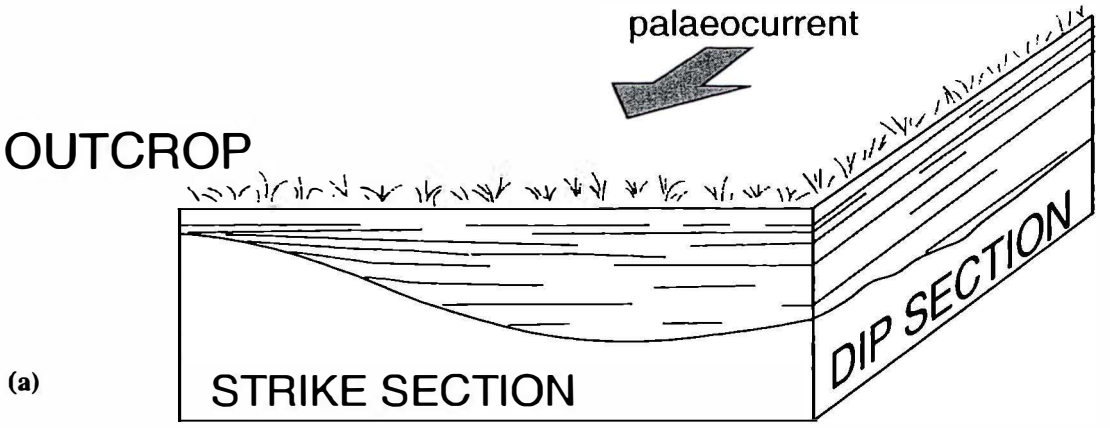

(a)

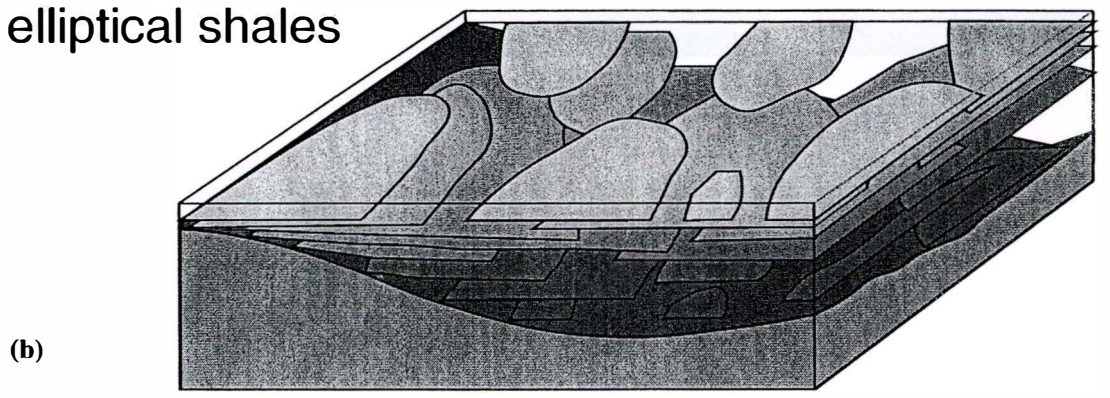

(b)

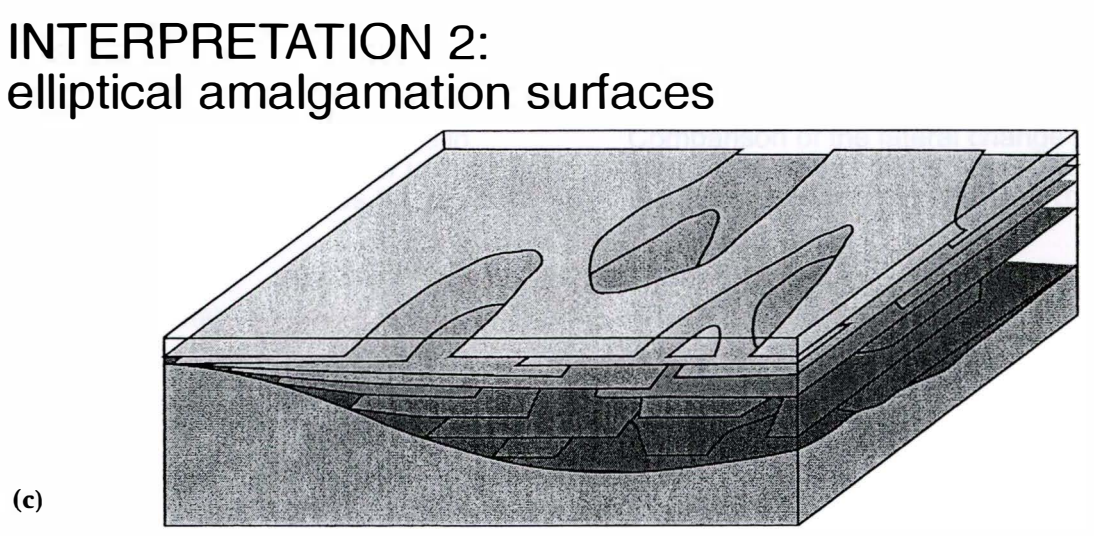

(c)

Figure 5.19 Schematic diagram to illustrate the three dimensional shape of discontinuous shales in turbidite sequences. (a) Discontinuous shales can be observed and measured in both dip and strike outcrop sections. (b) & (c) 3D interpretations of discontinuous shale shape. Both interpretations honour the outcrop data presented in (a), however, it is more likely that these shales are sheet-like with sub-elliptical or channel shaped holes as shown in (c).

Internal Channel-Sandbody Arctitecture & Lateral Net:Gross Changes at Channel Margins

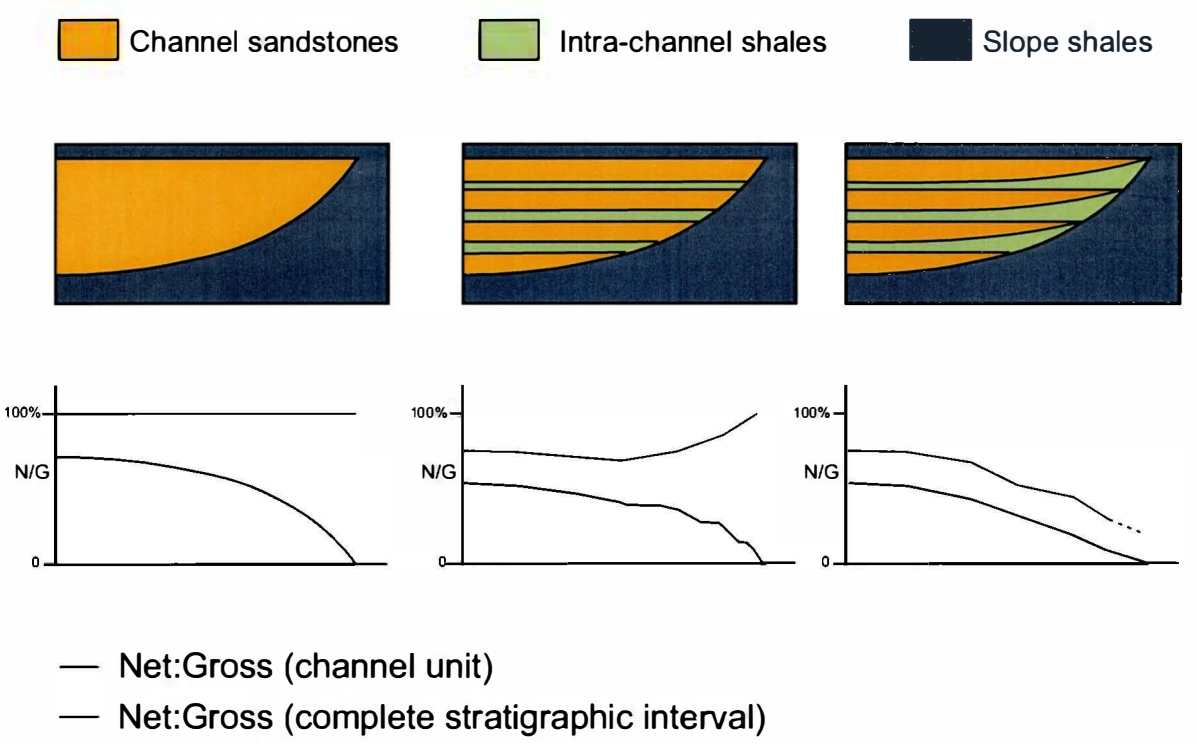

Comparison of the lateral change in Net:Gross ratio of the *channel unit* for the three channel scenarios (a), (b) & (c)

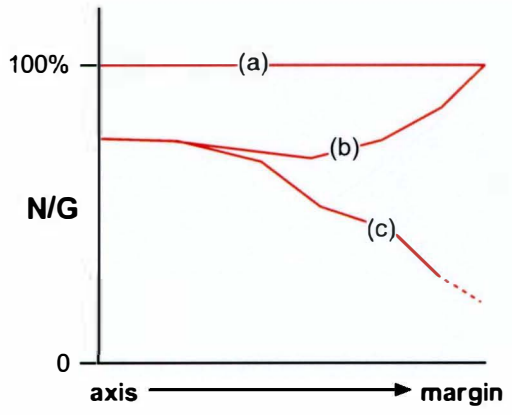

Comparison of the lateral change in Net:Gross ratio of the *stratigraphic unit* for the three channel scenarios (a), (b) & (c)

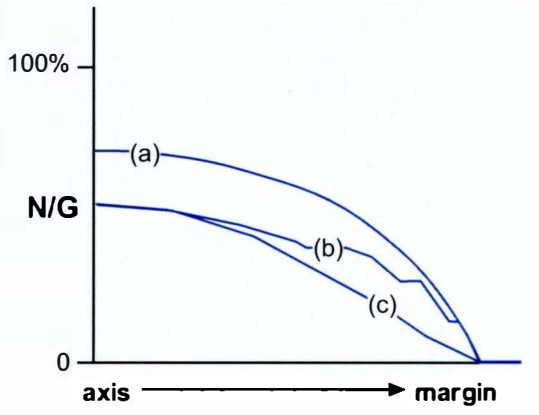

Figure5.20 Schematic diagrams indicating possible lateral changes in channel architecture and net:g

Section 6

Field localities in the Jaca sub-basin

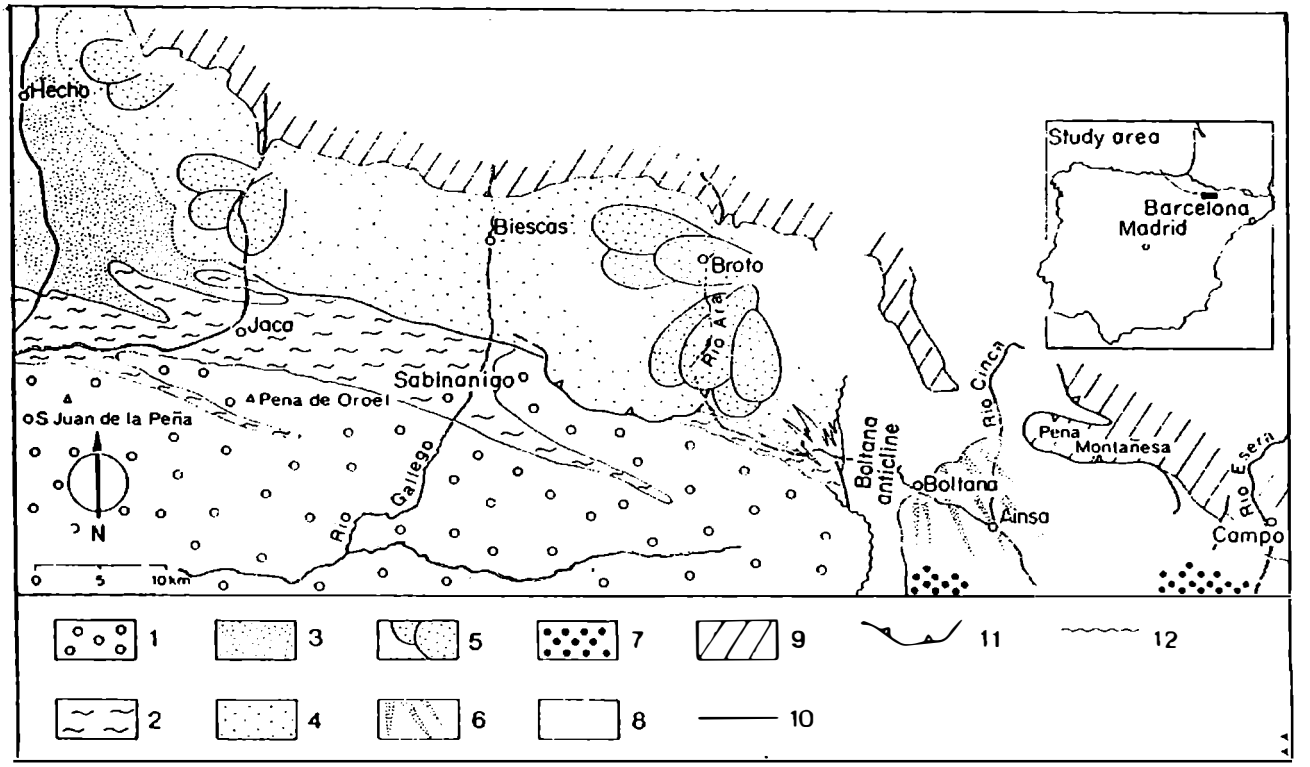

Figure 6.1 Sketch map showing the distribution of turbidite facies associations in the Eocene Hecho Group, between the Esera and Aragon Valleys. From Mutti, 1977.

Key

1. Fluvial and underlying deltaic and nearshore deposits (U Eocene to Oligocene)
2. Pamplona Marl (shelf and slope deposits - Cuisian to M. Eocene)
3. Hecho Group - basin plain deposits
4. Hecho Group - fan fringe and outer fan deposits
5. Hecho Group - outer fan deposits, with abundant sandstone lobes
6. Hecho Group - inner fan deposits
7. Hecho Group - deltaic deposits
8. Hecho Group - mudstone laterally between the deltaic deposits (7) and the inner fan sediments(6)
9. Pre-Cuisian rocks
10. Fault
11. Low-angle thrust
12. Unconformity

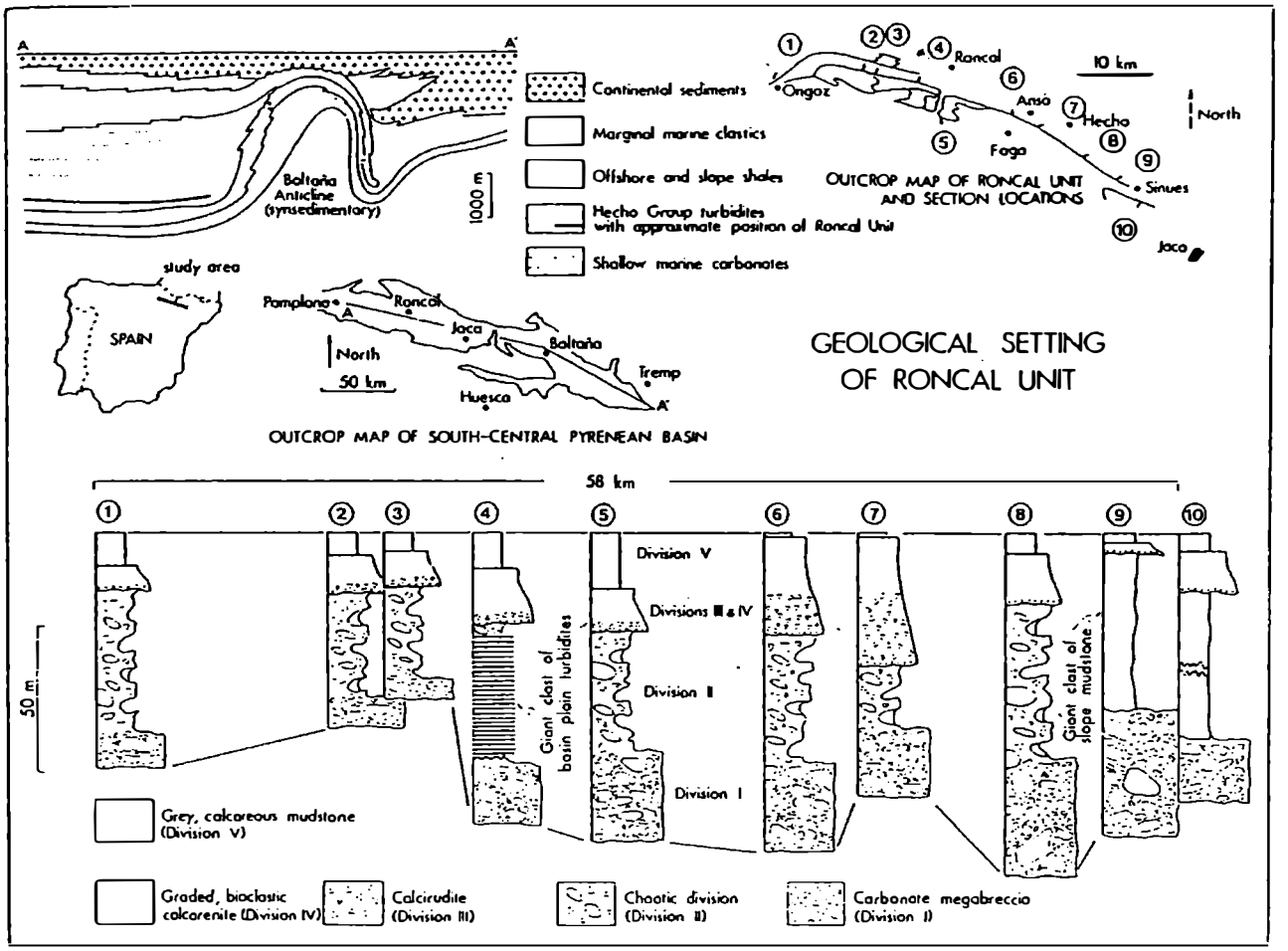

Figure 6.2 Geological setting of the Roncal Unit, a laterally extensive 'megabed'. The schematic section through the south-central Pyrenean Basin (upper left) shows the depositional setting. The outcrop map (top left) shows the extent of the unit and the location of the measured sections shown on the correlation panel below. From Johns *et al.*, 1981.

Section 7

Field localities in the Ebro Basin

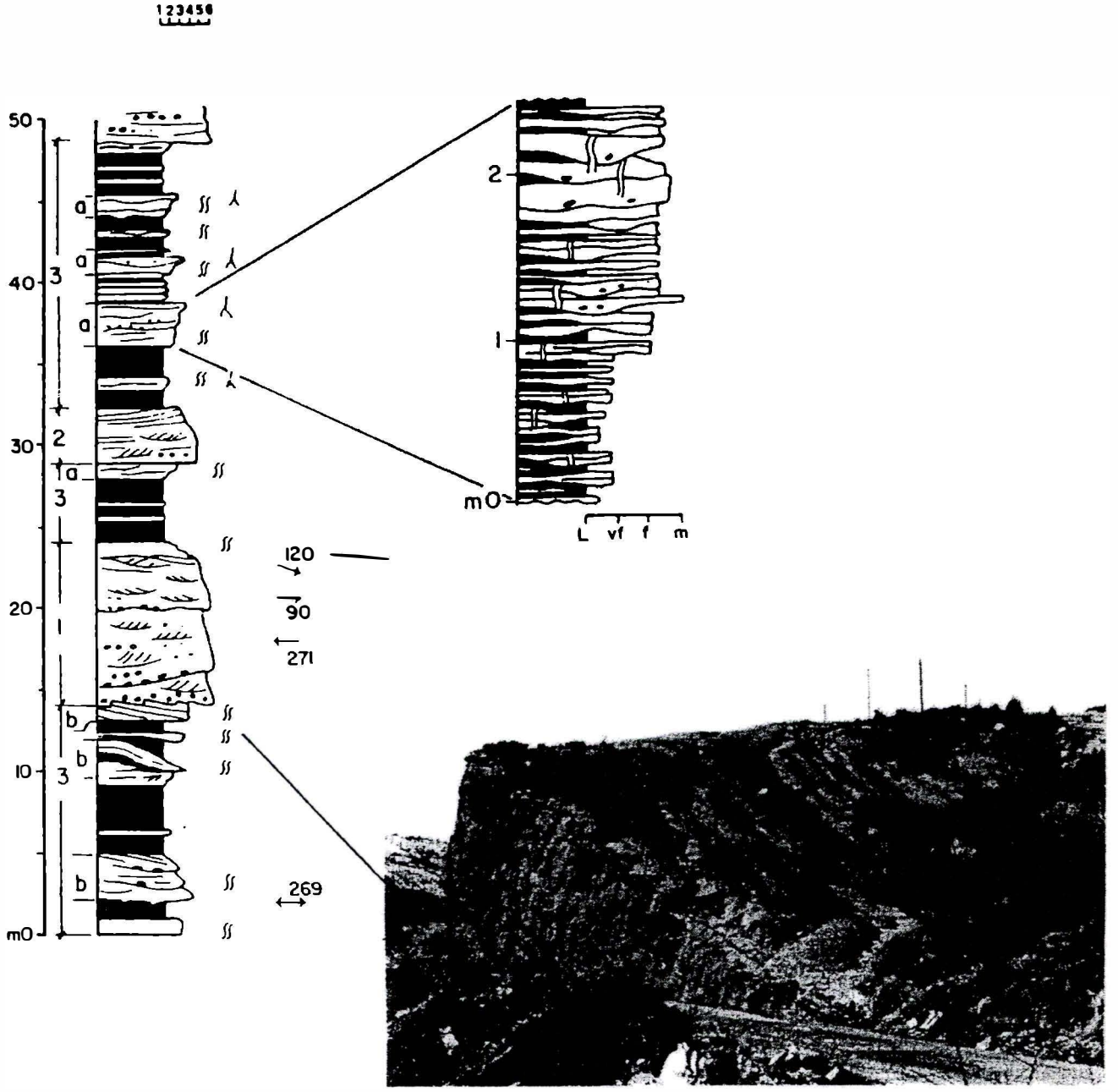

Figure 7.1 Channel sandbody composed of three stacked point bars, exposed near the Puerto de Monrepos. The top of the sandbody displays curved ridges which have been interpreted as scroll bars. From Friend *et al.*, 1981.

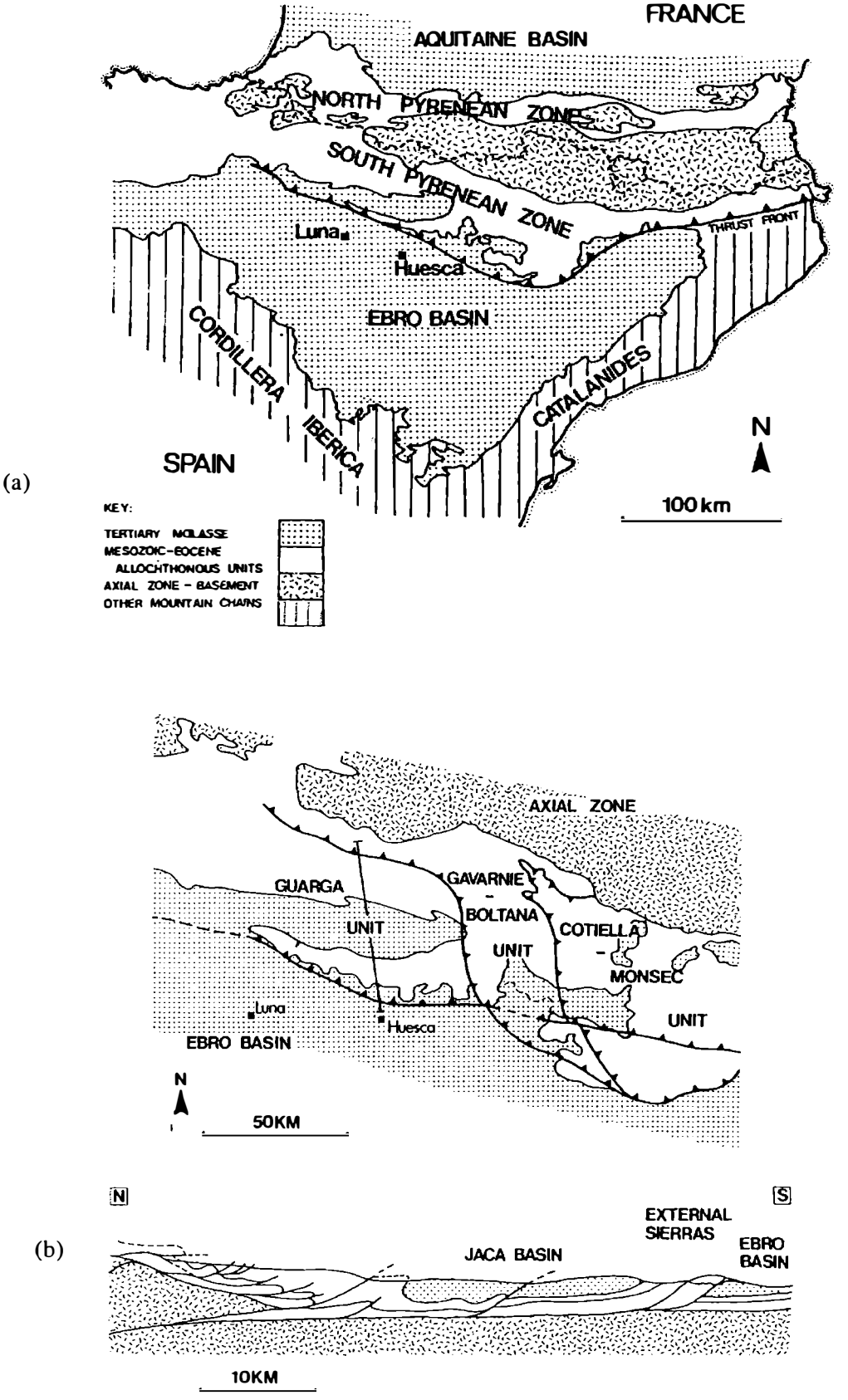

Figure 7.2 (a) Sketch geological map showing the position of the Ebro Basin. (b) Map and cross-section of the Ebro Basin. From Hirst and Nichols, 1986.

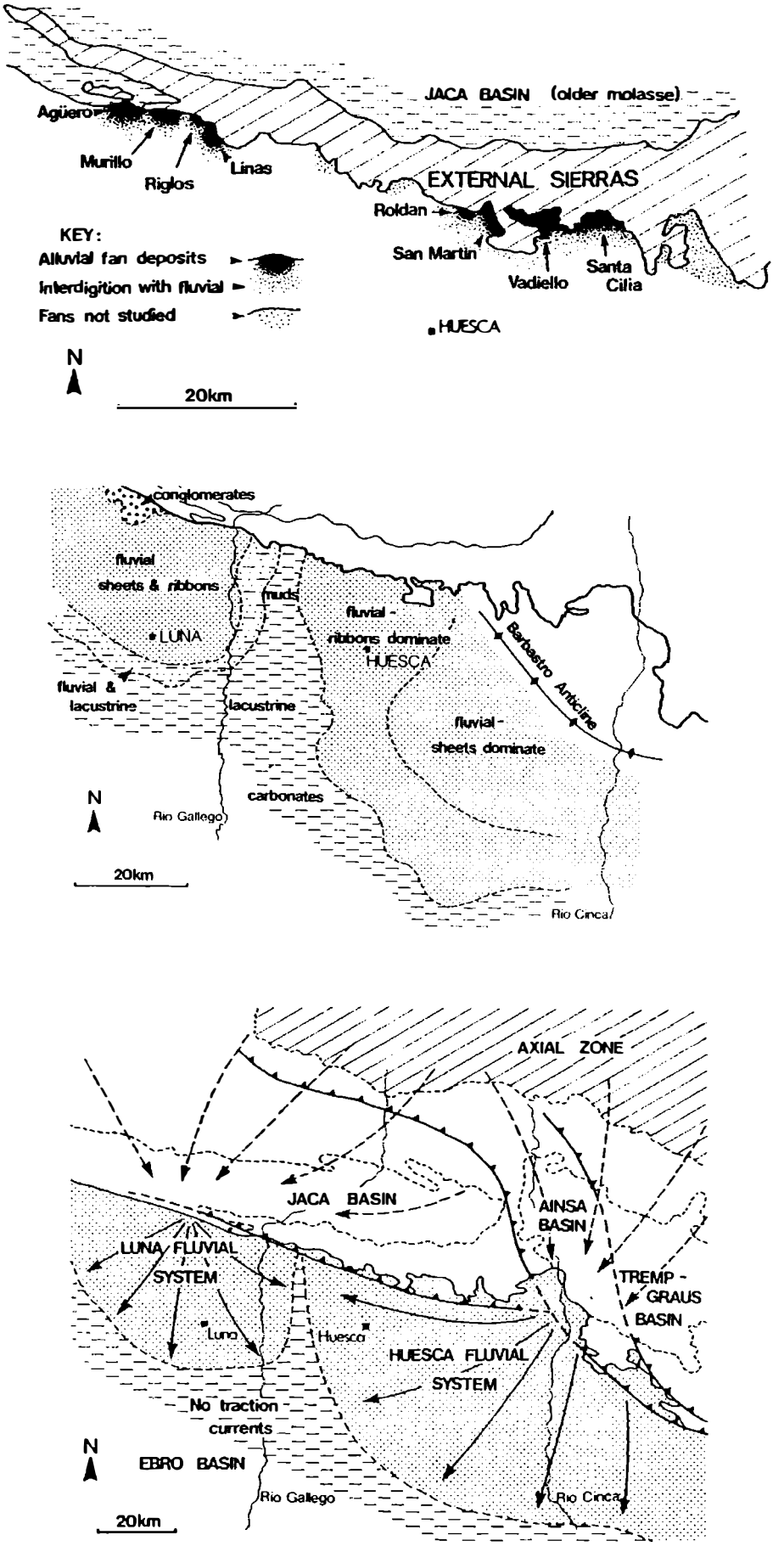

Figure 7.3 Maps showing the presence of many small, coarse grained alluvial fans along the External Sierras, and the location of the larger Luna and Huesca 'fans' (fluvial distributary systems). From Hirst and Nichols, 1986.

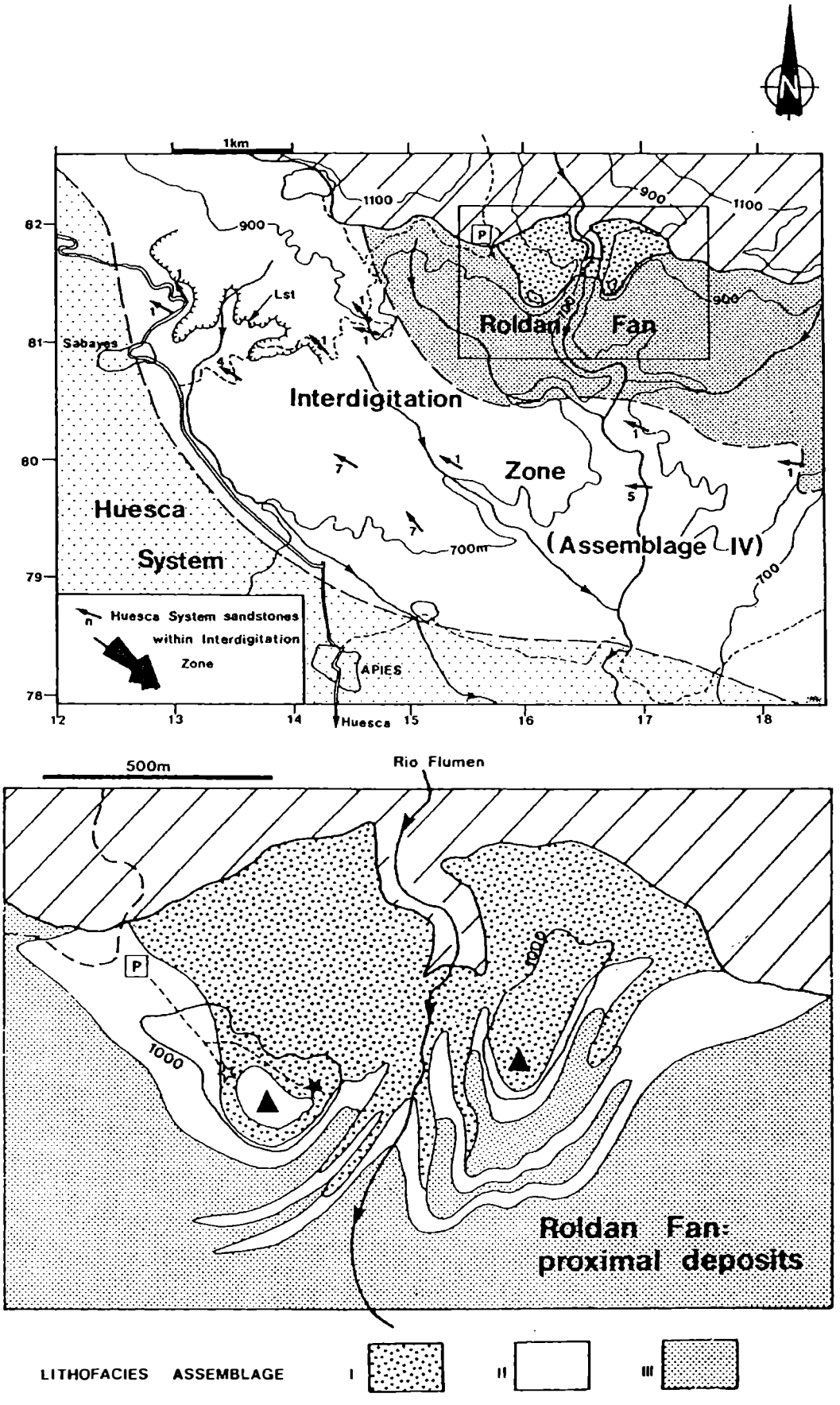

Figure 7.4 Facies disribution in the proximal part of the Roldan Fan, and the relationship of the fan with the larger Huesca system. From Friend *et al.*, 1989.

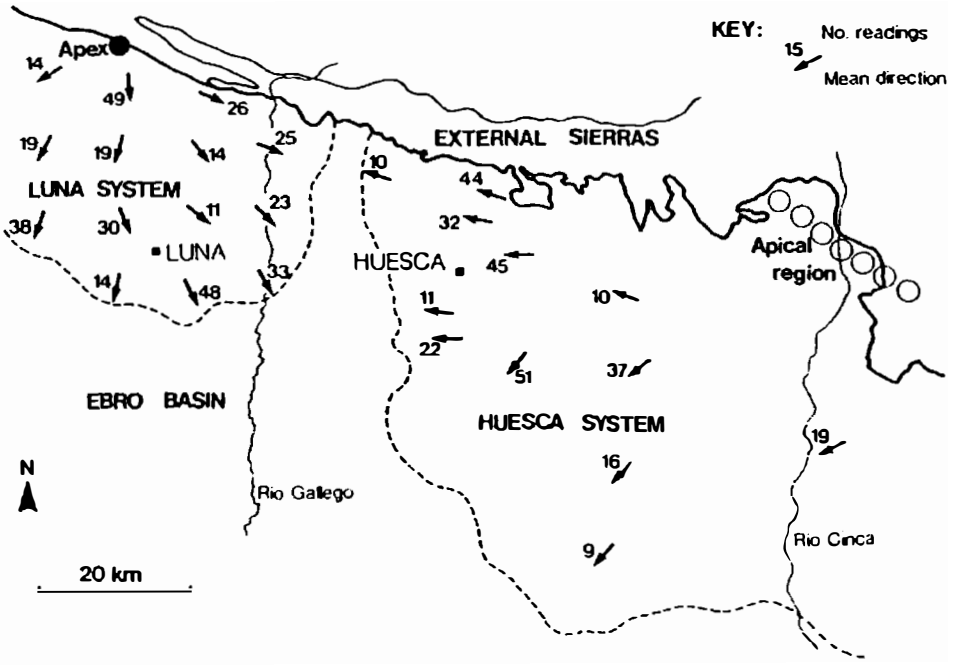

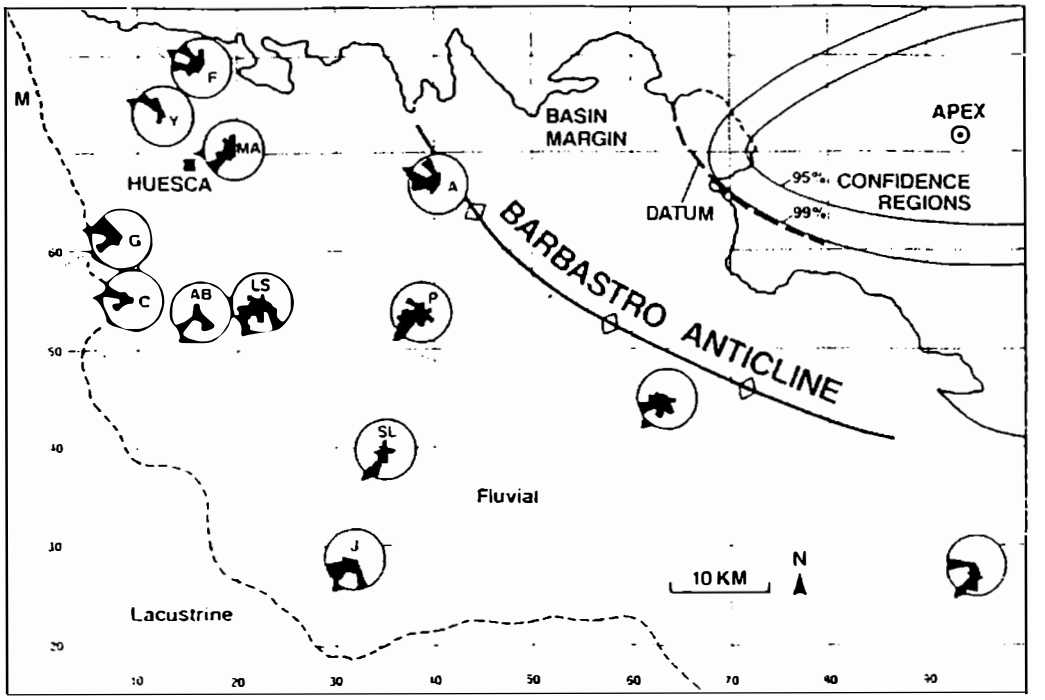

Figure 7.5 Measured palaeocurrents from channels in the Luna and Huesca systems. The radial pattern of the palaeocurrents can be used to localise the apex of the systems. From Hirst and Nichols, 1986.

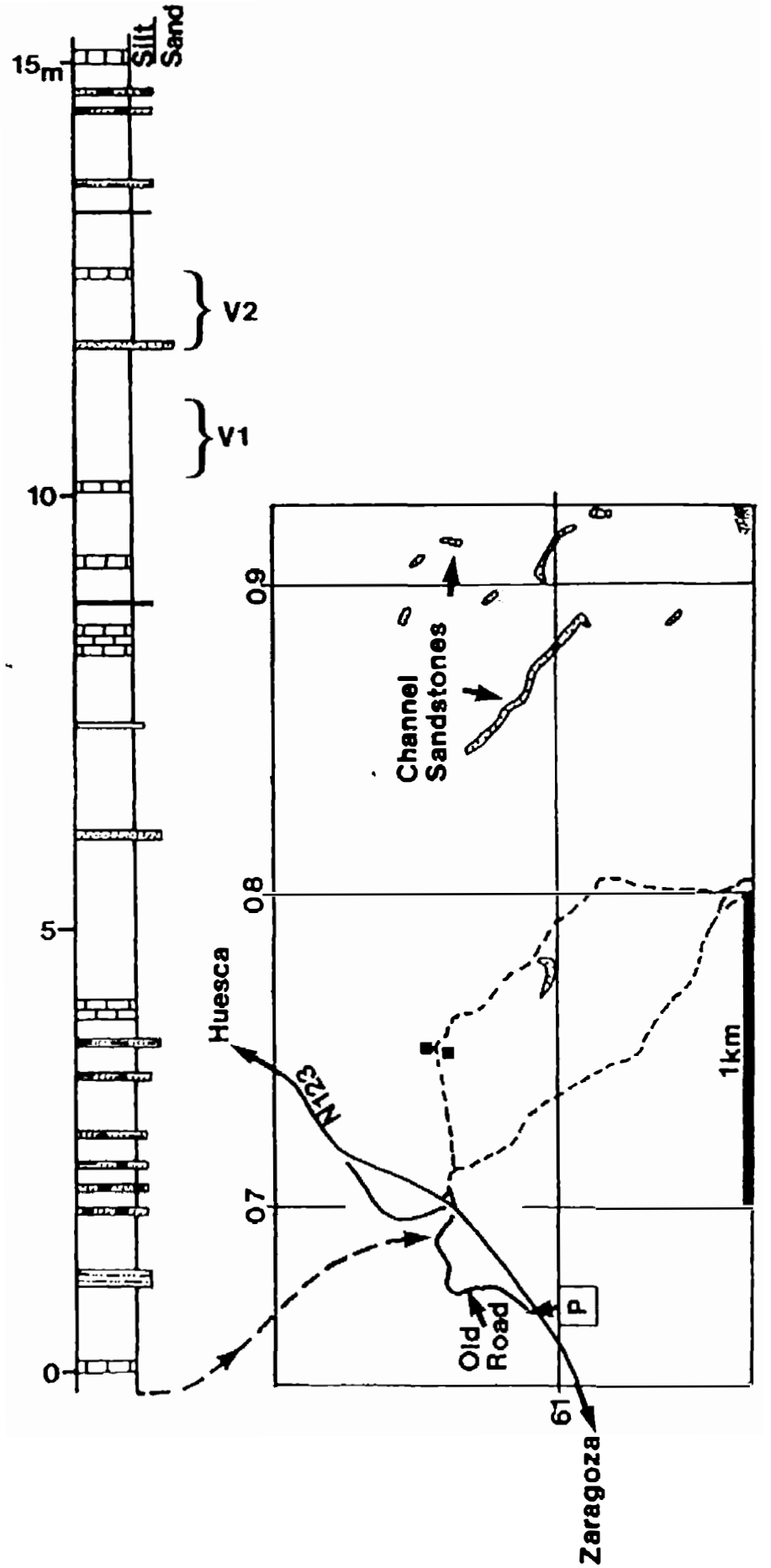

Figure 7.6 Sedimentary log showing the distal facies of the Huesca system at Sierra de la Galocha, SSW of Huesca. From Friend *et al.*, 1989.

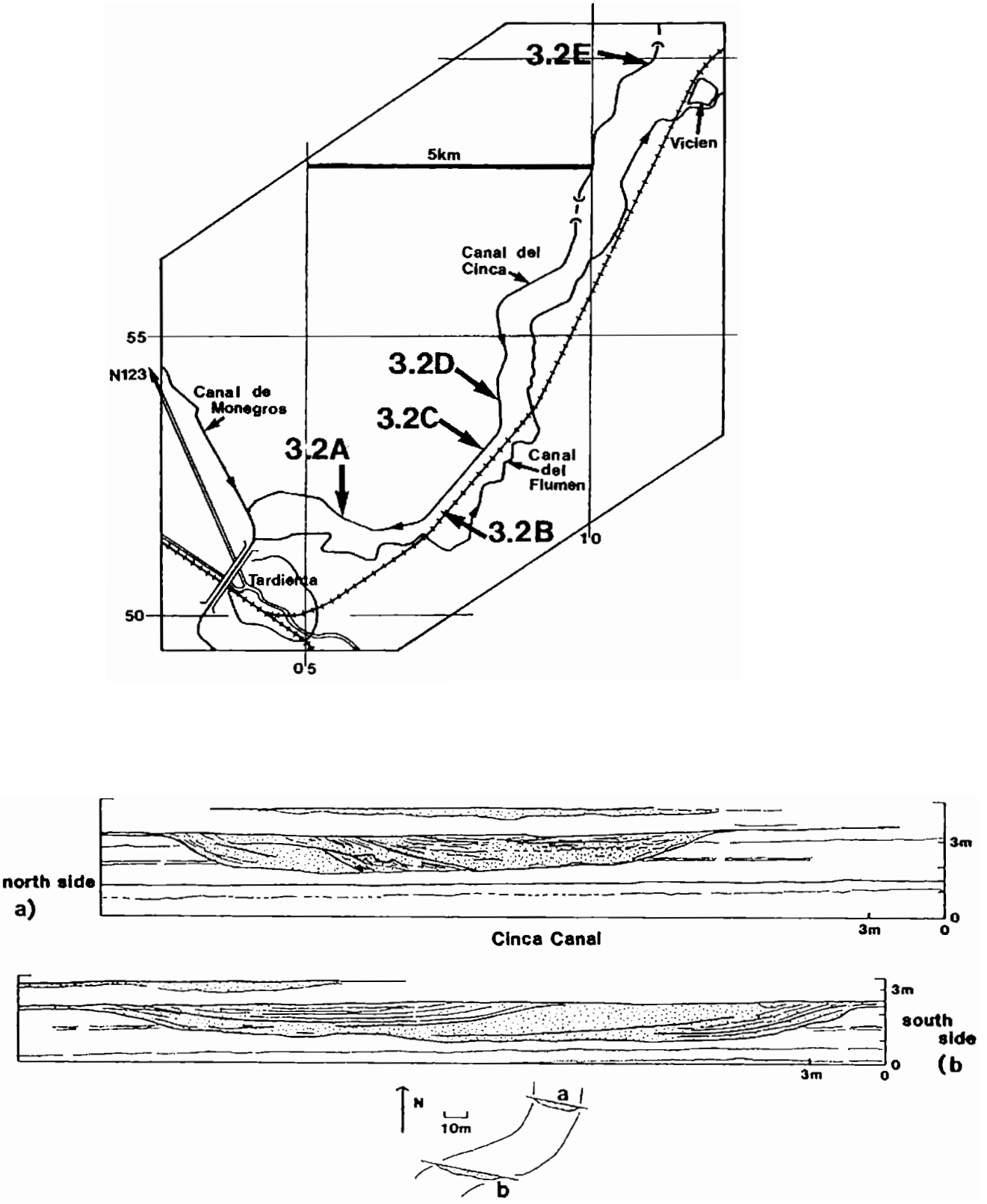

Figure 7.7 Location map for exposures along the Canal del Cinca, south of Huesca. The two channels seen at Locality 3.2A show lateral accretion surfaces dipping in opposite directions, which indicates that they were deposited on different point bars (see sketch). From Friend *et al.*, 1989.

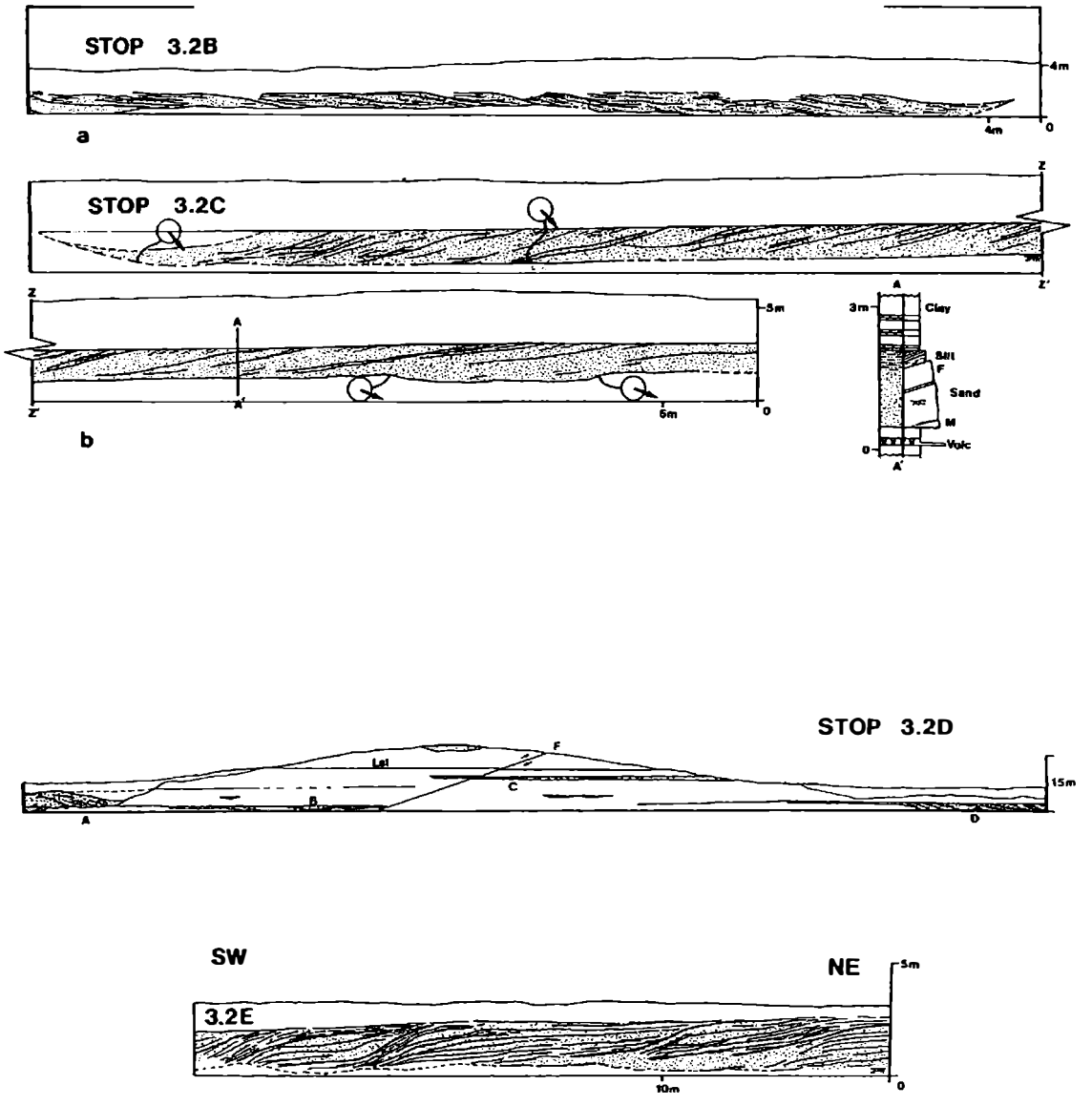

Figure 7.8 Fluvial channels with complex laterally-accreted units, alond the Canal del Cinca (see Figure 7.7 for localities). From Friend *et al.*, 1989.

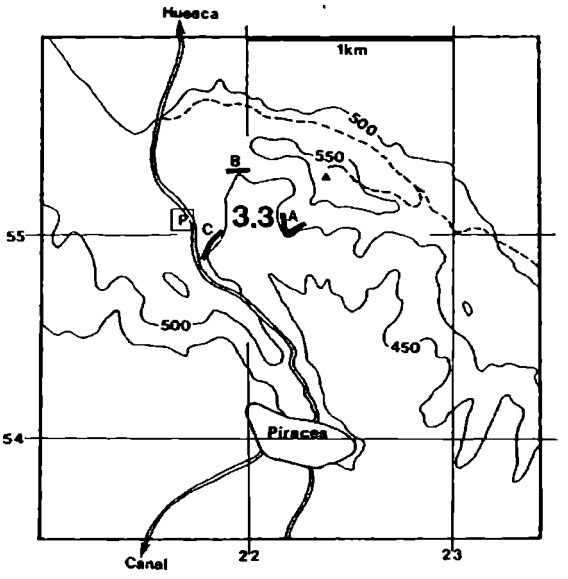

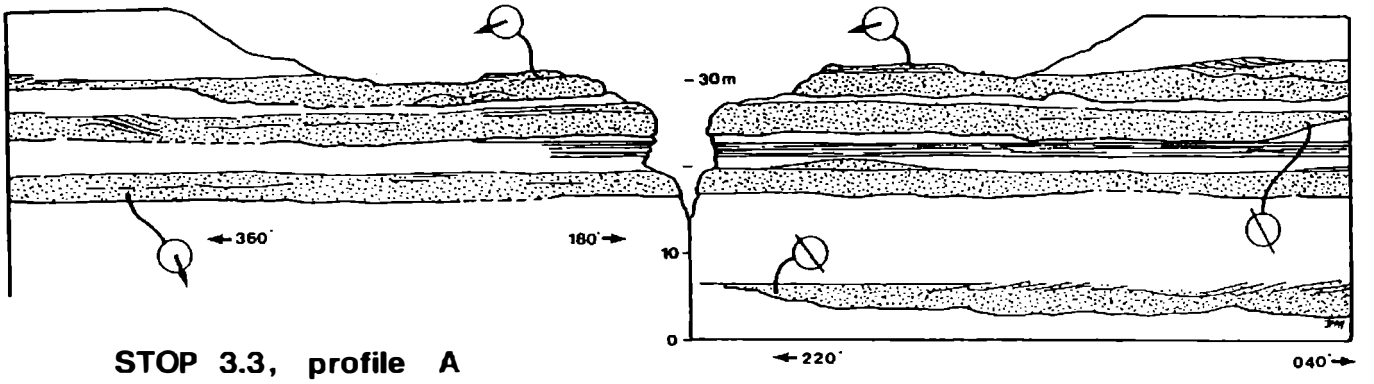

STOP 3.3, profile A

La Serreta

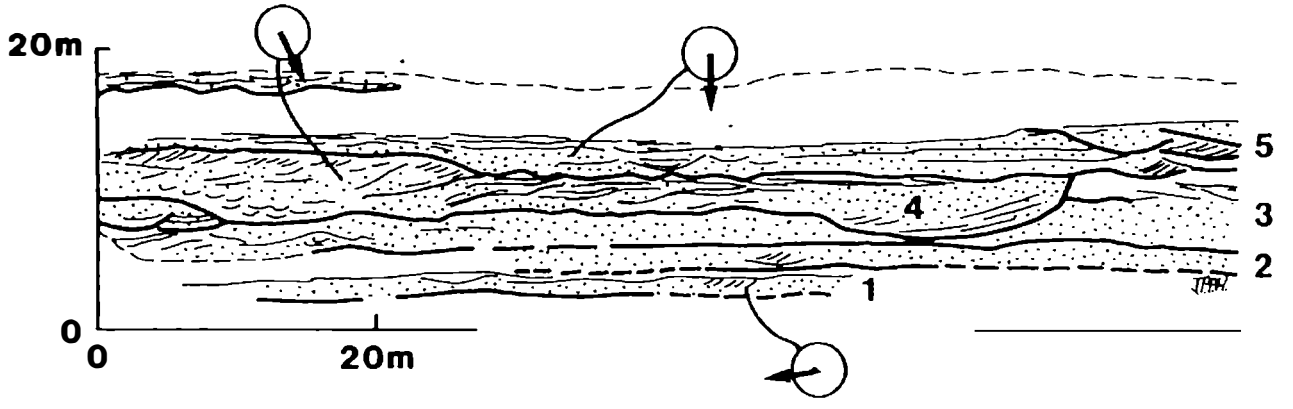

Figure 7.9 Locality map and sketch sections of the Huesca System at La Serreta. The two sketches are of localities A and B on the map. The sandstones here are more commonly multi-storey and multi-lateral than along the Canal del Cinca, and reflect a more proximal position on Huesca System. From Friend *et al.*, 1989.

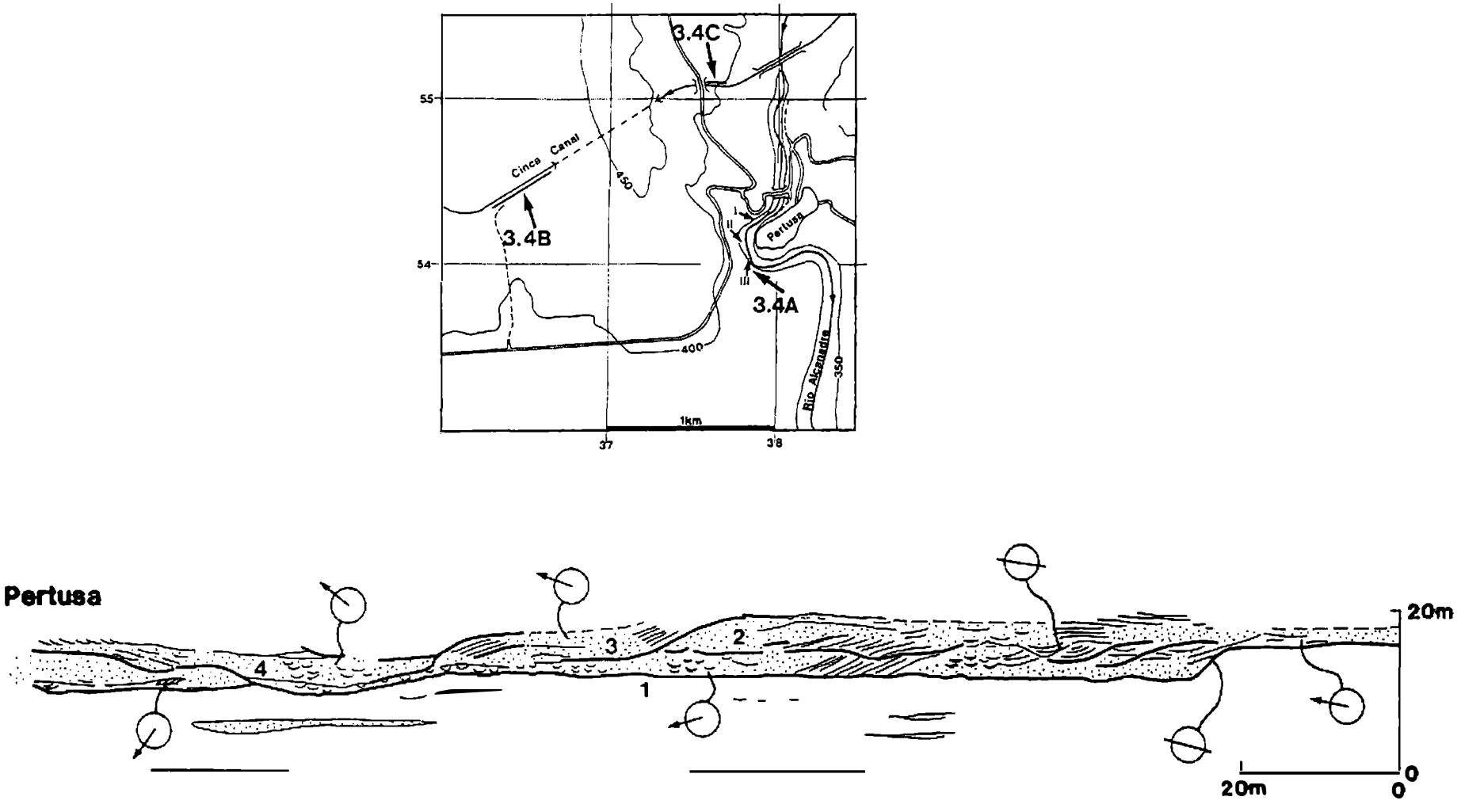

Figure 7.10 Locality map and sketch section of part of the extensive multi-storey/multi-lateral fluvial channel sandstone exposed at Pertusa. From Friend *et al.*, 1989

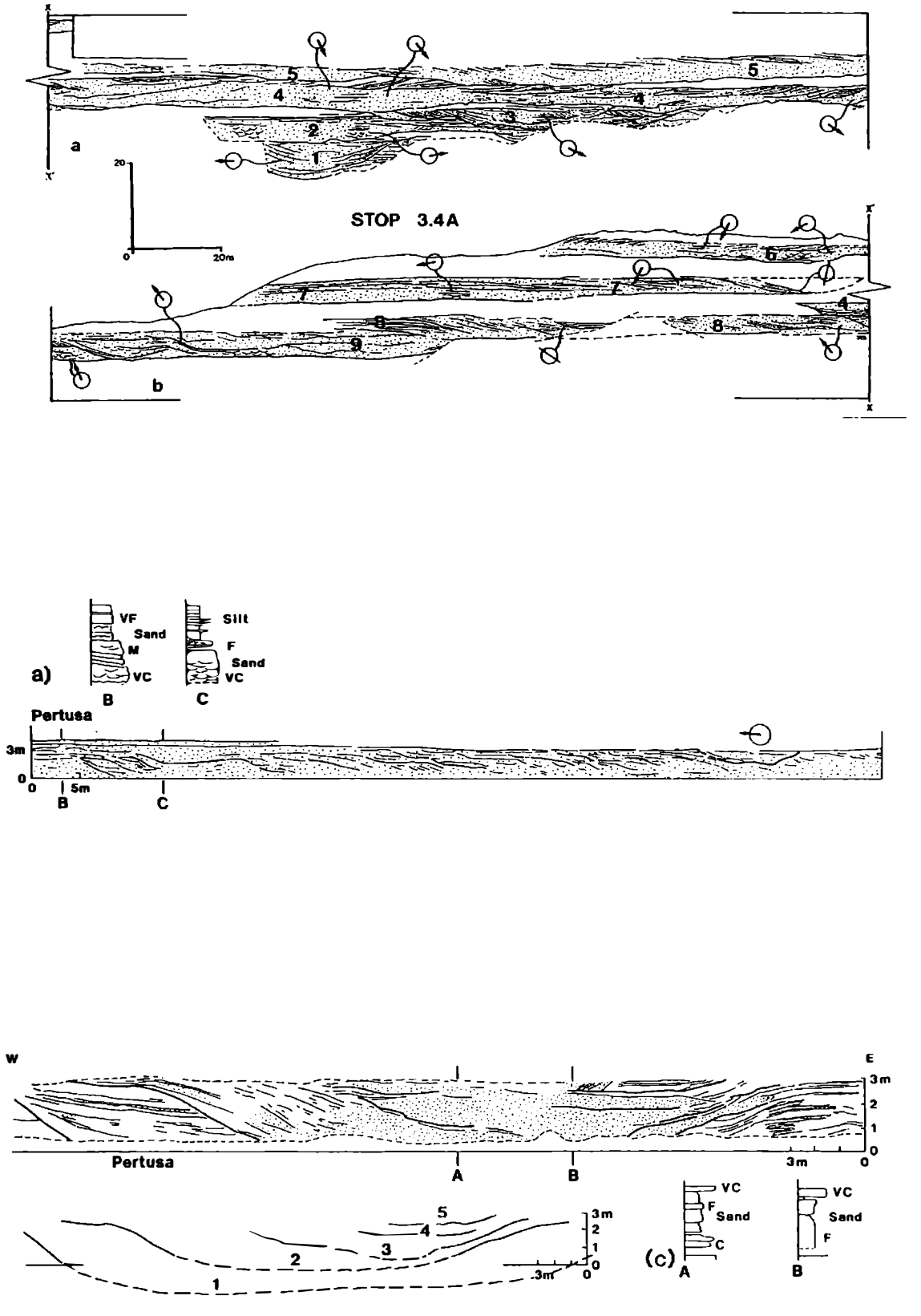

Figure 7.11 Further field sketches showing the multi-storey/multi-lateral nature of the channel sandstones at Pertusa (see Figure 7.10 for location). From Friend *et al.*, 1989.

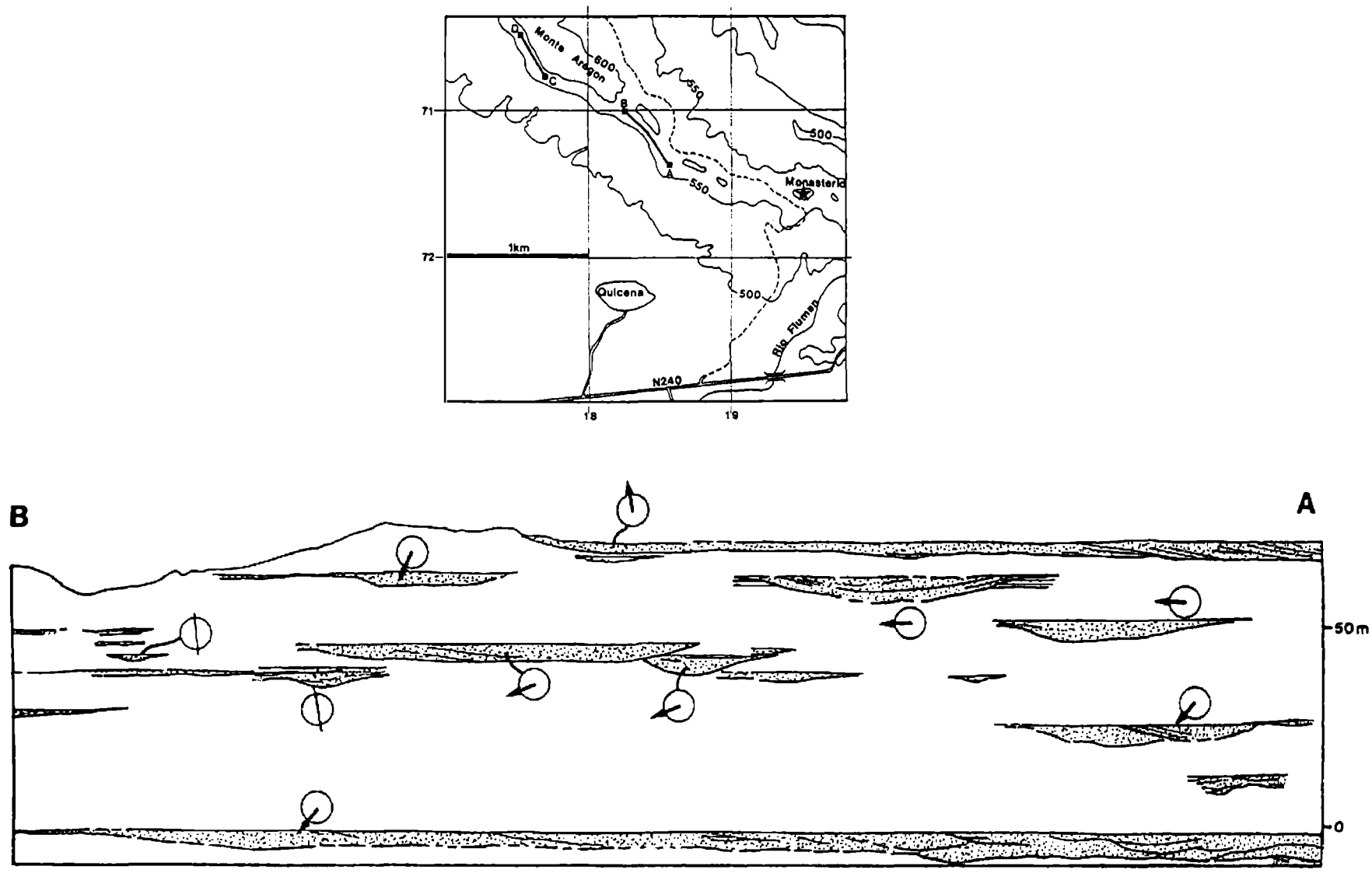

Figure 7.12. Location map and sketch of the Huesca System at Monte Aragon, east of Huesca. Both ribbon and sheet sandstones occur on the hillside; the sketch shows two extensive sheets separated by a lower net:gross interval dominated by ribbons. From Friend *et al.*, 1989

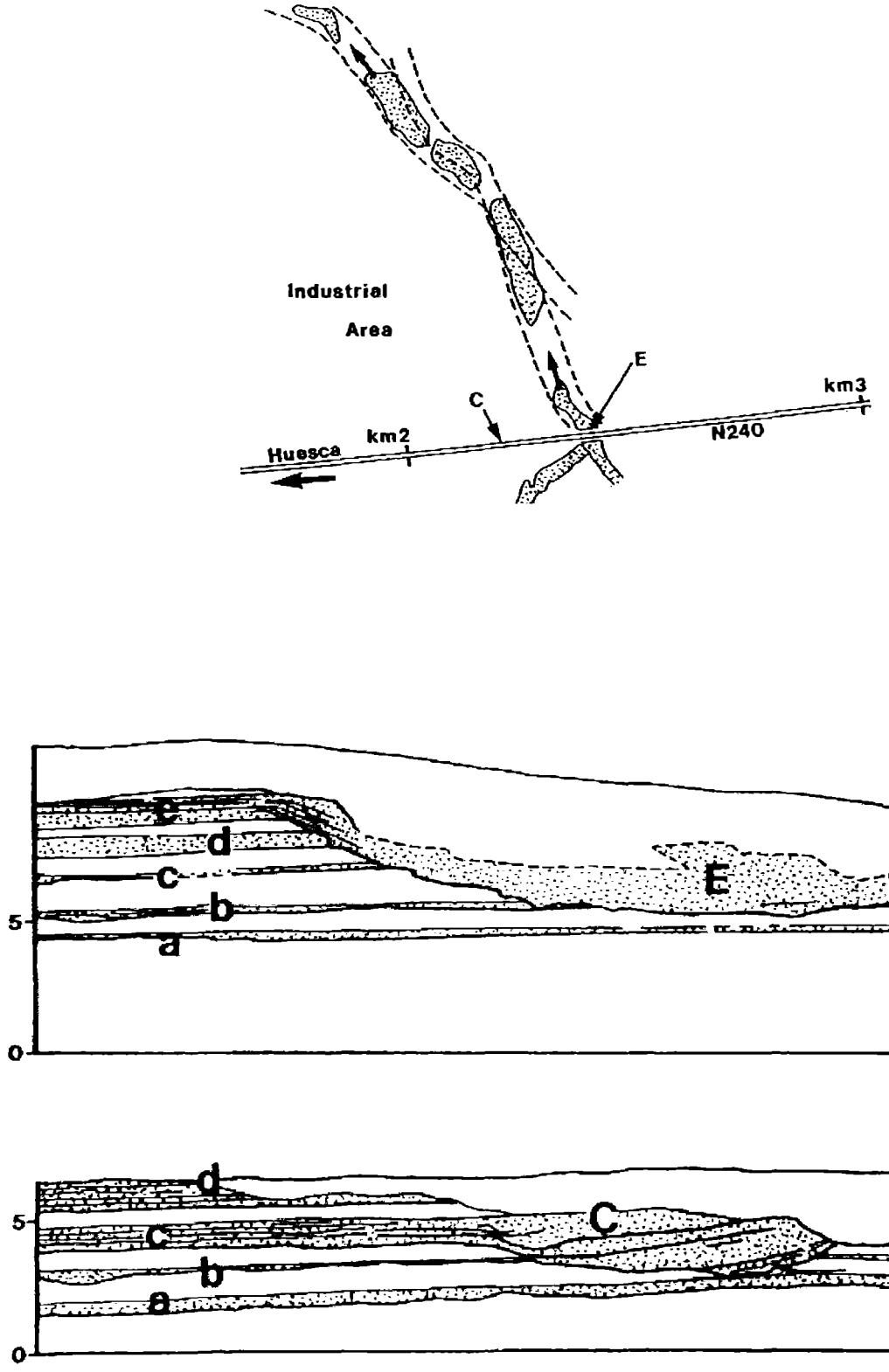

Figure 7.13 Ribbon-like channel sandstones with variably developed 'wings, exposed in a road cut east of Huesca. The reservoir behaviour of these channels would be influenced greatly by their relationship to the thinner sandstones in the surrounding floodplain deposits. From Friend *et al.*, 1989

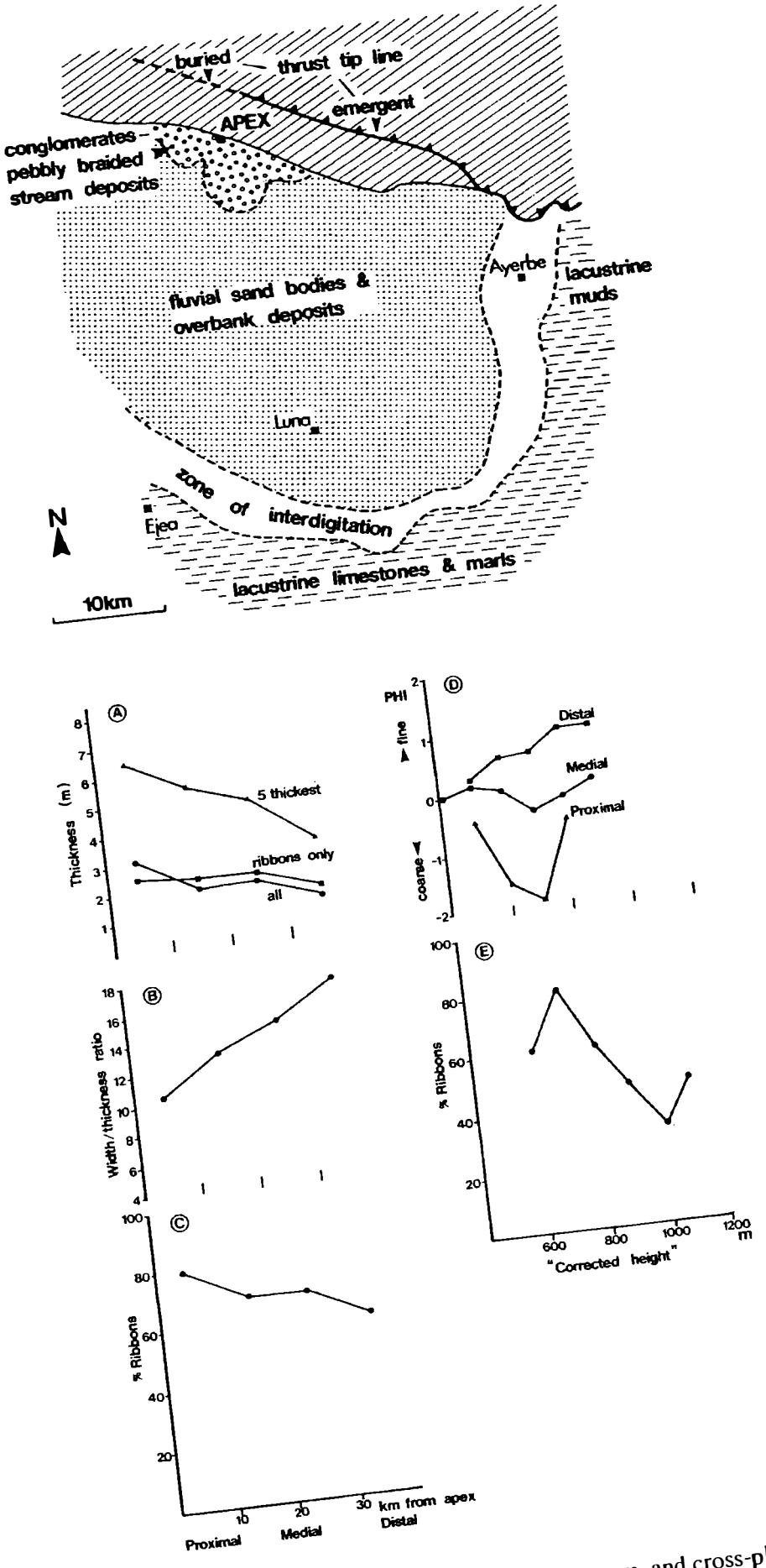

Figure 7.14 Map showing the facies belts in the Luna System, and cross-plots showing how the system varies both vertically and in a proximal to distal direction. From Nichols, 1987c.

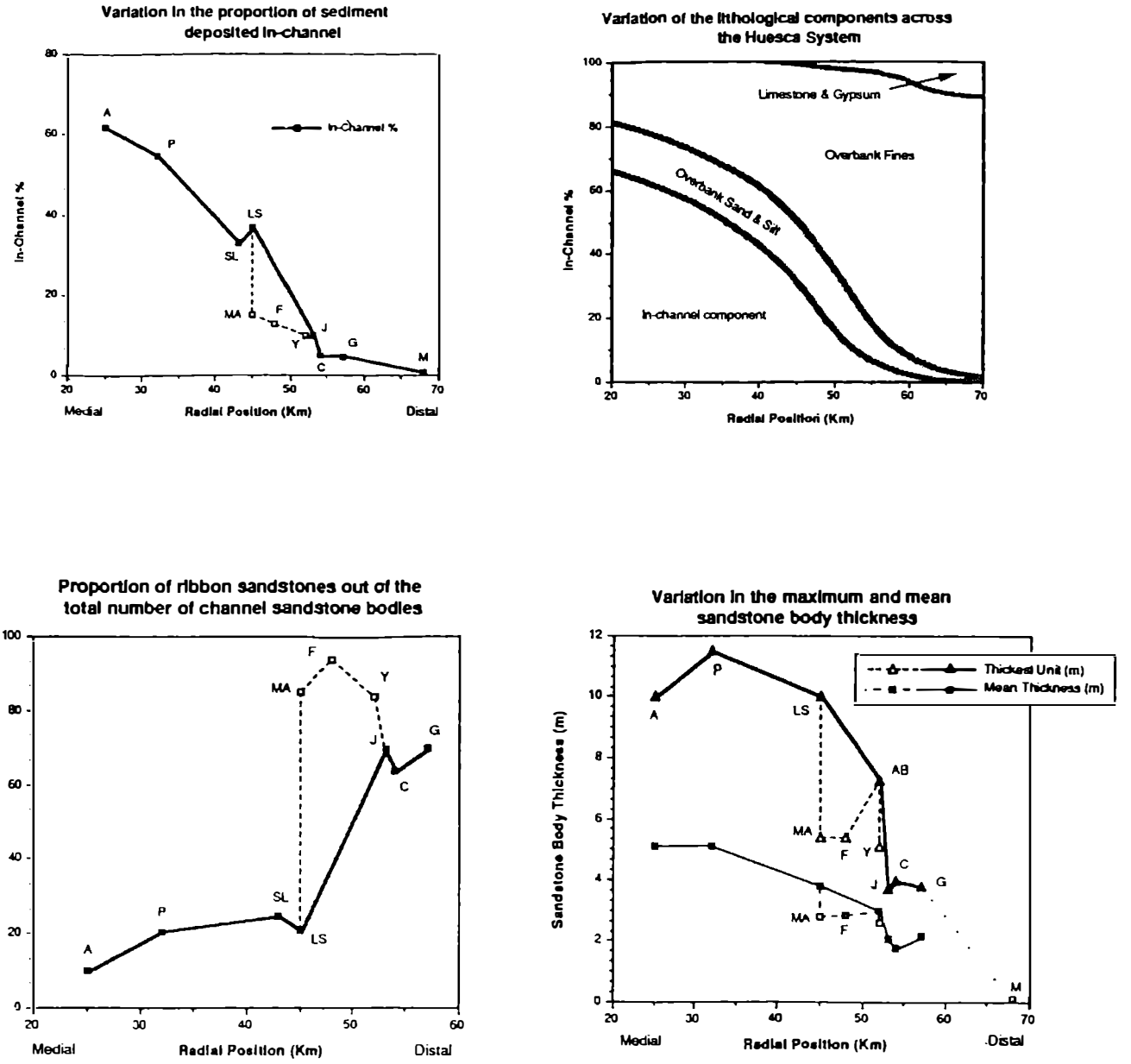

Figure 7.15 Cross-plots showing how channels in the Huesca System vary with radial position. From Hirst, 1991.

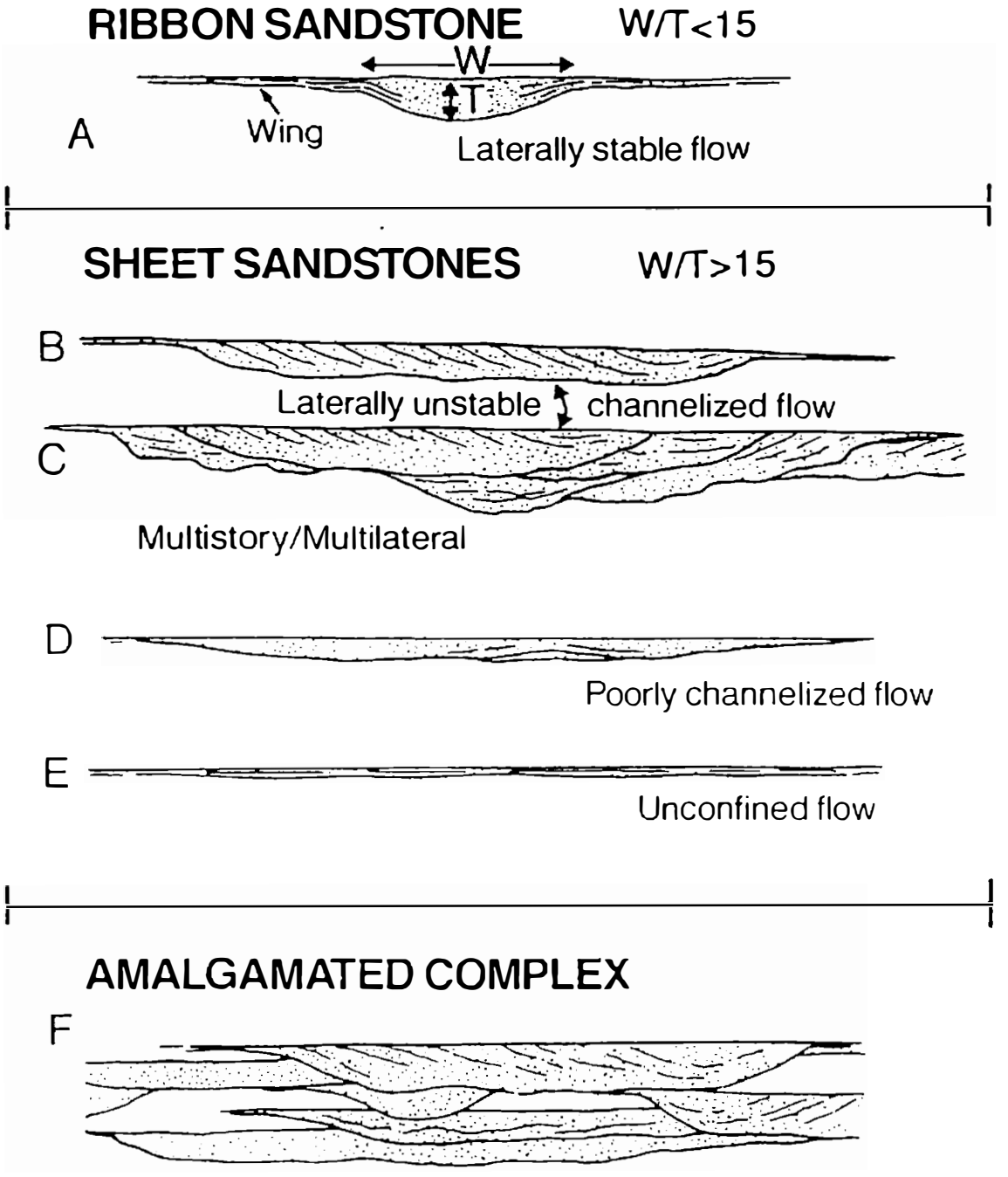

Figure 7.16 Geometry of fluvial channel sandbodies. From Hirst, 1991, after Slater *et al.*

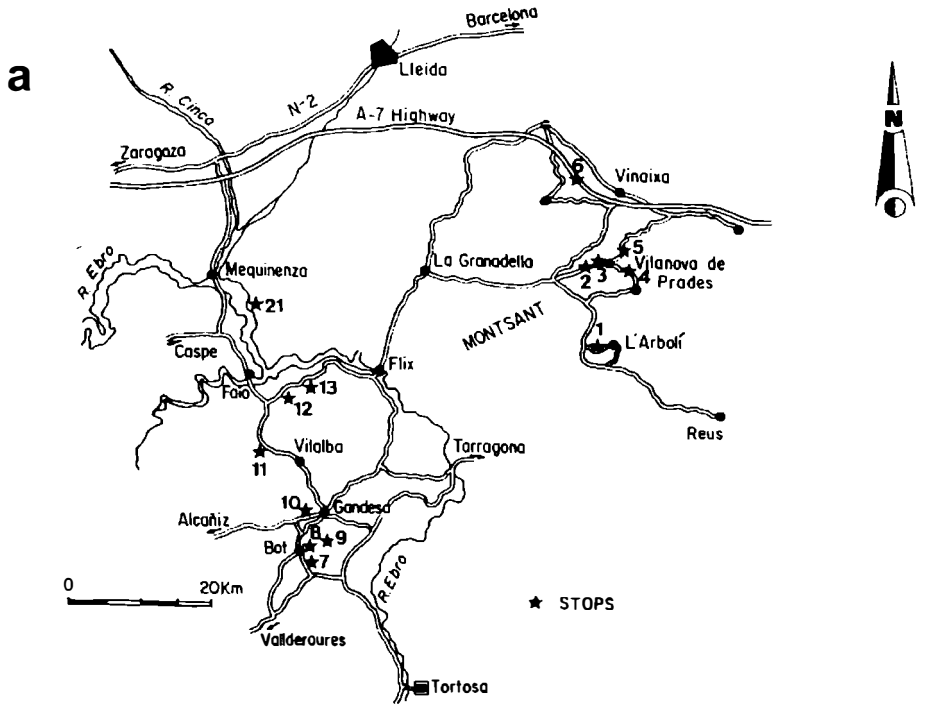

Location map of Montsant-Gandesa-Mequinenza area.

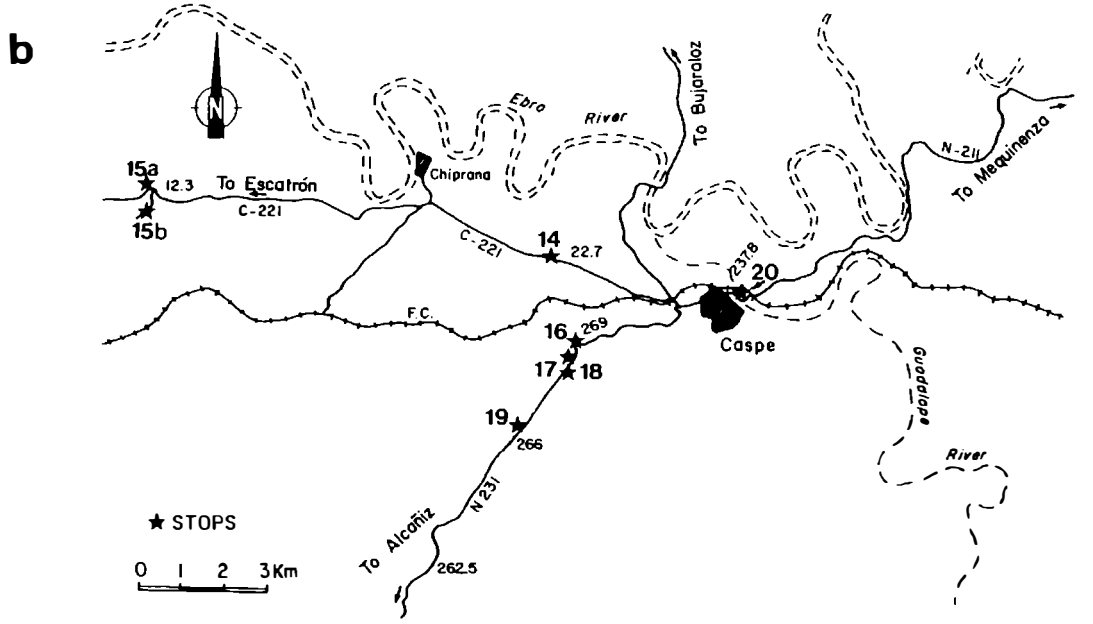

Location map of Caspe area.

Figure 7.17 Location maps for fluvial localities in the south-eastern Ebro Basin.
a. the Montsant-Gandesa-Mequinenza area; b. the Caspe area. From Anadon *et al.*, 1989.

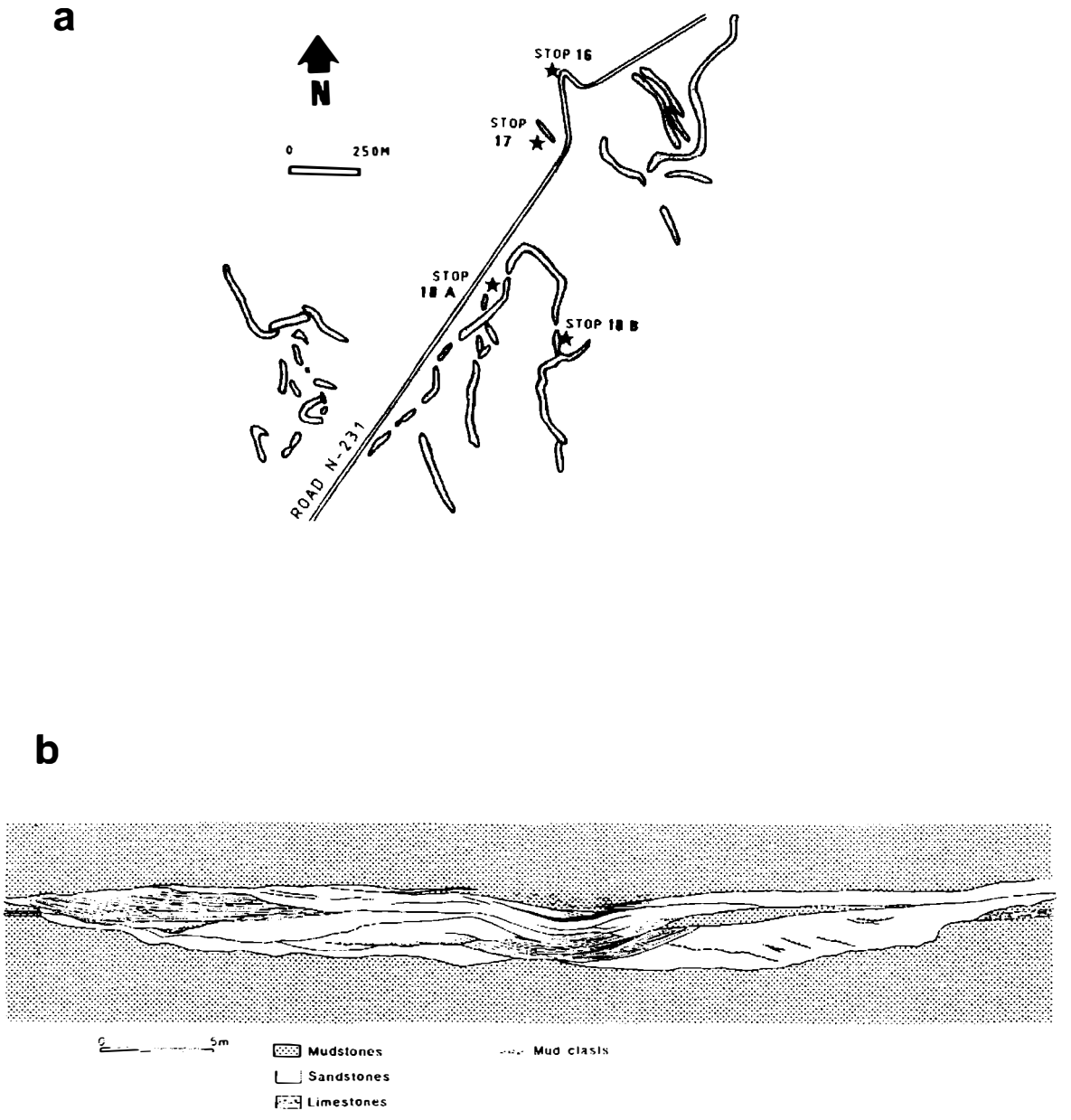

Figure 7.18 (a) plan view of exhumed ribbon sandbodies in the Caspe Formation (Oligo-Miocene), SW of Caspe and (b) cross-section showing amalgamation of two individual ribbons (at locality 16 of Fig. (a)). The two ribbons have orientations at approximately 90° to each other. A thin limestone bed (seen on the left of the figure) is eroded by the lower sandbody. From Anadon *et al.*, 1989.

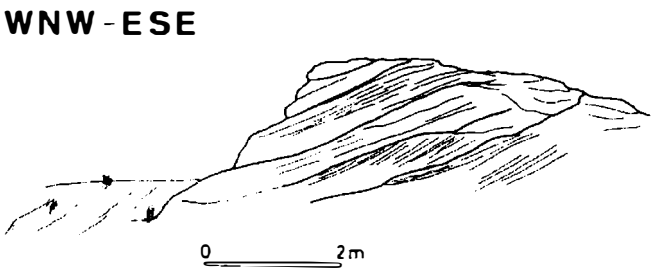

Large scale cross stratification surfaces resulting from the migration of lateral bars (see lower figure).

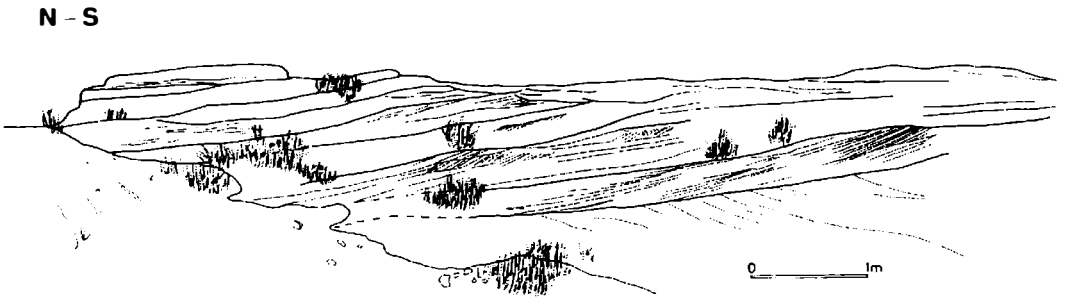

Low angle large scale cross stratification surfaces resulting from the downstream migration of transverse bars (see lower figure).

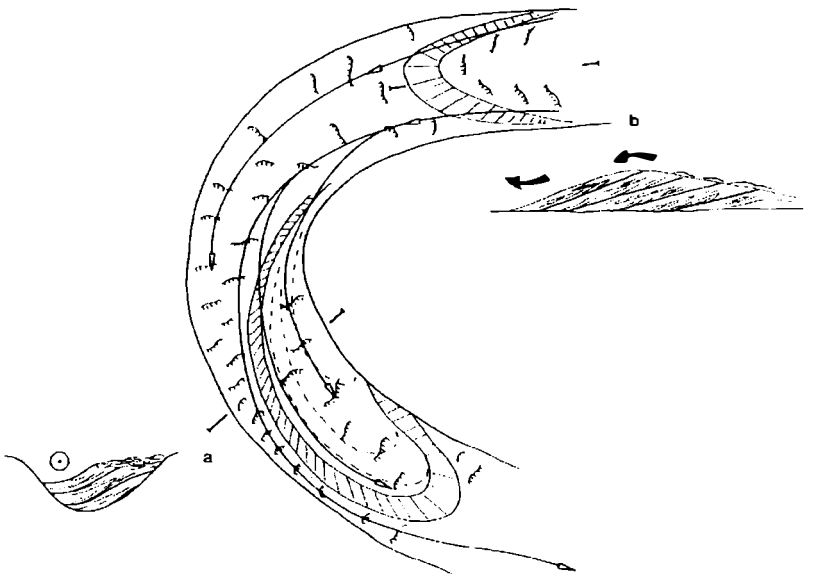

Interpretative sketch of the main sedimentological features of the sinuous ribbon infill shown in upper two figures.

Figure 7.19 Channel facies in a sinuous ribbon sandbody in the Caspe Formation SW of Caspe. Location 18 on Figure 7.17 and 7.18a. From Anadon *et al.*, 1989.

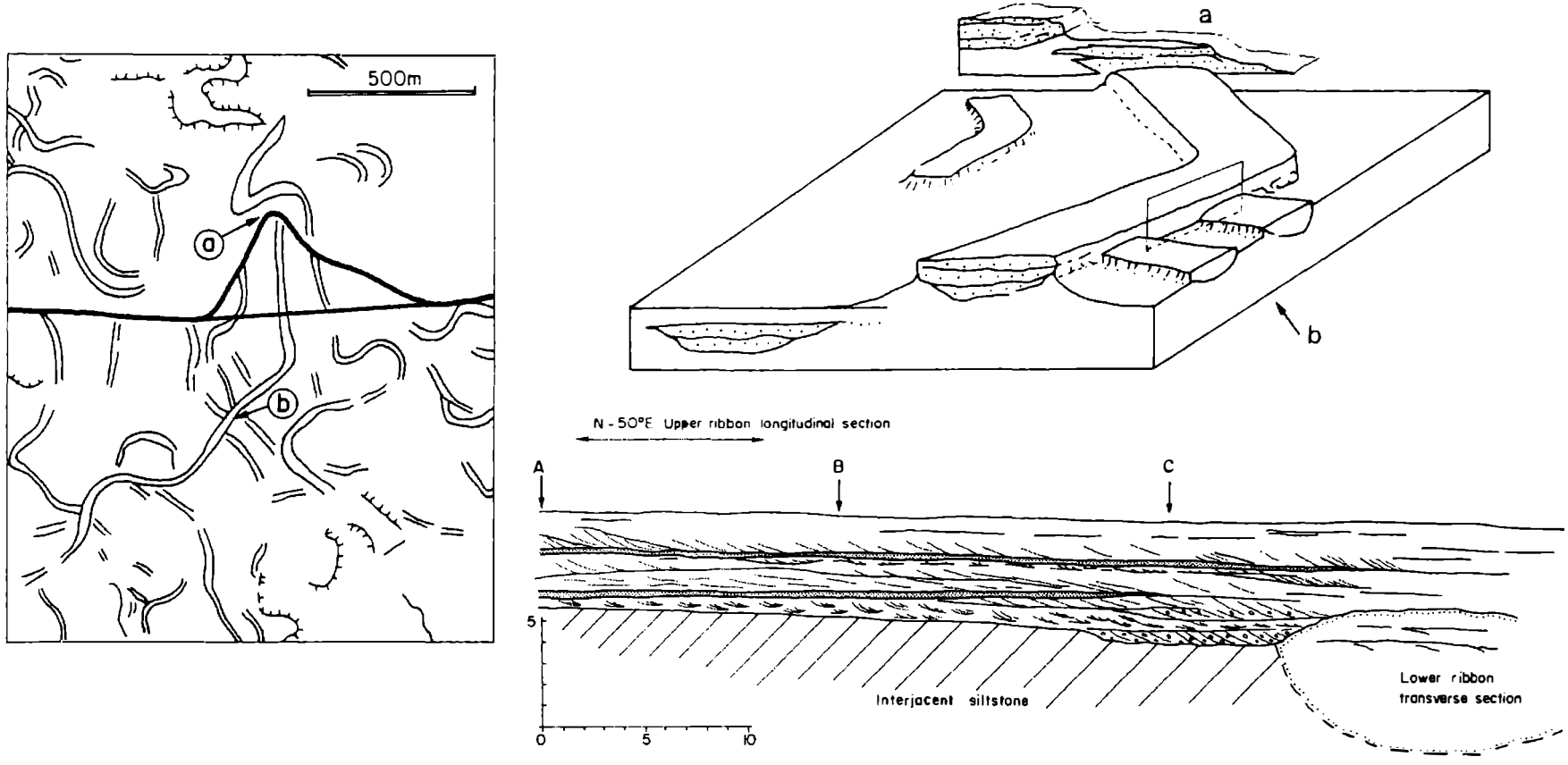

Figure 7.20 Plan geometry and vertical stacking of ribbon sandbodies in the Caspe Formation, WNW of Caspe (Location 15 on Figure 7.17). From Anadon *et al.*, 1989.

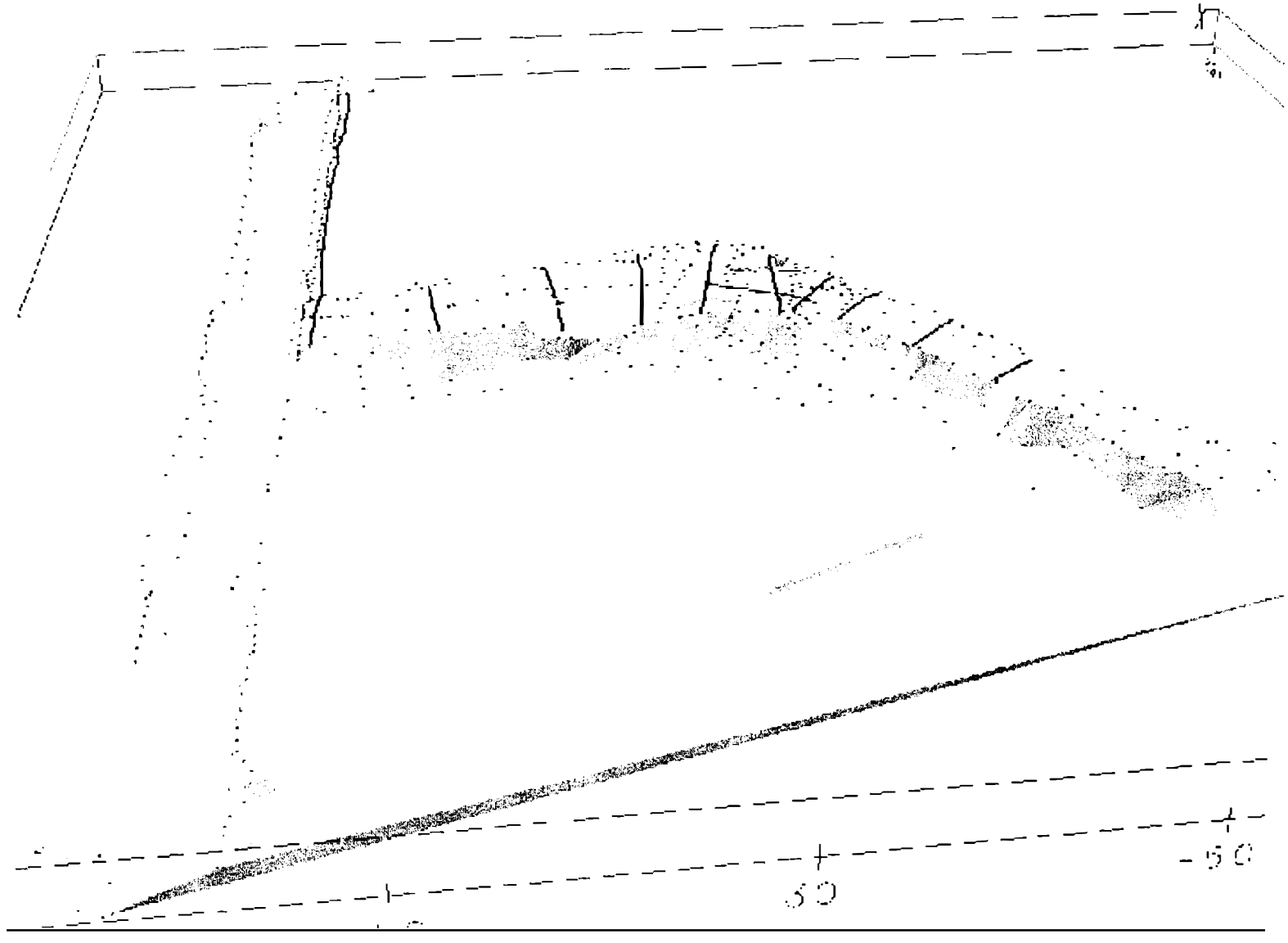

Figure 7.21 Initial digital terrain model (DTM) of the study site on the N211 road at km39. View is looking from the west towards the central channel belt deposit. Lines represent the Ground Penetrating Radar transects. The sandbody is to the north of locality b on Figure 7.20. The new road cutting (dashed line on Figure 7.20) can clearly be seen on the DTM.

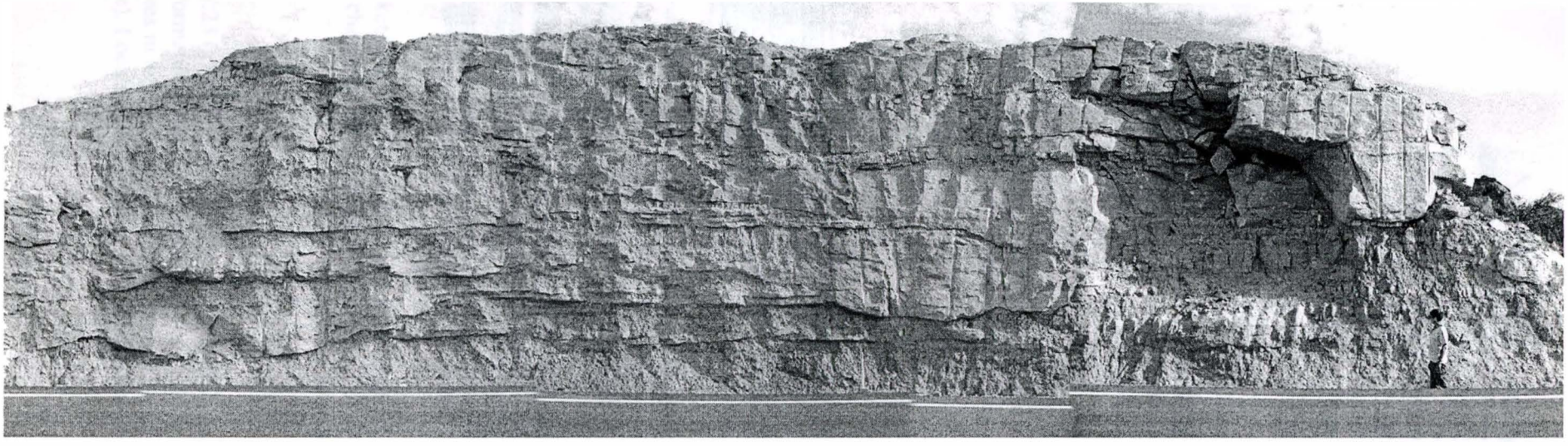

Figure 7.22 Photomontage of the central channel belt deposit at km39 on the N211. This face is the southern side of the road cut shown on Figure 7.21.

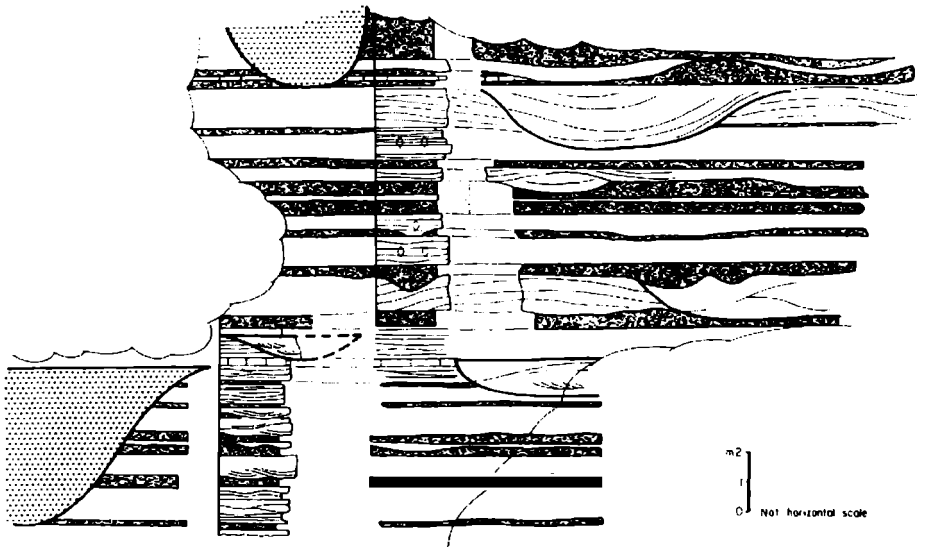

Architectural relationships between ribbons and sheet sandstone bodies in the Caspe Formation. The observed relationships show alternative aggradational and degradational episodes.

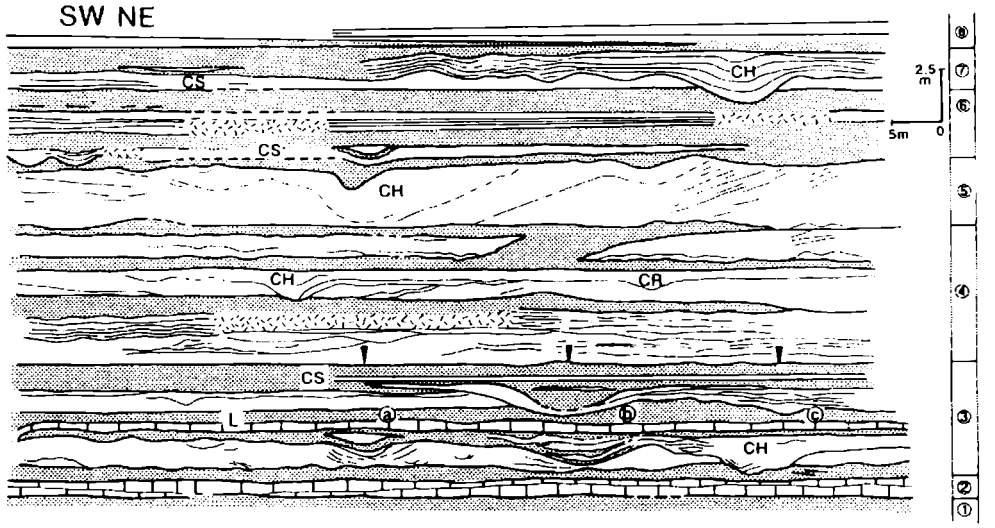

Field sketch of the fluvio-deltaic facies assemblages in the Barrance de l'Aguamoll. CH = channels; CR = crevasse channels; CS = crevasse splays and terminal lobes; L = lacustrine limestones.

Figure 7.23 (a) Architectural relationships between ribbon and sheet sandbodies in the Caspe Formation (locality 20 on Figure 7.17) (b) Stacking of channel and non-channel sandstones in a fluvio-deltaic interval in the Los Monegros lacustrine system (Oligo-Miocene). Locality 21 on Figure 7.17. From Anadon *et al.*, 1989.

Figure 17
Architecture of medial-distal alluvial fan facies (stop, 4 Montsant system).

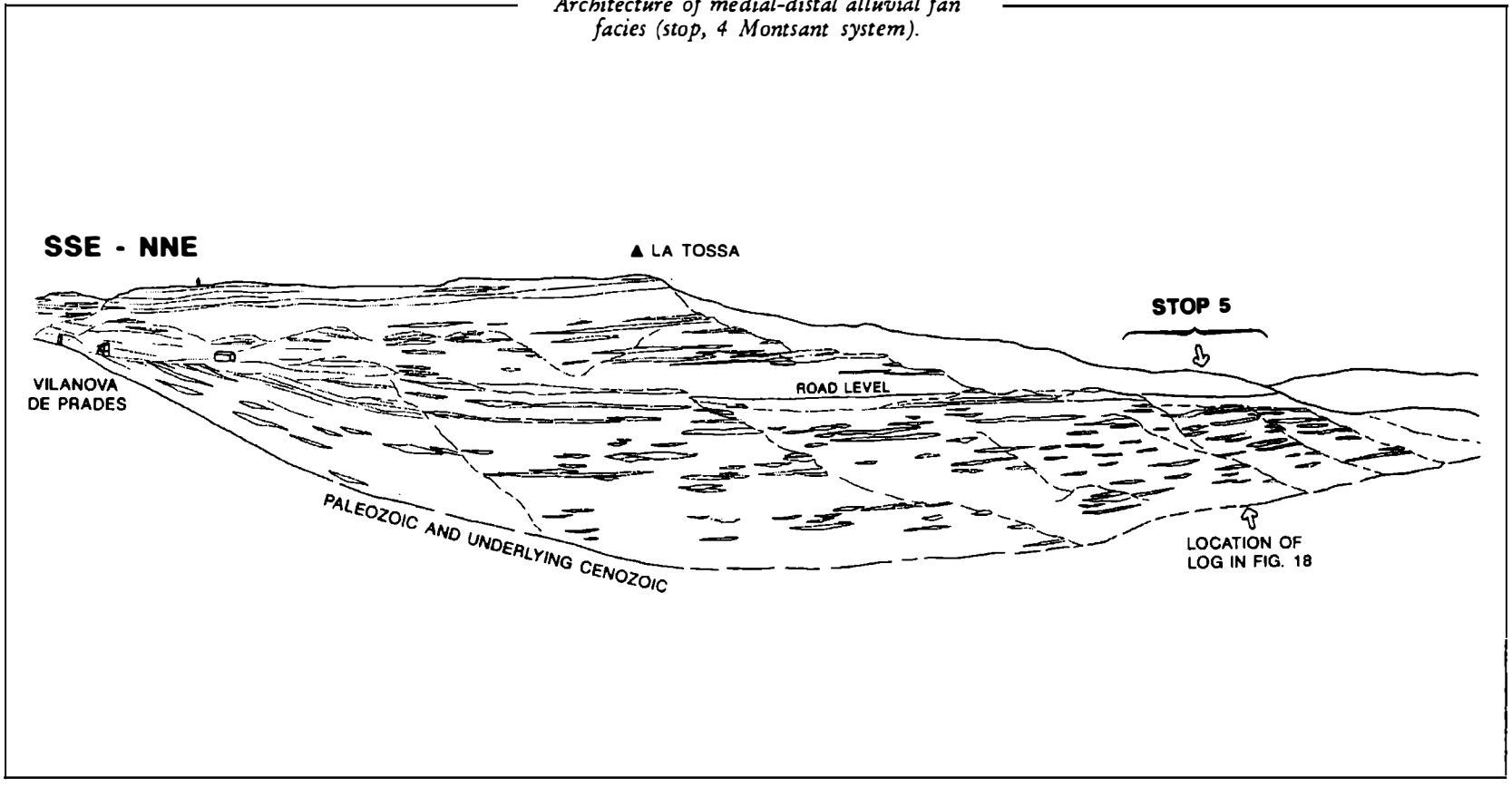

Figure 7.24 General architecture of the Montsant Alluvial System (Eocene to Oligocene). Note the upwards increase in net-to-gross and change from lenticular to more tabular conglomerate bodies. Location 4 on Figure 7.17. From Anadon *et al.*, 1989.

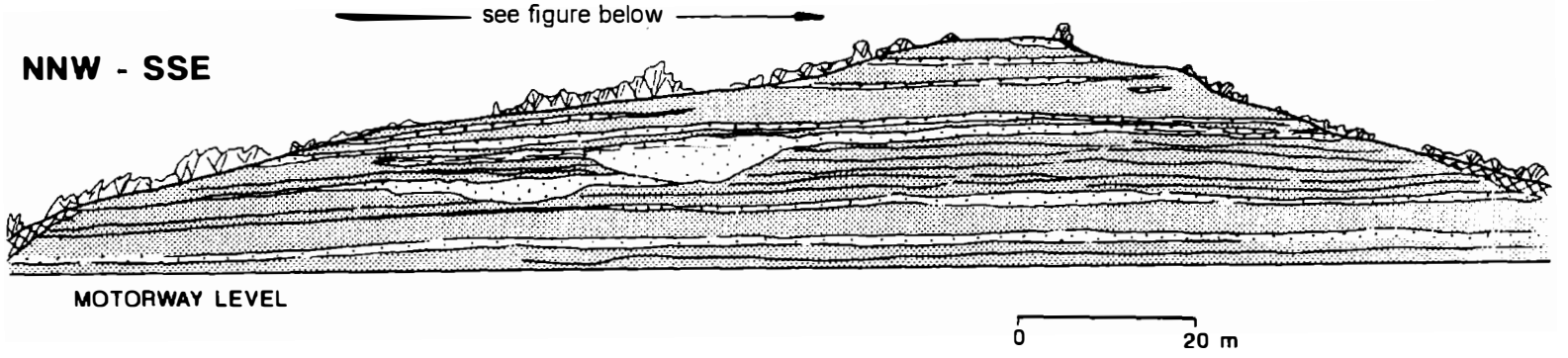

Sandy and conglomeratic ribbons in the distal alluvial fan facies of the Montsant system.

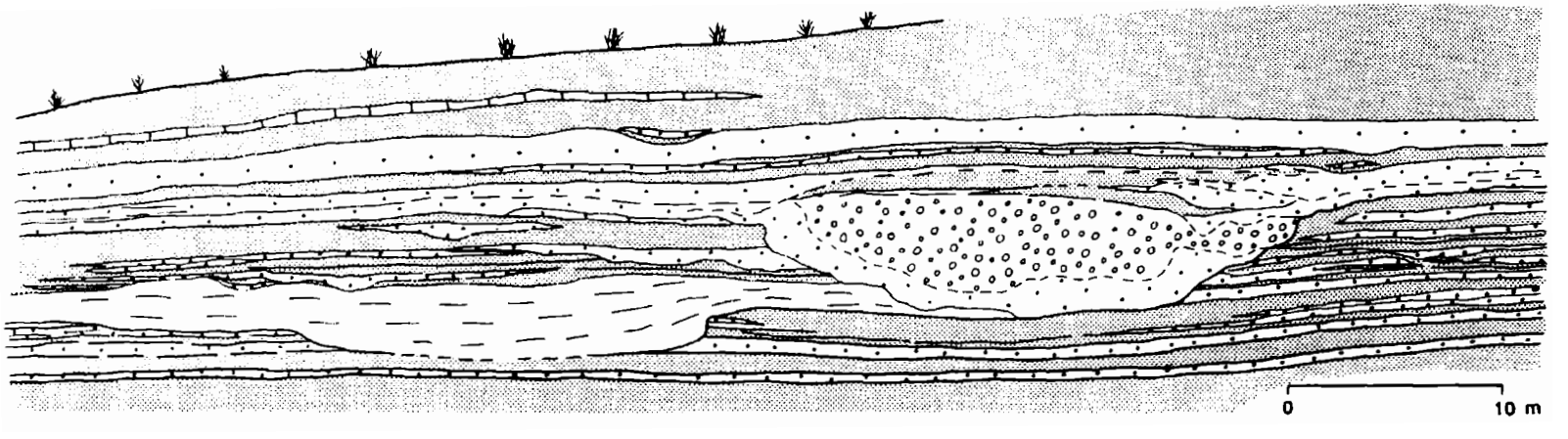

Detail of the ribbon channel infills (see figure above).

Figure7.25 Distal alluvial fan facies of the Montsant system, Locality 6 on Figure 7.17. Note the thin sheet sands and narrow sandstone and conglomerate ribbons. The ribbons commonly have a compound fill, with internal erosive surfaces. From Anadon *et al.*, 1989.

Section 8

General Diagrams

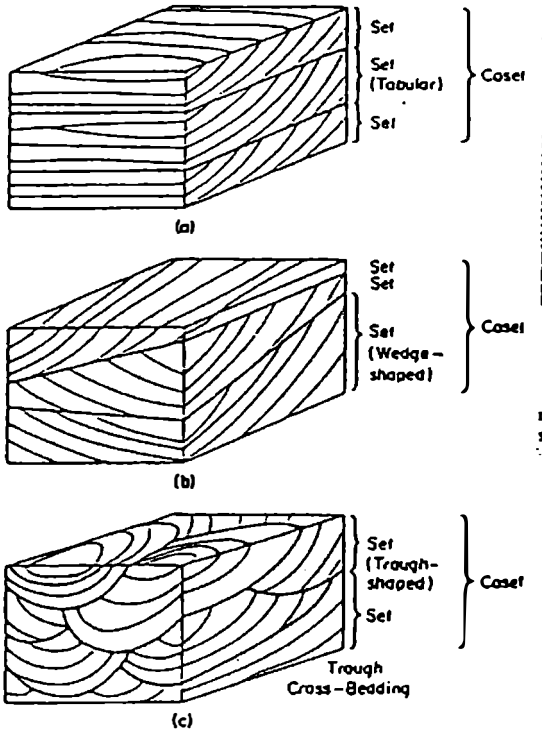

Terminology for cross-bedding. In (a) and (b) the cross-strata are tangential to angular in shape. In (a) the sets are tabular, but in (b) they are wedge-shaped. In (c) both cross-strata and sets are trough shaped. Terminology after McKee and Weir (1953).

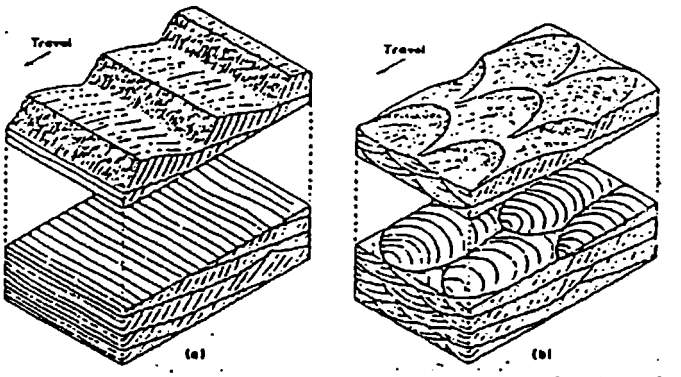

Relationship of internal cross-stratification pattern to surface shape of ripples or dunes. (a) Tabular cross-stratification due to bed forms with long and substantially straight crests. (b) Trough cross-stratification due to bed forms with short curved crests, as illustrated by lunate dunes.

SCALE OF STRATIFICATION THICKNESS
(after Ingram, 1954)

Very thickly bedded	Thicker than 1 m
Thickly bedded	30–100 cm
Medium bedded	10–30 cm
Thinly bedded	3–10 cm
Very thinly bedded	1–3 cm
Thickly laminated	0.3–1 cm
Thinly laminated	Thinner than 0.3 cm

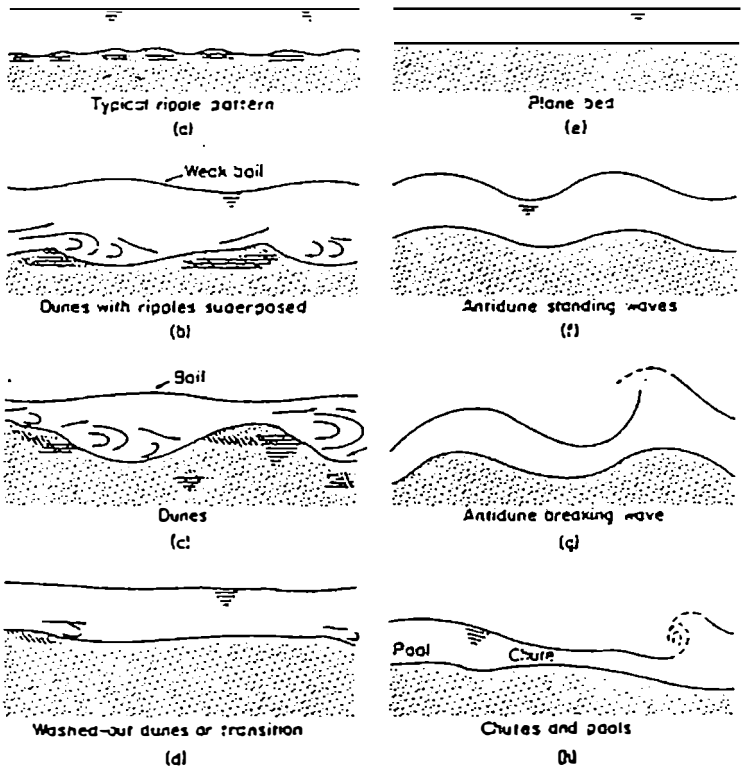

Types of bed-forms observed in steady, uniform flows in sand bed channels (after Simons and Richardson, 1961). The sequence (a) to (h) represents the idealized sequence observed in flumes as the stream power is increased (see Fig. 5-3). Forms (a) to (d) define the "lower flow regime" and the plane bed (e) and forms (f) to (h) define the "upper flow regime".

Figure 8.1 Current-generated bedforms and sedimentary structures

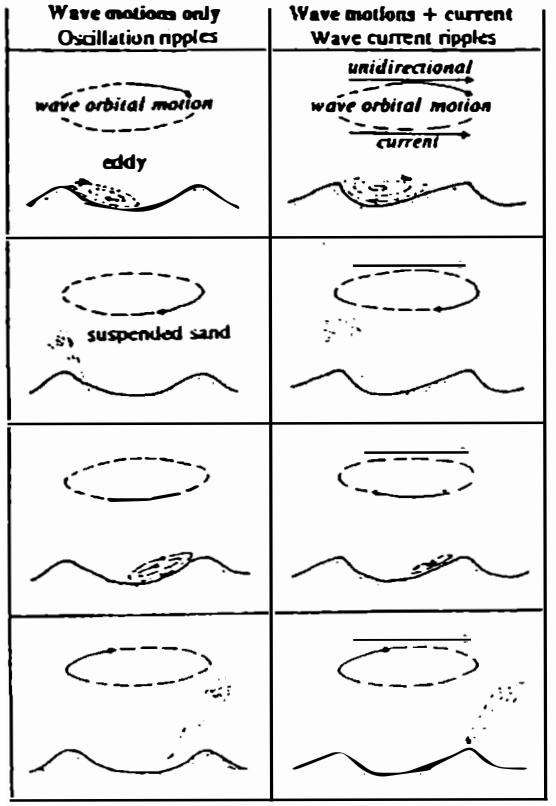

The relationship between sand transport over a rippled sand bed and the orbital motions of wave action with and without a superimposed unidirectional current (after Komar 1976 from original data of Inman & Bowen 1963).

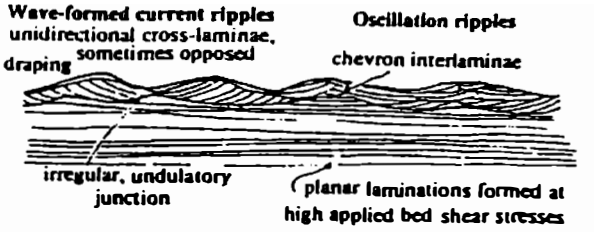

Some diagnostic internal features of wave-formed ripples (after de Raaf *et al.* 1977).

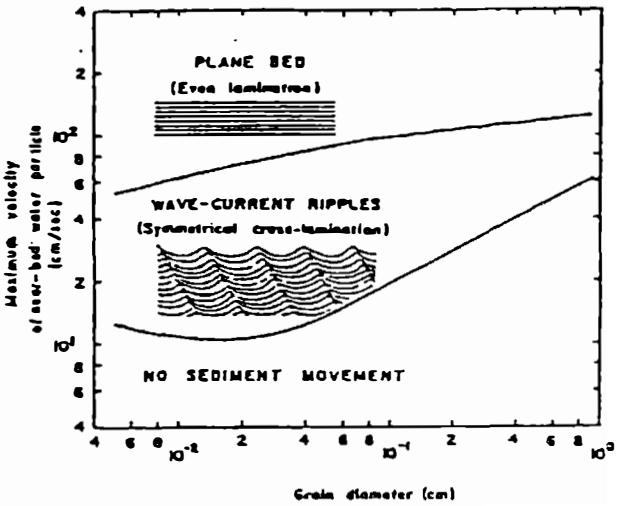

Bed forms in relation to maximum, wave-induced, near-bottom water particle velocity and calibre of quartz-density bed-material (data of M. Manohar and D. L. Inman).

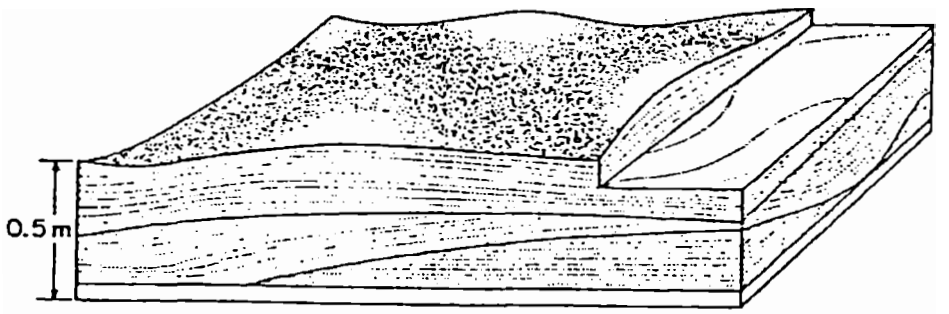

Characteristics of hummocky cross-stratification, published by Harms and others (1975, p. 88).

Figure 8.2 Wave-generated bedforms and sedimentary structures

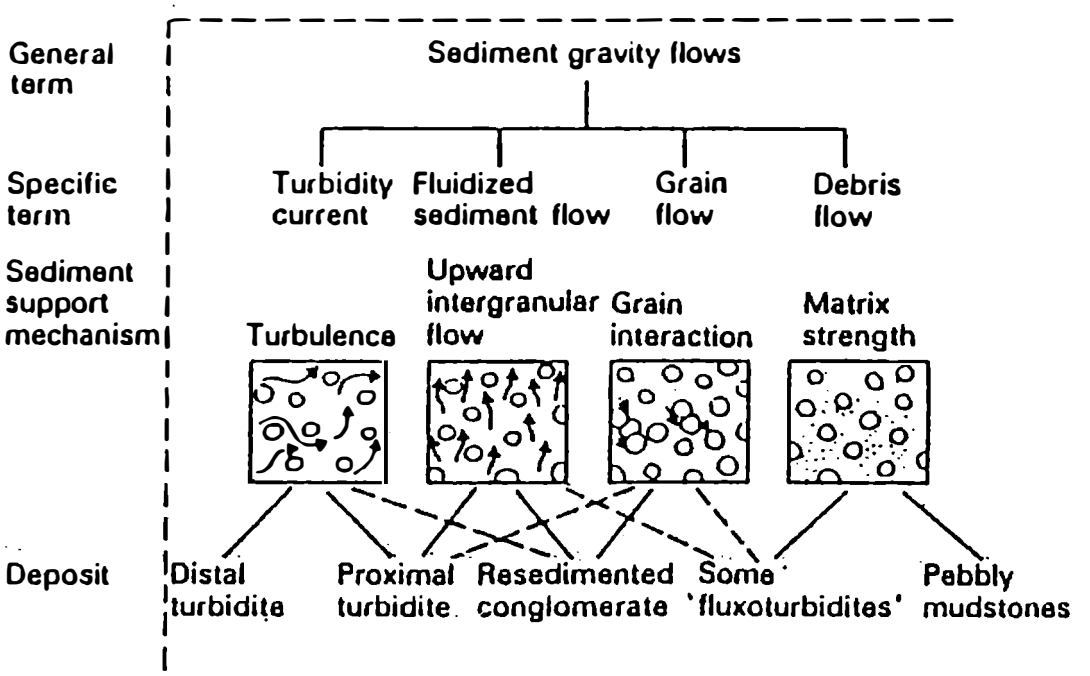

Classification of sediment gravity flows (after Middleton and Hampton, 1976).

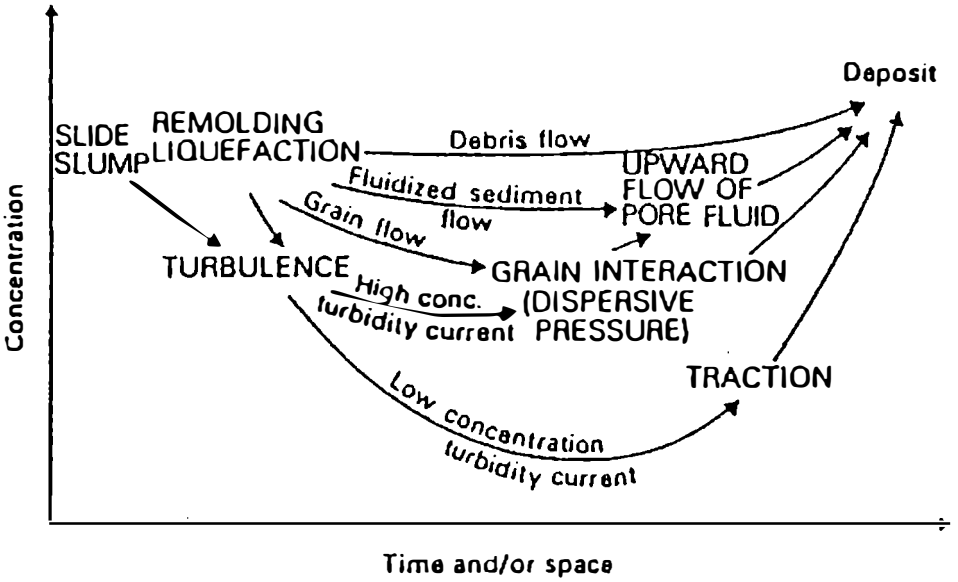

Hypothetical interrelation of processes in a single sediment gravity flow event (after Middleton and Hampton, 1976).

Figure 8.3 Classification and mechanisms of sediment gravity flows

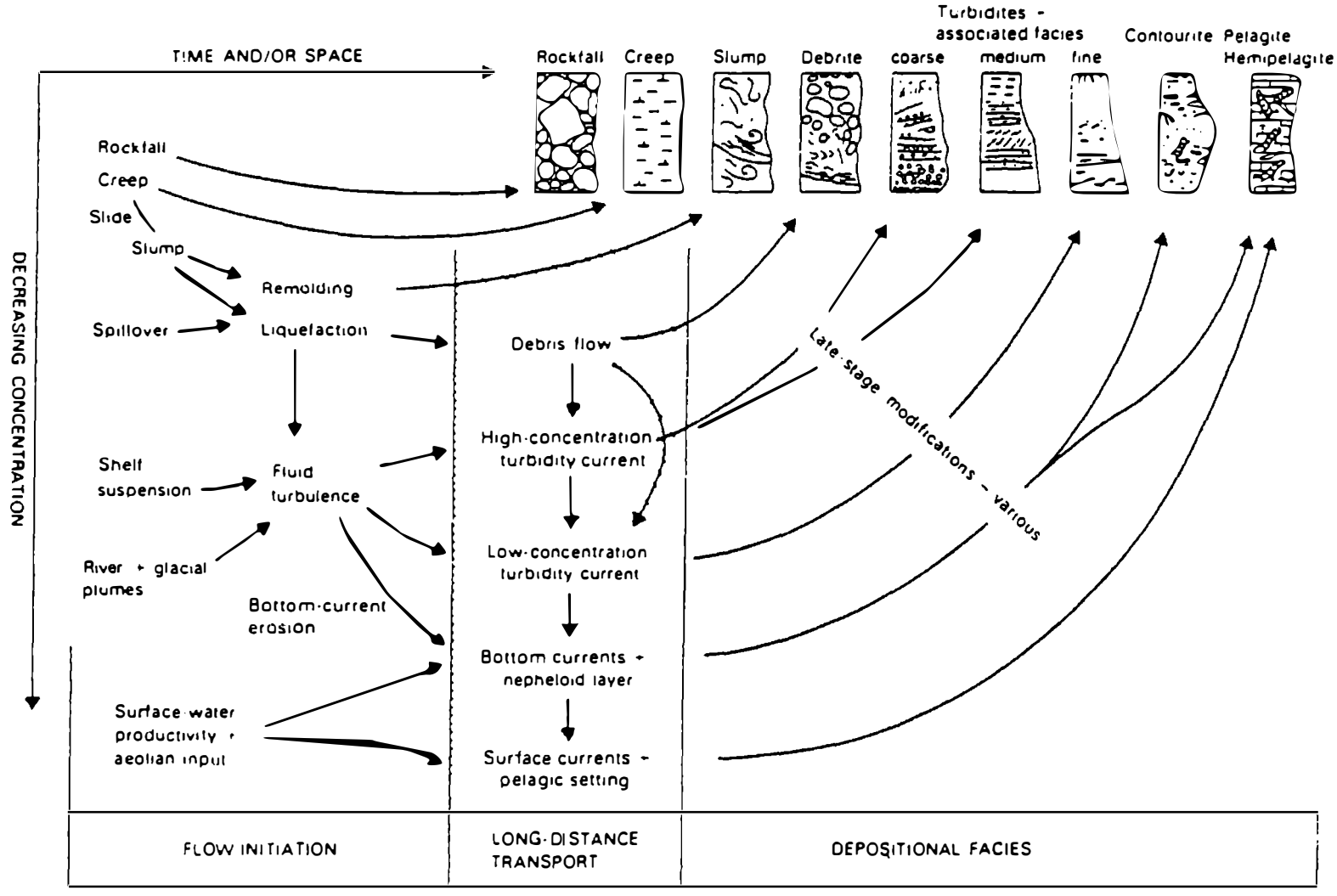

Figure 8.4 Probable inter-relationship of flow initiation, long distance transport and depositional processes in the deep sea. From Pickering et al., 1986

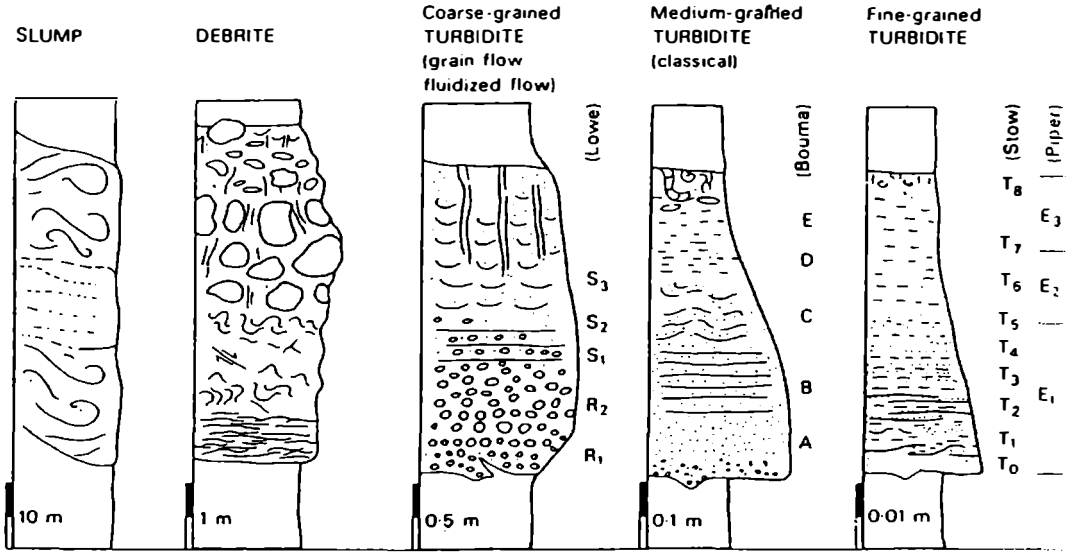

Re-sedimentated clastic facies models (from, Stow 1985).

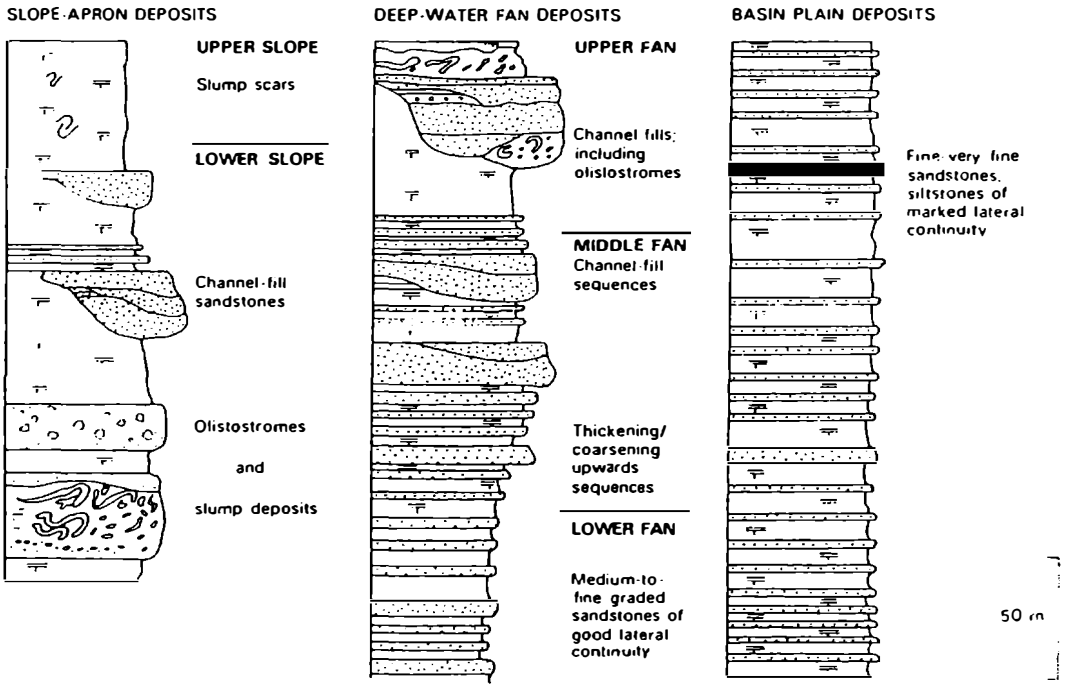

Facies associations and facies sequences (after Mutti and Ricci Lucci, 1972).

Figure 8.5 Clastic facies, facies associations and facies sequences for deep-water sediments

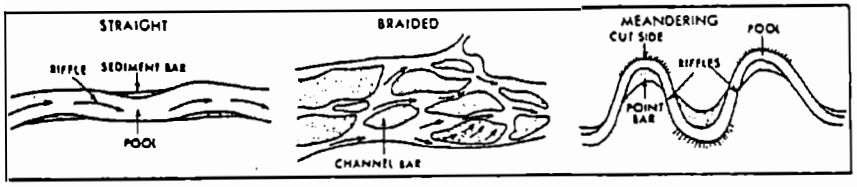

Channel patterns. (After Reineck and Singh, 1973).

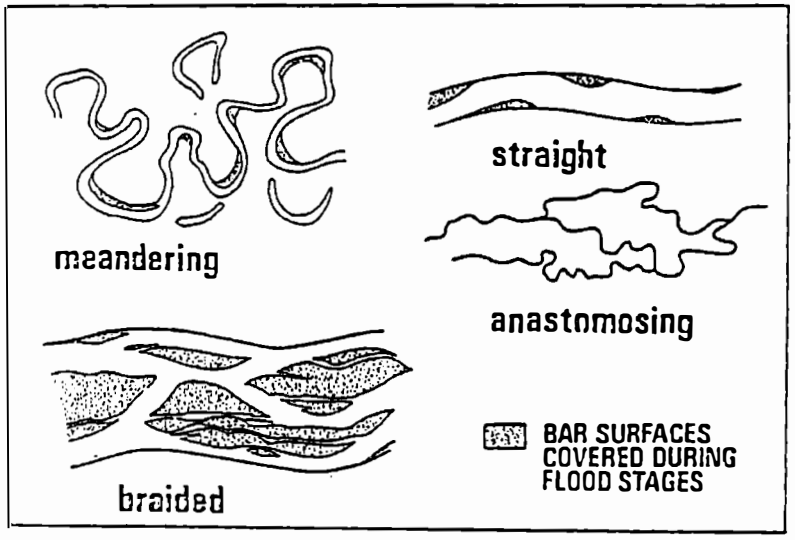

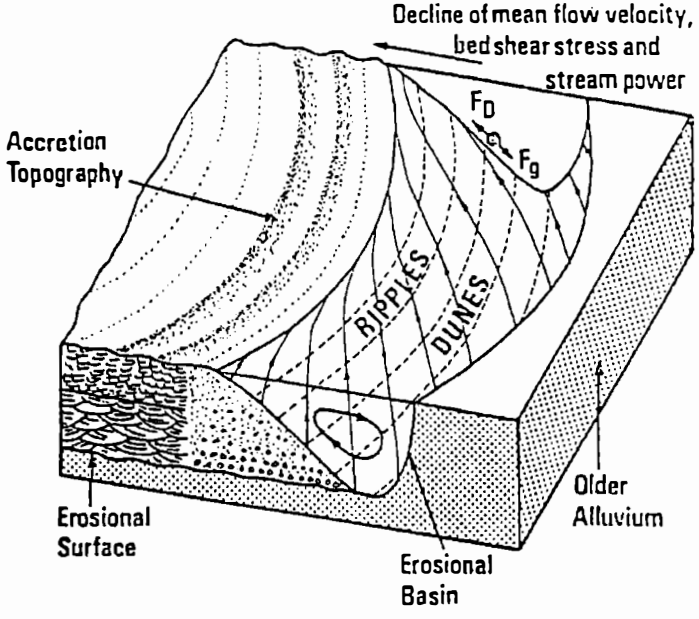

The classical point bar model for a meandering stream (after Allen, 1964, 1970b).

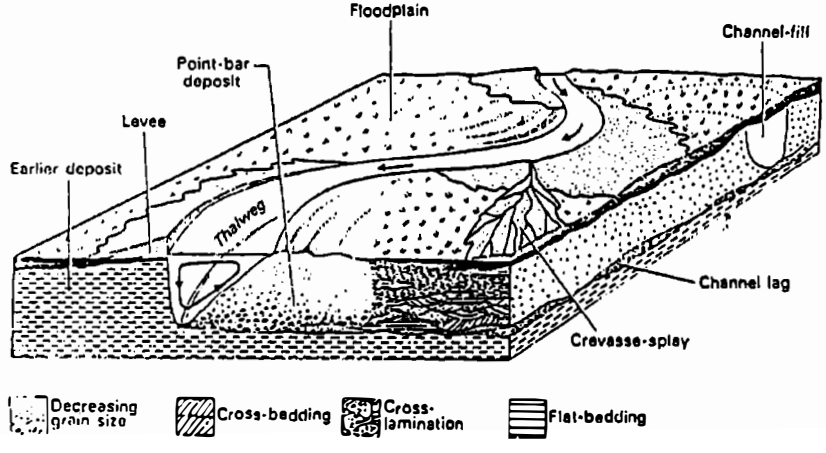

Figure 8.6 Fluvial channel morphologies and facies models.

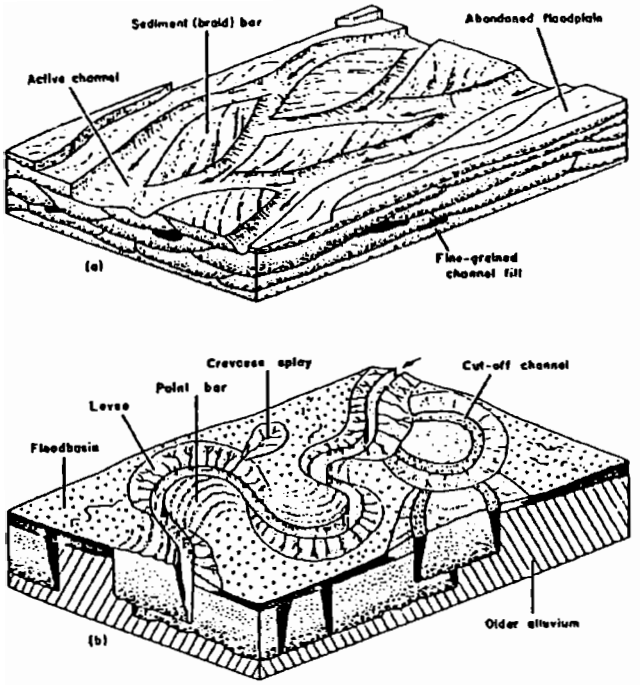

Models of fluviatile sedimentation. (a) Braided stream. (b) Meandering stream. Vertical scales exaggerated.

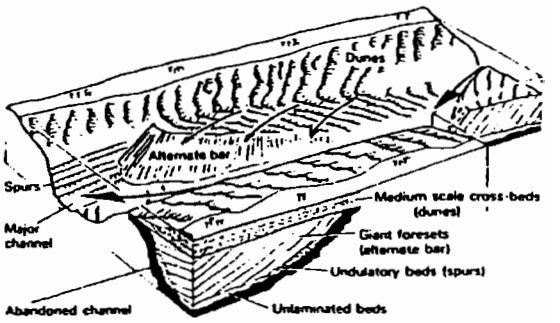

. Model for the large-scale delta-top, fluvial channels of the Namurian Kinderscout Grit of northern England. The channels are up to 40 m deep and about 1 km wide (after McCabe, 1975).

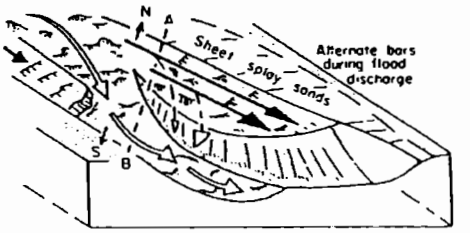

Maximum flow velocity at thalweg

Flow in the leeside surface

Flow component of the flow alternate to

A — B Quarry face

.. Alternate bar reconstruction for tangentially based foresets inclined obliquely to channel 3 axis. Note sheet splay overbank sands (modified from McCabe, 1975; Casey, 1960)

. The classical point bar model for a meandering stream (after Allen, 1964, 1970b)

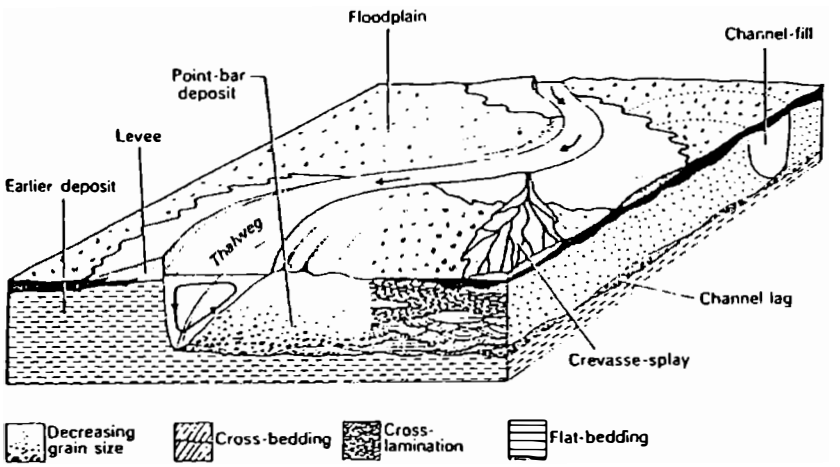

Figure 8.7 Block diagrams showing facies models for a range of fluvial channel types.

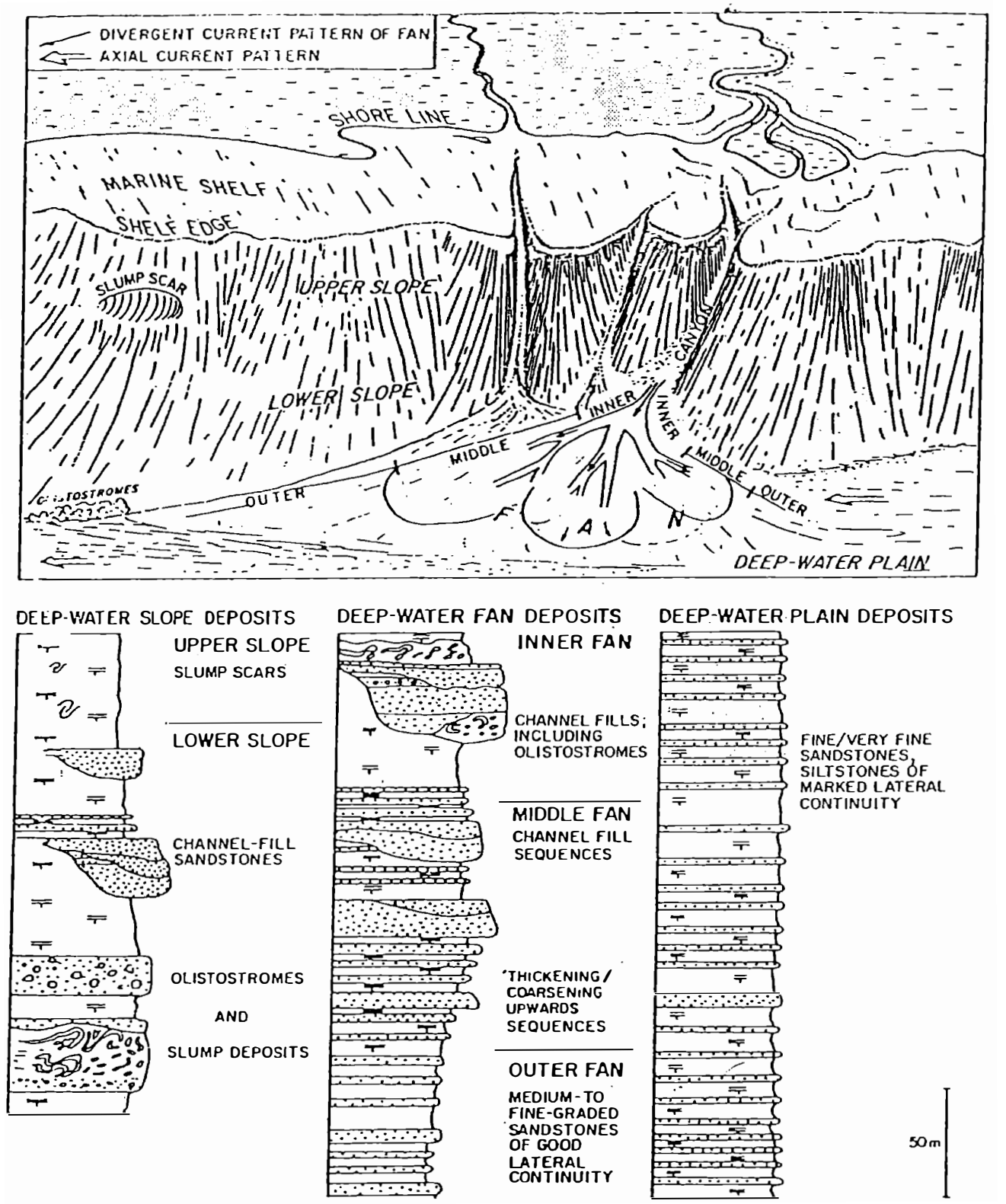

Figure 8.8 A model for deep-water slope and fan deposition. From Mutti.

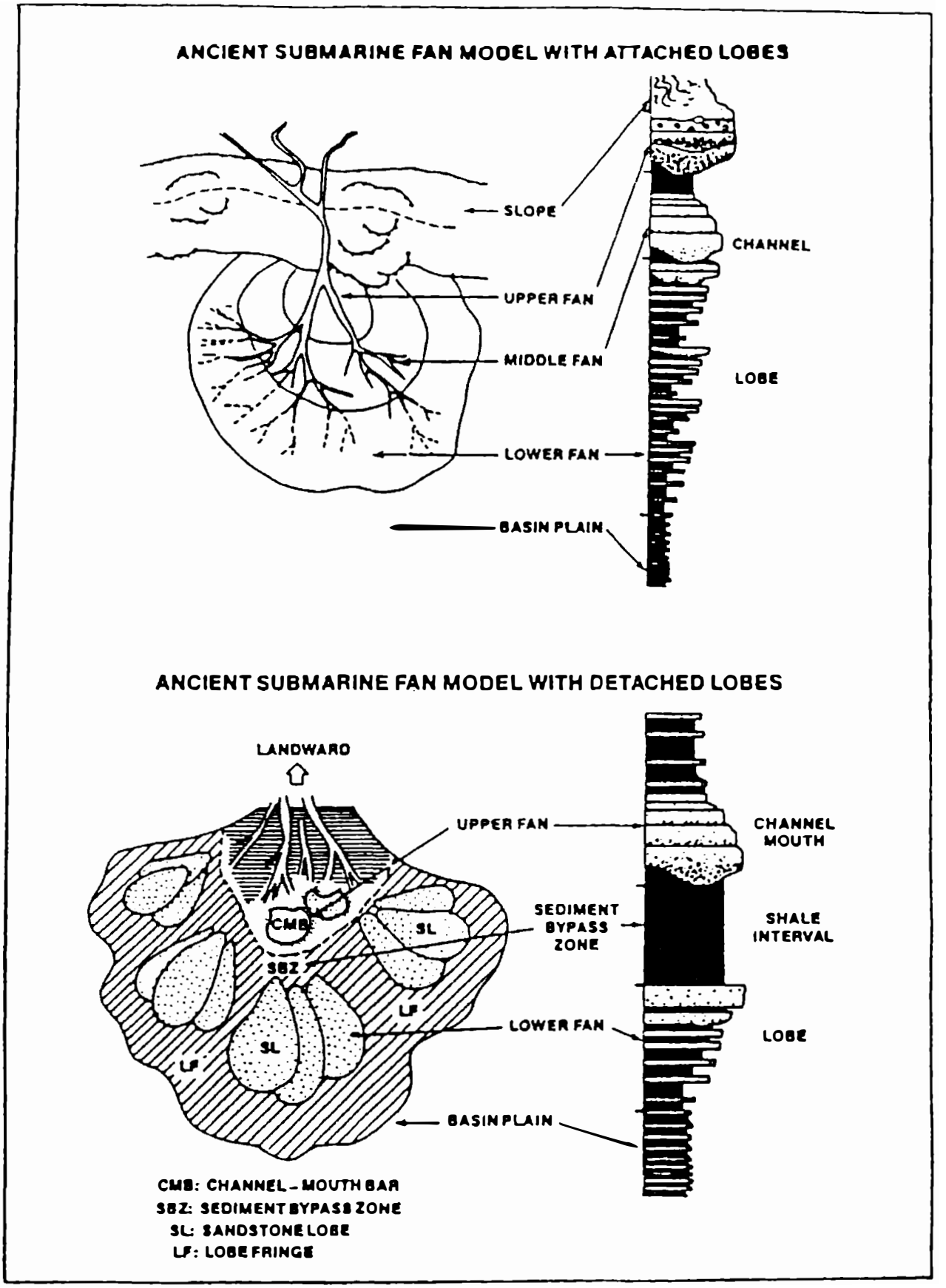

Figure 8.9 Submarine fan models (based on outcrop studies), showing upward-thinning channel sequences and upward-thickening progradational lobe sequences. (a) fan with attached lobes; (b) fan with detached lobes. After Shanmugan and Moiola, 1985.

Channel-margin facies

The facies relationships for the inner part of the Hecho Group system and terminology of channel and interchannel turbidites are shown in Fig. 3.

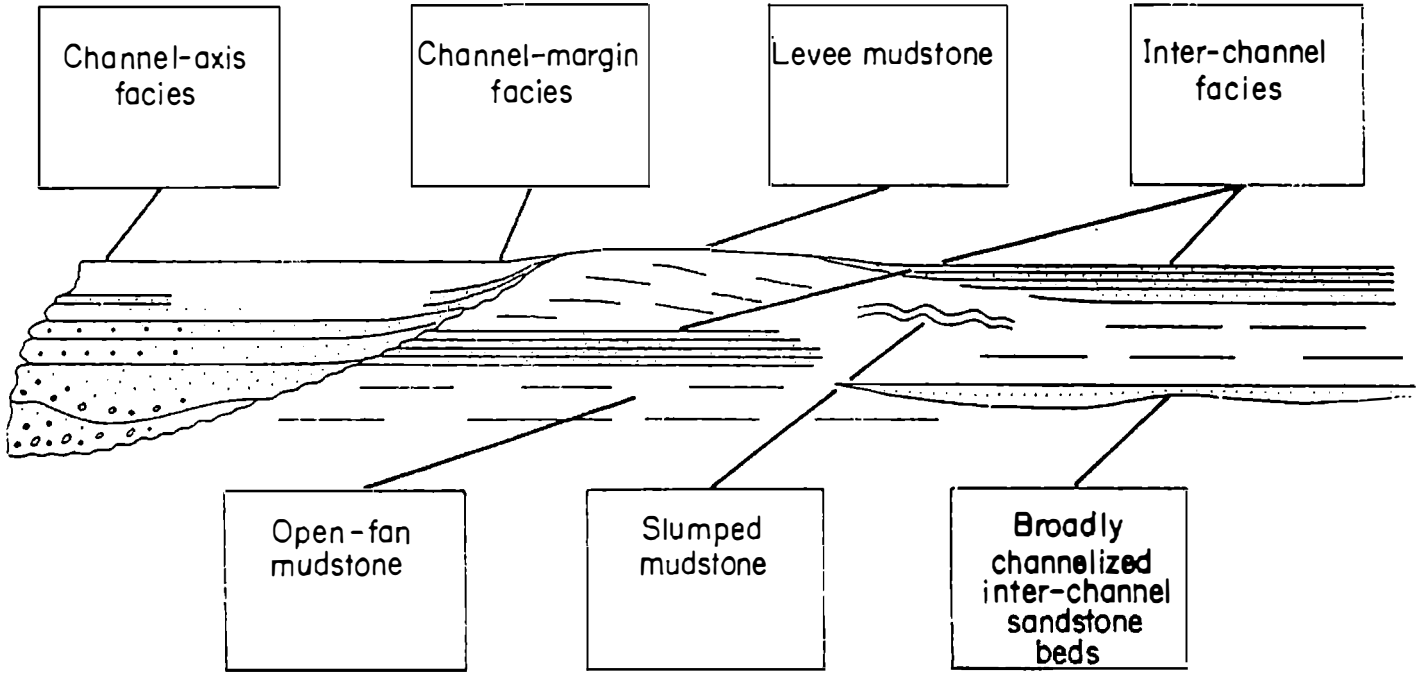

Figure 8.10 Relationships and terminology of channel and interchannel turbidite facies (as observed in the inner fan deposits of the Hecho Group). From Mutti et al.

Section 9

Notes

Sections 10 and 11

Locality map and geological map

Geological map of th

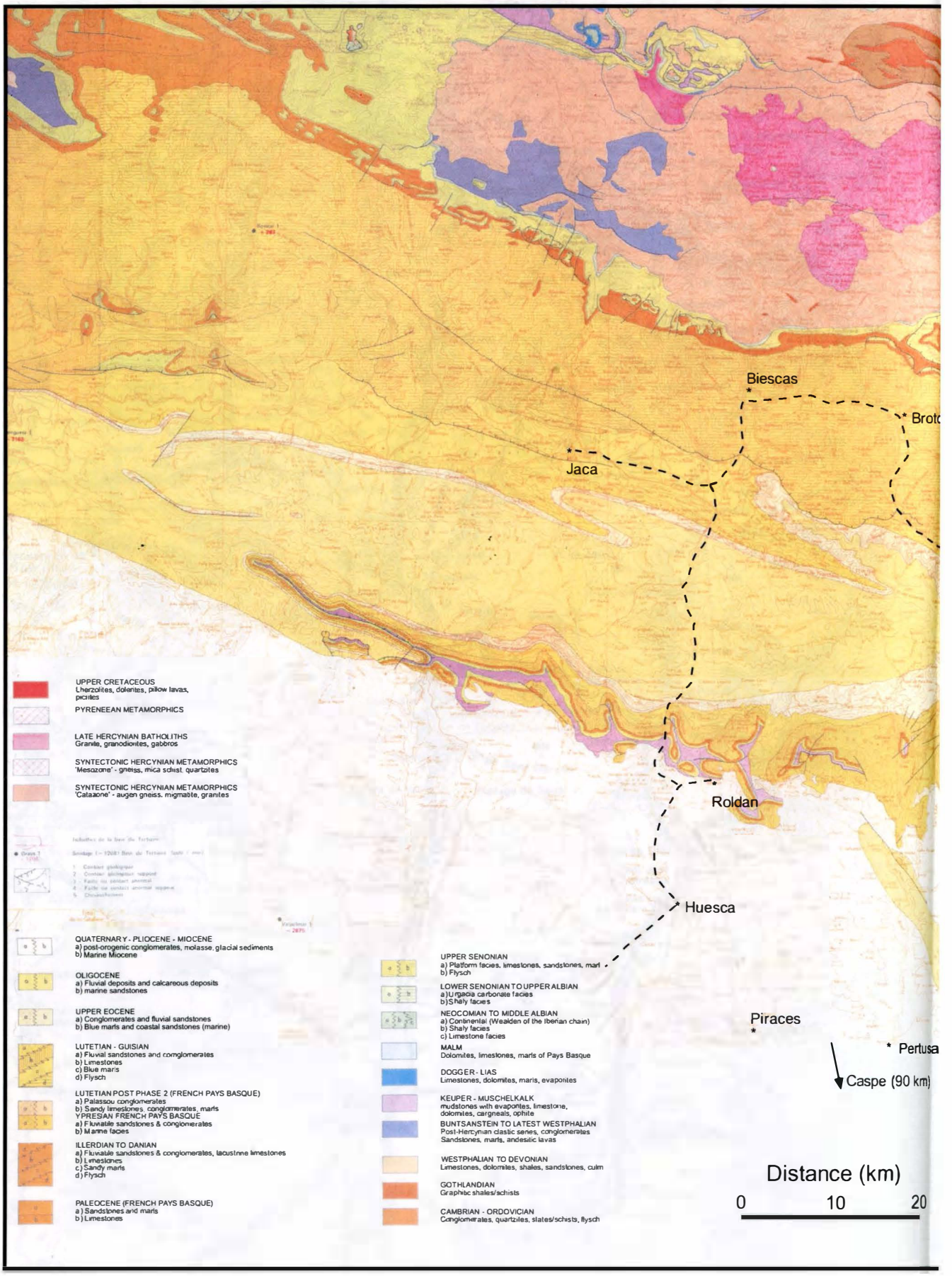

gical map of the south central Pyren

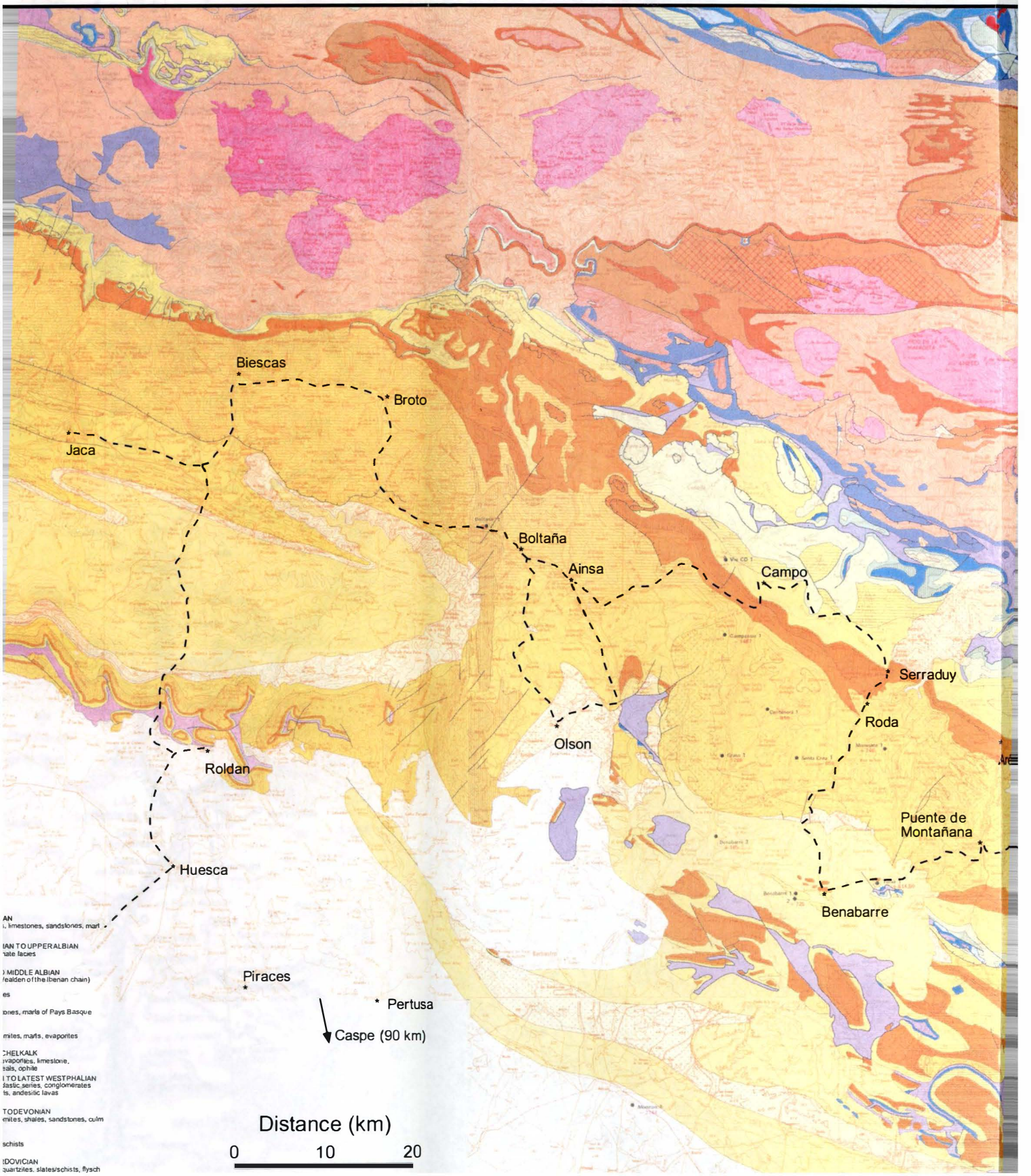

south central Pyrenees

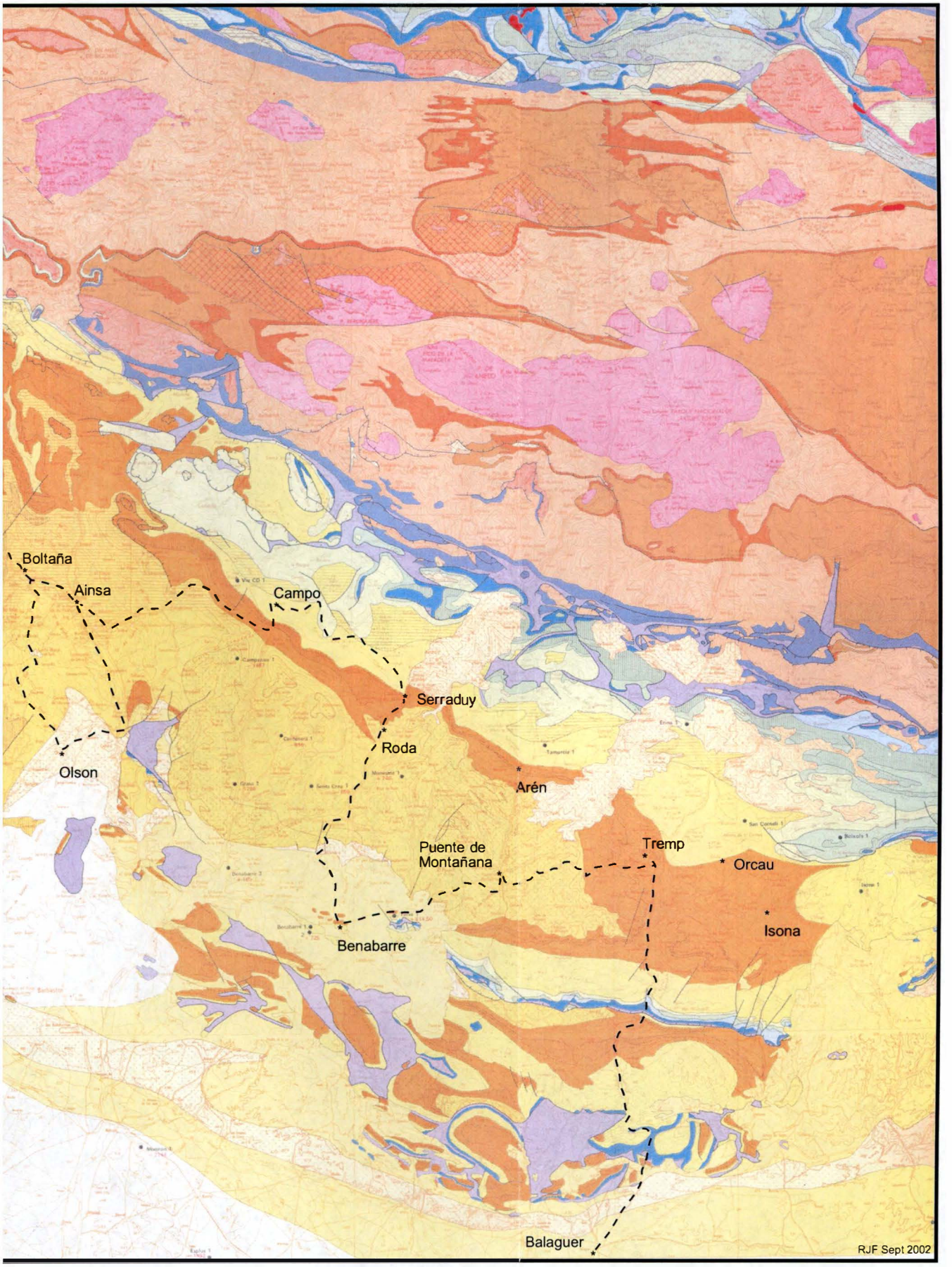

Based on Societe Nationale des Petroles D'Aquitane Carte Geologique des Pyrenees: Luz (Sheet NK 30-6) & Foix (Sheet NK 31-4) by M. Soler i Sampere, with M. J. Henry & E. Winnock, 1972.


28
4
989
29
OLORON-STE MARIE
LARUNS
ARGELÈS-GAZOST
COL DU TOURMALET
Pic d'Anie
Pic de Laraille
Puerto de Palo
Pic d'Arlet
Reserva nacional
de los Valles
Valle del Hecho
Etsaut
Urdos
Gabas
Pic de la Sagette
Pic des Tourettes
Pic du Midi d'Ossau
Parc National des Pyrénées
Balaïtous
Moun Né
Cauterets
Pont d'Espagne
Barèges
Luz-St Sauveur
St Sauveur
Pic d'Ardiden
Pic de Néouvielle
Pic Long
Gèdre
Gavarnie
Cirque de Gavarnie
Vignemale
Balneario de Panticosa
Panticosa
Pico de Baldairan
Gr de Fache
Picos del Infierno
Pto de Somport
Candanchú
Túnel de Somport
Canfranc-Estación
Canfranc
Sallent de Gállego
El Formigal
Anayet
Escarrilla
Sandiniés
Tramacastilla de Tena
Piedrafita
Búbal
Hoz de Jaca
El Pueyo
Sierra de Tendeñera
Bujaruelo
Taillón
Monte Perdido
Marboré
Parque nacional de Ordesa
Torla
Broto
Linás de Broto
Biescas
Villanúa
Collarada
Castiello de Jaca
Jaca
Sabiñánigo
Oroel
Monasterio de San Juan de la Peña
Puente la Reina de Jaca
Hecho
Siresa
Sierra de Guara
Santuario de S. Urbez
Puerto del Sarrablo
Boltaña
Aínsa
Fiscal
Valle de Solana
Sierra del Galardón
Castillo de Loarre
Loarre
Ayerbe
Los Mallos
Riglos
Murillo de Gállego
Arguis
Pto de Monrepós
Nueno
Salto del Roldán
Alquézar
Barbastro
HUESCA
Tierz
Siétamo
Monflorite
Almudévar
Tardienta
Grañén
Sariñena
Huerto
Alberuela de Tubo
Monasterio de Pueyo
N 240
N 260
N 330
A 132
E 7
HUESCA

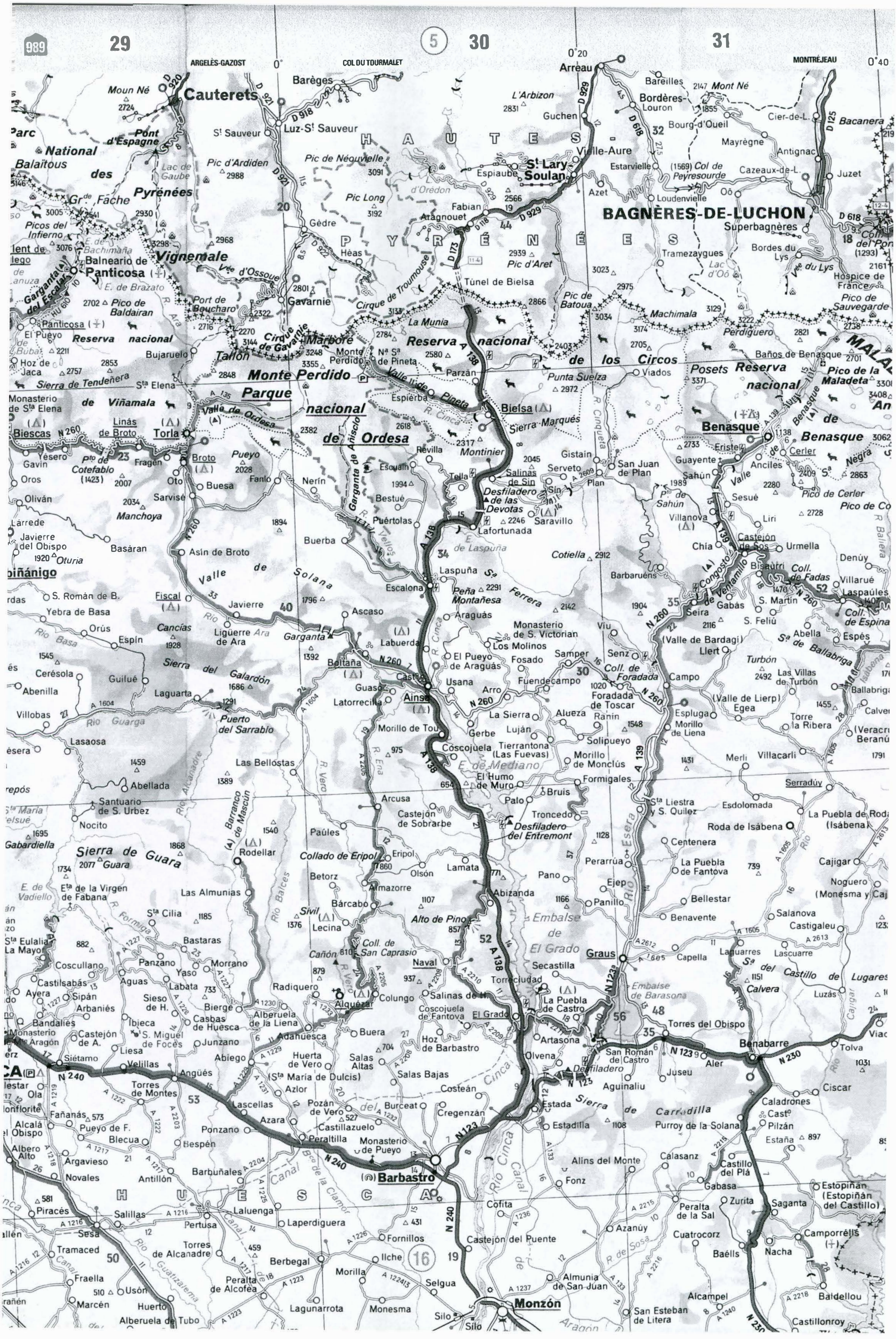

989
29
5
30
31
ARGELÈS-GAZOST
COL DU TOURMALET
MONTRÉJEAU
Cauterets
Barèges
Luz-St Sauveur
St Sauveur
Arreau
Bareilles
Mont Né
Bordères-Louron
Bourg-d'Oueil
Cier-de-L.
Bacanera
Mayrègne
Antignac
Juzet
Guchen
L'Arbizon
Vielle-Aure
St Lary-Soulan
Espiaube
Estarvielle
Col de Peyresourde
Cazeaux-de-L.
Azet
Loudenvielle
Oô
Fabian
Aragnouet
BAGNÈRES-DE-LUCHON
Superbagnères
Moun Né
Pont d'Espagne
Parc National des Pyrénées
Balaïtous
Pic d'Ardiden
Lac de Gaube
Pic de Néouvielle
d'Orédon
Pic Long
Gr.de Fache
Picos del Infierno
Gèdre
Héas
Vignemale
Balneario de Panticosa
Vde d'Ossoue
HAUTES PYRÉNÉES
Pic d'Aret
Túnel de Bielsa
Tramezaygues
Bordes du Lys
Lac d'Oô
Vée du Lys
Hospice de France
Pic de Sauvegarde
Port de Boucharo
Pic de Baldairan
Gavarnie
Cirque de Troumouse
Pic de Batoua
Machimala
Perdiguero
Cirque de Gavarnie
Marboré
La Munia
Reserva nacional de los Circos
Baños de Benasque
Pico de la Maladeta
Panticosa
El Pueyo
Reserva nacional
Bujaruelo
Taillón
Monte Perdido
Nª Sª de Pineta
Parzán
Punta Suelza
Viados
Posets
Reserva nacional
Hoz de Jaca
Sierra de Tendeñera
Sta Elena
Parque nacional de Ordesa
Valle de Pineta
Espierba
Bielsa
Sierra Marqués
Benasque
Valle de Benasque
Monasterio de Sta Elena
de Viñamala
Valle de Ordesa
Biescas
Linás de Broto
Torla
Revilla
Montinier
Gistain
San Juan de Plan
Eriste
Cerler
Yésero
Gavín
Fragen
Broto
Pueyo
Garganta de Añisclo
Escuaín
Tella
Salinas de Sin
Serveto
Sin
Plan
Guayente
Anciles
Sahún
Pto de Cotefablo
Oto
Buesa
Fanlo
Nerín
Bestué
Desfiladero de las Devotas
Saravillo
Pto de Sahún
Sesué
Pico de Cerler
Oros
Oliván
Sarvisé
Manchoya
Púertolas
Lafortunada
Villanova
Liri
Pico de Co
Lárrede
Javierre del Obispo
Oturia
Basarán
Asín de Broto
Buerba
Vellos
E. de Laspuña
Cotiella
Chía
Castejón de Sos
Urmella
Denúy
Sabiñánigo
Valle de Solana
Laspuña
Sª Ferrera
Barbaruens
Bisaurri
Coll. de Fadas
Villarué
Laspaúles
S. Román de B.
Fiscal
Javierre
Escalona
Peña Montañesa
Congosto de Ventamillo
Seira
Gabás
S. Martín
Coll. de Espina
Yebra de Basa
Ascaso
Araguás
Monasterio de S. Victorian
Los Molinos
Viu
S. Feliú
Espés
Orús
Espín
Cancías
Ligüerre de Ara
Garganta
Labuerda
El Pueyo de Araguás
Fosado
Samper
Senz
(Valle de Bardagí)
Llert
Abella
Sª de Ballabriga
Ceresola
Sierra del Galardón
Boltaña
Coll. de Foradada
Turbón
Las Villas de Turbón
Campo
Guilué
Abenilla
Laguarta
Guaso
Castejón
Usana
Fuendecampo
Foradada de Toscar
Ballabriga
Latorrecilla
Aínsa
Arro
Ranín
(Valle de Lierp)
Egea
Calvera
Villobas
Rio Guarga
Puerto del Sarrablo
La Sierra
Alueza
Espluga
Torre la Ribera
Morillo de Tou
Gerbe
Luján
Solipueyo
Morillo de Liena
Veracruz
Beranú
Lasaosa
Coscojuela
Tierrantona (Las Fuevas)
Morillo de Monclús
Villacarli
Merli
Las Bellostas
E. de Mediano
El Humo de Muro
Formigales
Serradúy
Abellada
Bruis
Santuario de S. Urbez
Arcusa
Palo
Sta Liestra y S. Quílez
Esdolomada
La Puebla de Roda (Isábena)
Nocito
Castejón de Sobrarbe
Troncedo
Desfiladero del Entremont
Roda de Isábena
Gabardiella
Paúles
Centenera
Sierra de Guara
Rodellar
Collado de Eripol
Eripol
Lamata
Perarrúa
La Puebla de Fantova
Cajigar
E.ta de la Virgen de Fabana
Olsón
Pano
Noguero
(Monesma y Cajigar)
Betorz
Almazorre
Ejep
Panillo
Bellestar
Las Almunias
Bárcabo
Abizanda
Benavente
Salanova
Sta Cilia
Sivil
Alto de Pino
Embalse de El Grado
Castigaleu
Sta Eulalia La Mayor
Bastaras
Lecina
Graus
Capella
Laguarres
Lascuarre
Coll. de San Caprasio
Cañón
Naval
Secastilla
Sª del Castillo de Lugares
Cosculluno
Panzano
Morrano
Yaso
Torreciudad
Calvera
Luzás
Castilsabás
Aguas
Labata
Radiquero
La Puebla de Castro
Embalse de Barasona
Ayera
Sipán
Arbaniés
Sieso de H.
Bierge
Alquézar
Colungo
Salinas de H.
Coscojuela de Fantova
El Grado
Bandaliés
Ibieca
Casbas de Huesca
Alberuela de la Liena
Adahuesca
Artasona
Torres del Obispo
Monasterio de Aragón
Castejón de A.
S. Miguel de Foces
Junzano
Buera
Hoz de Barbastro
San Román de Castro
Benabarre
Liesa
Abiego
Huerta de Vero
Salas Altas
Olvena
Aler
Viacamp
Tolva
Siétamo
Velillas
Angüés
(Sta María de Dulcis)
Salas Bajas
Desfiladero
Juseu
Aguinaliu
Torres de Montes
Azlor
Costeán
Estada
Sierra de Carrodilla
Ciscar
Caladrones
Castº
Pilzán
Estaña
Fañanás
Lascellas
Pozán de Vero
Burceat
Cregenzán
Estadilla
Purroy de la Solana
Alcalá del Obispo
Pueyo de F.
Azara
Castillazuelo
Ponzano
Albero Alto
Blecua
Bespén
Peraltilla
Monasterio de Pueyo
Alins del Monte
Calasanz
Argavieso
Castillo del Plá
Novales
Antillón
Barbuñales
Barbastro
Fonz
Gabasa
Estopiñán (Estopiñán del Castillo)
HUESCA
Cofita
Peralta de la Sal
Zurita
Saganta
Piracés
Salillas
Laluenga
Laperdiguera
Sesa
Pertusa
Azanúy
Cuatrocorz
Camporrélls
Tramaced
Torres de Alcanadre
Fornillos
Castejón del Puente
Baélls
Nacha
Berbegal
Ilche
Fraella
Peralta de Alcofea
Morilla
Selgua
Almunia de San Juan
Alcampel
Baldellou
Usón
Marcén
Huerto
Lagunarrota
Monesma
Monzón
San Esteban de Litera
Alberuela de Tubo
Silo
Castillonroy

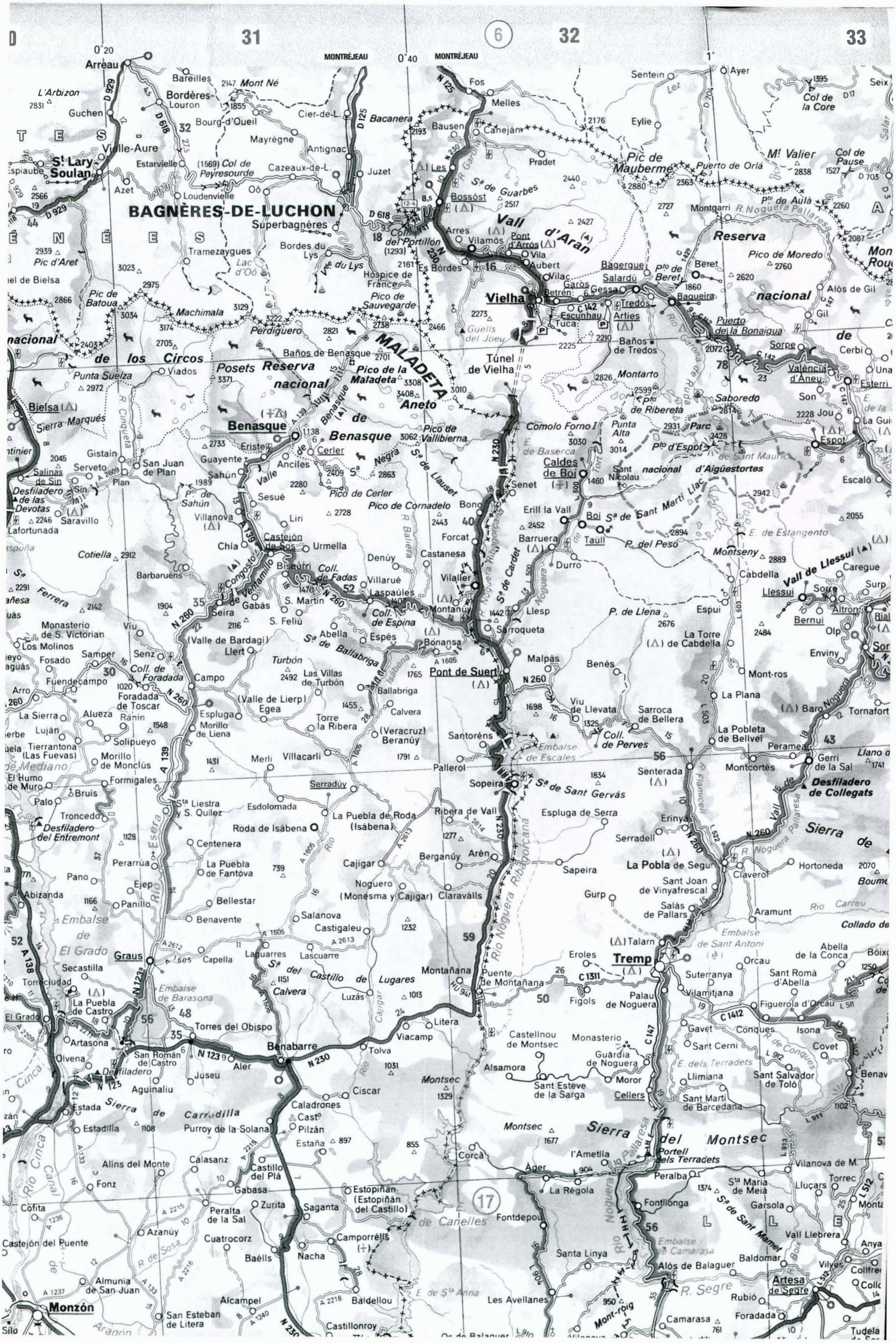
31
6
32
33
MONTRÉJEAU
MONTRÉJEAU
0°20
0°40
1°
Arreau
L'Arbizon
2831
Guchen
Bareilles
2147 Mont Né
Bordères-Louron
Bourg-d'Oueil
Mayrègne
Antignac
Cier-de-L.
Bacanera
Fos
Melles
Bausen
Canejàn
Sentein
Ayer
Lez
Eylie
2176
Col de la Core
Seix
Vielle-Aure
St Lary-Soulan
Estarvielle
(1569) Col de Peyresourde
Cazeaux-de-L.
Juzet
Les
Pradet
Pic de Maubermé
2880
2363
Puerto de Orlá
Mt Valier
2838
Col de Pause
1527
Azet
Loudenvielle
Oô
Bossòst
Sa de Guarbes
2517
2440
Montgarri
R. Noguera Pallaresa
Pto de Aulà
2260
BAGNÈRES-DE-LUCHON
Superbagnères
D 618
Coll del Portillón
(1293)
Arres
Vilamòs
Pont d'Arròs
Vall d'Aran
2427
2727
Reserva
Pico de Moredo
2760
2087
2939
Pic d'Aret
Tramezaygues
Bordes du Lys
Lac d'Oô
Vée du Lys
Es Bòrdes
Hospice de France
Vila
Aubert
Vilac
Bagergue
Salardú
Garòs
Gessa
Betrén
Pto de Beret
Beret
2620
1860
Baqueira
Alòs de Gil
nacional
Gil
3023
2975
Pic de Batoua
Machimala
3129
Pico de Sauvegarde
Vielha
C 142
Tredòs
Arties
Escunhau
Casarilh
Tuca
Puerto de la Bonaigua
Sorpe
de
Cerbi
2866
3034
3174
3222
Perdiguero
2821
2738
2466
2273
Guells del Joeu
2210
Baños de Tredós
2072
de los Circos
2705
2403
Baños de Benasque
2701
MALADETA
2225
Túnel de Vielha
Punta Suelza
2972
Viados
Posets
3371
Reserva nacional
Pico de la Maladeta
3308
3408
Aneto
3010
2826
Montarto
78
València d'Àneu
Una
Esterri
Bielsa
Sierra Marqués
Benasque
de Benasque
Pico de Vallibierna
3062
2599
Pto de Ribereta
Saboredo
2814
Son
2228
Jou
Espot
2733
Eriste
Gistain
Serveto
San Juan de Plan
Plan
2045
Guayente
Sahún
Anciles
Cerler
2409
Sa Negra
2863
Sa de Llauset
Cómolo Forno I
3030
Punta Alta
3014
2931
Parc
2428
Pto d'Espot
de Sant Maurici
Caldes de Boí
1460
Sant Nicolau
nacional d'Aigüestortes
Escaló
Salinas de Sin
Desfiladero de las Devotas
2246
Saravillo
Lafortunada
1989
Pto de Sahún
Villanova
2280
Pico de Cerler
Sesué
Liri
2728
Pico de Cornadelo
Bono
Senet
Erill la Vall
2452
Boí
Sa de Sant Martí
Llac
2942
2055
Cotiella
2912
Chía
Castejón de Sos
Urmella
2443
Forcat
Barruera
Taüll
2894
P. del Peso
E. de Estangento
Montseny
2889
Caregue
Sa Ferrera
2291
Barbaruéns
Bisaurri
Coll. de Fadas
Denúy
Villarué
Laspaúles
Castanesa
Vilaller
Sa de Cardet
Durro
Cabdella
Vall de Llessui
Llessui
Surp
Sorre
Altron
Bernui
2142
1904
Seira
Gabás
S. Martín
Coll. de Espina
Montanuy
1442
Llesp
P. de Llena
2676
Espui
2484
Monasterio de S. Victorian
Los Molinos
Viu
2116
S. Feliú
Abella
Espés
Bonansa
Sarroqueta
La Torre de Cabdella
Olp
Fosado
Samper
Senz
(Valle de Bardagí)
Llert
Sa de Ballabriga
Malpàs
Benés
Enviny
Fuendecampo
Coll. de Foradada
Campo
Turbón
2492
Las Villas de Turbón
1765
1605
Pont de Suert
N 260
Mont-ros
Foradada de Toscar
1020
Ballabriga
1698
La Plana
La Sierra
Alueza
Ranin
Espluga
(Valle de Lierp)
Egea
1455
Calvera
Viu de Llevata
Sarroca de Bellera
Baro
Tornafort
Luján
Morillo de Liena
1548
Torre la Ribera
(Veracruz) Beranúy
Santoréns
1325
Coll. de Perves
La Pobleta de Bellvei
Peramea
Tierrantona (Las Fuevas)
Solipueyo
Morillo de Monclús
1431
Merli
Villacarli
1791
Embalse de Escales
Gerri de la Sal
Llano
1741
de Mediano
El Humo de Muro
Formigales
Pallerol
Sopeira
Sa de Sant Gervàs
1834
Senterada
Montcortés
Desfiladero de Collegats
Palo
Bruis
Serradúy
Sta Liestra y S. Quílez
Esdolomada
La Puebla de Roda (Isábena)
Ribera de Vall
2614
Espluga de Serra
Erinyà
Sierra de
Troncedo
Desfiladero del Entremont
Roda de Isábena
1128
Centenera
1277
Serradell
Perarrúa
La Puebla de Fantova
739
Cajigar
Berganúy
Arén
Sapeira
La Pobla de Segur
Claverol
Hortoneda
2070
Pano
Ejep
Noguero (Monesma y Cajigar)
Claravalls
Gurp
Sant Joan de Vinyafrescal
Abizanda
Panillo
Bellestar
1166
Salàs de Pallars
Aramunt
Embalse de El Grado
Benavente
Salanova
Castigaleu
1232
Collado de
A 138
Graus
Capella
Laguarres
Lascuarre
Sa del Castillo de Lugares
59
Talarn
Tremp
Embalse de Sant Antoni
Abella de la Conca
Secastilla
Torreciudad
La Puebla de Castro
Embalse de Barasona
Sa de Calvera
1151
Luzás
1013
Montañana
Puente de Montañana
26
C 1311
Eroles
Figols
Palau de Noguera
Suterranya
Orcau
Vilamitjana
Sant Romà d'Abella
El Grado
56
48
Torres del Obispo
Litera
Viacamp
Castellnou de Montsec
Monasterio
Gavet
Conques
Isona
Figuerola d'Orcau
Artasona
35
Benabarre
Tolva
Guàrdia de Noguera
Sant Cerni
Covet
Olvena
San Román de Castro
N 123
Aler
N 230
1031
Montsec
Alsamora
Sant Esteve de la Sarga
Moror
Llimiana
Sant Salvador de Toló
Desfiladero
Juseu
Aguinaliu
Ciscar
1329
Cellers
Sant Martí de Barcedana
Benav
Estada
Sierra de Carrodilla
Caladrones
Castº
Pilzán
1102
Estadilla
1108
Purroy de la Solana
Montsec
1677
Sierra del Montsec
Estaña
897
855
l'Ametlla
Portell dels Terradets
Alins del Monte
Calasanz
Castillo del Plá
Corça
Àger
L 904
Vilanova de M.
Fonz
Gabasa
La Règola
Peralba
1374
Sta Maria de Meià
Llucars
Torrec
Cofita
Zurita
Estopiñán (Estopiñán del Castillo)
17
Saganta
Fontdepou
Fontllonga
Sa de Sant Mamet
Garsola
Peralta de la Sal
Embalse de Canelles
Castejón del Puente
Azanúy
Cuatrocorz
Camporrélls
Santa Linya
Embalse de Camarasa
Vall Llebrera
Anya
Baélls
Nacha
Alòs de Balaguer
Baldomar
Vilves
Collfred
Almunia de San Juan
R. Segre
Artesa de Segre
Colld
Monzón
Alcampel
Baldellou
Les Avellanes
950
Rubió
Foradada
San Esteban de Litera
Castillonroy
Mont-roig
Camarasa
761
Tudela
Silo

North Sea Tertiary

	Velocity (m/s)	Density (g/cc)	Impedance ($kgm^{-2}s^{-1}$)
Massive sandstone	3208	2.17	6961 x 10^3
Medium bedded sandstones and shales	2903	2.27	6590 x 10^3
Thinly bedded sandstones and shales	2703	2.21	5974 x 10^3
Shale and marl	2498	2.35	5870 x 10^3

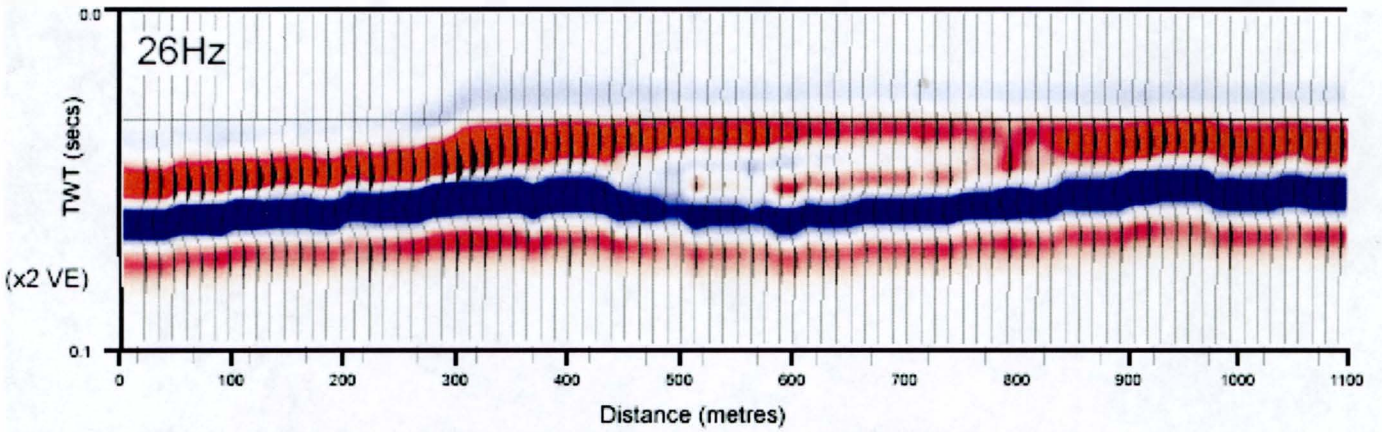

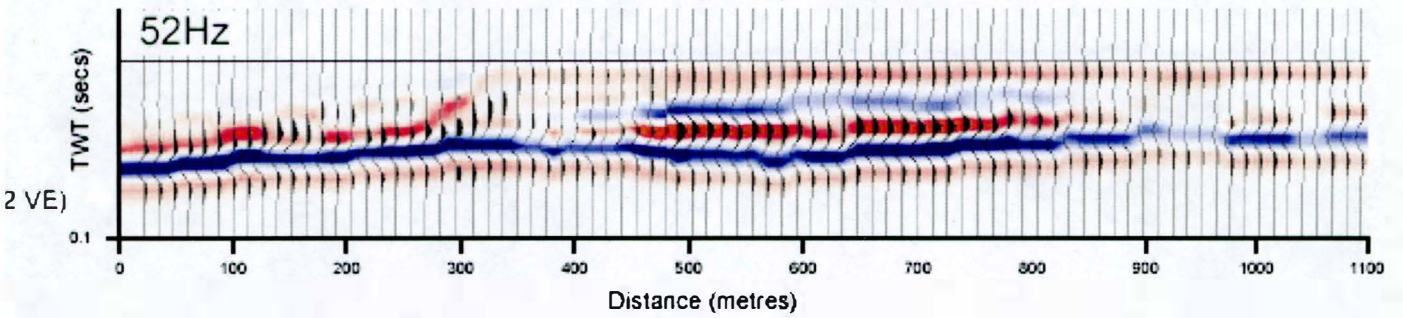

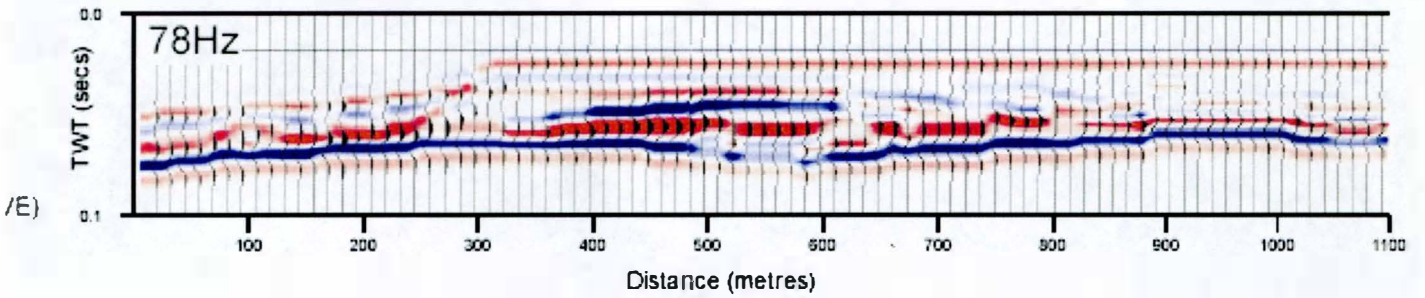

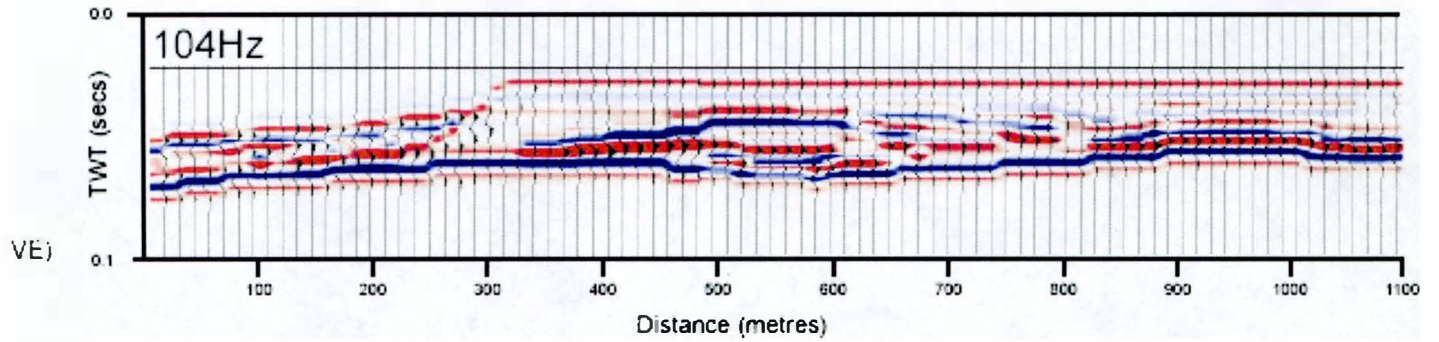

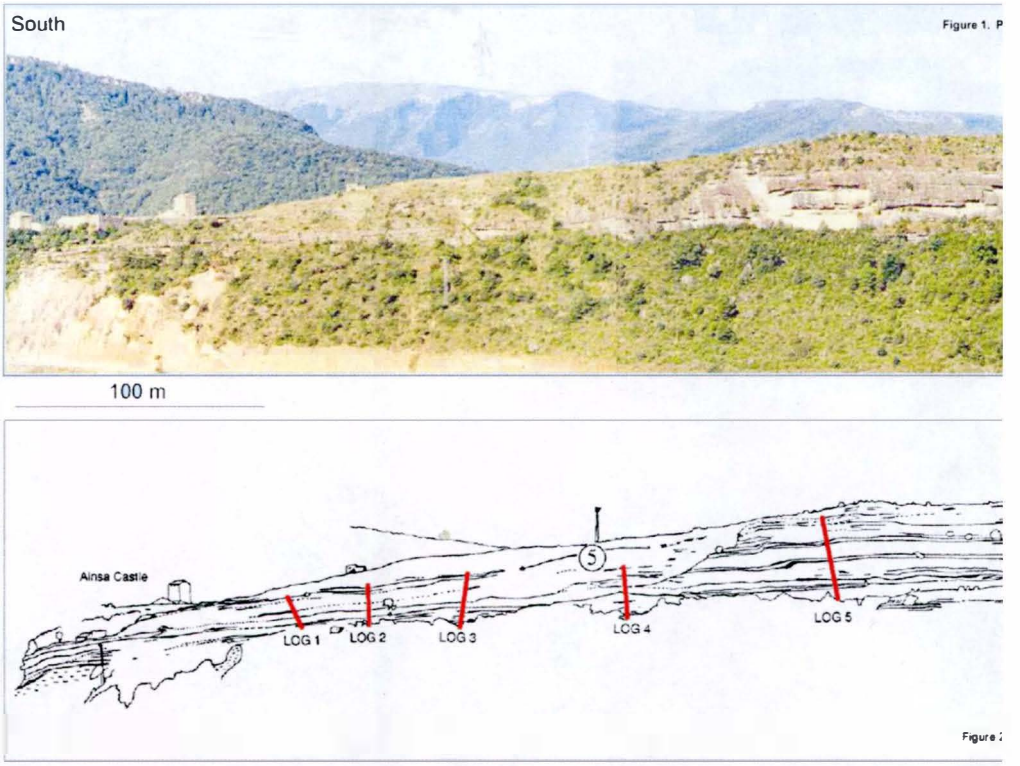

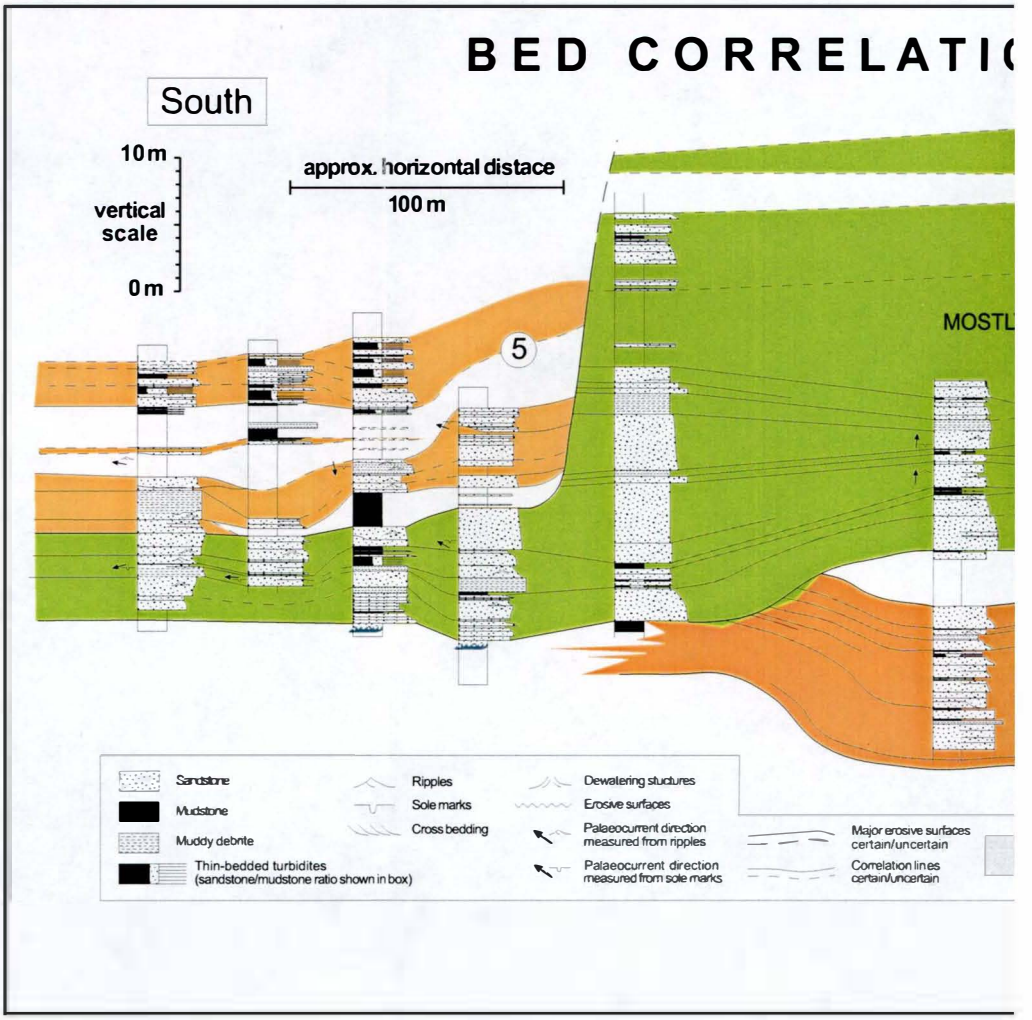

Bed correlation of the Ainsa II Channel showing five stacked channel eleme

Figure 1. Photomosaic of the Ainsa II Channel Complex viewed from across the Rio Cinca. The lateral southward shifting of channel bodies can be clear

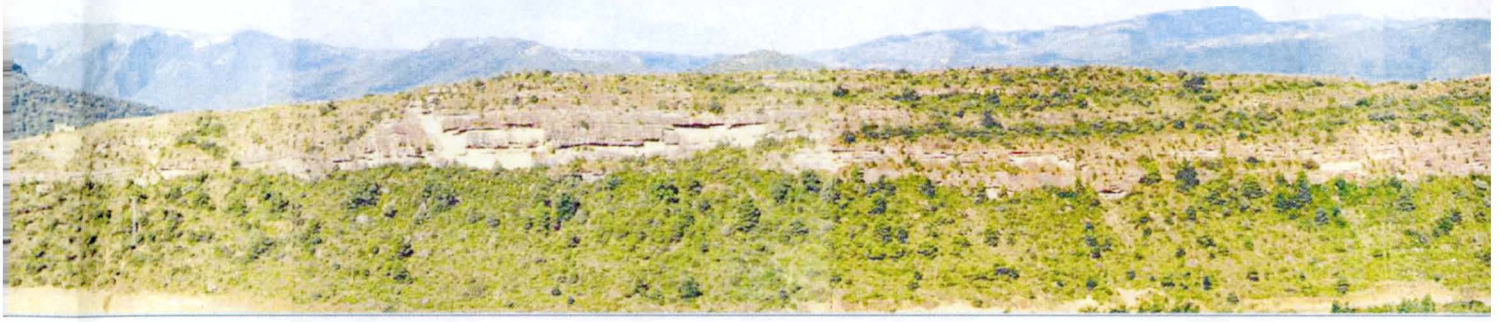

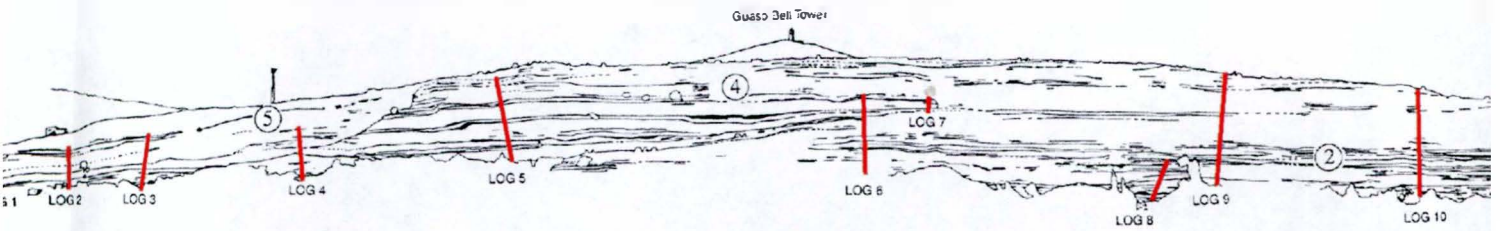

Figure 2. Photomosaic interpretation of the Ainsa II Channel Complex. Sedimentological logs through the section are shown in red labelled 1 - 14.

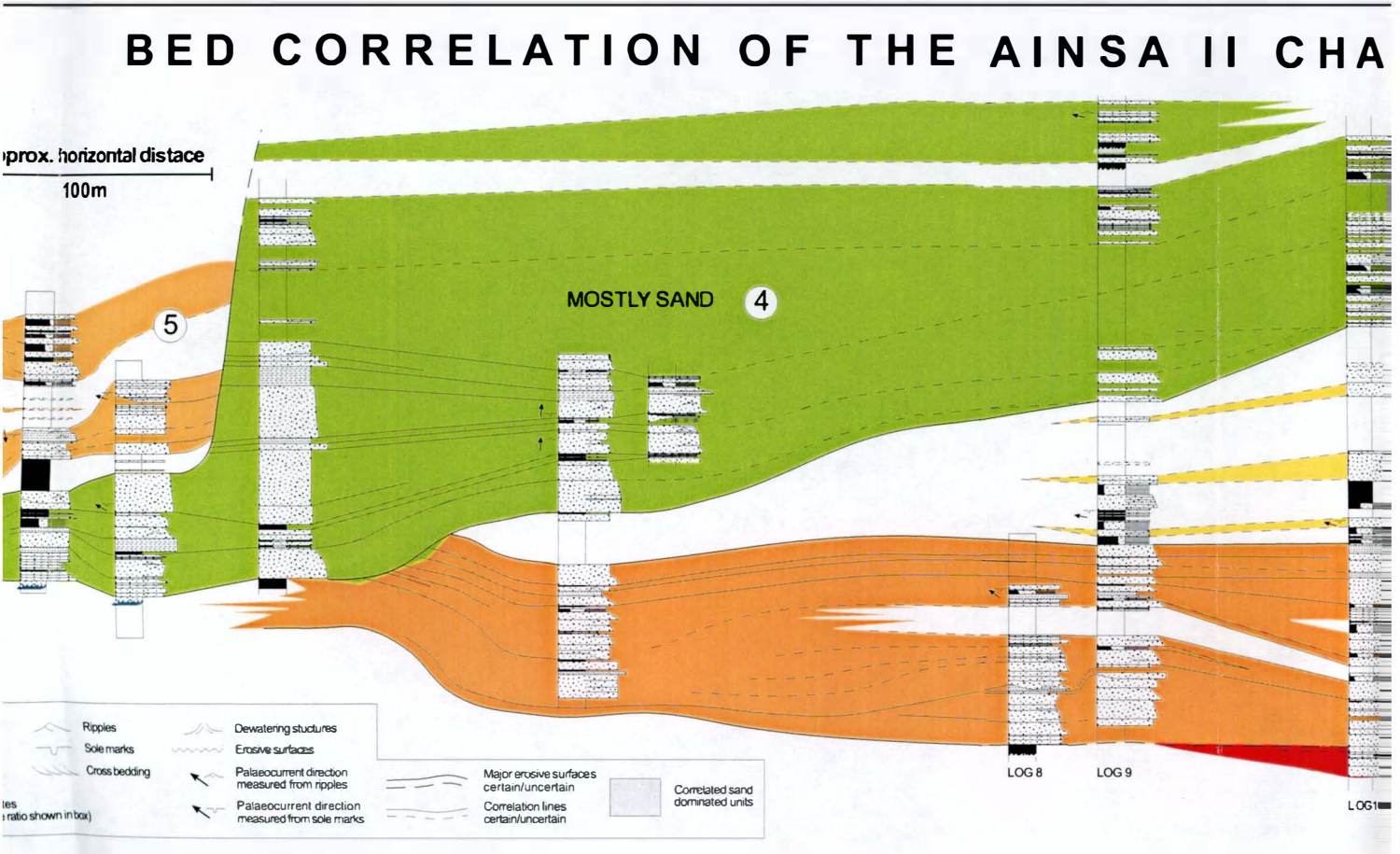

tion of the Ainsa II Channel showing five stacked channel elements numbered 1-5 (Clark 1994).

ica. The lateral southward shifting of channel bodies can be clearly seen in the photomosaic.

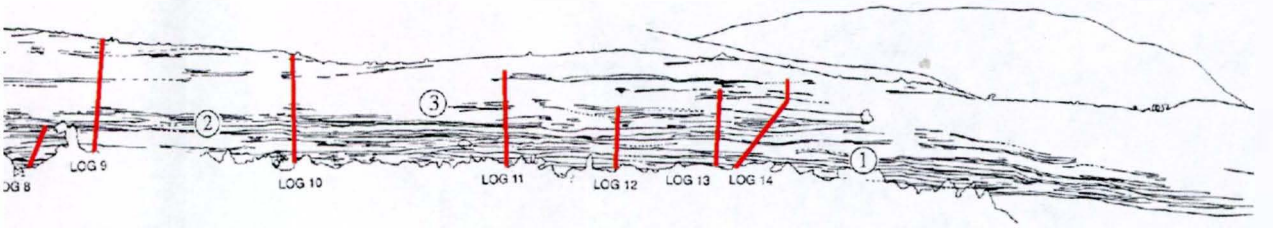

gical logs through the section are shown in red labelled 1 - 14. For details see Poster 2.

NSA II CHANNEL COMPLEX.

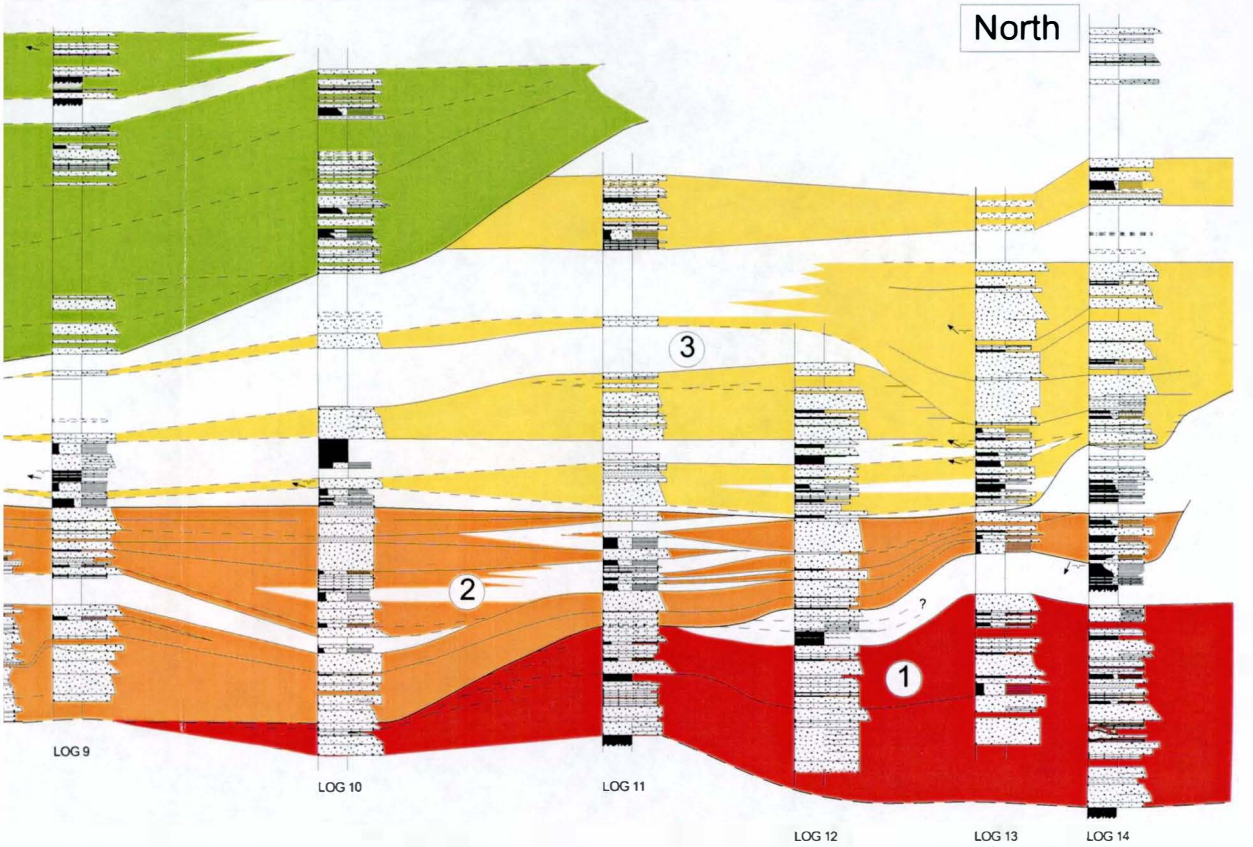

50 m

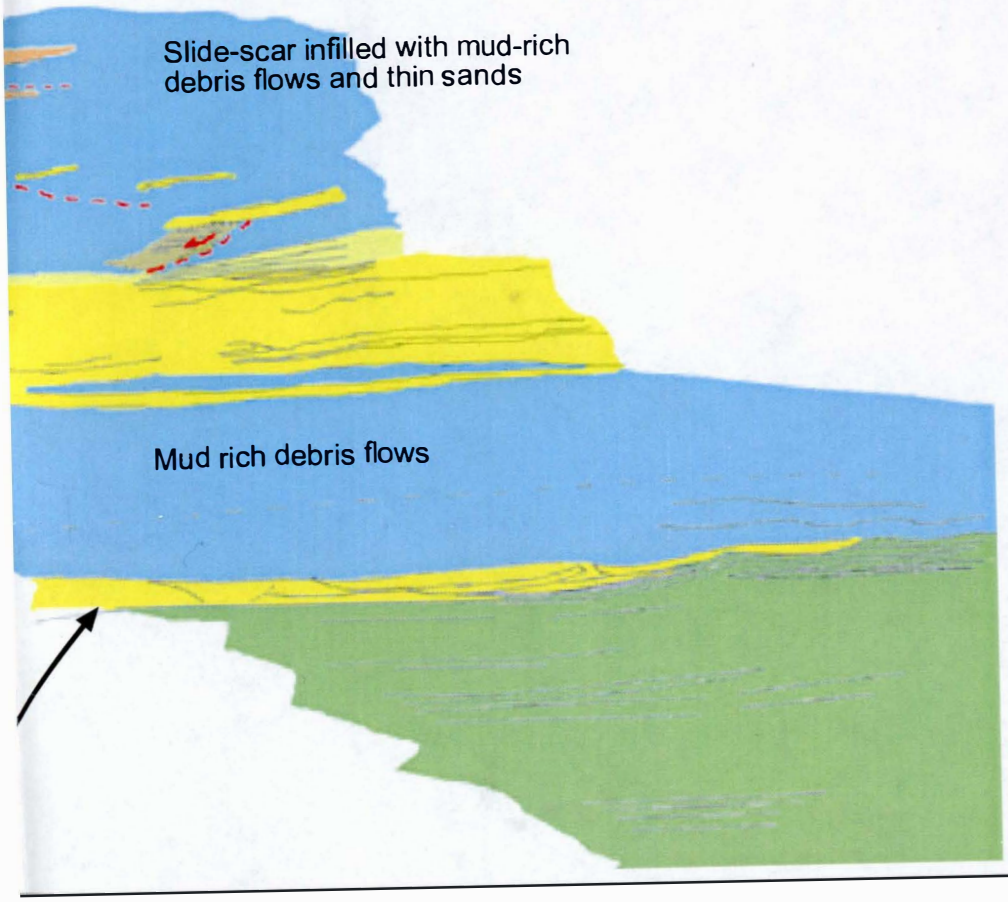
Slide-scar infilled with mud-rich
debris flows and thin sands
Mud rich debris flows

:hannel complex, Rio Ara section

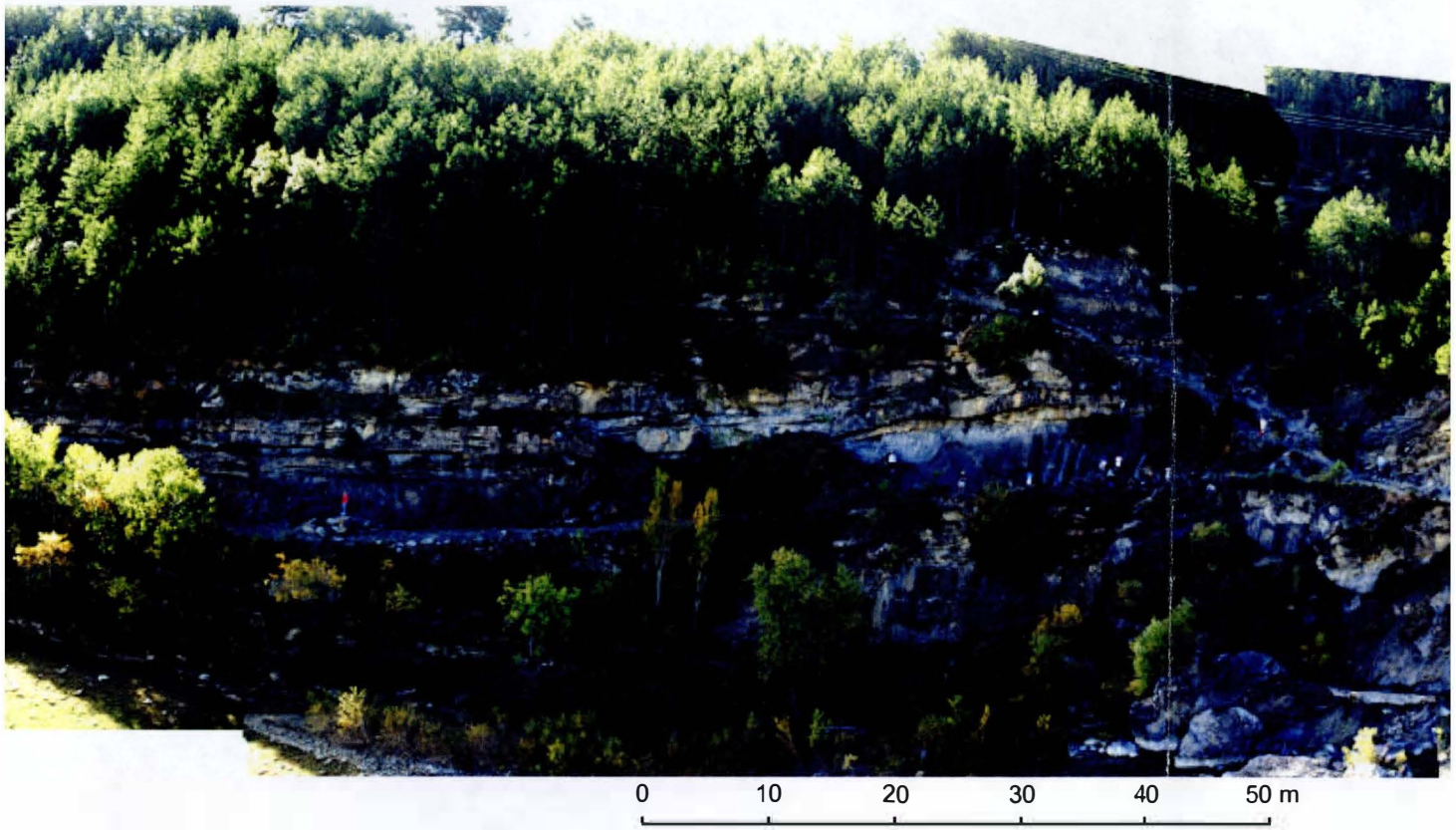

› l channel architecture, Rio Ara section

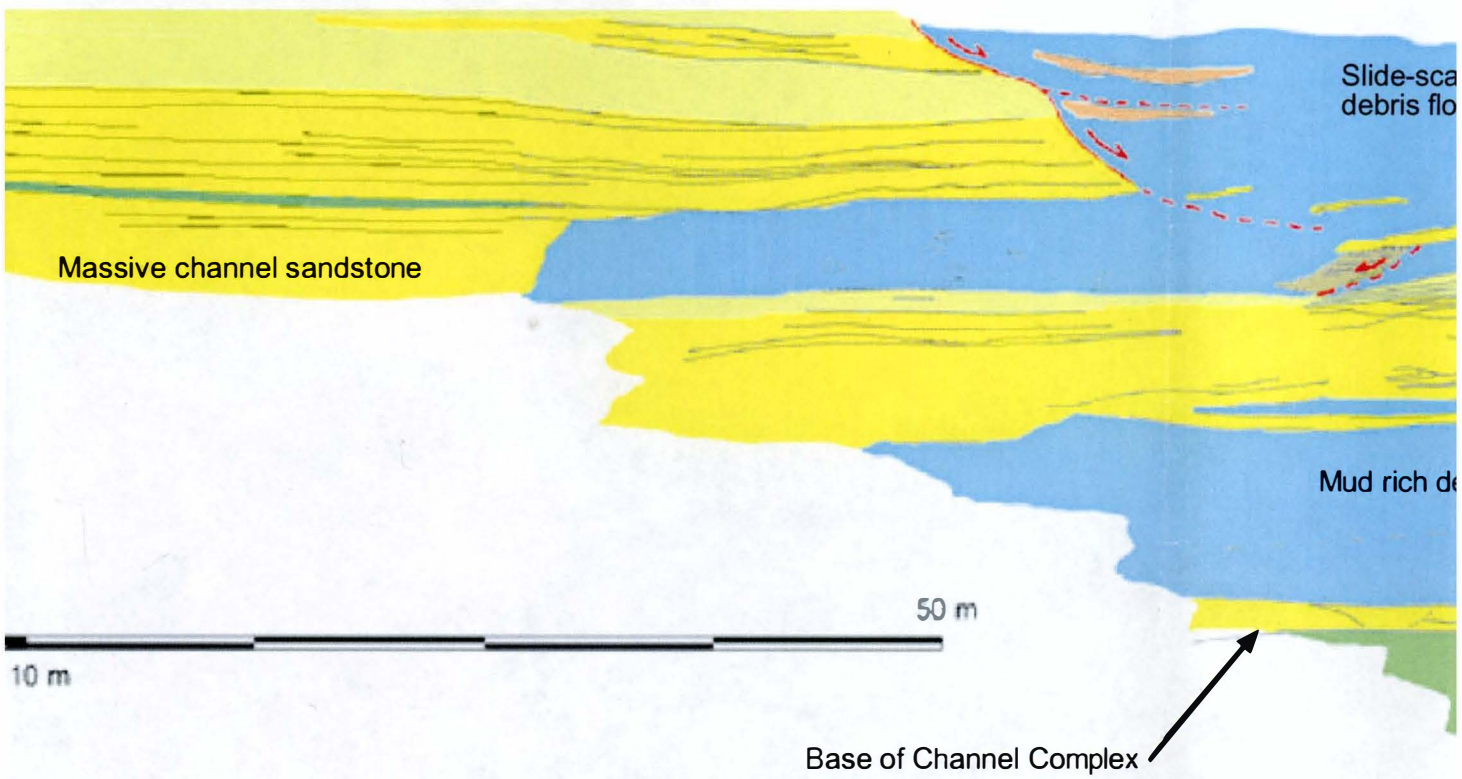

Aerial view of the Morillo I channel complex, Rio Ara section

Interpretation of the Morillo I channel architecture, Rio Ara section

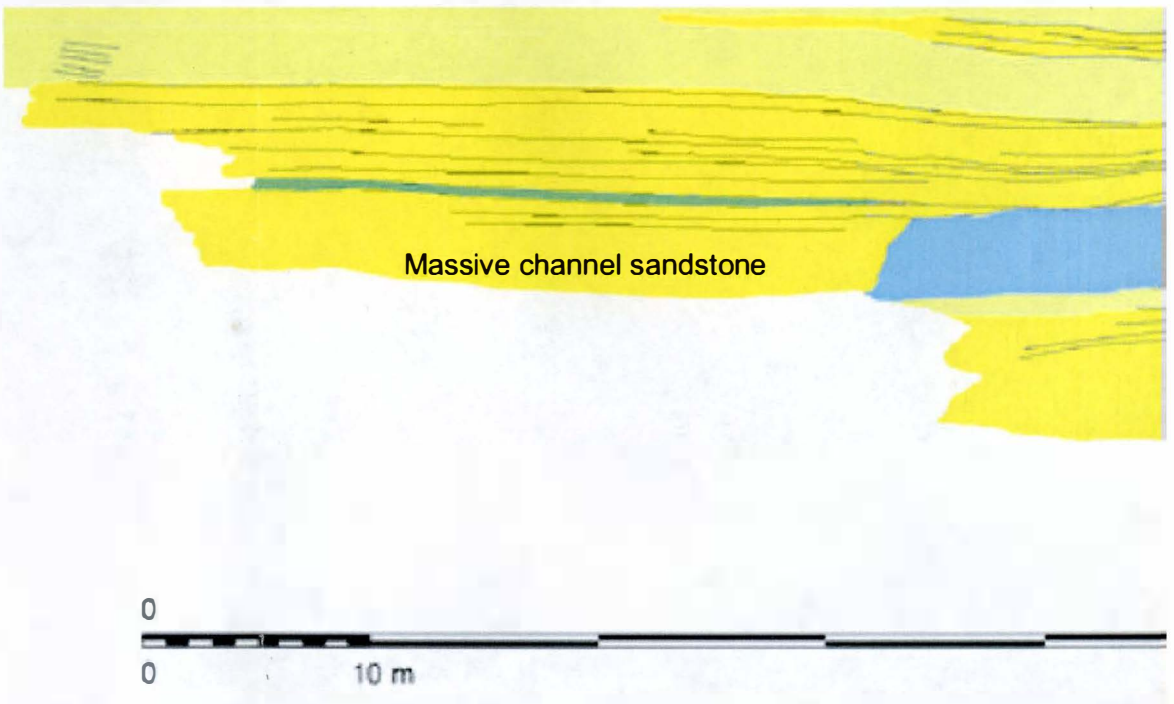

Ba

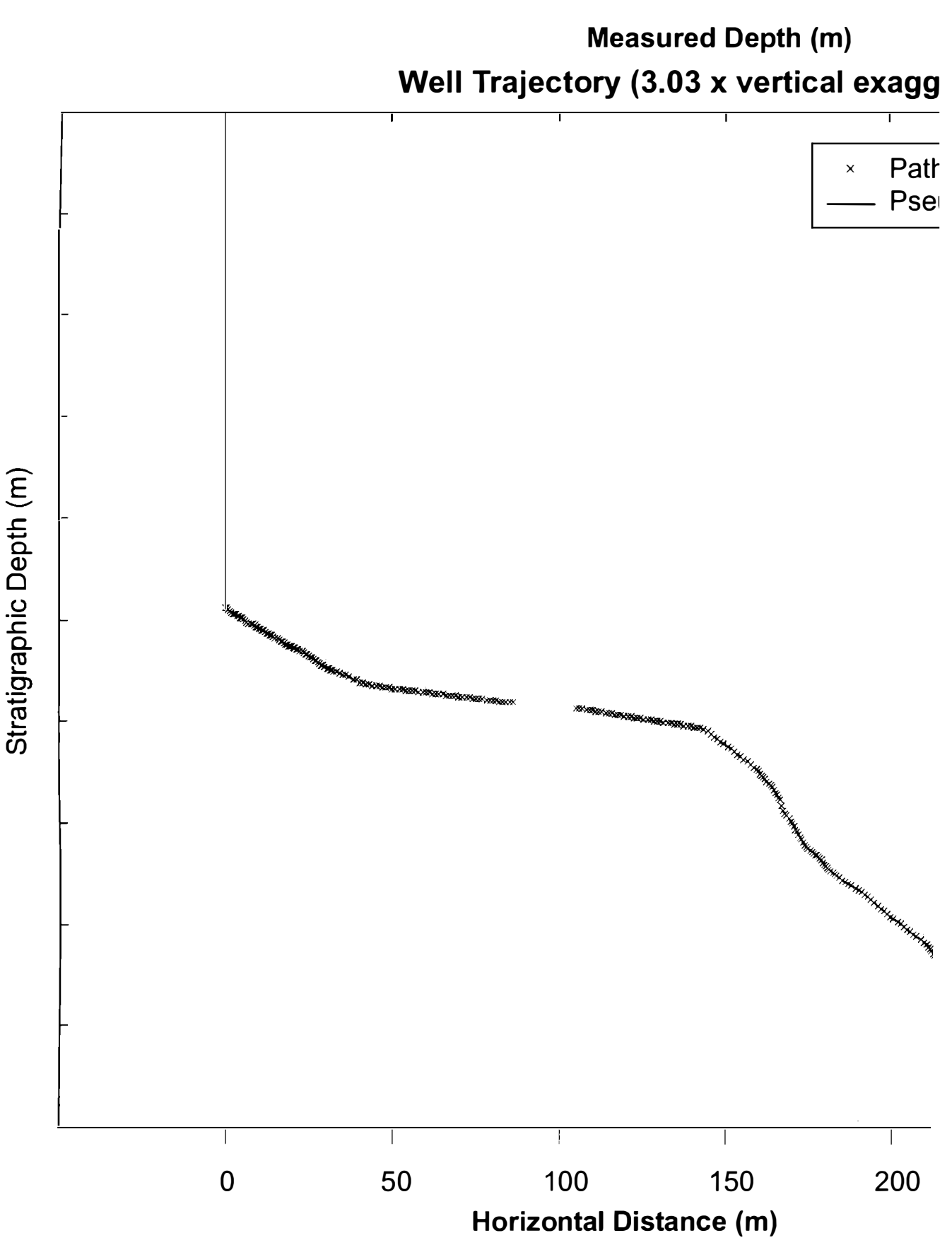
Measured Depth (m)
Well Trajectory (3.03 x vertical exagg
Path
Pseu
Stratigraphic Depth (m)
0
50
100
150
200
Horizontal Distance (m)

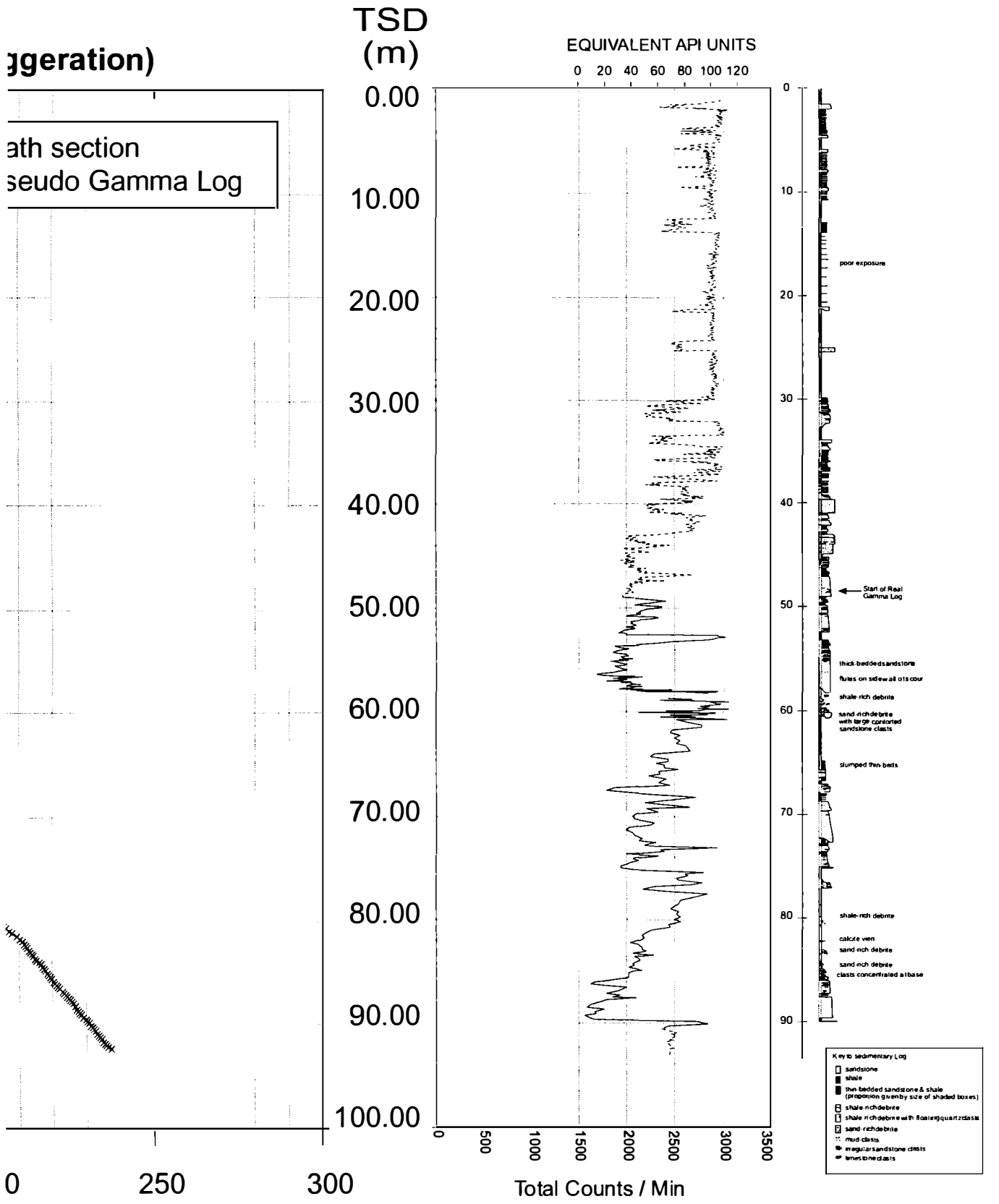
ggeration)
ath section
seudo Gamma Log
0
250
300
TSD
(m)
0.00
10.00
20.00
30.00
40.00
50.00
60.00
70.00
80.00
90.00
100.00
EQUIVALENT API UNITS
0 20 40 60 80 100 120
0
500
1000
1500
2000
2500
3000
3500
Total Counts / Min
poor exposure
Start of Real Gamma Log
thick-bedded sandstone
flutes on sidewall cts cour
shale-rich debrite
sand-rich debrite with large contorted sandstone clasts
slumped thin beds
shale-rich debrite
calcite vein
sand-rich debrite
sand-rich debrite
clasts concentrated at base
Key to sedimentary Log
sandstone
shale
thin-bedded sandstone & shale (proportion given by size of shaded boxes)
shale-rich debrite
shale-rich debrite with floating quartz clasts
sand-rich debrite
mud clasts
irregular sandstone clasts
limestone clasts

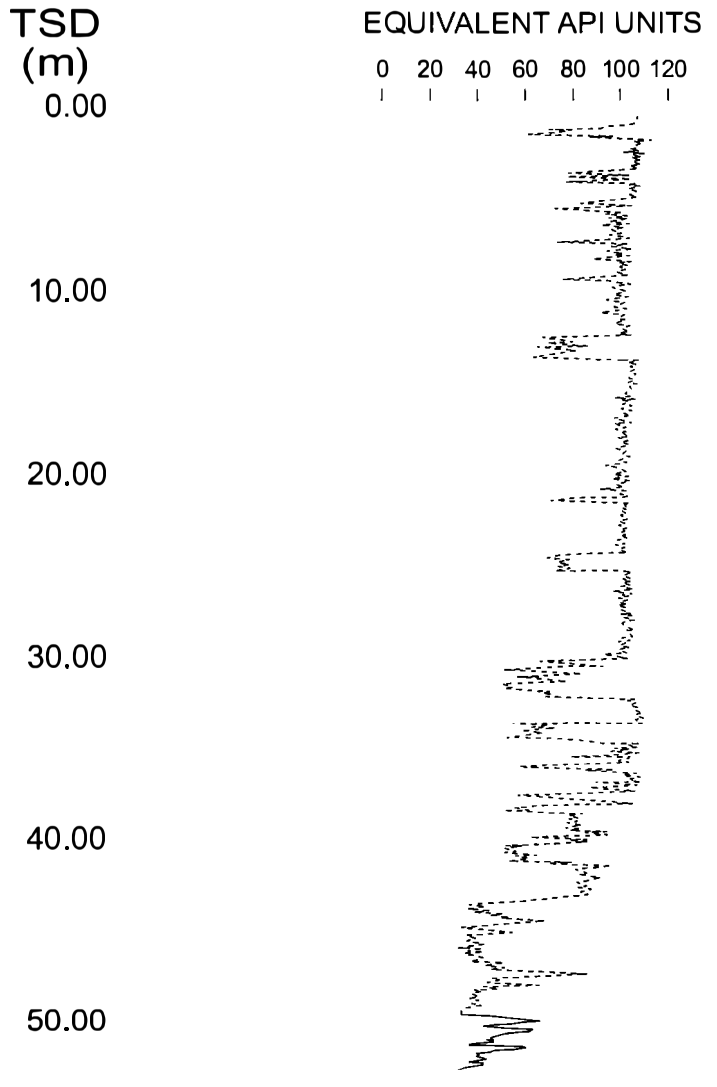
TSD
(m)
0.00
10.00
20.00
30.00
40.00
50.00
EQUIVALENT API UNITS
0 20 40 60 80 100 120

3500
3000
2500
2000
1500
1000
500
0
Total Counts / Min
30.00
40.00
50.00
60.00
70.00
80.00
90.00
100.00

3500
3000
2500
2000
1500
1000
500
0
Total Counts / Min
60.00
70.00
80.00
90.00
100.00